SYNTHESIS AND CHARACTERIZATIONS OF Co_3O_4 BASED NANOCOMPOSITE FOR ELECTROCHEMICAL SENSOR APPLICATIONS

SHAHID MEHMOOD

FACULTY OF SCIENCE
UNIVERSITY OF MALAYA
KUALA LUMPUR

2018

SYNTHESIS AND CHARACTERIZATIONS OF Co_3O_4 BASED NANOCOMPOSITE FOR ELECTROCHEMICAL SENSOR APPLICATIONS

SHAHID MEHMOOD

THESIS SUBMITTED IN FULFILMENT OF THE REQUIREMENTS FOR THE DEGREE OF DOCTOR OF PHILOSOPHY

DEPARTMENT OF PHYSICS
FACULTY OF SCIENCE
UNIVERSITY OF MALAYA
KUALA LUMPUR

2018

UNIVERSITY OF MALAYA

ORIGINAL LITERARY WORK DECLARATION

Name of Candidate: **Shahid Mehmood**

Registration/Matric No: **SHC160025**

Name of Degree: **Doctor of Philosophy**

Title of Thesis: **SYNTHESIS AND CHARACTERIZATIONS OF Co_3O_4 BASED NANOCOMPOSITE FOR ELECTROCHEMICAL SENSOR APPLICATIONS**

Field of Study: **Experimental Physics**

I do solemnly and sincerely declare that:

(1) I am the sole author/writer of this Work;
(2) This Work is original;
(3) Any use of any work in which copyright exists was done by way of fair dealing and for permitted purposes and any excerpt or extract from, or reference to or reproduction of any copyright work has been disclosed expressly and sufficiently and the title of the Work and its authorship have been acknowledged in this Work;
(4) I do not have any actual knowledge nor do I ought reasonably to know that the making of this work constitutes an infringement of any copyright work;
(5) I hereby assign all and every rights in the copyright to this Work to the University of Malaya ("UM"), who henceforth shall be owner of the copyright in this Work and that any reproduction or use in any form or by any means whatsoever is prohibited without the written consent of UM having been first had and obtained;
(6) I am fully aware that if in the course of making this Work I have infringed any copyright whether intentionally or otherwise, I may be subject to legal action or any other action as may be determined by UM.

Candidate's Signature Date:

Subscribed and solemnly declared before,

Witness's Signature Date:

Name: Dr. Chiu Wee Siong

Designation: Senior Lecturer

SYNTHESIS AND CHARACTERIZATIONS OF Co_3O_4 BASED NANOCOMPOSITE FOR ELECTROCHEMICAL SENSOR APPLICATIONS

ABSTRACT

Cobalt oxide (Co_3O_4), a metal oxide semiconductor has attained intensive interest and widely investigated due to its extraordinary characteristics such as facile synthetic methodologies, excellent catalytic properties, diverse morphologies and multiple applications. In recent years, enhancing the properties of Co_3O_4 by incorporating it into a conducting platform such as (in our case) graphene for its viable commercial applications, has been the focus of research, to explore its abilities towards the electrochemical sensing of target molecules. For an effective and sensitive sensing of a target molecule, Co_3O_4 with different morphologies was synthesized by a facile single-step hydrothermal method. The higher electrocatalytic performance was observed by Co_3O_4 nanocubes with low limit of detection i.e. 0.93 μM with the sensitivity value of 0.0485 ± 0.00063 $\mu A.\mu M^{-1}$ for the detection of 4-nitrophenol. 4-NP is an important toxic phenol-based nitro-compound that can be found in the waste-water released by the chemical and pharmaceutical industries. The Co_3O_4 with cubical morphology was selected as a model nanostructure due to its higher catalytic performance and Co_3O_4 based nanocomposites were synthesized for further studies. Graphene, a two-dimensional allotrope of carbon with *2D* honeycomb crystal lattice, having single atom thickness, large theoretical surface area with high conductivity at room temperature and wide electrochemical window, has attracted much attention by many researchers, was used as a conducting platform for Co_3O_4 nanocubes enrichment and to facilitate the electron transfer process. A Co_3O_4 based nanocomposite with different wt. % (2,4,8 and 12 wt.%) of graphene oxide (GO) was synthesized by the hydrothermal method and named as rGO-Co_3O_4 nanocomposite. The rGO-Co_3O_4 nanocomposite was used for the sensitive and selective detection of biological molecule serotonin (5-HT) a monoamine, present in enterochromaffin cells

located in the colonic mucosal epithelium widely distributed in the central nervous system. The rGO-Co_3O_4-4 % nanocomposite has shown higher current value of 36 μA with a lower potential value of 0.31 V. the limit of detection was found to be 1.128 μM. It is known that transition metals have high catalytic activity, high conductivity and ability to sense the target molecules. Hence, the deposition of a minimal amount of metal nanoparticle was proven to be an electrochemical signal enhancer in sensor application. Therefore, a nanocomposite consists of reduced graphene oxide, cobalt oxide and gold nanoparticle (rGO-Co_3O_4@Au) was synthesized by the same single-step hydrothermal method and utilized for the detection of hydrazine, a toxic, colorless and flammable molecule. Higher electrocatalytic performance was observed with a low limit of detection i.e. 0.443 μM for Hydrazine detection. Platinum (Pt) is considered a promising sensing element, due to its conducting nature and large surface area which boosts the electrochemical signal of the target analyte. Therefore, Co_3O_4 nanocubes deposited with Pt nanoparticle incorporated with graphene into a nanocomposite (rGO-Co_3O_4@Pt) was prepared by hydrothermal reaction and used as a sensor for the detection of nitric oxide (NO), a very important biological molecule responsible for vasodilation and blood pressure regulation in the nervous and cardiovascular systems of mammalian physiology. A limit of detection of 1.73 μM was calculated with a sensitivity value of 0.58304 $\mu A.\mu M^{-1}$. It will be worth mentioning that all the nanocomposites were synthesized for the first time by single step hydrothermal technique.

Keywords: cobalt oxide, graphene oxide, hydrothermal, electrochemical sensor.

SINTESIS DAN PENCIRIAN KOMPOSIT NANO BERASASKAN Co_3O_4 UNTUK APLIKASI PENGESAN ELEKTROKIMIA

ABSTRAK

Kobalt oksida (Co_3O_4) merupakan satu semikonduktor logam oksida yang menarik minat yang tinggi dan banyak dikaji kerana ciri luar biasanya seperti metodologi sintetik yang mudah, sifat pemangkin yang sangat baik, kepelbagaian morfologi dan aplikasi. Sejak beberapa tahun yang lalu, penambahbaikan sifat Co_3O_4 dengan memasukkan konduktor tunjang seperti grafin untuk aplikasi komersil yang berdaya maju, telah menjadi tumpuan penyelidikan, untuk meneroka keupayanya ke arah pengesanan elektrokimia molekul sasaran. Untuk penderiaan yang berkesan dan sensitif terhadap molekul sasaran, Co_3O_4 dengan morfologi yang berbeza telah disintesis dengan kaedah hidroterma sangat mudah (satu langkah). Prestasi elektropemangkin yang lebih tinggi telah dilihat apabila nanokubus Co_3O_4 mengesan 4-nitrofenol (4-NP) dengan kadar pengesanan yang rendah iaitu 0.93 μM dan nilai kepekaan 0.0485 ± 0.00063 $\mu A.\mu M^{-1}$. 4-NP merupakan sebatian penting yang boleh didapati di dalam sisa industri kimia dan farmaseutikal. Co_3O_4 dengan morfologi kubus dipilih sebagai model struktur nano untuk kajian seterusnya. Grafin, alotrop dua dimensi karbon dengan kekisi kristal sarang lebah 2D, mempunyai ketebalan atom tunggal, luas permukaan teoretikal yang besar serta kekonduksian yang tinggi pada suhu bilik, telah digunakan sebagai konduktor tunjang kepada nanokubus Co_3O_4 dalam memfasilitasikan proses pemindahan elektron. Nanokomposit berasaskan Co_3O_4 dengan komposisi berat (wt %) grafin oksida (GO) yang berbeza. (2, 4, 8 dan 12 %) disintesis mengunakan kaedah hidroterma dan dinamakan sebagai nanokomposit rGO-Co_3O_4. Nanokomposit rGO-Co_3O_4 digunakan untuk pengesanan sensitif dan selektif serotonin, satu molekul biologi (5-HT) monoamine yang terdapat di sel enterkhromafin yang terletak di epitel mukosa kolon yang tersebar luas dalam sistem saraf pusat. Nanokomposit yang mengandungi 4 % rGO-Co_3O_4 menunjukkan pengaliran arus yang tinggi iaitu 36 μA, nilai potensi yang rendah iaitu 0.31 V dan kadar pengesanan iaitu

1.128 μM. Logam peralihan secara umumnya mempunyai aktiviti pemangkin yang tinggi, kekonduksian yang tinggi dan keupayaan untuk mengesan molekul sasaran. Didapati juga, pemendapan nanopartikel logam pada kadar yang minimum terbukti menambah isyarat elektrokimia dalam aplikasi sensor. Oleh itu, nanokomposit yang terdiri daripada grafin oksida terturun, kobalt oksida dan nanopartikel emas (rGO-Co_3O_4 @ Au) disintesis melalui kaedah hidroterma yang sama dan digunakan untuk mengesan hidrazin, satu molekul toksik, tidak berwarna dan mudah terbakar. Prestasi elektrokatalik yang tinggi serta kadar pengesanan yang sangat rendah untuk hidrazin iaitu 0.443 μM ditemui. Platinum (Pt) diterima umum sebagai unsur penderiaan yang teguh atas sifat kekonduksian dan luas permukaan yang dapat meningkatkan isyarat elektrokimia dari molekul sasaran. Oleh itu, nanokubus Co_3O_4 dimendapkan bersama nanopartikel Pt yang telah digabungkan dengan grafin oksida terturun untuk menghasilkan nanokomposit (rGO-Co_3O_4@ Pt) melalui tindak balas hidroterma dan digunakan sebagai sensor untuk pengesanan nitrik oksida (NO), satu molekul biologi yang sangat penting terhadap vasodilasi dan peraturan tekanan darah dalam sistem saraf dan kardiovaskular fisiologi mamalia. Kadar pengesanan sebanyak 1.73 μM dan nilai sensitif sebanyak 0.58304 $\mu A.\mu M^{-1}$ telah dikira. Perlu dinyatakan bahawa semua nanokomposit telah disintesis buat kali pertama dengan teknik hidroterma yang melibatkan satu langkah sahaja.

Kata kunci: kobalt oksida, grafin oksida, hidrotermal, pengesan elektrokimia

ACKNOWLEDGEMENTS

All Praises be to **Allah**, His Majesty for His uncountable blessings, the **Allah** who is the most Gracious and the most Merciful. The best prayers and peace be unto his best messenger **Mohammad,** his pure descendant, family and his noble companions. Firstly, I would like to express my sincere gratitude to my advisors Dr. Huang Nay Ming, Dr. Chiu Wee Siong and Professor Dr. Wan Jeffrey Basirun for their continuous support during my Ph.D. study and related research, their critical review which allowed me to enhance the quality of my research writings, and immense knowledge. Next, I would like to express my gratitude to Dr. Alagarsamy Pandikumar, Dr. Perumal Rameshkumar, Dr. Sohail Ahmed for their guidance and discussions. I would like to extend my gratitude to my teachers: Mr. Amir Shehzad, Mr. Rehman wali khattak, Mr. Nazir Muhammad, Mr. Waheed Qureshi and Mr. Rashid Iqbal. Sincere thanks to Norazriena Binti Yusoff, Numan Arshed, Syed Tawab Shah, Syed Shahabuddin, Eraj Humayun Mirza, Chong Mee Yoke and all who supported me. I thankfully acknowledge the funding source, High Impact Research grant (UM.C/625/1/HIR/MOHE/05), supported me during my PhD work and Low Dimensional Materials Research Center's (LDMRC) members. Finally, my sincere gratitude e goes to my deceased father for his hard work, undemanding love, innumerable sacrifices and unconditional support throughout my life. It is possible for me to complete my studies and fulfil his dream because of his sacrifices which he made for me to reach until this point. I feel honored and deeply indebted for the support, encouragement, sacrifices, patience and prayers of my loving mother, sisters, brothers, aunties and my dearest Rafia. Without their love and support over the years none of this would have been possible. They have always been there for me and I am gratified for everything they have helped me to achieve.

Shahid Mehmood

January 2018

TABLE OF CONTENTS

LIST OF FIGURES

LIST OF TABLES

LIST OF SYMBOLS AND ABBREVIATIONS

AA	:	Ascorbic acid
AFM	:	Atomic force microscope
BDD	:	Boron-doped diamond
CME	:	Chemically modified electrode
CMG:	:	Chemically modified graphene
CPE	:	Carbon paste electrode
CV	:	Cyclic voltammetry
CVC	:	Chemical vapor condensation
CVD	:	Chemical vapor deposition
EDRF	:	Endothelium-derived relaxation factor
EDX	:	Energy-dispersive X-ray
EG	:	Ethylene glycol
EIS	:	Electrochemical impedance spectroscopy
EPA	:	Environment protection agency
ERGO	:	Electrochemically reduced graphene oxide
FESEM	:	Field emission scanning electron microscopy
FET	:	Field effect transistors
GC	:	Glassy carbon
HIR	:	High Impact Research
HRTEM	:	High resolution transmission electron microscopy
HTSC	:	High temperature super-conductors
LDMR	:	Low Dimensional Materials Research Center
LOD	:	Limit of detection
LOQ	:	Limit of quantification

MOCVD	:	Metal-organic chemical vapor deposition
ORR	:	Oxygen reduction reaction
PBS	:	Phosphate buffer solution
SCE	:	Saturated calomel electrode
SPR	:	Surface plasmon resonance
STM	:	Scanning tunneling microscope
SWV	:	Square wave voltammetry
UA	:	Uric acid
UM	:	University of Malaya
VLS	:	Vapor-Liquid-Solid
VS	:	Vapor-Solid
WE	:	Working electrode
XRD	:	X-ray diffraction

LIST OF APPENDICES

CHAPTER 1: INTRODUCTION

1.1 Background

1.1.1 Nanotechnology

The introduction to nanoscience and nanotechnology has revolutionized the whole world. Recently, great efforts have been paid to materials that were thought of being inactive in bulk form for different technological applications. Now it is proven that these bulk materials can exhibit extraordinary physical and chemical properties at nanoscale dimensions (Zhang *et al.*, 2008). The idea to synthesize materials at nanoscale dimensions was presented by Richard Feynman during his lecture "There is Plenty of Room at the Bottom" in 1959 at an American Physical Society meeting in Caltech. He said that with nanoscale components, it will be possible to successfully manipulate and control materials on the atomic and molecular size for electronic and mechanical systems; the development of technologies into such small systems would be created from combined fields such as chemistry, biology and physics. Similarly, the term "nanotechnology" was first introduced in 1974 by a Japanese scientist Norio Taniguchi at The International Conference on Production Engineering, Tokyo, from 26-29th August. He said that "nanotechnology" is the process of separation, integration and deformation of material by using one atom or one molecule. The idea of nanotechnology had been applied in 1980s by Gerd Binning and Heinrich Rohrer in the invention of scanning tunneling microscope (STM) which they won the Nobel Prize in Physics in 1986 (Demuth *et al.*, 1986). Furthermore, the idea of nanotechnology was also used in the development of the atomic force microscope (AFM), invented by Calvin Quate and Christoph Gerber.

More attention are being paid by many researchers from the past few decades to develop nanostructures because of their unique properties, such as:

1. The large surface area to volume ratio which increases the surface reactivity of nanomaterials which is useful for chemical and sensing applications.
2. Increased optical emission and absorption due to the electron transfer from one state to another state which is useful for optoelectronic nanodevices.

It has been also found that the magnetic, optic, catalytic and electronic properties of nanomaterial strongly depend on their crystallinity, size, structure and morphology (Rahman *et al.*, 2009).

Recently, nanostructured semiconductors have attracted much attention owing to their technological applications and fascinating properties (Ng *et al.*, 2003). The transition metal oxides have been studied intensively and it was found that these metal oxides play a very crucial role in the field of chemistry, physics and material science, and are widely used in these fields (Fernandez-Garcia *et al.*, 2004; Sun *et al.*, 2015). A large variety of oxide compounds can be formed from metal elements that can adopt a vast number of structural geometries with an electronic structure that can exhibit metallic, semiconductor or insulator character. Metal oxide nanostructures due to their widespread structural, physical and chemical properties and functionalities, stand out as one of the most common, diverse and richest class of material, and among the most versatile groups of semiconductor nanostructures. Metal oxides proved to be very promising for a variety of technological applications due to their unique and tunable optical (Cho *et al.*, 2017), optoelectronic (Allag *et al.*, 2016), magnetic (Xiao *et al.*, 2008), electrical (Cho *et al.*, 2017), mechanical (Cinthia *et al.*, 2015), thermal (Bala *et al.*, 2009), catalytic (Li *et al.*, 2017) and photochemical (Stroyuk *et al.*, 2005) properties . Metal oxides nanostructures have been at the heart of many dramatic advances in materials science. For example, these

metal oxides have been used as chemical sensors (Shahid *et al.*, 2015) , gas sensors and biosensor (Dalkıran *et al.*, 2017; Xu *et al.*, 2017), fuel cells (Shahid *et al.*, 2014), supercapacitors (Numan *et al.*, 2016), secondary battery materials (Park *et al.*, 2006), solar cells (Baek *et al.*, 2017), alkaline and lithium ion batteries (Chen *et al.*, 2017), piezoelectric (Jeong *et al.*, 2006), lasers (Pravinraj *et al.*, 2017), solar absorbers (Shimizu *et al.*, 2014) and so on. Hence, it was observed that metal oxide nanostructures have been explored widely by researchers, therefore the understanding of metal oxide nanostructures is the topic of main interest in term of their synthesis, properties and applications.

In recent years, cobalt oxide amongst the various types of metal oxides has attracted intensive attention from researchers due to its tremendous electrical, optical, magnetic and transport properties (Mini *et al.*, 2016; Xiao *et al.*, 2008). Due to the properties such as well-defined electrochemical redox activity (Ming-Jay *et al.*, 2009), low cost, stable chemical state (Xue *et al.*, 2014) and high theoretical capacity (890 mA hg^{-1}) (Shahid *et al.*, 2015), cobalt oxide nanostructures are considered as very promising candidate in the field of material science for electrochemical applications. Nevertheless, Co_3O_4 nanostructures have great potential as anode materials for electrochemical devices (Shahid *et al.*, 2017), rechargeable electronic devices (Numan *et al.*, 2016), Li ion batteries (Xue *et al.*, 2014), gas sensors (Li *et al.*, 2010), and high-temperature selective solar-radiation absorbers (Choudhury *et al.*, 1983).

However, Co_3O_4 is type of semiconductor which suffers from poor conductivity, low ion transport problem, larger band gap, low electrocatalytic activity and low stability as compared to metals. To mitigate these issues, researchers have utilized other material such as metals and conducting platform (graphene, carbon nanotubes and conducting polymers) and fabricated nanocomposites with Co_3O_4 which enhances the physical and

physiochemical properties of Co_3O_4. Therefore, Co_3O_4 based nanocomposite has attained immense interest in the field of electrochemistry. The major reason towards the interest in Co_3O_4 nanostructures and Co_3O_4 based nanocomposites is due to their technological application in various fields stated above and versatile morphological structures of Co_3O_4 which help in boosting the electrocatalytic performance of the nanocomposite.

In recent years, Co_3O_4 nanostructures and Co_3O_4 based nanocomposites have been used intensively as efficient electrode material for electrochemical applications, such as sensing of water pollutants like phenol based compounds, dyes, bleaches, salts, pesticides, insecticides, metals, toxins produced by bacteria and human or animal drugs etc. Moreover, Co_3O_4 and its nanocomposites are also used to detect the biological molecules such as serotonin (5-HT), dopamine (DA), ascorbic acid (AA), uric acid (UA) and nitric oxide (NO) etc. Thus, Co_3O_4 based nanocomposites provide promising features towards sensing of target molecules.

1.2 Aim and Objectives

Co_3O_4 is a very suitable candidate for various applications especially electrochemical applications. In view of these facts, different structures of Co_3O_4 could contribute to electrochemical sensing of target molecule, since the performance of nanomaterial significantly depends on the size, morphology, crystallinity and distribution of the particles. Similarly, the specific structure of Co_3O_4 with higher electrochemical performance can be used to fabricate a nanocomposite with graphene, which further contributes to the electrochemical sensing of target molecules, by increasing the effective surface area of the nanocomposite. Moreover, Co_3O_4 behaves like impurities on graphene matrix which increases the defect level and creates an interlayer spacing between the different layers of GO, which allows the electrolytes to diffuse between the layer of GO. This could ultimately increase the electrocatalytic activity of the nanocomposites through

the interaction of the HOMO-LUMO of graphene with the d-orbital electrons in the Co atom which significantly enhances the electrocatalytic performance of the nanocomposite. Metal atoms can be doped into Co_3O_4 nanoparticles to boost the performance, as stated above that metals have significant role in improving the performance of the sensor material. So, the main objectives of the reseach are:

A) Investigation of optimized parameters for the synthesis of different structures of metal oxides.
B) To Optimize the parameter for the synthesis graphene-metal oxide nanocomposite.
C) Deposition of metal nanoparticle on the surface of metal oxides to further enhance the electrocatalytic performance of electrode material.
D) To investigate the performance of electrode material for the detection of target molecules.

Based on the objectives stated above, the main research focus of the thesis are:

1) Synthesis of different nanostructures of Co_3O_4 by using simple one step hydrothermal route by varying the temperature and time. The synthesized material can be used as a catalyst for the sensing of a water contaminant such as 4-NP.
2) Synthesis of a specific nanostructure of Co_3O_4 as a composite with rGO chosen from different synthesized nanostructures which is based on the performance/electrocatalytic activity for electrochemical sensor studies of serotonin a biological molecule. To synthesize the rGO-Co_3O_4 nanocomposite, ammonia is used which promotes the reduction of GO into rGO and precipitation of Co_3O_4. The same one-step hydrothermal route can be used for the synthesis of rGO-Co_3O_4 nanocomposite.

3) A ternary nanocomposite can be synthesized by the addition of Au i.e. rGO-Co_3O_4@Au by using the same synthesis route as mentioned above in the 2nd hypothesis. The nanocomposite can be used for the electrochemical sensing of hydrazine.

4) The synthesis of ternary nanocomposite by using the hydrothermal route as stated above and by replacing Au with Pt i.e. rGO-Co_3O_4@Pt since Pt is a more efficient catalyst compared to Au. The electrochemical studies can be carried out for the sensing of nitric oxide (NO) a very important physiological molecule.

1.3 Structure of Thesis

This thesis is divided into seven chapters, chapter one includes the background studies of the metal oxides and their nanocomposites used for various applications based on their properties. Chapter one further includes the aims and objectives of the thesis. Chapter two provides a brief literature review on metal oxide and metals nanoparticles, graphene and graphene oxide and metal oxide based nanocomposite and their applications. Chapter three, four, five and six presents with the research work conducted during the Ph.D. candidature period which includes experimental details, and results and discussions involving different type of Co_3O_4 based nanocomposites and their electrochemical applications:

1. Morphology dependent electrocatalytic properties of hydrothermally synthesized cobalt oxide nanostructure.
2. Amperometric detection of depression biomarker using a glassy carbon electrode modified with nanocomposite of cobalt oxide nanocubes incorporated into reduced graphene oxide
3. An electrochemical sensing platform of cobalt oxide@gold nanocubes interleaved reduced graphene oxide for the selective determination of hydrazine.

4. An electrochemical sensing platform based on reduced graphene oxide-cobalt oxide nanocubes@platinum nanocomposite for nitric oxide detection.

The summary of the research works is included in Chapter 7 by covering the important findings from each study. The suggestions of possible future work arising from this research are proposed at the end of 7th Chapter. The flowchart of the research work is illustrated in Figure 1.1.

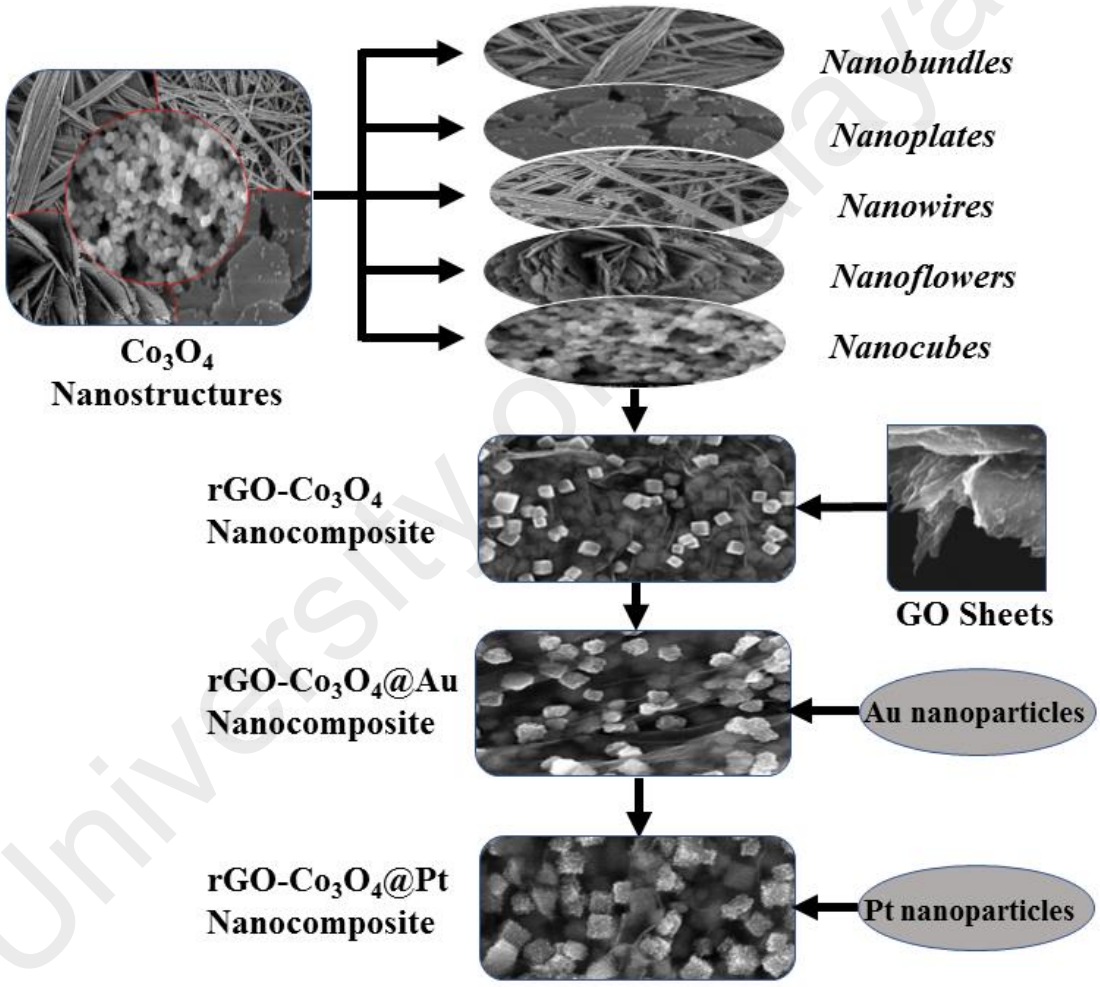

Figure 1.1: Flow chart of research studies.

CHAPTER 2: LITERATURE REVIEW

2.1 Metal Oxide Nanoparticles

Metal oxides are an important class of materials which are widely used as catalysts in addition to a wide range of diverse applications in materials science, chemical sensing, microelectronics, nanotechnology, environmental decontamination, analytical chemistry, solid state chemistry and fuel cells.

The oxides of metals such as iron, nickel, cobalt, copper and zinc have many important applications, such as magnetic storage media, solar energy conversion, electronics, semiconductor and catalysis. The use and performance for different properties and applications are however, strongly influenced by the crystalline structure, the morphology and the size of the particles. Therefore, it is very important to develop methods for the synthesis of metal oxide nanoparticles where the particle size and the crystal structure of the products can be controlled.

2.1.1 Synthesis Processes of Metal Oxides Nanoparticle

The principal necessity of any innovative research in the field of nanometal oxides is the preparation of the material. The design of an efficient method for the synthesis of metal oxide nanoparticles, is a present-day challenge. The synthetic methodologies for metal oxide nanoparticles can be subdivided into the following categories:

The synthesis of nanomaterials with desired morphology and composition is the most challenging task in the field of nanoscience and nanotechnology. In the past several decades, the synthesis of metal oxides nanostructures has stimulated great interest due to their novel properties which provide intense research efforts to fabricate efficient miniaturized devices in various nanoelectronics and photonics applications. Thus, various fabrication techniques have been explored in the literature for the synthesis of these metal oxide nano-structures.

Methods for fabricating nanomaterials can be generally subdivided into two groups: top-down methods and bottom-up methods. In the first method, nanomaterials are derived from a bulk substrate and obtained by progressive removal of the material, until the desired nanomaterials are obtained. A simple way to illustrate the top-down method is to think of carving a statue out of a large block of marble. Bottom-up methods work in the opposite direction: the nanomaterials, such as a nanocoating, are obtained starting from the atomic or molecular precursors and gradually assembling it until the desired structure is formed.

In both methods two requisites are fundamental: the control of the fabrication conditions (e.g. energy of the electron beam) and the control of the environmental conditions (presence of dust, contaminants, etc.). For these reasons, nanotechnology requires highly sophisticated fabrication tools that are mostly operated in vacuum or clean-room laboratories.

An overview is given on the experimental techniques used for the synthesis and characterization of nanomaterials. The synthesis of nanomaterials with desired morphology and composition is the most challenging task in nanoscience and nanotechnology. In several decades, the synthesis and characterization of metal oxide nanostructures have stimulated great interest due to their novel properties which provide intense research efforts to fabricate efficient miniaturized devices in various nanoelectronics and photonics applications. Therefore, various fabrication techniques have been explored in the literature for the synthesis of these metal oxide nanostructures but typically, they can be divided into two categories: (1) solution phase growth processes and (2) vapor phase growth processes.

2.1.1.1 Chemical Process/Solution Phase Growth Processes

Solution phase growth process is the successful and generic method for the synthesis of various nanostructures. Unlike the vapor phase synthesis, this method provides different environment for the growth of the nanostructures. Thus, it considerably reduces the cost and complexity of the fabrication of nanostructures. Although large yields of desired nanomaterials are produced based on the solution method, but it also produces large amount of impurities, which in turn could hamper the applications of the products. However, the obtained products can be cleaned and hence the impurities can be decreased by the filtration and washing of the obtained products. In this way, pure products make this technique commercially applicable for nanostructured formations. To develop strategies that control and confine the growths, several approaches have been used and is reported in the literature, such as sol-gel, electrochemical deposition, surfactant assisted growth process, sonochemical, solvothermal, chemical precipitation methods etc.

Chemical method for the synthesis of metal oxide nanoparticles is referred to as bottom-up approach where the nanoparticle synthesis is achieved by the chemical reduction of metal salts, electrochemical procedures or from the metastable organometallic compounds by their precisely controlled decomposition. Numerous kinds of stabilizers such as surfactants, donor ligands, polymeric compounds etc. are utilized for controlling the growth of nanoparticles and restraining them from agglomeration. The important types of chemical method for the synthesis of metal oxide nanoparticles are discussed as follows:

(a) ***Co-precipitation Process***

Metal oxides are prepared using the chemical precipitation route. The selection of proper reactants is the most important factor in any chemical synthesis process. For this purpose, an extensive knowledge on the chemical reactivities of the reagents, and the reaction mechanism is required. The morphology and the composition of a nanomaterial can be controlled efficiently if each reaction step is fully understood. The chemical reaction could be initiated by mixing the reactants in a beaker or in a round-bottom flask. The concentration of reactants, reaction time and order of addition of reactants to the solution, temperature, pH, viscosity and surface tension of the solution are the parameters which must be controlled. When the reaction products are supersaturated, spontaneous nucleation occurs and subsequently, it passes through the growth mechanism. Nanomaterials, with different morphology, can be prepared during this step if proper care is taken. The major difficulty in the chemical precipitation method is the contamination, particularly due to the by-product generated in chemical reaction. The optimization procedure is certainly a tedious task. Numerous experiments at different parameters must be investigated to achieve the desired results. Even working conditions such as stirring speed, vibration, exposure to light, cleanliness of glassware etc. can significantly affect the quality of nanomaterial produced. Hence, the synthesis of nanomaterials of desired morphology and composition through chemical methods is considered to be an art and also a skill. (Ajayan *et al.*, 2000)

(b) ***Sol-gel Process***

Sol-gel chemistry has recently evolved into a general and powerful approach for preparing inorganic materials. This method typically entails hydrolysis of a solution of a precursor molecule to obtain, first a suspension of colloidal particles (the sol) and then a gel composed of an aggregate of sol particles. The gel is then thermally treated to yield

the desired material. This method is a versatile solution process for preparing ceramic and glass materials (Interrante *et al.*, 1997).

(c) Electrochemical Deposition Process

This method has been widely used for the fabrication of metallic nanowires in porous structures and is convenient for the fabrication of metal oxide nanostructures. Electrodeposition uses dissolved precursors, especially in aqueous solution, is a low cost and a scalable technique, well suited to produce large scale semiconductor thin films. Recently, the electrochemical deposition has attracted much attention due to its short reaction times and low cost. Yang et al. in 2007 reported the synthesis of highly ordered ZnO ultrathin nanorod and hierarchical nanobelt arrays on zinc substrate with an electrochemical route in mixed H_2O_2 and NaOH solution (Yang *et al.*, 2007) Different materials produced with this method using porous or non-porous structures, substrates and metal foils etc. are reported in the literature (Rout *et al.*, 2006).

(d) Sonochemical Method

This method of synthesizing materials has proven to be a valuable technique for producing novel materials with uncommon properties. The sonochemical method of synthesis basically arises from the acoustic cavitation phenomenon, this phenomenon includes formation, growth and collapse of bubbles in the aqueous solution (Thompson *et al.*, 1999). The process occurs under extreme reaction conditions, for example high pressure greater than 500 atm, very high temperature more than 5000K, and cooling rate (>1010 K/s, attained during cavity collapse). This method leads to many unique properties of the irradiated solution, resulting in the formation of nanostructures via the chemical reaction. A variety of nanostructures are already prepared by the sonochemical method and reported in the literature (Dhas *et al.*, 1997; Kumar *et al.*, 2000).

(e) ***Hydrothermal or Solvothermal Process***

The hydrothermal synthesis is a method of synthesis of single crystals which depends on the solubility of minerals in hot water under high pressure. The crystal growth occurs in an apparatus consisting of a steel pressure vessel called autoclave, in which a nutrient is supplied along with water. A gradient of temperature is maintained at the opposite ends of the growth chamber so that the hotter end dissolves the nutrient and the cooler end causes the seeds to grow continuously. The hydrothermal process was initiated in the middle of the 19th century by geologists and was aimed at laboratory simulations of natural hydrothermal phenomena. In the 20th century, the hydrothermal synthesis was clearly identified as an important method for material synthesis, predominantly in the fields of hydrometallurgy and single crystal growth (Byrappa *et al.*, 2012). Advantages of the hydrothermal synthesis method include the ability to synthesize crystals of substances which are unstable near to the melting point, and the ability to synthesize large crystals of high quality. The solubility of many oxides in hydrothermal solutions of salts is much higher than in pure water; such salts are called mineralizers. Among the disadvantages are the high cost of equipment and the inability to control the crystal growth process (O'Donoghue, 1983).

(f) ***Template Process***

Amongst the numerous synthetic route for the synthesis of controlled sized metal oxide nanoparticles, the template technique is one of the encouraging approaches to prepare nanoscale metal oxides. In the template based nanoparticles synthesis, porous materials comprising of uniform void spaces are utilized as the host to trap nanoparticles as the guest. The template methods are commonly used in some of the previously stated approaches and specifically applies to two types of templates, soft-templates (surfactants) and hard templates (porous solid materials such as silica or carbon).

2.1.1.2 Physical Process / Vapor Phase Growth Processes

Physical method is also generally known as the top-down approach for the synthesis of nanoscale material. In this approach, the bulk material is transformed into nanomaterial by using physical forces such as milling, grinding, vapor phase deposition etc. Some of the important physical approaches for the synthesis of nanomaterials are discussed below:

For the growth of a group of nanostructures, vapor phase deposition is the most versatile technique. In vapor-phase synthesis of nanoparticles, the vapor phase mixture is thermodynamically unstable relative to the formation of solid material in nanoparticulate form. This includes the usual situation of a supersaturated vapor. It also includes a third process 'chemical supersaturation' where it is thermodynamically favorable for the vapor phase molecules to react chemically to form a condensed phase. If the degree of supersaturation and reaction/condensation kinetics are sufficient, the particles will nucleate homogeneously. Once nucleation occurs, the remaining supersaturation can be relieved by condensation or reaction of the vapor-phase molecules on the resulting particles, thus particle growth will supersede further nucleation. Therefore, to prepare smaller particles, a high degree of supersaturation by inducing a high nucleation density is necessary, and immediately quenching the system, either by removing the source of supersaturation or slowing the kinetics, to stop the growth of the particles. In most cases, this happens rapidly (milliseconds to seconds) in a relatively uncontrolled fashion, and lends itself to continuous or quasi continuous operation.

To control the diameter, the aspect ratio and crystallinity of nanomaterial, diverse techniques have been explored such as thermal evaporation, pulse laser deposition (PLD), metal organic chemical vapor deposition (MOCVD), sputtering process, thermal chemical vapor deposition, cyclic chemical vapor deposition (CFCVD) etc. Generally, two growth mechanisms have been explored for the formation of these metal oxide

nanostructures by the aforesaid techniques: (a) Vapor-Liquid-Solid (VLS) and (b) Vapor-Solid (VS) process.

(a) ***Thermal Evaporation Method***

Various nanostructured materials are grown by the thermal evaporation process. In this technique, there is a need of high temperature thermal furnace, used for vaporizing the source material to facilitate the deposition of the nanostructures at relatively lower temperatures. The vapor species of the source materials are generated first by physical or chemical methods, and subsequently condensed under certain conditions such as temperature and pressure on silicon substrate. Numerous nanomaterials have been grown by this method which ranges from elemental nanowires to a variety of semiconductor materials (Frohlich *et al.*, 2006; Greene *et al.*, 2003; Wang *et al.*, 2002). Generally, the thermal evaporation process contains a horizontal quartz tube furnace with rotary pump and gas supply system.

(b) ***Pulsed Laser Deposition***

A pulsed-laser beam leads to a rapid removal of material from a solid target and to the formation of an energetic plasma plume, which then condenses onto a substrate. In contrast to the simplicity of the technique, the mechanisms in PLD including ablation, plasma formation and plume propagation, as well as nucleation and growth are rather complex. In the laser ablation process, the photons are converted first into electronic excitations and then into thermal, chemical and mechanical energy (Kelly *et al.*, 1994; Miotello *et al.*, 1999) resulting in the rapid removal of material from the surface. This process has been studied extensively because of its importance in laser machining. Heating rates as high as 1011 K s^{-1} and instantaneous gas pressures of 10–500 atm are observed at the target surface (Kelly *et al.*, 1994).

PLD has been used extensively in the growth of high-temperature curates and numerous other complex oxides, including materials that cannot be obtained via an equilibrium route. Earlier on, it has been shown that the growth process of materials from a PLD plume are fundamentally different compared to thermal evaporation (Sankur *et al.*, 1989). The method has been successful for the film synthesis of Y-type magnetoplumbite (with a c-axis lattice parameter of 43.5 Å) (Ohkubo *et al.*, 2001) and garnets with 160 atoms per unit cell (Willmott *et al.*, 2000).

(c) ***Sputtering Process***

A final means of vaporizing a solid is via sputtering with a beam of inert gas ions. Urban et al. in 2002 demonstrated the formation of a dozen different metal nanoparticles using magnetron sputtering of metal targets. They formed collimated beams of the nanoparticles and deposited them as nanostructured films on silicon substrates. This process must be carried out at relatively lower pressures (~1 mTorr), which makes further processing of the nanoparticles in aerosol form difficult. It is largely driven by the momentum exchange between ions and atoms in the material, due to collisions. The surface diffusion process is usually used to explain the formation of nanoscale islands or rod growth during the sputtering process. Recently this method has been used for the synthesis of various nanostructures such as ZnO, W, Si, B, etc. (Cao *et al.*, 2001; Cao *et al.*, 2002; Karabacak *et al.*, 2003).

(d) ***Mechanical Attrition***

One of the important physical method for the synthesis of nanoparticles is mechanical attrition or mechanical milling of bulk material to produce low dimensional materials. This technique yields nanoparticles by using milling equipment which are categorized as “low energy milling” and “high energy milling” based on the material to be transformed into nanomaterials. The main goal of the milling technique is the reduction

of particle size and merging of particles in new phases. In contrast to the several procedures cited earlier, mechanical attrition leads to the formation of nanostructures through the structural decomposition of crude grained structures, instead of cluster assembly due to mechanical deformation. The ball milling and rod milling systems are potent tools to produce numerous advanced materials. Mechanical attrition is a distinctive technique which can be carried out at room temperature. The procedure of mechanical attrition has been performed on high energy mills, vibratory type mill, centrifugal type mill and low energy tumbling mill. Some of the important milling techniques includes attrition ball mill, planetary ball mill, vibrating ball mill, low energy tumbling mill and high energy ball mill.

(e) ***Metal-organic Chemical Vapor Deposition***

This technique MOCVD is widely used for the preparation of epitaxial structures by atom deposition on a wafer substrate. The operational principle of this method is simple and has been extensively used for various thin film growths. For the specific crystal growth, the desired atoms, which are bonded with complex organic gas molecules are passed over a hot semiconductor wafer. Due to the heat, the complex organic molecules decompose and are deposited as the desired atoms, via layer by layer deposition onto the substrate surface. The undesired remnants are removed or deposited on the walls of the reactor. By varying the composition of the gas, crystal properties approaching the atomic scale can be achieved. Using this technique, layers of the precisely controlled thickness can be obtained, which is important for the fabrication of materials with specific optical and electrical properties. By MOCVD, it is possible to build a range of semiconductor photodetectors and lasers. Furthermore, scientists are recently inclined to grow nanostructures with this technique, in addition to thin film growth. Various semiconductor nanostructures have been synthesized by this technique as reported in the literature (Baxter *et al.*, 2005; Kang *et al.*, 2006; Su *et al.*, 2005)

(f) Chemical Vapor Deposition and Chemical Vapor Condensation

A CVD is well renowned technique where a solid material is deposited on a pre-heated surface of a substrate through a chemical reaction from the vapor or gas phase. This process need an appropriate amount of activation energy to initiate the nanoparticle synthesis which can be supplied through numerous ways. In thermal CVD, the energy to initiate the reaction is provided by elevated temperature (up to 900 °C). In plasma CVD, the reaction is triggered by plasma at temperatures between 300 and 700 °C. In laser equipped CVD technique, the pyrolysis of bulk solid takes place upon the adsorption of heat from laser thermal energy which eventually leads to nanoscale material synthesis. In photo-laser equipped CVD, the ultra violet radiation induces the chemical reaction which has adequate amount of photon energy to breakdown the chemical bond in the reactant molecules. An alternative method known as CVC was established in Germany in 1994. It comprises pyrolysis of the metal-organic precursors into vapors, under reduced pressure atmosphere. Nanoparticles of metal oxides such as ZrO_2, Y_2O_3 and nano-whiskers have been synthesized by the CVC method (Chang *et al.*, 1994; Rajput, 2015).

2.1.2 Properties of Metal Oxides

2.1.2.1 Surface Properties

Little is known about the surface structures of transition metal oxides, but their bulk crystal structures are well researched. The physical and chemical properties of any material depend mainly on its surface properties regardless of its bulk or nanoscale nature. The surface of any type of material is different compared to the bulk, as the movement and exchange of matter and energy occur through an area called the interface. In addition, they also can either initiate or terminate a chemical reaction, like in the case of catalysts. When a bulk solid material is further segmented into nano-regime material, the total collective surface area is significantly enhanced although the total volume remains the same. Therefore, the surface-to-volume ratio of the material is increased as compared to

the bulk parent material. How could the total surface area increase if a cube of 1 m^3 is progressively cut into smaller and smaller cubes, until it is composed of 1 nm^3 cubes? Table 1 summarizes the result (Fiiipponi *et al.*, 2012).

Table 2.1: Effect of size on surface area of cube.

Dimension of cubic side	No. of cubes	Total effective surface area
1 m	1	6 m^2
0.1 m	1000	60 m^2
0.01 m = 1 cm	10^6 (1 million)	600 m^2
0.001 m 1 mm	10^9 (1 billion)	6000 m^2
10-9 m = 1 nm	10^{27}	6 x 10^9 = 6000 km^2

2.1.2.2 Electrical Properties

Materials can be grouped in many ways and such as the ability to conduct electricity. There are three main categories which they belong i.e. insulators, semiconductors or conductors, depending on the electric current flow through the material. The boundaries between the three sets are somewhat arbitrary and overlap occurs. There are, however, fundamental differences between the mechanism of conduction in metals and semiconductors/insulators. The electrical properties of solid-state materials depend on the band structure. The highest filled electronic state at 0 K is called the Fermi energy E_f. Figure 2.1 demonstrates the three different band structures of solids at 0 K.

i. A conductor, typical of many metals *e.g.*, copper which has a partially filled outermost band. Each copper atom has one 4*s* electron to make the 4*s* band half filled. The electrons in this band are free to move whenever an electric field is applied.

ii. A conductor *e.g.*, magnesium in which filled and empty bands overlap each other. In the case of magnesium, there is an overlap between the 3*s* and 3*p* band.

iii. A semiconductor, where a small gap separates the filled valence band from an empty conduction band, because electrons can gain sufficient energy to excite into the empty conduction band.

iv. An insulator where all the electrons are restricted in the valence band with the conduction band completely empty. The band gap, that is several electron volts, means it is energetically unlikely for an electron in the valence band to be promoted to the empty conduction band.

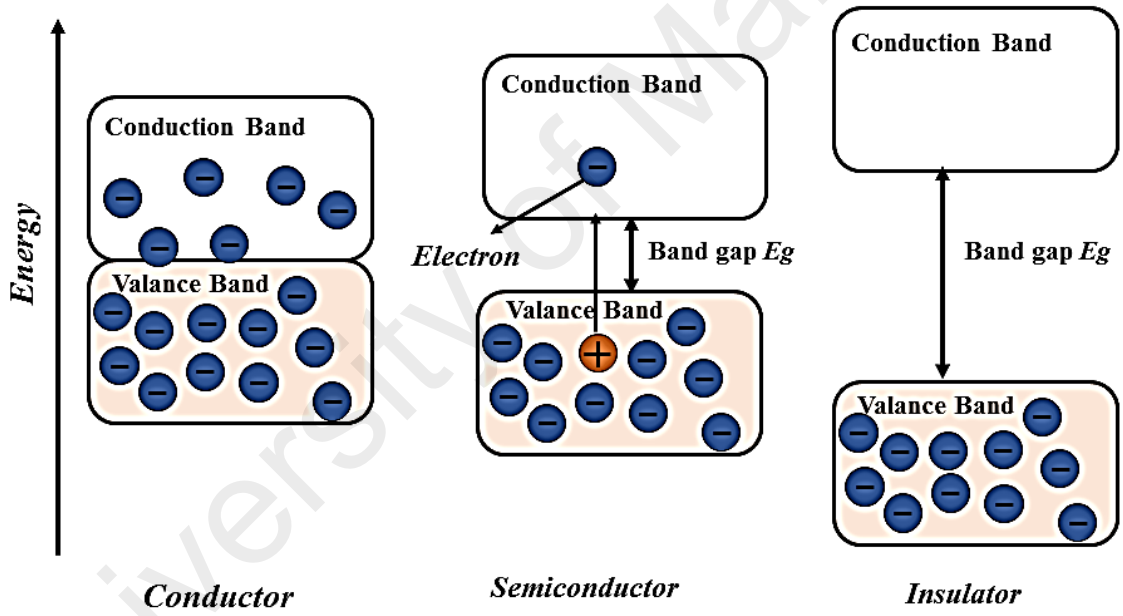

Figure 2.1: Various band structures in solids at 0 K representing conductor, semi-conductors and insulator.

Most of the structural ceramics are electrical insulators, while some electroceramics are very good electronic conductors. Semiconducting ceramics can be either p-type or n-type which depends on the number of holes or negative charges. They mostly undergo redox reactions, i.e., oxidation-reduction reactions with surroundings and are highly useful as chemoresitive gas sensors. Developments in the various subclasses of

electroceramics have paralleled the growth of emerging technologies, examples are such as optical properties.

2.1.2.3 Optical Properties

Additionally, metal oxides display optical characteristics and have shown ground state electronic structures, as well as numerous excitations of charge, spin, orbital and lattice degrees of freedom. The optical features of metal oxides have broadened their field of technological applications such as optical and optoelectronic devices, by applying the optical responses, magneto-optical effect, photo-refractive effect and elasto-optic effect. Moreover, the conductivity of a semiconductor depends on the current or voltage applied to a control electrode or to the intensity of irradiation by infrared, visible light, ultraviolet (UV) or X-ray.

2.1.2.4 Redox Properties

Metal oxides are one of the most important and widely employed classes of solid catalysts, either as active phases or as supports. Metal oxides especially containing transition metals possess redox properties in addition to their acidic and basic nature. This is due to the interaction with reactant molecules such as CO, H_2, and O_2 which could lead to electron transfer from the surface to the adsorbed species and modify the valence state of the metal centers.

Metal oxides are used because of their acid-base and redox properties and constitute the largest family of heterogeneous catalysis (Brückner, 2003; Henrich *et al.*, 1996; Henry *et al.*, 1998; Kung, 1989; Noguera, 1996; Védrine, 2002; Zecchina *et al.*, 2001). The three key features of metal oxides, which are essential for applications in catalysis, are

(i) *Coordination environment of the surface atoms.*

(ii) *Redox properties of metal oxides.*

(iii) *Oxidation state of the surface.*

The control of surface coordination environment can be done by the choice of crystal plane exposition and by the preparation methods employed; however, specification of redox properties is mainly due to the type of oxide. Many oxide catalysts correspond to more or less complex transition metal oxides containing cations of available oxidation state which introduce redox properties in addition to acid-base properties. The acid-base properties of the oxides are usually interrelated to their redox behavior. In particular, the redox behavior of the metal oxide being used and the effect of various additives on its redox properties are the principal factors for the formulation of a catalyst for oxidation and related reactions (Fierro, 2005).

2.1.2.5 Magnetic Properties

Inorganic solids that have magnetic effects other than diamagnetism (a property of all substances), are characterized by the presence of unpaired electrons, usually located on metal cations. Just like electronic properties, the magnetic properties of three dimensional solids result from the interaction of metal centers. Magnetic behavior is thus restricted to the compounds having transition metals and lanthanides due to the presence of unpaired d and f electrons, respectively. In a discrete molecule in solution, the unpaired electrons are totally independent and are randomly oriented. The metal oxides show a variety of phenomena, such as magnetism, dielectricity, superconductivity etc., which are remarkably sensitive to their chemical compositions, crystal structures, carrier concentrations and the applied external field. Long time ago, the study of magnetic properties in metal oxides was done for fundamental aspects as well as applications (Adler, 1968; Tsuda *et al.*, 2013). Magnetic oxides, especially ferrites e.g., $MgFe_2O_4$, are new materials which are used in transformer cores, magnetic recording and information storage devices, etc. After the discovery of high temperature super-conductors (HTSC) cupperates, metal oxides has been studied from the modern point of view and the most

attractive compound after HTSC is the manganites with perovskite structure ($R_{1-x}A_xMnO_3$), whose study started as early as the 1950s (Jonker *et al.*, 1950).

2.1.2.6 Other Properties

In addition to the properties discussed earlier, metal oxides exhibit distinctive chemical, mechanical, catalytic and adsorption properties. Metal oxide nanoparticles have been extensively employed for industrial applications in the field of catalysis as active compositions or as supports materials. Metal oxides possess photocatalytic abilities which can be exploited to solve the present-day energy crises. In 1972, Fujishima and Honda first reported the photocatalytic splitting of water using TiO_2, which was the first photocatalyst used for water splitting and the commencement of a new field of modern heterogeneous photocatalysis (Fujishima *et al.*, 1972; Ni *et al.*, 2007). Currently, metal oxide nanoparticles, owing to large surface to volume ratio and enhanced surface binding properties have been employed as adsorbent to remove environmental pollutants. Metal oxide nanoparticles exhibit stability towards radioactive radiations, thermal and mechanical changes and are exploited for the irreversible, selective and efficient removal of large amounts of pollutants from contaminated water. Thus, metal oxide in nanoscale have demonstrated unique and distinctive properties and have been applied extensively in the field of chemical, nuclear-energy, pharmaceutical, food, bioengineering, dairy, water treatment and electronic industries.

2.2 Cobalt Oxide

Cobalt oxide (Co_3O_4), a magnetic p-type semiconductor, is an important class of inorganic metal oxide which belongs to normal spinel structure based on a cubic close packing array of oxide ions. Spinel cobalt oxide (Co_3O_4) nanomaterials have been widely explored recently, as they possess facile synthetic methodologies, excellent catalytic properties and diverse morphologies (Jiao *et al.*, 2010). Thus, Co_3O_4 appears as a

promising candidate for various applications such as fuel cells, lithium ion batteries, photocatalysis, artificial photosynthesis, gas sensors, etc., due to its eclectic abundance and economic cost (Hu *et al.*, 2008; Jiao *et al.*, 2009; Li *et al.*, 2005; Shahid *et al.*, 2014).

Cobalt (II, III) oxide is one of two well characterized cobalt oxides. As shown in scheme 1, cobalt (II, III) oxide is a mixed valence compound, and its formula is sometimes written as $Co^{II}Co^{III}_2O_4$ and sometimes as CoO & Co_2O_3. Like Fe_3O_4, Co_3O_4 has a spinel structure. The Co^{2+} occupies the tetragonal 8(a) sites, while Co^{3+} occupies the octahedral 16(d) sites. The 32(e) sites are occupied by 32 O^{2-} ions. As known, the spinel minerals have the generic formula AB_2O_4, where A is a cation with a +2 charge and B is a cation with +3 charges. The oxygen atoms in a spinel are arranged in a cubic close-packed structure, and the cations A and B occupy some or all of the octahedral and tetrahedral sites in the lattice (Wang *et al.*, 2012).

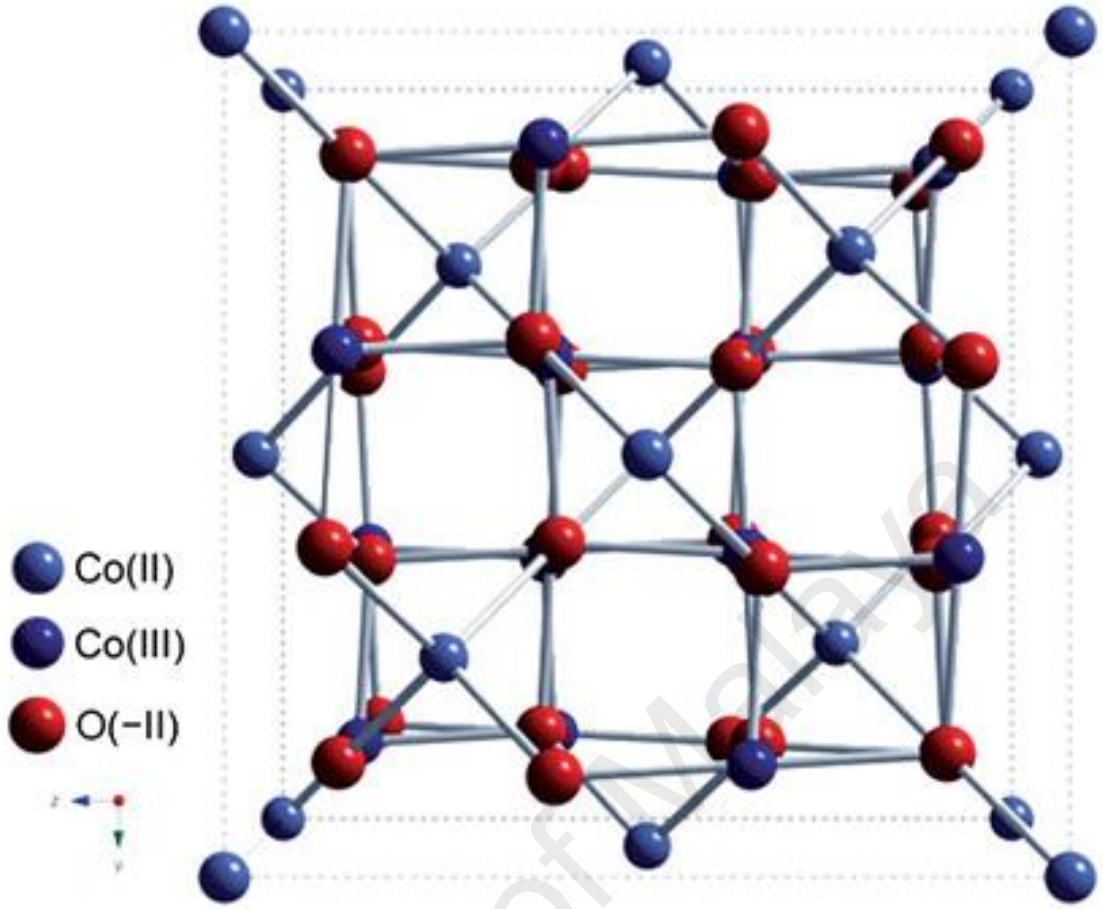

Figure 2.1: The spinel structure of cobalt (II, III) oxide.

The difference in oxygen defects, oxygen holes and oxygen adsorbed in different states of cobalt in Co_3O_4 (a mixed valance material that is formally $Co^{II}\ Co^{III}_2\ O_4$) are thought to be the reason for high activity and selectivity of this metal oxide catalysts (Sharifi *et al.*, 2013).

The Co_3O_4 adopts the normal spinel structure, with Co^{2+} ions in tetrahedral interstices and Co^{3+} ions in the octahedral interstices of the cubic close-packed lattice of oxide anions (Greenwood *et al.*, 1997).

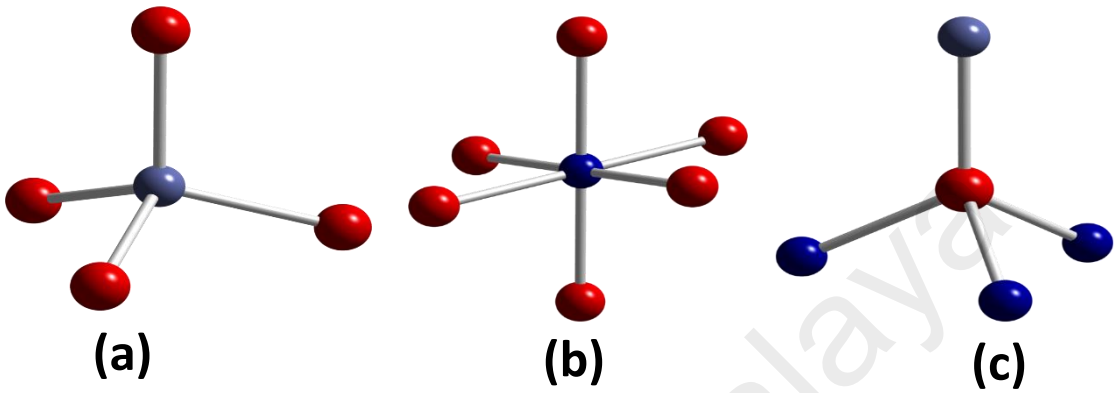

Figure 2.2: Co_3O_4 normal spinel structure coordination geometry (a) tetrahedral coordination geometry Co(II) (b) distorted octahedral coordination geometry Co(III) and (c) distorted tetrahedral coordination geometry of O.

Co_3O_4 is an important form among the various cobalt oxides based on its distinctive structural features and properties (Shi *et al.*, 2012). It has been demonstrated that these nanostructured transition metal oxides have even more attractive applications such as heterogeneous catalysts, gas sensors, lithium ion batteries, electrochromic devices, solar energy absorbers, ceramic pigments and optical devices, etc. (Ando *et al.*, 2004; Chou *et al.*, 2008; Li *et al.*, 2005; Lou *et al.*, 2008; Makhlouf, 2002; Rahman *et al.*, 2012; Wu *et al.*, 2003). Further details and synthesis procedures of cobalt oxide is explained briefly in chapter 3, 4, 5 and 6.

2.3 Graphene Oxide and Graphene

2.3.1 Graphene

Graphene a two-dimensional material is one of the allotropes of carbon. It is an isolated single layer in graphite composed of sp^2 hybridized carbon atoms. It is composed of sp^2 hybridized carbon atoms arranged in a *2D* honeycomb crystal lattice having C-C

bond length of about 0.142 nm. The possibility of wrapping graphene into 0D fullerenes, rolling into 1D carbon nanotubes (CNTs) and stacking into 3D graphite makes graphene the central building block for all graphitic materials as can be seen in Figure 2.3. (Geim *et al.*, 2007).

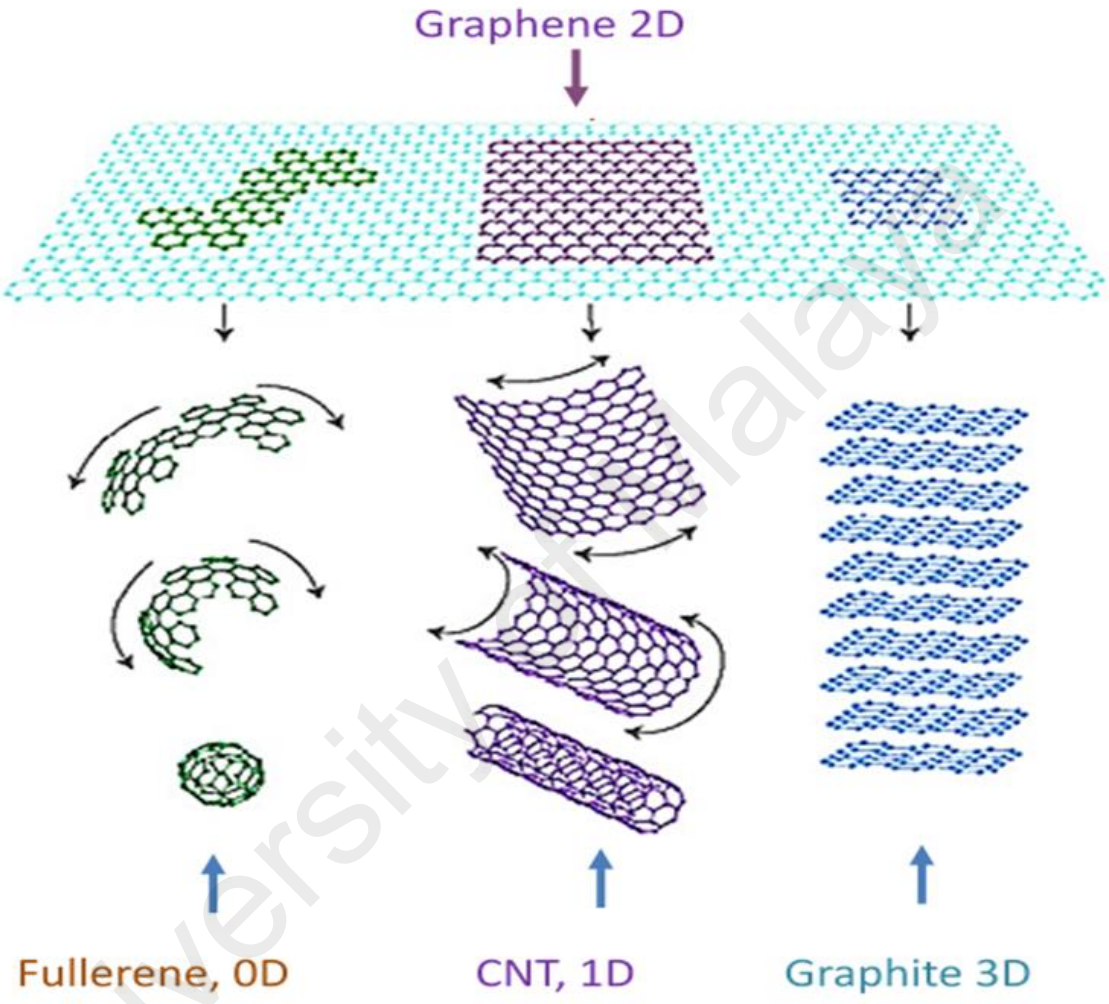

Figure 2.3: Carbon materials as fullerenes (0D), carbon nanotubes (CNTs) (1D) and graphite (3D) can be derived from single layer graphene (*2D*).

Graphene is composed of sp^2 hybridized carbon atoms arranged in a *2D* honeycomb crystal lattice. Three valence electrons of carbon atoms in graphene form bonds (σ) with their nearest neighbors while the fourth electron of each carbon atom is localized in the pi (π) orbitals perpendicular to the planar sheet, forms highly delocalized bonds (π) with others. Graphene is a zero band gap semiconductor and charge carriers in graphene have very small effective mass, so that the carrier mobilities are as high as 200000 $cm^2\ V^{-1}\ s^{-1}$

at a carrier density of 1012 cm^{-2} (Du *et al.*, 2008). Electrons can flow through graphene more easily compared to copper metal. The edges of graphene are also known as an armchair or a zig-zag edge, due to the individual lattice arrangement on the atomic scale (see Figure 6.1(a)).

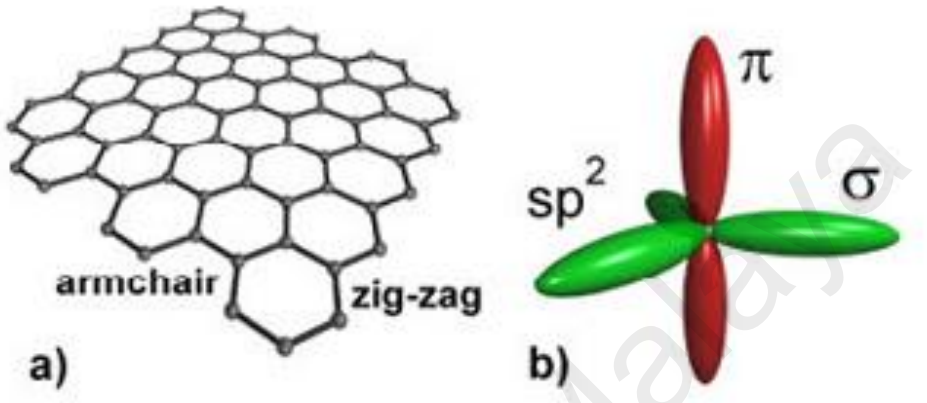

Figure 2.4: Armchair and zig-zag edges in graphene (a), *sp²* hybridization illustrated in graphene (b).

The opacity of a single graphene layer is 2.3 % so its optical transparency is 97.7 % observed in the visible range, but decreases linearly as the number of layers increases The mechanical properties of graphene have been investigated by numerical simulations and experimental measurements using AFM (Van Lier *et al.*, 2000). Graphene is one of the strongest materials with a mechanical strength higher than diamond and over 300 times greater than a steel film of the same thickness (Lee *et al.*, 2008). Reported values for defect-free graphene are Young's modulus of 1.0 TPa and a fracture strength of 130 GPa that are higher than CNTs (Van Lier *et al.*, 2000). Graphene is flexible and stretchable up to 20 % of its initial length. In addition to these outstanding properties, graphene has a thermal conductance (>5000 W/m K) (Chen *et al.*, 2012) that is also higher than all the other carbon structures and theoretical surface area of 2600 m^2/g (Stankovich *et al.*, 2007).

2.3.2 Graphene Oxide

During the last few years, chemically modified graphene (CMG) has attracted great interest in the perspective of several applications such as sensors, energy related materials, polymer composites, field effect transistors (FET), paper-like materials and biomedical relevance due to the remarkable mechanical, thermal and electrical, properties (Park *et al.*, 2009). Chemically modified graphene oxide has been a favorable route to obtain mass produced CMG platelets. Like graphite, graphite oxide also has a layered structure, but in graphite oxide the carbon planes are highly decorated by oxygen containing functional groups. These functional groups not only make the layers hydrophilic, but they also expand the interlayer distance. With moderate ultrasonication,

these oxidized layers can be exfoliated in water resulting in the exfoliated sheets with one or few carbon layers like graphene.

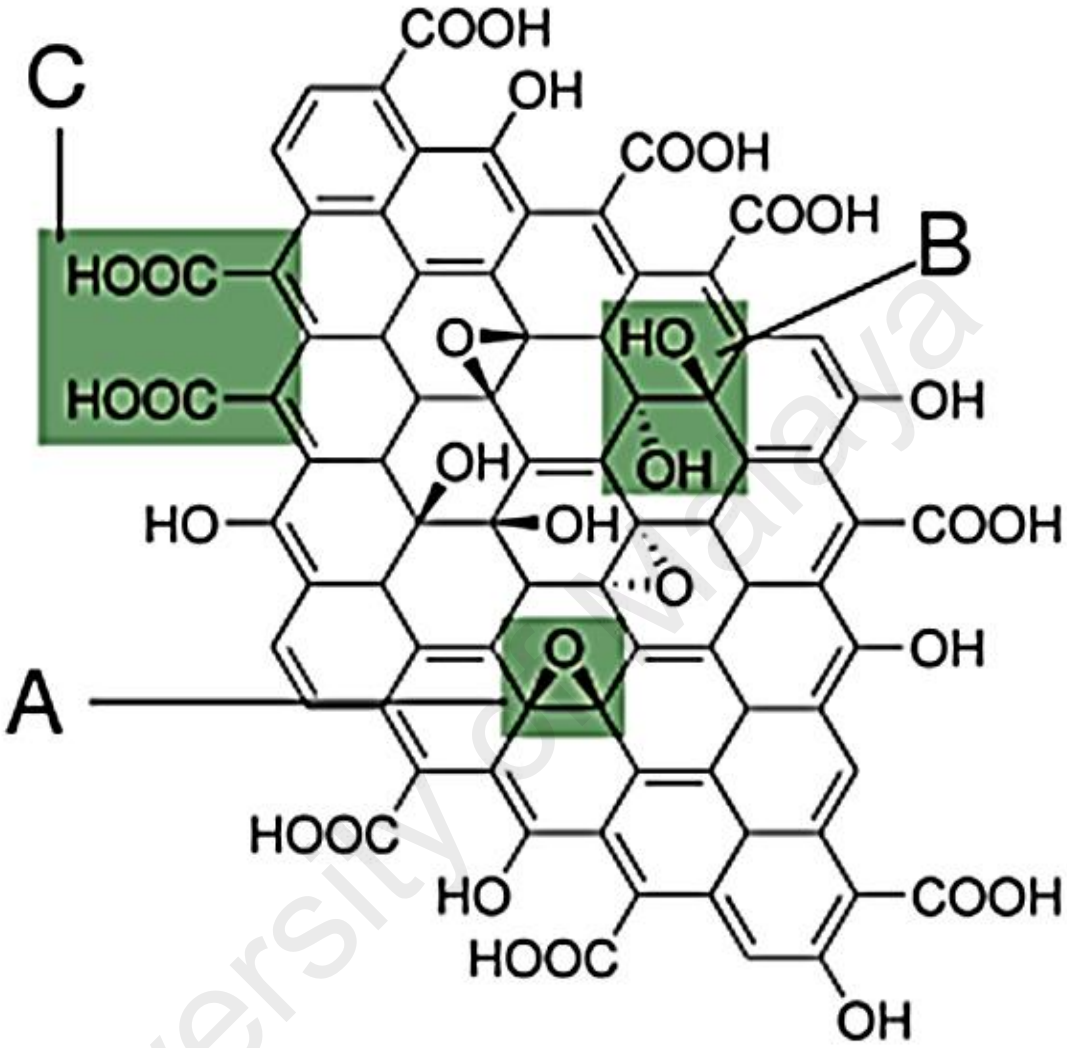

Figure 2.5: Graphene oxide with functional groups. A: Epoxy bridges, B: Hydroxyl groups, C: Pairwise carboxyl groups.

These sheets are also called graphene oxide (GO) (Novoselov *et al.*, 2004). Graphene oxide consists of pseudo two-dimensional carbon layers usually generated from graphite oxide. The primary precursor for synthesizing graphene oxide is graphite flakes which are first oxidized to graphite oxide (Jang *et al.*, 2009). Graphene oxide contains reactive oxygen with functional groups such as carboxylic, hydroxyl and epoxy groups which render it the best precursor in the above-mentioned applications. The epoxy and hydroxyl groups are attached on the GO basal plane, while the carboxylic groups are

present on the edges of graphene oxide. However, due to these functional groups, GO is strongly hydrophilic in nature and disperse easily in water and intercalation of water molecules readily occur between the GO sheets. Depending upon the relative humidity within the stacked GO sheets, the interlayer spacing between GO sheets varies significantly from 0.6 to 1.2 nm (Buchsteiner *et al.*, 2006). Consequently, the interaction between GO sheets is weakened, while the inter-sheet spacing is increased which in turn enables the exfoliation of GO sheets. Mechanical stirring, thermal shock, ultra-sonication in water, or polar solvents are used to exfoliate GO into two dimensional individual nanosheets (Hu *et al.*, 2010). However, many studies claimed that too much ultrasonication could decrease the lateral dimension of the GO sheets. The resulting individual GO sheets are mostly single or few layer sheets that disperse readily in water to make a stable colloidal GO suspension. The GO suspension stability originates from the negative electrostatic repulsion due to the ionization of phenolic hydroxyl groups and carboxylic groups (Li *et al.*, 2008). Because of the introduction of oxygen functional groups on the carbon basal planes, the thickness of single-layer GO sheets has been reported approximately between 1–1.4 nm. In other words, the individual GO sheet thickness is approximately three times greater than an ideal single graphene layer (de Moraes *et al.*, 2015). Indeed, the graphite oxide exfoliation into individual GO sheet can also occur in polar organic solvents such as N-methylpyrolidine (NMP), ethylene glycol (EG) and N, N-dimethylformamide (DMF). It forms a non-aqueous colloidal suspension that is analogous to aqueous GO colloidal suspension (Paredes *et al.*, 2008). Generally, the GO sheet concentration, dispersed in water, is up to 3 mg/ml. The aqueous GO colloidal suspension offers an appropriate setting for an electrochemical method of converting GO into electrochemically reduced graphene oxide (ERGO). However, the properties of ERGO are different from pristine graphene because of various residual oxygen containing functional groups on the carbon basal plane (Viinikanoja *et al.*, 2012).

2.3.3 Synthesis of Graphene Oxide

The oxidation of graphite is carried out by mixing graphite flakes into H_2SO_4:H_3PO_4 (320:80 mL) and $KMnO_4$ (18 g) with continuous stirring. After the slow addition of all materials, the one-pot mixture was left stirring for 3 days to allow the oxidation of graphite. The color of the mixture changed from dark purplish green to dark brown. Later, H_2O_2 solution was added to stop the oxidation process in the presence of ice to control the temperature, and the color of the mixture changed to bright yellow, indicating a high oxidation level of the graphite. The graphite oxide product was washed three times with 1 M of HCl aqueous solution and repeatedly with deionized water until a pH of 4–5 was achieved. The washing process was carried out using simple decantation of supernatant via a centrifugation technique with a centrifugation force of 11,500 g. During the washing process with deionized water, the graphite oxide experienced exfoliation, which resulted in the thickening of the graphene solution, forming a GO gel. The synthesis of graphene oxide can be summarized into three steps:

1. In first step, the graphite flakes are treated with strong acids and a strong oxidizing agent i.e. $KMnO_4$, the product obtained after the treatment is named as graphite oxide since it has oxygen containing hydroxyl and epoxide groups across the basal planes of graphite oxide and carbonyl groups situated at the edges of lattice.
2. In the second step, the oxidation will be stopped by H_2O_2 and ice, and the washing process will be carried out to remove the acids and to raise the pH of graphite oxide, i.e. the washing process will also contribute in the exfoliation of graphite oxide.
3. Lastly, the sonication of the washed product will be carried out to exfoliate the graphite oxide to graphene oxide.

   The following figure shows the synthesis process of GO.

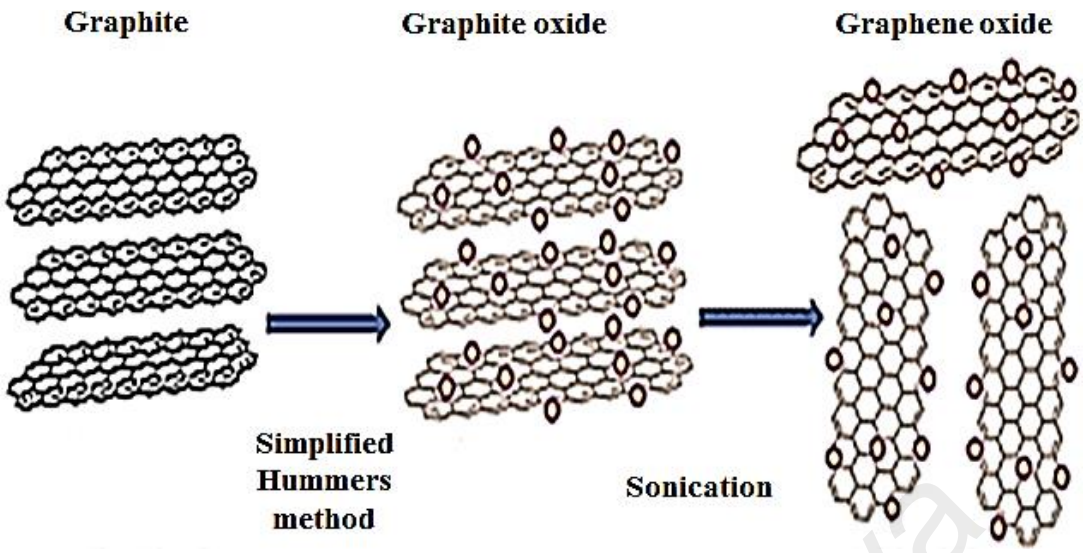

Figure 2.6: Schematic representation for synthesis of GO using Simplified Hummers' method.

The Hummer's method of preparation of graphene was modified by many researchers and named as the "Modified Hummers method", "Improved Hummers method", and "simplified Hummers method" etc. Or the typical method for the synthesis of graphene is also known as the "simplified Hummers method" by our group (Huang *et al.*, 2011).

2.4 Metal Nanoparticles

Metal nanoparticles such as gold (Au), silver (Ag), platinum (Pt), palladium (Pd), copper (Cu), zinc (Zn) etc, have attracted much attention because of their extraordinary properties in different fields of optics (Augustine *et al.*, 2014), optoelectronics (Borsella *et al.*, 1999; Conoci *et al.*, 2006), catalysis (Lesiak *et al.*, 2014; Li *et al.*, 2014), solar cell (Hai *et al.*, 2013; Kang *et al.*, 2010) and sensors (Li *et al.*, 2014). The unique chemical and physical properties of metal nanoparticles make them potentially useful for designing new and improved sensing devices, especially electrochemical sensors. Their excellent electrocatalytic properties and high load capacity for biomolecules have given advantages for metal nanoparticles to be employed as electrochemical signal enhancer in sensor application. With regard to this, silver nanoparticles (AgNPs) have been extensively

investigated as an effective electrocatalyst for electrochemical sensor applications (Yusoff *et al.*, 2017). AgNPs continue to gather enormous attention because they require low production cost, are environmentally friendly, have low toxicity and good biocompatibility. Moreover, AgNPs possesses advantages of excellent catalytic activity, high conductivity and high surface energy, which makes them a promising catalyst material. Furthermore, the high surface to volume ratio allows the exposition of large fraction of metal atoms to the reactant molecules and is very much desirable for sensor applications (Rastogi *et al.*, 2014). Besides that, they are also the best conductors among all the noble metals (Jiang *et al.*, 2013). Due to these properties, AgNPs may facilitate more efficient electron transfer than the other noble metal nanoparticles. Besides AgNPs, gold nanoparticles (AuNPs) have recently drawn increasing attention from many researchers in the field of sensors (Yusoff *et al.*, 2017) due to their novel chemical, optical and physical properties such as high effective surface to volume ratio, excellent electrical and heat conductivity, and strong absorption in the visible and near infrared wavelength region (380 to 750 nm). Among the important physical properties of AuNPs are the surface plasmon resonance (SPR) and the ability to quench fluorescence (Yeh *et al.*, 2012). Besides that, they have excellent biocompatibility and low toxicity which are suitable for biotechnology applications (Khlebtsov *et al.*, 2011). AuNPs also exhibit high chemical stability and inertness under physiological conditions as well as excellent electrocatalytic properties. All these properties make AuNPs an attractive material for electrochemical and biological devices. More interestingly, the properties of AuNPs can be controlled by tuning the shape and size (Jain *et al.*, 2006). Because of its smaller size, Au could provide high active surface area, thus, improve the electron transfer process. This will lead to the enhancement in sensitivity and signal to noise ratio, therefore improves the analytical performance. Another noble metal that has the potential of a catalyst in electrochemical sensors is palladium nanoparticles (PdNPs) (Liu *et al.*, 2016).

PdNPs have attracted extensive attention because of their good chemical and physical properties, such as wear and corrosion resistance, as well as good stability. Their high specific surface area could increase the mass transport and enhance the electron transfer kinetics, thus improves the electrocatalytic activity. PtNPs have been used for electrochemical sensor application in composite with graphene and metal oxides, due to their potential electrical communication, resulting in an efficient electron transfer process at the modified electrode. The Pt nanoparticles also provide a larger surface area for the effective interaction of target molecules and thereby improves the electron-transfer kinetics and the electrocatalytic performance (Shahid *et al.*, 2015).

2.5 Cobalt Oxide Based Nanocomposites

Nanocomposites are material composites where at least one of the phases shows dimensions in the nanoscale range (1 nm = 10^{-9} m). Nanocomposite materials have emerged as suitable alternatives to overcome limitations of microcomposites and monolithic, while posing preparation challenges related to the control of elemental composition and stoichiometry in the nanocluster phase. They are the advanced materials of the 21st century due to the unique design and property combinations that are not found in conventional composites. The general understanding of these properties is yet to be reached, although the first inference about them was reported as early as 1992.

2.5.1 Synthesis of Cobalt Oxide and its Composites with Graphene Oxide

Co_3O_4 nanoparticles and Co_3O_4 based nanocomposite can be synthesized through many routes such as mechanical, sonication, electrochemical, chemical, hydrothermal/solvothermal methods of synthesis and so on.

2.5.1.1 Hydrothermal Method

Co_3O_4 nanoparticles and its nanocomposite have been synthesized with graphene, carbon nanotubes, metals and polymers etc. by hydrothermal routes. The hydrothermal

synthesis is generally defined as crystal synthesis or growth under high temperature and water pressure conditions from substances which are insoluble in normal temperature and pressure (<100 °C, <1 atm). Since the ionic product (K_w) has a maximum value around 250–300 °C, the hydrothermal synthesis is usually carried out below 300 °C. The critical temperature and water pressure are 374 °C and 22.1 MPa, respectively. The solvent properties for many compounds, such as dielectric constant and solubility, change dramatically under supercritical conditions. The dielectric constant of water is 78 at room temperature where polar inorganic salts can be dissolved in water. The dielectric constant of water decreases with increasing temperature and decreasing pressure. When the dielectric constant is below 10 under supercritical conditions, the contribution of the dielectric constant to the reaction rates increases based on the electrostatic theory. Thus, supercritical water gives a favorable reaction medium for particle formation, owing to the enhancement of the reaction rate and large supersaturation, based on the nucleation theory, due to the lower solubility. The formation mechanism of metal oxide nanoparticles from metal nitrate solution is as follows: First, the hydrated metal ions are hydrolyzed to metal hydroxide. Then, the metal hydroxides precipitate as metal oxides through the dehydration step.

$$M(NO_3)_2 + xH_2O = M(OH)_x + xHNO_3$$

$$M(OH)_x = MO_{x/2} + \frac{x}{2}H_2O$$

Hydrolysis is regarded as an electrostatic reaction between metal ions and hydroxyl ions.

2.5.2 Application of Cobalt Oxide Based Nanocomposite

2.5.2.1 Electrochemical Detection/Sensing of Target Molecules

Electrochemical techniques have been used to measure the concentration of biomolecules due to the direct transformation of electrochemical information produced

by biochemical mechanism into an analytically useful signal. Electrochemical biosensors have advantages such as high sensitivity and selectivity towards the electroactive target molecules, rapid and accurate response and most importantly it is portable and inexpensive compared to another existing biosensor.

Besides that, it also offers advantages of wide linear response range, good stability and reproducibility. There are two basic components of an electrochemical sensor which works together as a working or sensing electrode, that are a chemical recognition system and physicochemical transducer. Other than the working electrode (WE), the reference and counter electrodes are also required in this sensor and are enclosed in the sensor housing in contact with a liquid electrolyte and biomolecules. As a biosensor, the recognition layers must interact with the target biomolecules and the physicochemical transducer will translate the bio-recognition event into a useful electrical signal which can be detected by electrochemical workstation. Amperometry, cyclic voltammetry (CV) and potentiometry are some of the examples of electrical signal resulting from the transduction of a biological signal. One of the most important components in electrochemical sensing technique is the WE because it is the place where all the electrochemical oxidation and reduction occur. There are various types of WE that have been commercialized such as platinum (Pt), gold (Au), mercury (Hg) and carbon electrode. Even though Pt electrode demonstrates good electrochemical inertness, the high cost for production and contamination from the presence of small amounts of water or acid in the electrolyte limits the application. The catalytic reduction of protons to form hydrogen gas (hydrogen evolution) at low negative overpotential obscures any useful analytical signal.

Another metal electrode that behaves almost like Pt electrode is the Au electrode. The Au electrode provides good electron transfer kinetics and a wide anodic potential

range; however, it exhibits weakness in the positive potential range due to the oxidation of the surface. The mercury electrode is another type of WE that has been used in electrochemical sensing technique due to its high hydrogen overvoltage which can extend the cathodic potential window. Besides that, it also possesses highly reproducible, renewable and smooth surface, which is very beneficial in electrochemical analysis. The most common form of mercury electrode is the dropping mercury electrode, hanging mercury drop electrode and mercury film electrode. Nevertheless, the toxicity and limited anodic range of mercury limits the applications. Among the different types of electrodes, the carbon electrode such as carbon paste electrode (CPE) and glassy carbon (GC) electrode has been commonly used as WE, due to the wider negative and anodic potential range compared to other electrodes. Moreover, carbon electrodes also have a low background current, rich surface chemistry as well as comparative chemical inertness. Therefore, researchers commonly utilize the carbon electrode as the WE in electrochemical sensing.

Razmi et al. reported the amperometric detection of acetaminophen by an electrochemical sensor based on cobalt oxide nanoparticles. They reported the suitability of a carbon ceramic electrode for the uniform formation of cobalt oxide nanoparticles with an average size of approximately 70 nm by a simple and inexpensive CV method. They demonstrated that the electrode exhibited good electrocatalytic activity toward the oxidation of acetaminophen in an alkaline medium because of the good stability, short response time, low detection limit, high sensitivity and relatively low operational potential (Razmi *et al.*, 2010). Batsile et al. reported the catalytic activity of mesoporous cobalt oxides with controlled porosity and crystallite size evaluation using the reduction of 4-nitrophenol. They claimed that mesoporous cobalt oxide can be a cost effective catalyst for the reduction of 4-nitrophenol and also for other environmentally hazardous phenolic organic compounds (Mogudi *et al.*, 2016). Dinesh et al. reported an *in-situ*

electrochemical synthesis of reduced graphene oxide-cobalt oxide nanocomposite modified electrode for the selective sensing of depression biomarker in the presence of AA and DA. They demonstrated that for the first time, a new route of synthesis i.e. *in-situ* electrochemical synthesis of RGO/Co_3O_4 nanocomposite without any binder, organic solvent, strong reducing agents and bulk deposition methods. The synthesized nanocomposite is utilized for the selective detection of serotonin in the presence of other coexisting species like AA and DA with a very low detection limit and remarkable current sensitivity in physiological conditions (Dinesh *et al.*, 2017). Thi et al. synthesized cobalt oxide/reduced graphene oxide composites for electrochemical capacitor and sensor applications. In their report, reduced graphene oxide sheets decorated with cobalt oxide nanoparticles (Co_3O_4/rGO) were produced using a hydrothermal method without surfactants and used for non-enzymatic H_2O_2 sensing. The developed sensor showed good sensing ability toward the detection of H_2O_2 with limit of detection (LOD) = 0.62 mM and the sensitivity was 28,500 $mAmM^{-1}$ cm^{-2} (Nguyen *et al.*, 2016). Other than this, other material based on metal, metal oxides and graphene have been prepared for a sensitive and selective determination of water contaminants and biological molecules. Numerous reports are available on Co_3O_4 based nanocomposites for the detection of water contaminants as well as biological molecules due to the unique properties of Co_3O_4 as discussed earlier in this Chapter and Chapter 1.

CHAPTER 3: MORPHOLOGY DEPENDENT ELECTROCATALYTIC PROPERTIES OF HYDROTHERMALLY SYNTHESIZED COBALT OXIDE NANOSTRUCTURES[1]

3.1 Introduction

The introduction of nanoscience and nanotechnology and the ability to synthesize various nanomaterials have breathed new life into catalysis science. In recent years, nanostructured metal oxides have attracted much attention because of their applications in electronics, optics, magnetic storage devices, and electrochemical sensors for environmental analyses (Poizot *et al.*, 2000; Rahman *et al.*, 2009; Zhang *et al.*, 2008). Nanostructured of metal oxides such as TiO_2, Fe_3O_4, NiO, MnO_2 and Co_3O_4 have been used in various applications such as lithium ion batteries, supercapacitors, solar cells, fuel cells and catalysis to overcome the high cost of noble metals (Huang *et al.*, 2009; Liu, 2008; Zhai *et al.*, 2009). Recently, electrodes modified with metal oxide nanostructures have been thoroughly investigated for the electrochemical determination of several biologically important analytes because of their interesting electrocatalytic properties (Asif *et al.*, 2011; Jiang *et al.*, 2014). Among the various metal oxides, the Co_3O_4 nanostructure shows some interesting magnetic, optical and transport properties (Ahmed *et al.*, 2002; Takada *et al.*, 2001), and are considered to be one of the more promising materials for electrochemical applications because of their well-defined electrochemical redox activity, high theoretical capacity (890 mAh g^{-1}), low cost and stable chemical state (Xue *et al.*, 2014).

[1] This chapter is published as: Shahid, M. M., Rameshkumar, P., & Huang, N. M. (2015). Morphology dependent electrocatalytic properties of hydrothermally synthesized cobalt oxide nanostructures. *Ceramics International, 41*(10), 13210-13217.

Further, Co_3O_4 nanoparticles have shown their potential utility in anode materials for rechargeable Li ion batteries (Rahman *et al.*, 2009), electronic devices (Cheng *et al.*, 1998), gas sensors (Li *et al.*, 2005), electrochromic devices (Xia *et al.*, 2010) and high-temperature selective solar-radiation absorbers (Shalini *et al.*, 2001). With the goal of profitable utilization, much effort has been exhausted to develop synthetic techniques for growing Co_3O_4 nanostructures, including hydrothermal (Rahman *et al.*, 2009), pulsed laser deposition (Ahmed *et al.*, 2002), chemical vapour deposition (Cheng *et al.*, 1998) and radiolysis (Alrehaily *et al.*, 2013). Generally, hydrothermal synthesis is highly preferred for the synthesis of metal oxide nanostructures because of its simplicity. An appropriate amount of powdered reagents and water are placed in a Teflon-lined autoclave and heated without stirring from moderate to high temperatures and pressures for the desired time. Further, it is possible to predict the optimum reaction conditions using the electrolyte thermodynamics, and the problem of impurities can be overcome by varying the ratios of the precursors in the hydrothermal synthesis (Lencka *et al.*, 2000). Recently, more attention has been given to controlling the morphology of the metal oxide nanostructures in the synthesis, as the novel functionalities of nanostructures depend not only on their compositions but also on their shapes and sizes.

Phenol-based nitro-compounds are extensively used in the pharmaceutical and chemical industries and are considered to be toxicants, which cause damage to organisms and plants even at a very low concentration and can create various problems in humans (Madhu *et al.*, 2014; Wang *et al.*, 2012). As an example, 4-nitrophenol (4-NP) is one of the important toxic phenol-based nitro-compounds that can be found in the waste-water released by the chemical and pharmaceutical industries, and it is a common intermediate in the production of analgesics, leather products, dyes and pharmaceuticals. Acute exposure to 4-NP can cause headache, fever, breathing problems and even death at a high level of exposure. It also tends to remain in agricultural crops, vegetables, fruits and water

sources when used as an ingredient in a fertilizer or pesticide (Madhu *et al.*, 2014; Santhiago *et al.*, 2014). Because of its high stability in water, low biodegradation, high toxicity and persistence, 4-NP is on the priority list of the US environment protection agency (EPA) (Liu *et al.*, 2014; Madhu *et al.*, 2014; Tang *et al.*, 2013; Yang *et al.*, 2012). Based on the facts described above, it is vitally important to develop simple and reliable techniques for the detection of trace amounts of 4-NP in environmental water samples. Out of the various available techniques, electrochemical techniques have drawn much attention because of the advantages such as simplicity, excellent selectivity and sensitivity, easy operation with a rapid response, and cost effectiveness (Madhu *et al.*, 2014; Tang *et al.*, 2013). In addition, it is well known that nitro groups can be electrochemically reduced easily in aromatic or heterocyclic compounds, thus permit the sensitive determination of 4-NP through electrochemical methods utilizing a very good electrocatalytic material (Liu *et al.*, 2009; Zeng *et al.*, 2014). Metal oxides such as TiO_2 (Lin *et al.*, 2013; Shaoqing *et al.*, 2010), Fe_3O_4 (Du *et al.*, 2012), NiO (Pan *et al.*, 2012), MnO_2 (Wu *et al.*, 2014), and Co_3O_4 (Pan *et al.*, 2013) were previously exploited for the detection of 4-NP.

In this study, nanostructured Co_3O_4 with different morphologies (nanocubes, nanowires, nanobundles, nanoplates and nanoflowers) were synthesized using the hydrothermal process and their electrochemical properties in the electrochemical reduction of 4-NP were investigated. The nanostructures were characterized by field emission scanning electron microscopy (FESEM), X-ray diffraction (XRD), and Raman spectroscopy. The electrochemical impedance spectroscopy (EIS) measurements showed the lowest charge transfer resistance (R_{ct}) value for Co_3O_4 nanocubes toward the $[Fe(CN)_6]^{3-/4-}$ redox couple among all the modified electrodes. The Co_3O_4 nanocubes modified electrode showed higher electrocatalytic activity toward the electrochemical reduction of 4-NP, and the detection of 4-NP was performed at the same modified

electrode using square wave voltammetry (SWV). A linear relationship was observed between the current response and the concentration (R^2 = 0.997), and LOD was 0.93 µM.

3.2 Experimental Section

3.2.1 Materials

Cobalt acetate ($Co(CH_3COO)_2.4H_2O$) was purchased from Sigma Aldrich. Ethanol (99.8 %) and urea (99 %) were received from Systerm Malaysia. NaOH (99 %), while ammonia (25 %) and 4-NP (> 98 %) were purchased from R & M chemicals. Distilled water was used throughout the experiments unless stated.

3.2.2 Synthesis of Co_3O_4 Nanostructures with Different Morphologies

Co_3O_4 nanostructures with different morphology were synthesized using a simple one-step hydrothermal process with the aid of a Teflon-lined stainless-steel autoclave with a total capacity of 100 mL filled to 75 % with the solution. Co_3O_4 nanocubes were synthesized using the same procedure as previously reported by our group (Shahid *et al.*, 2014). During the synthesis of different morphologies, the cobalt precursor was dissolved in deionized water, and structure-directing agents such as ethanol, ammonia, NaOH and urea were added drop-wise under stirring. After the formation of a homogeneous slurry, it was transferred to the autoclave for the hydrothermal process at different temperatures. The total reaction volume was maintained as 75 mL using distilled water for the synthesis of the Co_3O_4 nanostructures. After the hydrothermal treatment, the solid Co_3O_4 product was collected, washed with DI water and ethanol, and dried in a hot air oven at 60 °C for 24 h to evaporate the water content. The dried solid product was then crushed to obtain a powder form and was further used in the electrochemical experiments. The experimental details of the synthesis of the Co_3O_4 nanostructures with different morphologies are summarized in Table 3.1.

Table 3.1: Experimental parameters for the synthesis of different morphologies of Co_3O_4 nanostructures.

Morphology of Co_3O_4	Cobalt salt (mM)	Temperature (°C)	Reaction time (h)	Structure directing agents
Nanocubes	2	180	12	15 mL ammonia (6 %)
Nanowires	2	150	5	30 mL ethanol (99.9 %) and 3 mmol urea
Nanobundles	2	120	12	2 mmol urea
Nanoplates	2	150	15	13 mL NaOH solution (3.25 mM) with 2 mL ammonia (25 %)
Nanoflowers	2	180	12	30 mL ethanol and 15 mL ammonia (6 %)

3.2.3 Modified Electrode Preparation and Electrochemical Measurements

The GC electrode modified with one of the Co_3O_4 nanostructures was fabricated by drop-casting 5 µL (1 mg/mL) of a homogenous aqueous solution of the Co_3O_4 nanostructure onto the GC electrode (d = 3 mm) surface and allowing it to dry at room temperature (25 °C) for 2 h. The fabricated GC was used as a WE. Prior to the modification, the GC electrode was polished with 0.05 µm alumina slurry and cleaned by potential cycling between + 1 and - 1 V in 0.1 M H_2SO_4 before the experiments. All the electrochemical studies were carried out under a nitrogen atmosphere using a VersaSTAT-3 electrochemical analyzer (Princeton Applied Research, USA) with a conventional three-electrode system. A platinum (Pt) wire and Ag/AgCl were used as the counter and reference electrodes, respectively. Phosphate buffer solution (PBS) (pH 7) was used as the supporting electrolyte for the detection of 4-NP. The square wave voltammograms were recorded by applying a step potential of 4 mV, amplitude of 25 mV, and frequency of 15 Hz. All the potentials were measured with reference to the Ag/AgCl electrode unless otherwise mentioned.

3.2.4 Characterization Techniques

The morphologies of the Co_3O_4 nanostructures were studied using (FESEM) (JEOL JSM-7600 F). A high-resolution transmission electron microscopy (HRTEM) image of the Co_3O_4 nanocubes was collected using the JEOL JEM-2100F instrument operated at 200 kV. The crystalline nature of the nanostructures was analyzed using a Philips X'pert X-ray diffractometer with Cu Kα radiation (λ=1.5418 nm) at a scan rate of 0.02° s^{-1}. Raman spectra were obtained using the Renishaw inVia 2000 system green laser emitting at 514 nm.

3.3 Results and Discussions

3.3.1 Morphological Characterization of Co_3O_4 Nanostructures

Field emission scanning electron microscopic (FESEM) analysis was performed to investigate the Co_3O_4 nanostructures, and the FESEM images are displayed in Figure 3.1. Almost uniform-sized nanocubes were formed while using aqueous ammonia as the structure-directing agent. Ammonia was used for the precipitation of Co^{2+} ions and their oxidation (Dong *et al.*, 2007). The Co_3O_4 nanowires were formed with a length of several hundred nanometers. The formation of some smaller-sized Co_3O_4 nanoparticles was also observed on the nanowires, which may have been due to the initial nucleation of the Co_3O_4 nanoparticles during the stirring process in the presence of urea with ethanol, before treatment in the hydrothermal process. The Co_3O_4 nanobundles were formed in the presence of urea alone as the structure-directing agent. The Co_3O_4 nanoplates were obtained due to the presence of NaOH and ammonia solution under hydrothermal treatment at 120 °C, and the nanoplates were vertically arranged to form a flower-like Co_3O_4 nanostructures in the presence of ethanol and ammonia below 180 °C. This is due to the initial nucleation of the nanoparticle formation during the stirring process, where aggregates of the smaller-sized Co_3O_4 nanoparticles were decorated on the nanoplates

and to form flower-like nanostructures. Figure 3.2 displays the HRTEM images to provide a better understanding of the cubical morphology of the Co_3O_4 nanocubes.

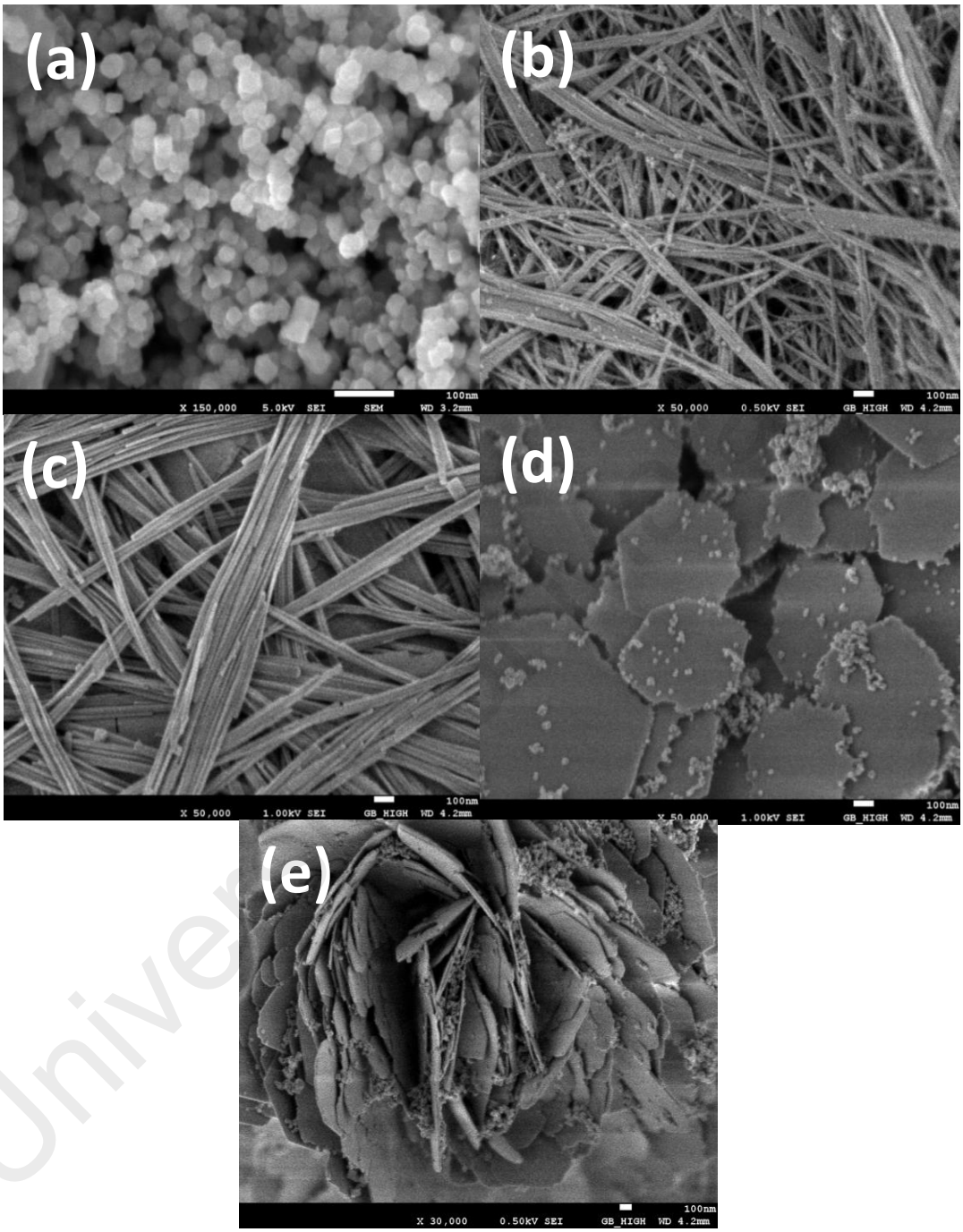

Figure 3.1: FESEM images of different morphologies of Co_3O_4 (a) Nanocubes, (b) Nanowires, (c) Nanobundles, (d) Nanoplates and (e) Nanoflowers.

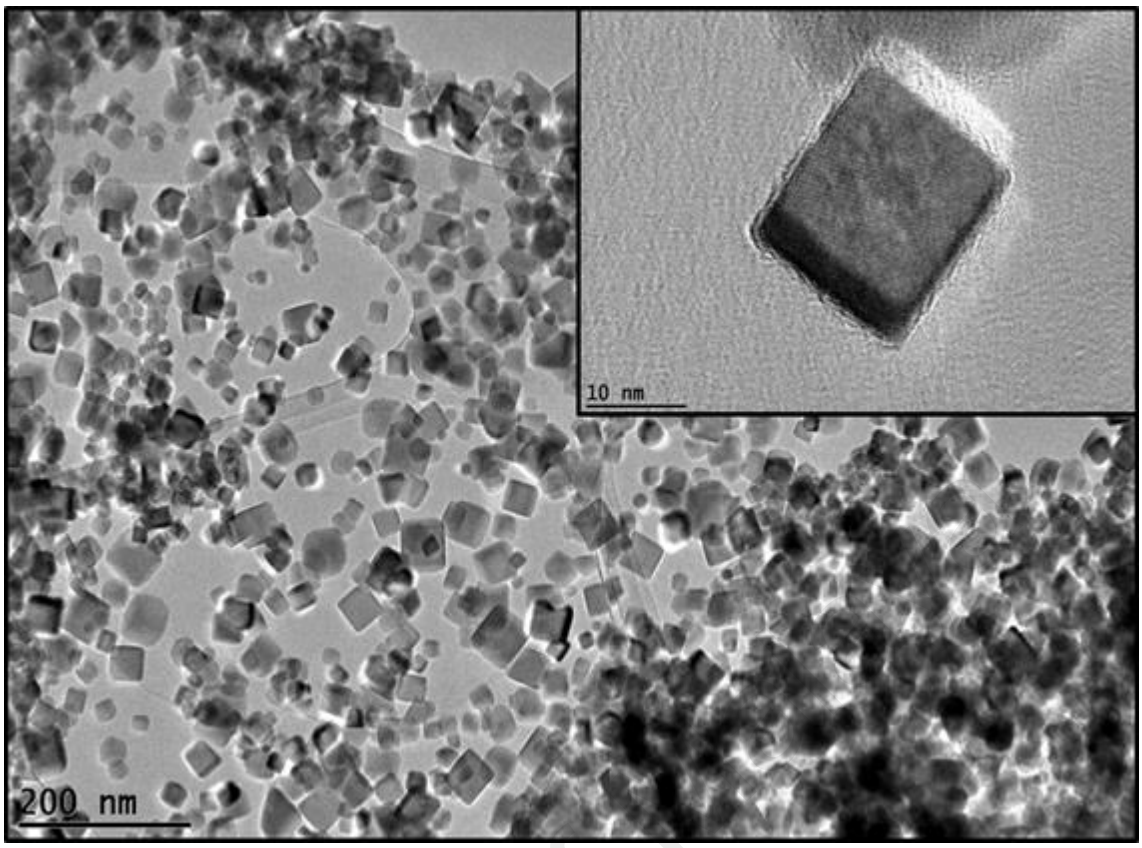

Figure 3.2: TEM image of Co_3O_4 nanocubes. Inset shows the TEM image at higher magnification.

3.3.2 XRD and Raman Analyses of Co_3O_4 Nanostructures

The crystalline nature of the Co_3O_4 nanostructures was studied by recording the XRD patterns, as shown in Figure 3.3. The characteristic diffraction peaks at 31.1°, 37.0°, 44.6°, 55.6°, 59.2°, and 65.1° correspond to the (220), (311), (222), (400), (422), and (511) diffraction planes of the face-centered cubic Co_3O_4 spinel phase, respectively (JCPDS card No. 42-1467) (Yao *et al.*, 2013). All the morphologies showed the well-identified diffraction peaks of Co_3O_4.

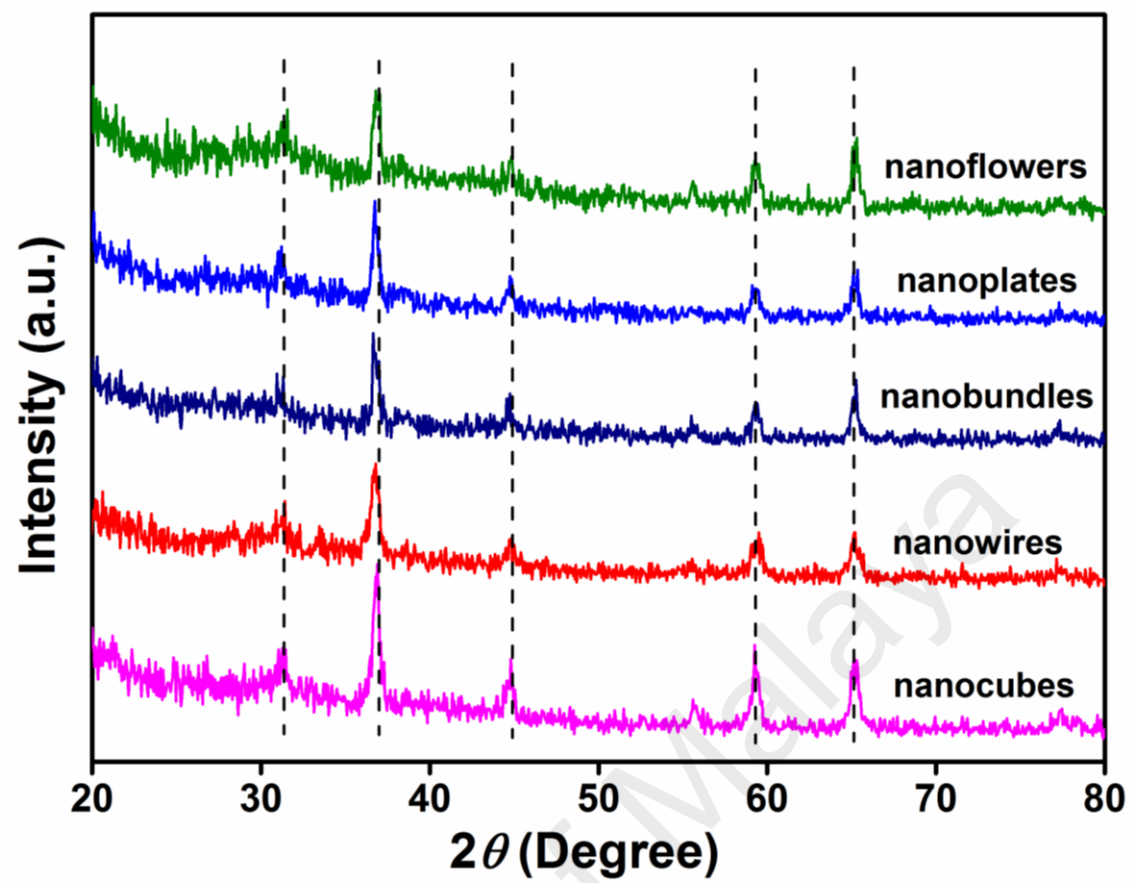

Figure 3.3: XRD patterns of Co_3O_4 nanostructures

The Raman spectra of all the morphologies of the Co_3O_4 structures are shown in Figure 3.4. These show peaks at 192, 476, 516, 612, and 680 cm^{-1}, which correspond to the E_g, F^1_{2m}, F^1_{2g} and A_{1g} modes of Co_3O_4, respectively (Liu *et al.*, 2007). The Raman peak positions of all the synthesized Co_3O_4 structures are almost identical to one another.

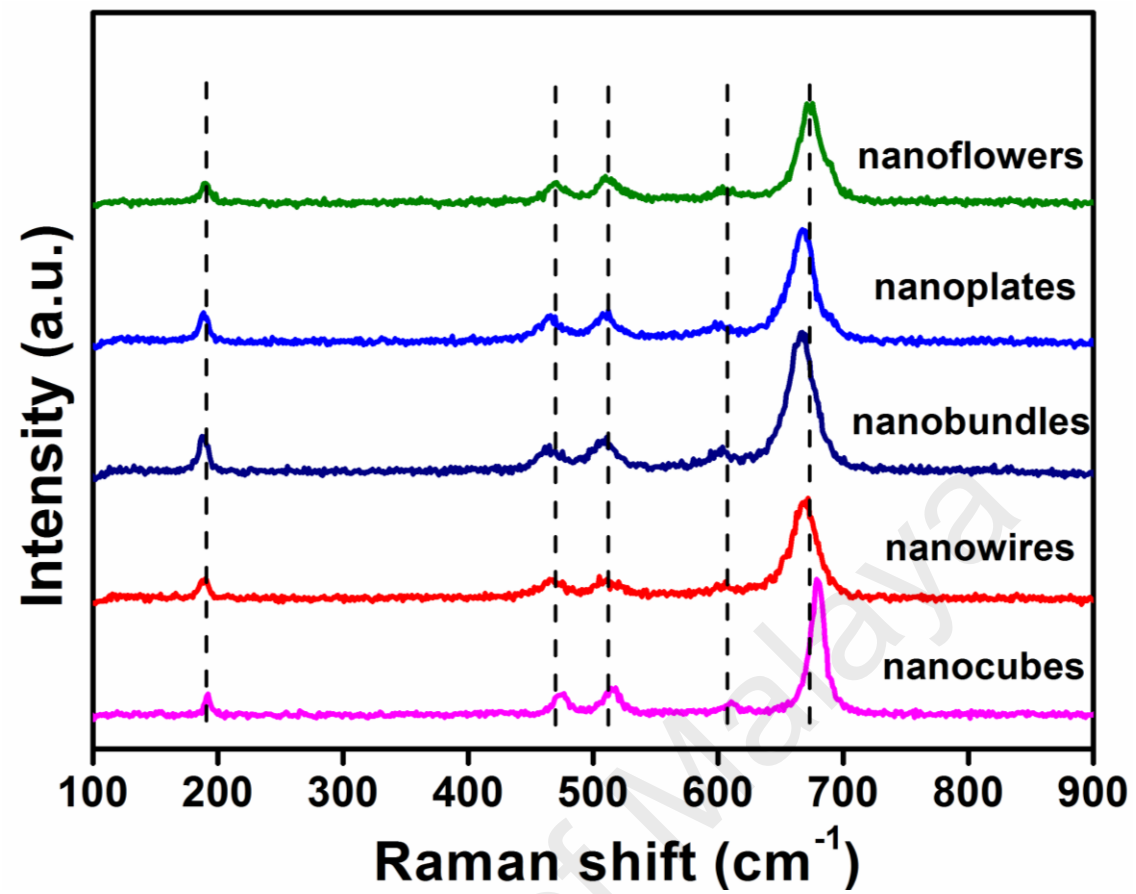

Figure 3.4: Raman spectra of Co_3O_4 nanostructures.

3.3.3 Electrochemical Iimpedance Spectroscopy Analysis

The interfacial properties of the surface-modified electrodes were studied using the EIS (Rubio-Retama *et al.*, 2006). The $[Fe(CN)_6]^{3-/4-}$ couple was used as a redox analyte to study the conducting behaviors of the electrodes modified with the Co_3O_4 nanostructures with different morphologies (Figure 3.5(a & b)). The charge transfer resistance (R_{ct}) values of the modified electrodes using the $[Fe(CN)_6]^{3-/4-}$ redox probe, measured as the diameters of the semicircles in the Nyquist plots, were 3200, 4100, 28000, 300, 1490, and 740 Ω for the bare GC, nanowires, nanobundles, nanocubes, nanoplates and nanoflowers, respectively. The R_{ct} of the Co_3O_4 nanocubes was much smaller than those of the other modified electrodes, which implies faster electron transfer kinetics of the nanocube modified electrode. The Bode-impedance plots of the modified electrodes were also collected between the frequency range of 0.01–10000 Hz (Figure

3.5(c)). The phase peaks that appears between the frequency range of 100–1000 Hz indicates the charge-transfer resistance of the modified electrodes. The less intense peak obtained for the Co_3O_4 nanocubes modified electrode reveals a faster electron transfer process at the modified electrode surface, and the phase angles of all the electrodes were less than 90° at higher frequencies, which suggests that the electrodes did not behave like an ideal capacitor (Matemadombo *et al.*, 2007).

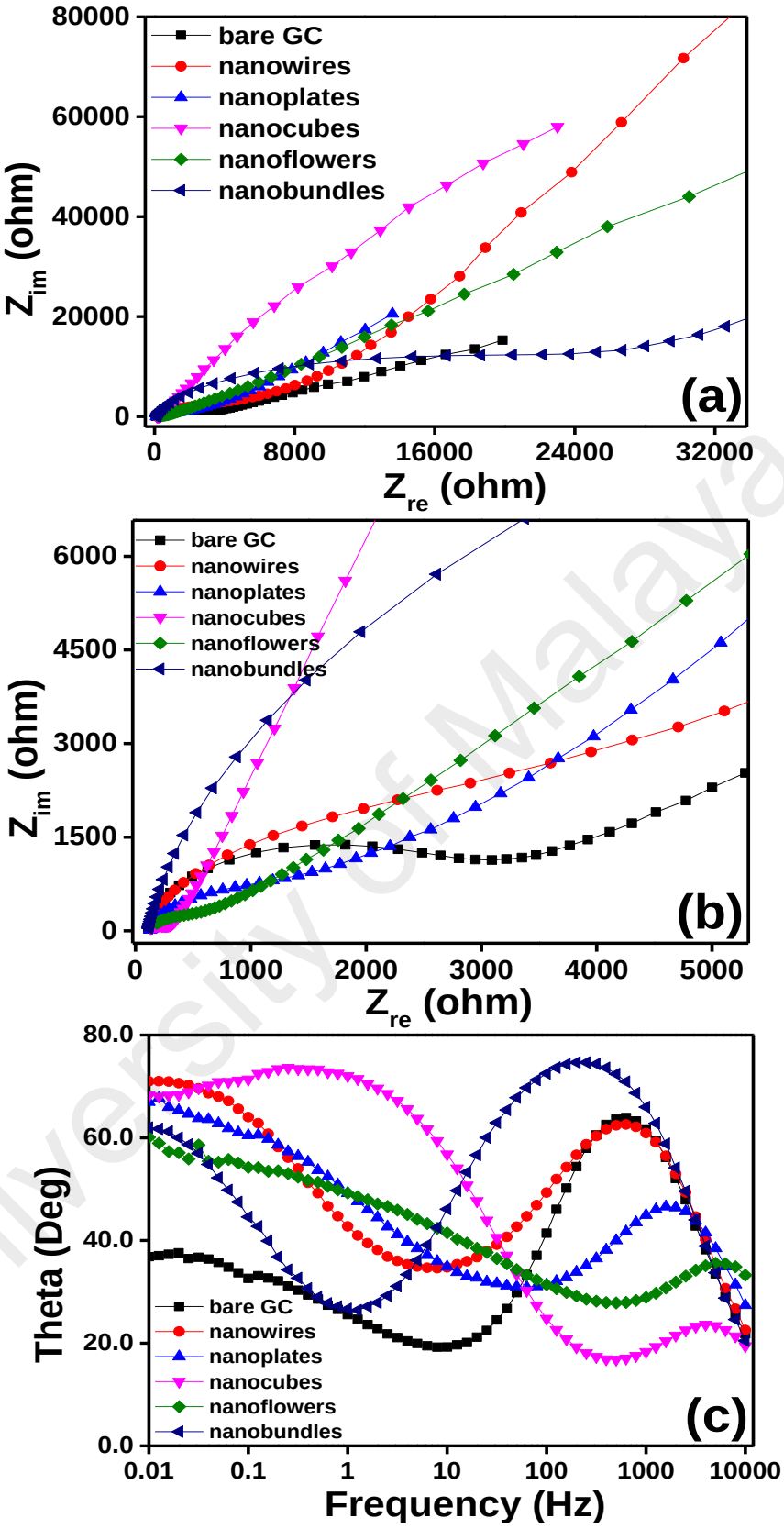

Figure 3.5: Normal and expanded views of Nyquist plots (a & b) and Bode impedance plots (c) obtained for bare GC and GC electrodes modified using Co_3O_4 nanostructures with different morphologies for 1 mM $K_3[Fe(CN)_6]$ in 0.1 M KCl a: bare GC, b: nanowires, c: nanoplates, d: nanocubes, e: nanoflowers and f: nanostrips nanobundles.

3.3.4 Electrocatalytic Reduction of 4-Nitrophenol

The electrocatalytic reduction of 4-NP was chosen as a model system to study the electrocatalytic behaviors of the Co_3O_4 nanostructures modified electrodes with the different morphologies. Irrespective of the morphology, all the Co_3O_4 nanostructures showed the increased catalytic current for the reduction of 4-NP (Figure 3.6). Among the morphologies, Co_3O_4 nanocubes displayed the highest catalytic current (-15 µA) for the reduction of 100 µM 4-NP. The Co_3O_4 nanowires and nanobundles showed smaller catalytic currents of -8.3 and -7.4 µA, respectively, at more negative potentials for the same concentration of 4-NP. The higher catalytic performance of the nanocubes can be attributed to the uniformly formed smaller-sized nanostructures compared to the other morphologies. Notably, the Co_3O_4 nanocube modified electrode did not show any electrochemical feature in the absence of 4-NP (Appendix 1). The Co_3O_4 nanoplates and nanoflowers produced almost the same catalytic responses for the reduction of 4-NP in terms of the peak potential and catalytic current. The bare GC electrode also showed the minimum catalytic current for the reduction of 4-NP in the given potential window.

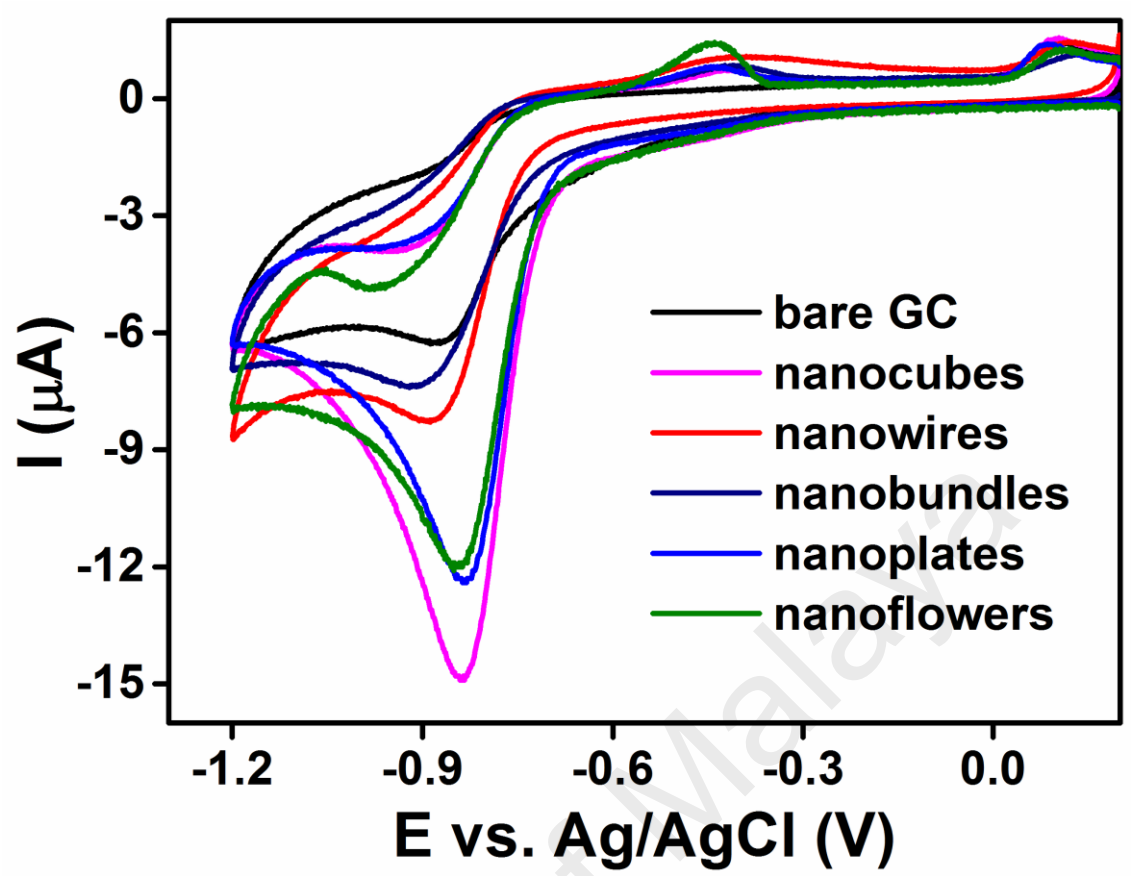

Figure 3.6: Cyclic voltammograms recorded at bare GC and GC electrodes modified using Co_3O_4 nanostructures with different morphologies in presence of 100 µM 4-NP in 0.1 M PBS (pH 7) at scan rate of 50 mVs^{-1}.

Figure 3.7 explains the formation of the various products during cathodic and anodic scans of 4-NP reduction. The observation of a reduction peak for 4-NP at –0.8 V (a) is ascribed to the reduction of a nitro group ($–NO_2$) to hydroxylamine (–NHOH) through a single-step four-electron transfer process (Li *et al.*, 2007; Zhang *et al.*, 2006). It has been reported that the reduction products of the $–NO_2$ group at peak "a" should contain a radical anion and hydroxylamine. The peaks observed at -0.4 V (b) and +0.1 V (c) can be attributed to the oxidized products of the products obtained at peak "a". The oxidation peak at "c" is due to the oxidation of hydroxylamine (–NHOH) to the nitroso group (-NO) *via* a two–electron transfer process (Li *et al.*, 2007; Zhang *et al.*, 2006). This oxidized product (c) is further reduced at +0.02 V during the negative scan at the second cycle (peak "d"). The electrochemical reduction of nitroaromatic compounds has been widely studied using different types of electrode materials (Chen *et al.*, 2012;

Maduraiveeran *et al.*, 2009; Yuan *et al.*, 2014). Generally, the electroreduction of Ar-NO_2 to Ar-NH_2 *via* a six-electron transfer process requires an acidic electrolyte, and the formation of Ar-NHOH is facilitated in a neutral or alkaline medium through a four-electron transfer process (Zhang *et al.*, 2000). The dependence of the peak current and peak potential on the pH variation of PBS for the reduction of 4-NP was studied using the nanocubes modified electrode.

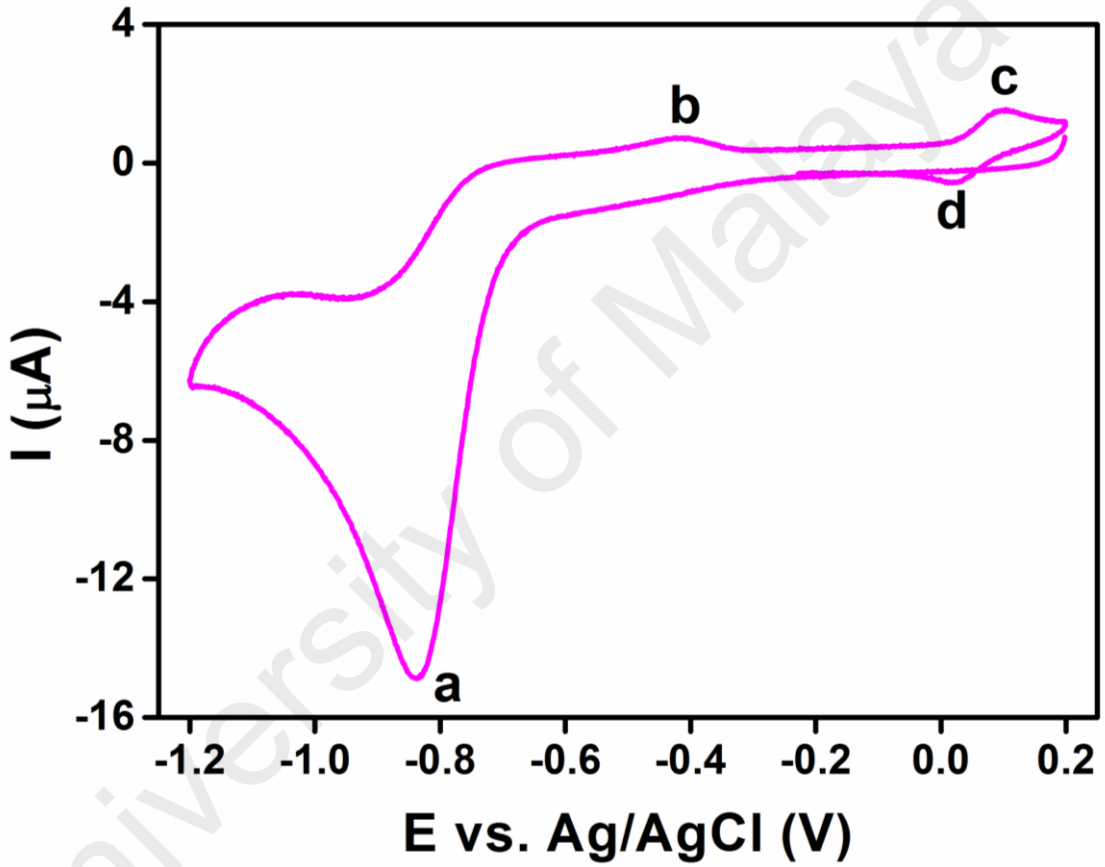

Figure 3.7: Cyclic voltammogram recorded at Co_3O_4 nanocubes modified electrode in presence 100 µM 4-NP in 0.1 M PBS (pH 7) at scan rate of 50 $mV.s^{-1}$.

Figure 3.8(a) displays voltammograms of the 4-NP reduction in 0.1 M PBS at various pH values, where the reduction peak potential is shifted toward more negative value when the pH is increased from 3 to 8. The plot of the reduction peak potential versus pH shows a linear relation (Figure 3.8(b)) with a slope of -54 mV/pH, which suggests that an equal number of protons and electrons are involved in the electrochemical reduction of 4-NP (Xu *et al.*, 2014). Further, the catalytic current observed for the reduction of 4-

NP at pH 7 is higher than those observed at other pH solutions (Figure 3.8(b) (inset)). Since most waste-water has a neutral pH, it is advantageous to perform the catalytic reduction and detection of 4-NP at pH 7. Moreover, adjusting the pH of the PBS to much lower values requires the addition of acid, which may increase the cost of the catalytic process.

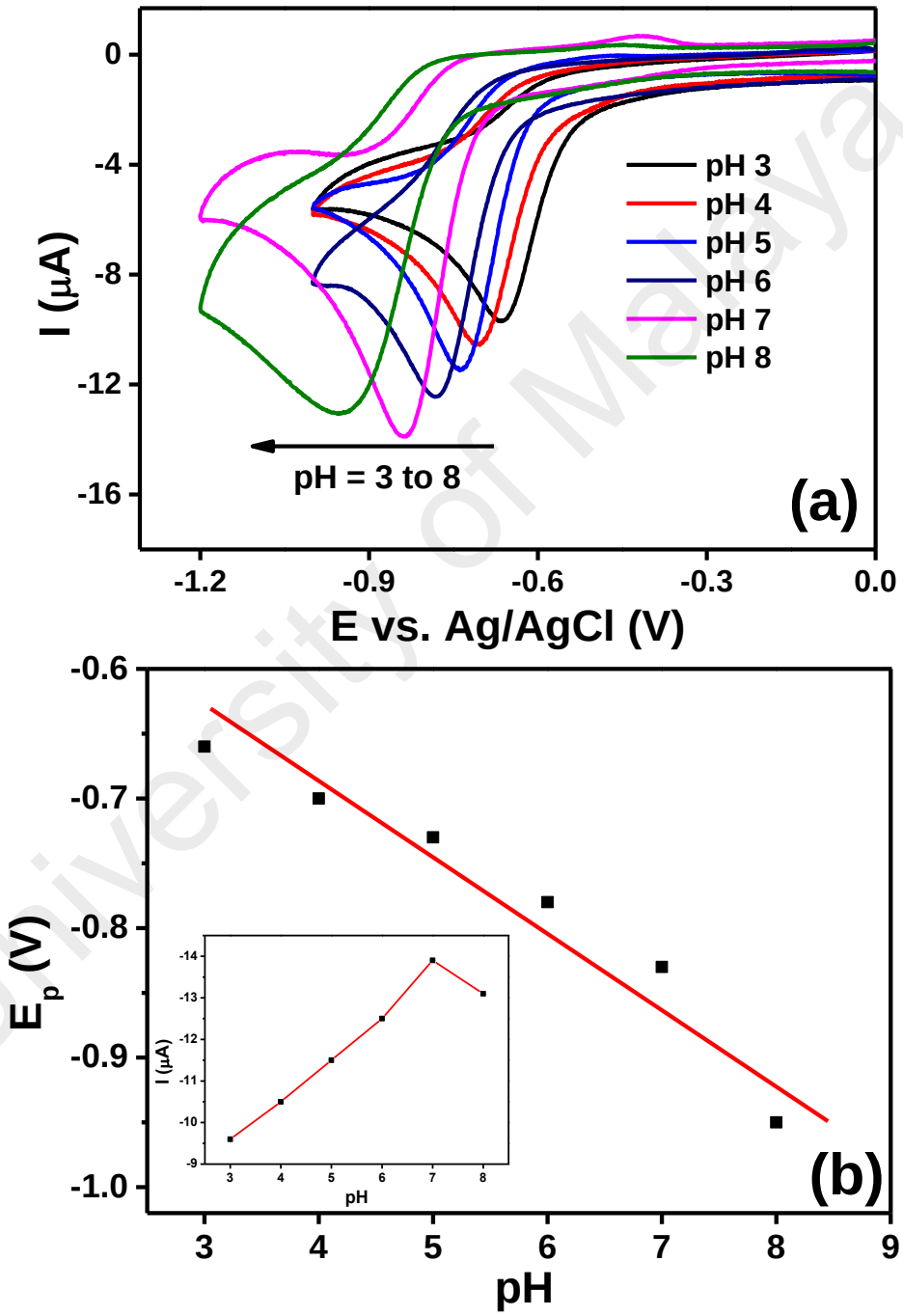

Figure 3.8: (a) Cyclic voltammograms recorded at Co_3O_4 nanocubes modified electrode in presence of 100 µM 4-NP in 0.1 M PBS with different pH levels (pH = 3 to 8) at scan rate of 50 mV s^{-1}. (b) Plot of shift in peak potential versus pH. Inset: Plot of peak current versus pH.

3.3.5 Square Wave Voltammetric Detection of 4-Nitrophenol

The Co_3O_4 nanocubes modified electrode was chosen to detect the lowest detected concentration of 4-NP because of its better performance in catalysis. The square wave voltammetric technique was used to study the sensing ability of the modified electrode and Figure 3.9(a) displays the voltammetric responses observed for successive additions of 4-NP at the nanocubes modified electrode dipped in 0.1 M PBS (pH 7). During the successive additions (both 2 and 5 µM additions), the peak current corresponding to the reduction of 4-NP increased at the potential of – 0.83 mV, and the plot of the peak current difference (I_d) versus the concentration of 4-NP showed a linear relation (R^2=0.997) (Figure 3.9(b)). After some additions of 4-NP, the voltammogram showed the formation of a pre-peak at a less negative potential, due to the strong adsorption of 4-NP at the Co_3O_4 nanocubes modified electrode surface. It is well known that a split in the peak is observed in the square wave voltammograms, due to the adsorption of redox analytes (Rameshkumar *et al.*, 2014). The sensitivity and LOD of the modified electrode were 0.0485±0.00063 µA/µM and 0.93 µM, respectively, for the detection of 4-NP. The voltammetric responses were reproducible for different GC electrodes modified with Co_3O_4 nanocubes and for repeated experiments. The analytical performance of the Co_3O_4 nanocubes modified GC electrode toward the detection of 4-NP was compared with those of different electrode materials (Table 3.2), and a good LOD was attained without employing any polymeric binder material or tedious electrode modification process.

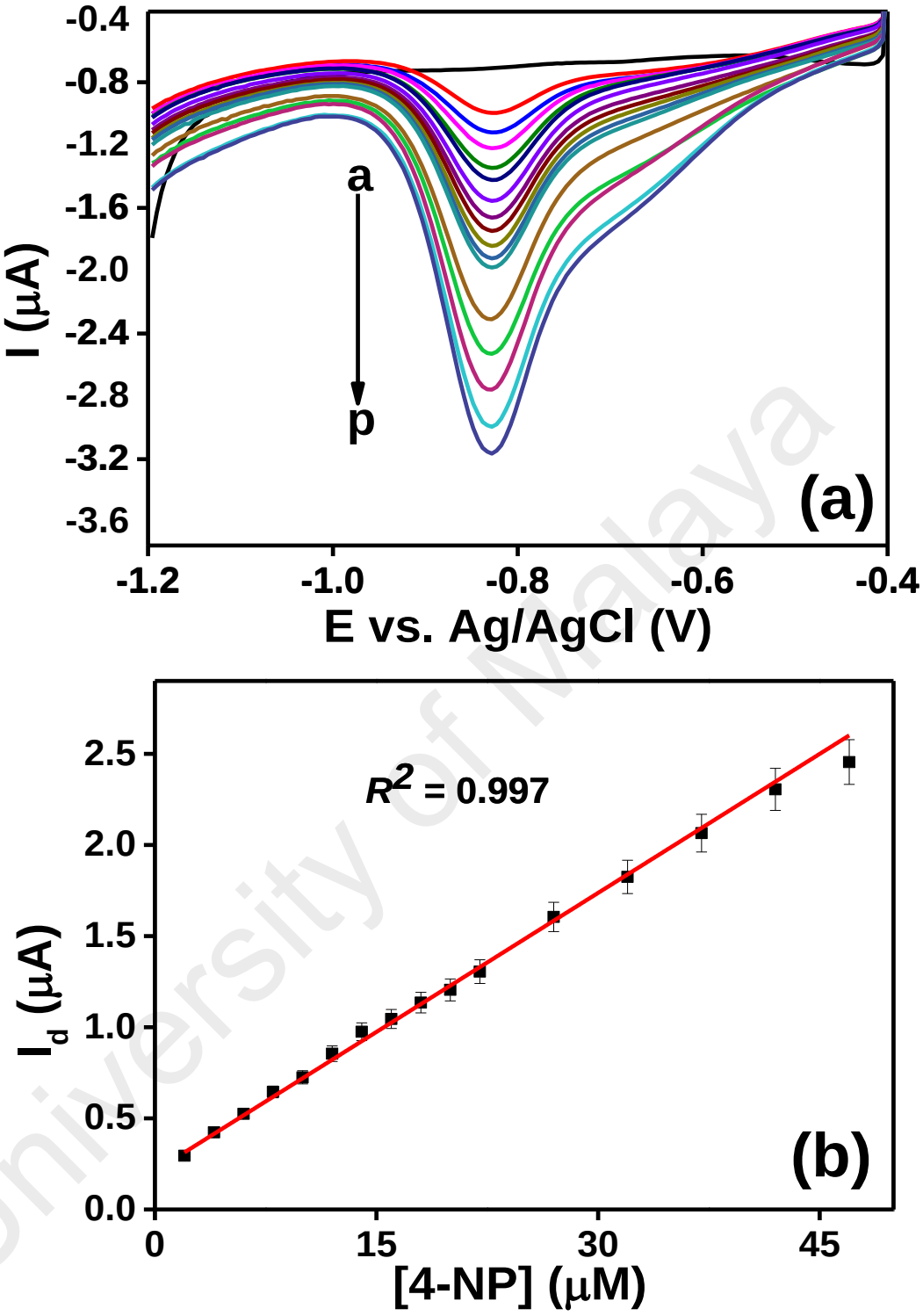

Figure 3.9: (a) Square wave voltammetric responses obtained at Co_3O_4 nanocubes modified electrode for successive additions of 4-NP (a-k: 2 µM additions and l-p: 5 µM additions) in 0.1 M PBS (pH 7) and (b) Corresponding calibration plot.

Table 3.2: Comparison of the present sensor with some of the previously reported electrochemical sensors for 4-NP.

Modified electrode	Analytical technique	pH of the buffer	LOD	Reference
GC/Nano-Cu_2O	Differential pulse voltammetry	6.0	0.5 µM	(Yin *et al.*, 2012)
GC/TPDT–SiO_2/Ag NPs	Square wave voltammetry	7.2	0.5 µM	(Rameshkumar *et al.*, 2014)
GC/GO	Linear sweep voltammetry	4.2	0.02 µM	(Li *et al.*, 2012)
GC/nano–gold	Semi–derivative voltammetry	6.0	8 µM	(Chu *et al.*, 2011)
CPE/CD–SBA	Differential pulse voltammetry	5.0	0.01µM	(Xu *et al.*, 2011)
GC/MWNT-Nafion	Differential pulse voltammetry	4.0	0.04 µM	(Huang *et al.*, 2003)
Pt electrode/Nano Cu_2O	Amperometry	6.0	0.1	(Gu *et al.*, 2010)
SPCE/Graphene/Nf	Differential pulse voltammetry	5.0	0.6 µM	(Arvinte *et al.*, 2011)
GC/ Poly(propyleneimine)–gold	Square wave voltammetry	5.0	0.45 µM	(Ndlovu *et al.*, 2010)
GC/α-MnO_2 nanotube	Amperometry	7.0	0.1 mM	(Wu *et al.*, 2014)
GC/Co_3O_4 nanocubes	Square wave voltammetry	7.2	0.93 µM	Present work

3.4 Conclusion

Cobalt oxide (Co_3O_4) nanostructures with different morphologies were successfully synthesized using a simple hydrothermal process and were characterized with FESEM, XRD and Raman analysis. Further, GC electrodes modified with Co_3O_4 nanostructures with different morphologies were characterized with EIS, and the results showed the lowest charge transfer resistance (R_{ct}) value for the Co_3O_4 nanocubes toward the $[Fe(CN)_6]^{3-/4-}$ redox couple among the modified electrodes. The electrochemical reduction of 4-NP was chosen as a model system to study the electrochemical properties of the Co_3O_4 nanostructures, and the reduction of 4-NP was performed with electrodes modified with the different Co_3O_4 nanostructures using PBS (pH 7). It was found that the Co_3O_4 nanocubes modified electrode displayed a better catalytic current response and the detection of 4-NP at lower concentration levels was studied with the nanocubes modified

electrode using SWV. A LOD of 0.93 µM was achieved using the Co_3O_4 nanocubes, and the current responses were reproducible for the detection of 4-NP.

CHAPTER 4: AMPEROMETRIC DETECTION OF DEPRESSION BIOMARKER USING A GLASSY CARBON ELECTRODE MODIFIED WITH NANOCOMPOSITE OF COBALT OXIDE NANOCUBES INCORPORATED INTO REDUCED GRAPHENE OXIDE

4.1 Introduction

Serotonin (5-hydroxytryptamine, 5-HT) is a monoamine, present in enterchromaffin cells located in the colonic mucosal epithelium widely distributed in the central nervous system. It has an enormous biological importance, the deficiency of 5-HT leads to mental disorders such as Alzheimer's disease, infantile autism, mental retardation, mood, sleep disorders, appetite and depression (Abbaspour *et al.*, 2011; Wang *et al.*, 2013). A series of studies were carried out on human and animal which shows the effect of changes in motility and 5-HT signaling in ageing in terms of, obesity and gastrointestinal diseases such as inflammatory bowel diseases (Morris *et al.*, 2016). Therefore, the sensitive and selective detection of 5-HT with a measurement levels is of great worth and can contribute in understanding the role of 5-HT in depression and other neurological disorders. There are plenty of analytical techniques available which are being used for the detection of 5-HT, these techniques includes fluorimetry (Panholzer *et al.*, 1999), enzyme immunoassay (Chauveau *et al.*, 1991) radioimmunoassay (Jeon *et al.*, 1992) chemiluminescence (Tsunoda *et al.*, 1999) and mass spectrometry (Middelkoop *et al.*, 1993).

Although these techniques are available and has been used for the detection of 5-HT but there are some limitations in using these technique as they are time-consuming and often require sample pre-treatment. On the other hand, electrochemical methods are highly efficient for the detection of a target molecule. But one of the main requirements is that the analyte must be electrochemically active. Since 5-HT is an electroactive

compound, it can be determined by electrochemical methods (Anithaa *et al.*, 2017; Crespi *et al.*, 1991; Dinesh *et al.*, 2017; Fagan-Murphy *et al.*, 2012; Gueell *et al.*, 2010; Gupta *et al.*, 2014; Liu *et al.*, 2011; Liu *et al.*, 2010; Ran *et al.*, 2015; Wang *et al.*, 2013). Nonetheless, the electrochemical technique also endures some issues that limit the detection of 5-HT. The first is that the concentration of 5-HT is very low under physiological conditions. Secondly, the co-existence of other biological molecules like such as AA, DA and UA, which have their oxidation potential nearby to each other and almost overlaps with that of 5-HT at conventional solid electrodes. These concerns make the detection of 5-HT a much more challenging task. A conventional unmodified electrode will not be able to detect this type of molecule in a challenging environment. In recent years, the surface modification of the conventional electrode by special coatings has been the state-of-the-art area in the development of electrochemical sensors (Gupta *et al.*, 2014; Niu *et al.*, 2013; Xu *et al.*, 2012). To resolve these problems, one of the most common ways is the utilization of a modified electrode to improve the sensitivity of 5-HT detection and remove the interference from AA and DA and UA in the 5-HT determination. So, carbon-based electrodes are widely used in voltammetric analysis due to their several advantages such as low cost, chemical stability, wide potential window, good electrocatalytic activity and easy availability. The biocompatibility of carbon electrode makes them a suitable candidate to study the biologically relevant redox systems and *in vivo* analysis. A GC electrode, polycrystalline boron doped diamond electrode and carbon nanotubes are materials which present a wide range of characteristics that are interesting to compare. However, GCE is one of the widely used WE material in electrochemistry.

In recent years, the construction of a competitive sensor material is a difficult and challenging job. A list of nanocomposite material has been used to modify the GCE surface for electrochemical detection of target molecules (Numan *et al.*, 2017; Shahid *et*

al., 2015; Yusoff *et al.*, 2017). The different types of materials which has been used for the detection of 5-HT are GC and boron-doped diamond (BDD) electrodes (Fagan-Murphy *et al.*, 2012), MWCNTs–CS–poly(p-ABSA) (Ran *et al.*, 2015), CUCR/GCE (Wang *et al.*, 2013), Nafion/$Ni(OH)_2$/MWCNT/GC (Babaei *et al.*, 2013), rGO-Co_3O_4/GCE (Dinesh *et al.*, 2017) and 100 kGy GI-WO_3/GCE (Anithaa *et al.*, 2017). In this report, reduced graphene oxide and cobalt oxide (rGO-Co_3O_4) nanocomposite synthesized by a very simple single step hydrothermal route, was utilized for the detection of 5-HT. As it is well known that graphene, a two-dimensional carbon sheet having single-atom thickness, large theoretical surface area (2630 $m^2.g^{-1}$) with high conductivity at room temperature (106 $s.cm^{-1}$), with a wide electrochemical window has a great contribution in catalysis science (Shahid *et al.*, 2017). Graphene sheets are the excellent host material for growing nanomaterials for high performance electrochemical applications (Kim *et al.*, 2009; Zhou *et al.*, 2010). Until now large number of graphene based materials has been synthesized for applications in fuel cell (Shahid *et al.*, 2017), electrochemical sensor (Thanh *et al.*, 2016) , supercapacitors (Numan *et al.*, 2016; Rafique *et al.*, 2017), solar cells (Rafique *et al.*, 2017) and Li-ion batteries (He *et al.*, 2010), etc. The Co_3O_4 nanocubes have been utilized with graphene oxide as a composite material due to its extraordinary characteristics (Shahabuddin *et al.*, 2015).

Our group has used rGO-Co_3O_4 nanocomposite as a cathode and anode material for fuel cell applications (Shahid *et al.*, 2014; Shahid *et al.*, 2017). Until now, there are no reports on rGO-Co_3O_4 nanocomposite prepared by the hydrothermal method utilized for the detection of 5-HT. The presence of the rGO-Co_3O_4 nanocomposite was characterized by FESEM, energy-dispersive X-ray spectroscopy (EDX) mapping, XRD and Raman analyses. The rGO-Co_3O_4 nanocomposite was utilized for the sensitive and selective detection of 5-HT, in the presence of other co-existing interference molecules such as AA and DA and UA. The LOD and limit of quantification (LOQ) were 1.128 μM and 3.760

μM, respectively, with a sensitivity of 0.133 $\mu A.\mu M^{-1}$ on a rGO-Co_3O_4 nanocomposite modified GCE. Furthermore, the as prepared nanocomposite modified electrode was stable, reproducible and showed excellent selectivity toward the detection of 5-HT.

4.2 Experimental Section

4.2.1 Materials

Graphite flakes were purchased from Asbury Inc. (USA). Sulfuric acid (H_2SO_4, 98 %), phosphoric acid (H_3PO_4), hydrochloric acid (HCl, 35 %), potassium permanganate ($KMnO_4$, > 99 %) and ammonia solution (NH_3, 25 %) were purchased from R & M Chemicals. Cobalt acetate tetrahydrate $Co(CH_3COO)_2.4H_2O$ was purchased from Sigma Aldrich. Hydrogen peroxide (H_2O_2, 35 %) was obtained from Systerm, Malaysia. Serotonin hydrochloride was obtained from abcr GmbH Germany. DI water was used throughout the experimental work.

4.2.2 Synthesis of rGO-Co_3O_4 Nanocomposite

GO was prepared by a simplified Hummers method route (Ming, 2010). Graphite flakes (3 g), H_2SO_4 (360 mL), H_3PO_4 (40 mL), and $KMnO_4$ (18 g) were mixed under stirring at room temperature. The mixture was stirred for three days to achieve the complete oxidation of the graphite. The color of the mixture changed from dark green to dark brown. Ice containing H_2O_2 solution was used to stop the oxidation process and control the temperature. The color of the mixture changed to bright yellow, indicating a high level of oxidation of the graphite oxide. The formed graphite oxide was washed three times with 1 M HCl aqueous solution and repeatedly several times with de-ionized water to achieve a pH of 5-6. The washing process was carried out using a simple decantation of supernatant *via* the centrifugation technique. During the process of washing with de-ionized water, the graphite oxide was exfoliated, which resulted in the thickening of the GO solution and finally formation of the GO gel. In the typical procedure for the synthesis

of rGO-Co_3O_4 nanocomposites, the GO was synthesized by a simplified Hummer's method (Shahid *et al.*, 2015). A 1 mmol of Co $(CH_3COO)_2.4H_2O$ was mixed in 12 mL of DI water and added drop by drop into a GO solution of 1 $mg.mL^{-1}$ under continuous stirring. Four samples of rGO-Co_3O_4 nanocomposites were prepared with the same procedure but with different wt. % of GO (2, 4, 8, and 12 wt. %) and stirred for 2 h to obtain a homogeneous solution. After that, 15 mL of 6 % ammonia was slowly added drop-wise into the above reaction mixture under vigorous stirring to raise the pH to almost 10. Then, the as prepared 75 mL of the reaction mixture was transferred into a 100 mL of Teflon lined stainless steel autoclave and subjected to hydrothermal treatment at 180 ^oC for 12 h. Finally, the obtained precipitate of rGO-Co_3O_4 nanocomposite was washed many times with DI water, followed by ethanol to remove the extra impurities and dried in a hot air oven at 60 ^oC. For comparison, unaided Co_3O_4 and rGO were prepared using the same method but without the presence of GO and $Co(CH_3COO)_2.4H_2O$, respectively.

4.2.3 Preparation of Modified Electrode and Electrochemical Measurements

Prior to the modification of GC electrode, it was polished mechanically and electrochemically in both ways. In the mechanical cleaning, 0.5 µm alumina slurry was used and the GC electrode was gently rubbed on alumina coated cloth. After that the GC electrode was sonicated for less than 5 min to remove the adherent particles on its surface. The electrochemical cleaning was carried out by potential cycling between - 1 and + 1 V in 0.1 M H_2SO_4, and washing with DI water after sonicating for 5 min. The rGO-Co_3O_4 nanocomposite modified GC electrode was prepared by using a well sonicated homogenous solution with an optimized concentration of 1 $mg.mL^{-1}$ using DI water as the solvent. The electrochemical studies for the 5-HT was carried out using an Autolab analyzer fitted with a conventional three-electrode system in a 0.1 M phosphate buffer (PB) (pH 7.2) as the supporting electrolyte. The GC electrode with an area of 0.707 cm^2, modified with 5 µL of as syntheised ink was used as the WE, while a saturated calomel

electrode (SCE) and platinum wire were the reference and counter electrodes, respectively. All the electrode potentials were quoted with respect to the SCE reference electrode.

4.2.4 Characterization Techniques

Characterization techniques are as mentioned in Section 3.2.4 with elemental mapping and energy dispersive X-ray (EDX) analysis were performed in addition (JEOL JSM-7600F).

4.3 Results and Discussions

4.3.1 Morphological Characterization of the rGO-Co_3O_4 Nanocomposites

The structural studies of the prepared nanocomposite are shown in Figure 4.1. The GO sheets appear as a cloudy wrinkled shaped structure is shown in Figure 4.1(a). After the hydrothermal process, GO is reduced to rGO and become more agglomerated and wrinkled due to the removal of oxygen functional groups which are responsible for preventing the GO sheets from stacking Figure 4.1(b). The Co_3O_4 nanostructures are in a cubical form as shown in Figure 4.1(c), with high aggregation. Figure 4.1(d) shows the nanocomposite of rGO and Co_3O_4. Interestingly in Figure 4.1(b), the cloudy wrinkled rGO sheet become stretched and smooth. This is due to the cobalt oxide nanocubes which stretch the rGO sheets and act as a nanospacers between the different layers of rGO sheets. The graphene sheets usually appears in stacked form after reduction, due to the removal of the oxygen functional groups, which can be confirmed by the shift in *2D* band in the Raman spectrum, which is explained in next section (Wang *et al.*, 2008). Another interesting phenomenon is that the nanocomposite of rGO-Co_3O_4 also prevents the Co_3O_4 nanocubes from agglomeration, as can be seen in Figure 4.1(c). So, it can be concluded that both the Co_3O_4 nanocubes and rGO nanosheets form a synergistic relationship during the formation of the rGO-Co_3O_4 nanocomposite. The Co_3O_4 nanocubes help the graphene

sheet to stretch and prevents the stacking of the graphene sheets thus increases the effective surface area of the graphene, while the graphene sheets also prevented the Co_3O_4 nanocubes from agglomerations due to strong interaction between the Co_3O_4 and the rGO through interfacial Co–O–C bonds formed by the high reactivity of sp^2 carbon atoms of rGO with the electron-rich oxygen species of Co_3O_4 (Shahid *et al.*, 2015). The use of ammonia facilitated the reduction of graphene oxide and also played an important role in the precipitation of cobalt Co^{2+} ions and their oxidation (Dong *et al.*, 2007). In addition, the density of Co_3O_4 nanocubes decreased when the wt. % of GO is varied from lower to higher concentration (2 wt. % to 12 wt. %). This is because of the presence of a sufficient number of graphene sheet which help to optimize the best nanocomposite for detection of 5-HT, as explained in electrocatalysis of 5-HT section.

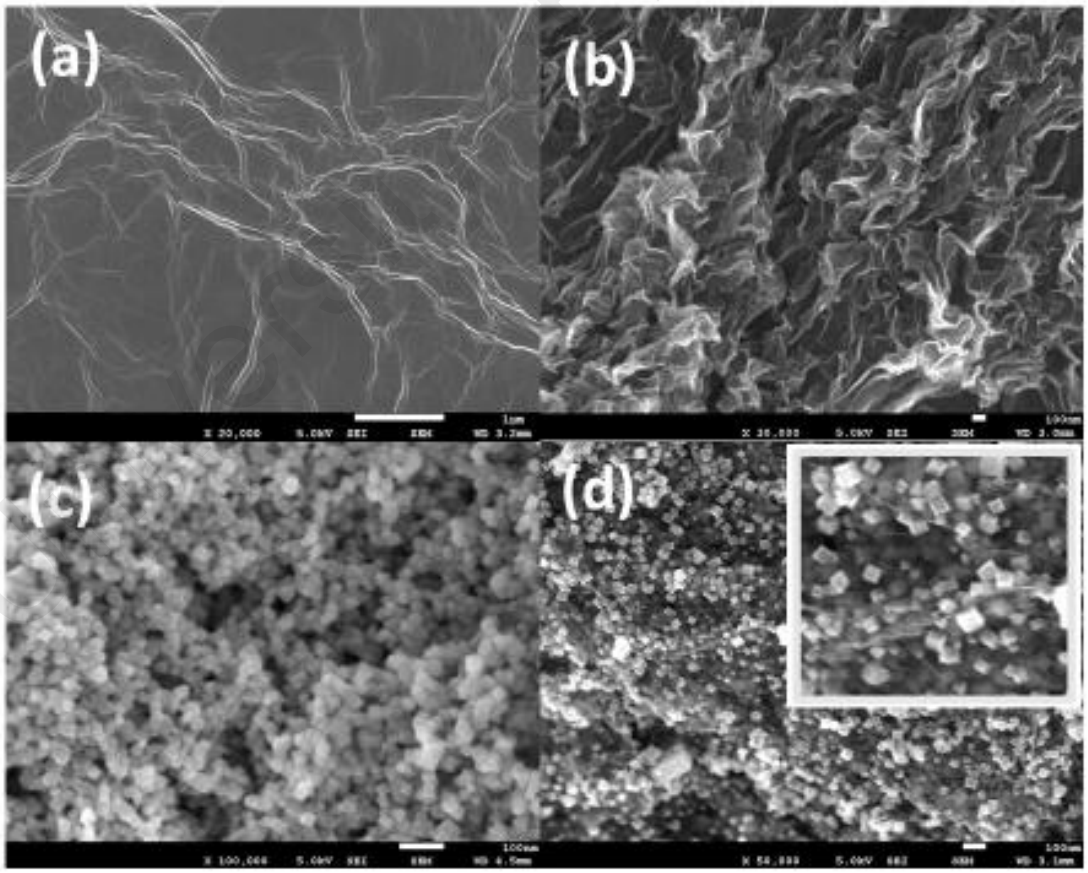

Figure 4.1: FESEM images of (a) GO sheets, (b) rGO (c) Co_3O_4 nanocubes and (d) rGO-Co_3O_4-4 % nanocomposite.

The EDX elemental mapping analysis was carried out for the rGO-Co_3O_4-4 % to check the distribution of elements (Figure 4.2). The FESEM image of rGO-Co_3O_4-4 % nanocomposite and the elements C (green), Co (magenta), Si (blue) and O (red) are shown in Figure 4.2(a & b). For clarity, the independent elemental distribution of C, Co, Co and Si is shown in Figure 4.2(c-f). Figure 4.2(c) shows the presence of GO as carbon material while Figure 4.2(d) (magenta) and Figure 4.2(e) (red) shows large area coverage due to the densely packed Co_3O_4 nanocubes. Silicon (Si) was used as a substrate for the preparation of the sample [Figure 4.2(f) (blue color)]. The presence of elemental O (18.28 wt. %), C (18.3 wt. %), Si (0.64 wt. %) and Co (62.77 wt. %) is shown in in Appendix 2 which confirms the presence of the same elements in the nanocomposite.

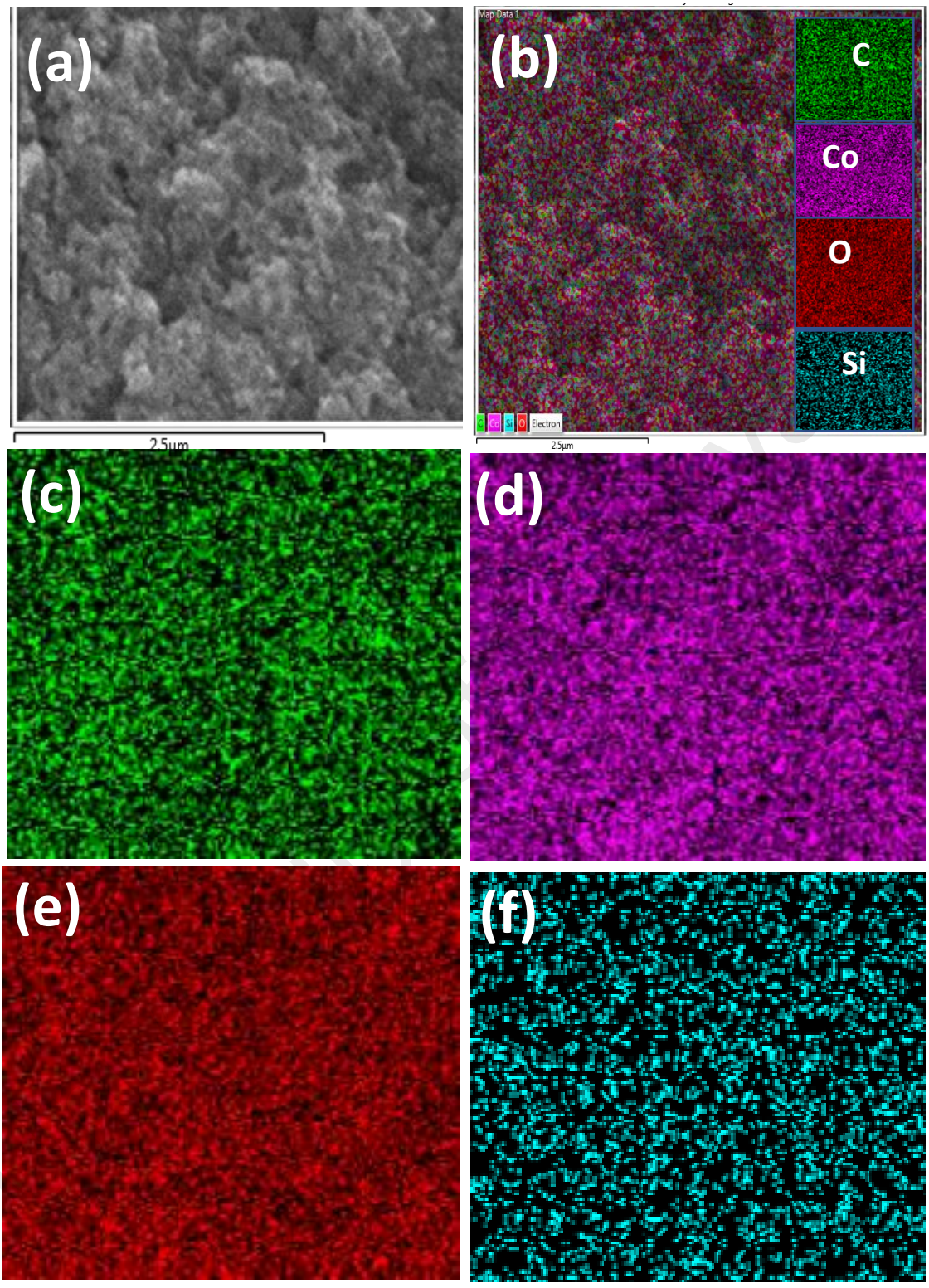

Figure 4.2: (a) FESEM image, (b) EDX elemental mapping of the rGO-Co_3O_4-4 % nanocomposite, (c) green, (d) magenta, (e) red and (f) blue, corresponding to the elements C, Co, O and Si, respectively.

4.3.2 XRD and Raman Analysis

The XRD analysis was conducted to evaluate the crystalline nature of the rGO-Co_3O_4-4 % nanocomposite (Figure 4.3). The diffraction peaks at 2θ values of 19.1°, 31.2°, 37.0°, 38.7°, 45.0°, 59.4°, 65.4° and 77.4° correspond to the crystal planes of (111), (2 2 0), (3 1 1), (222), (4 0 0), (5 1 1), (4 4 0) and (5 3 3) of the face centered cubic Co_3O_4 (JCPDS Card No. 42-1467) (Song *et al.*, 2013). The observed peaks for rGO-Co_3O_4-4 % nanocomposite has higher intensity (Figure 4.3d) as compared to the peaks obtained for unaided Co_3O_4 (Figure 4.3c). The high intensity peaks show that the presence of graphene in the nanocomposite prevented the Co_3O_4 from agglomeration, which in turn appears as highly crystalline nanostructures, and the XRD results agrees well with the FESEM results. The high intensity diffraction peak of GO at 10.6° corresponds to lattice plane of (001) which confirms the presence of GO in Figure 4.3a (Chen *et al.*, 2010) . Additionally, the disappearance of the high intensity peak of GO at 10° in Figure 4.3b and the appearance of other two peaks at 25.5° and 43.2° corresponds to lattice plane of (002) and (100) respectively, which indicates the reduction of GO to rGO. Interestingly, the absence of rGO peak in the rGO-Co_3O_4-4 % nanocomposite confirms the exfoliation of the graphene sheets as well as the interleaved Co_3O_4 nanocubes into different layers of rGO sheets, which can be seen in the FESEM (Figure 4.1(d)).

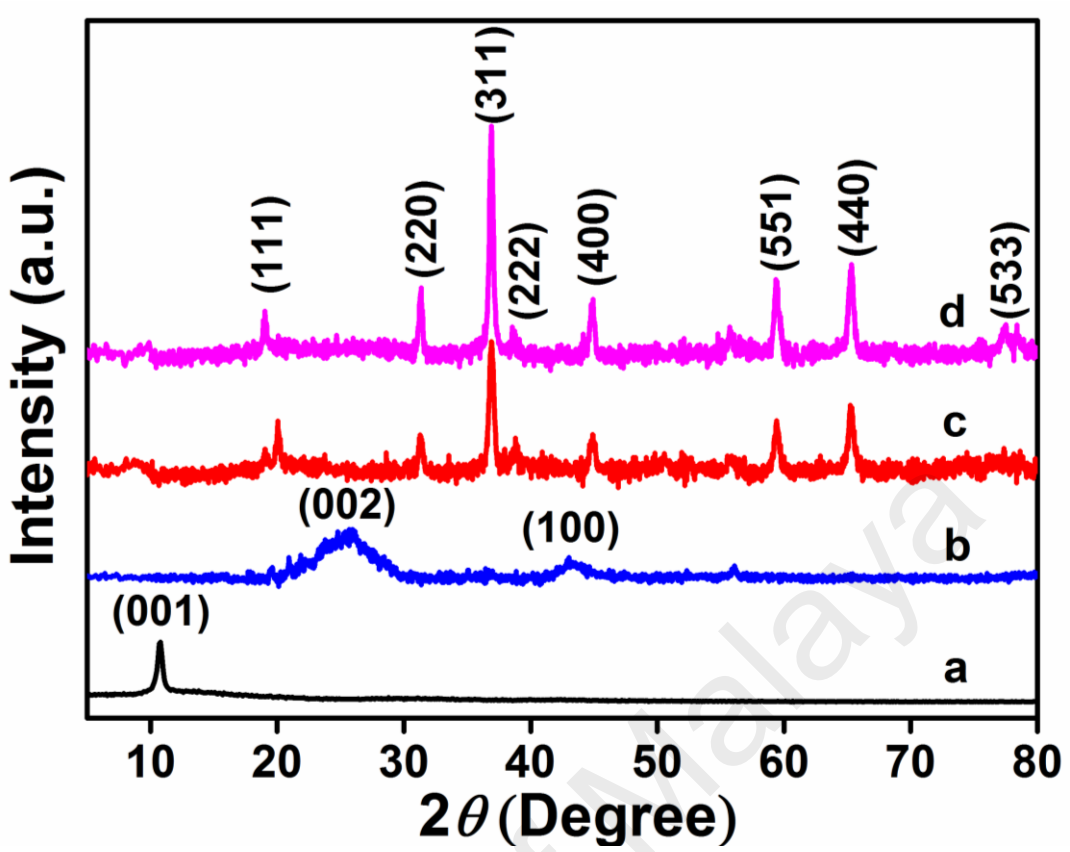

Figure 4.3: XRD patterns of (a) GO, (b) rGO, (c) Co_3O_4 and (d) rGO-Co_3O_4 nanocomposite.

The Raman spectra of GO and rGO-Co_3O_4-4 % nanocomposite is shown in the Figure 4.4. The rGO-Co_3O_4-4 % nanocomposite shows the *D* (1349 cm^{-1}) and *G* (1601 cm^{-1}) band of reduced graphene oxide with higher intensity of $D/G > 1$ which confirms the reduction of GO into rGO. The *D* band in Raman spectra refers to the defects which arises from the vibration of sp^3 carbon atoms while the *G* band arises from sp^2 hybridized carbon atoms (Yusoff *et al.*, 2017). The slight shifting of the *G* band to 1601 cm^{-1} for rGO-Co_3O_4-4 % nanocomposite also confirms the reduction of GO into rGO, as shown in Appendix 3 (inset). The successful synthesis of rGO-Co_3O_4-4 % nanocomposite can be supported further by the Raman modes in Figure 4.4, which shows different values at 194, 482, 525 and 691 cm^{-1} which corresponds to the F_{2g}^2, Eg, F_{2g}^1 and A_{1g} Raman modes respectively, of the Co_3O_4 along with rGO peaks (Jiang *et al.*, 2016). The Raman mode are given in Appendix 3 which further justify the formation of pure Co_3O_4 nanocubes.

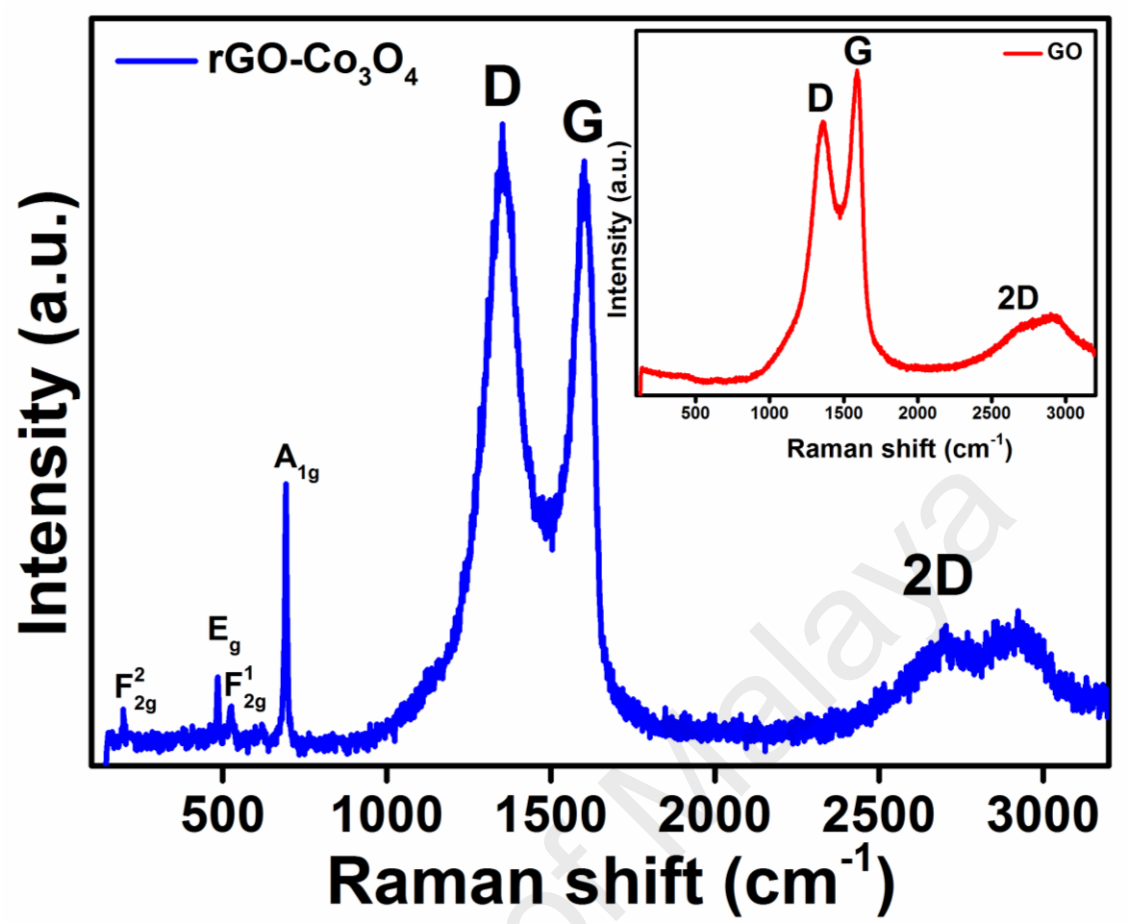

Figure 4.4: Raman spectra of rGO-Co_3O_4-4 % nanocomposite and GO (inset).

4.3.3 Electrocatalysis of 5-HT

The electrochemical oxidation of 5-HT with bare GC electrode and chemically modified GC electrodes has been investigated *viz*. Co_3O_4, rGO and rGO-Co_3O_4-4 % nanocomposite in 0.1 M phosphate buffer (pH 7.2) as shown in Figure 4.5(a). The cyclic voltammograms were recorded for the oxidation of 5-HT (0.5 mM) under deaerated conditions. The oxidation peak of 5-HT at bare GC electrode showed poor electrocatalytic response with a current value of 9.3 μA at higher oxidation peak potential of 3.5 mV in Figure 4.5(a). All other three chemically modified GC electrodes showed higher electrocatalytic current compared to the bare GC electrode with a shift in oxidation potential towards lower potential, as can be seen in Figure 4.5(a). It is interesting to note that favorable result for the oxidation of 5-HT has been shown by rGO-Co_3O_4-4 %

modified GC electrode with the highest current (36 mA) and is four times higher compared to the bare GC electrode with an oxidation potential of 3.1 mV in Figure 4.5(a). The considerable higher oxidation peak current of 5-HT at rGO-Co_3O_4-4 % modified GC electrode shows a faster electron transfer process facilitated at the modified electrode. The poor electrocatalytic performance of the Co_3O_4 modified GC electrode was due to the Co_3O_4 nanocubes aggregation, which prevent faster electron transfer kinetics. The higher electrocatalytic detection of 5-HT was shown by the rGO modified GC electrode with lower oxidation potential, due to the higher electrical conduction of the rGO. The cyclic voltammogram in Figure 4.5(b) shows the comparison of rGO-Co_3O_4-4 % modified GC electrode in the presence and absence of 0.5 mM of 5-HT. There was no peak observed in the absence of 5-HT at the modified GC electrode, while a well resolved oxidation peak appears in the presence of 5-HT, which further confirms the electrocatalytic oxidation of 5-HT at the chemically modified electrode (CME).

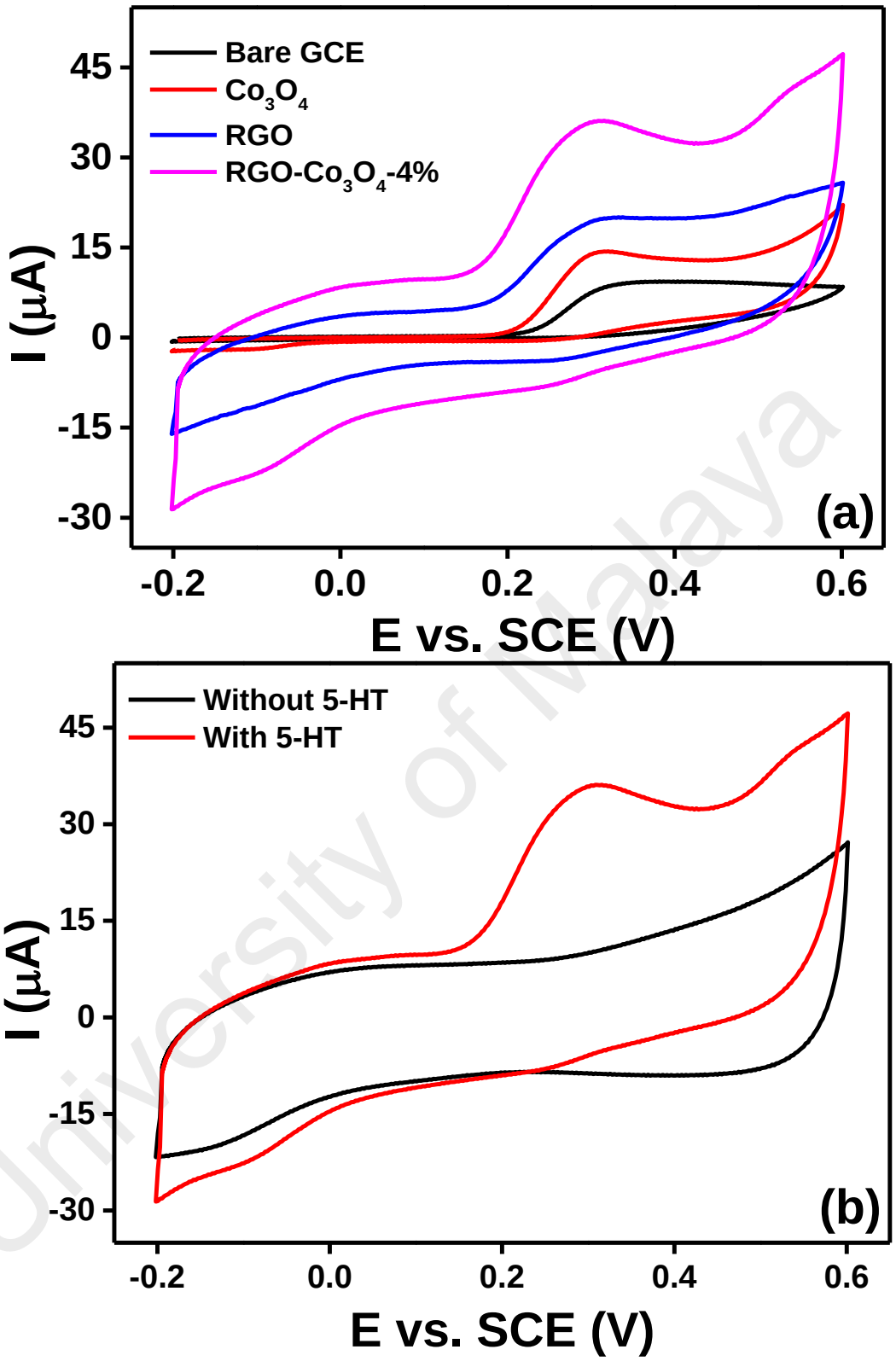

Figure 4.5: (a) Cyclic voltammograms recorded at bare GCE, Co_3O_4, rGO and rGO-Co_3O_4-4 % nanocomposite modified electrode for 0.5 mM 5-HT in 0.1 M PB (pH 7.2) with a scan rate of 50 $mV.s^{-1}$ and (b) the cyclic voltammogram curves of rGO-Co_3O_4-4 % nanocomposite in presence and absence of 5-HT.

Appendix 4 shows the electrocatalytic performance comparison of the rGO-Co_3O_4 modified GC electrode at different concentrations of GO (2 wt. % to 12 wt. %). The rGO-Co_3O_4-4 % modified GC electrode gave the best electrocatalytic activity. On the other hand, the rGO-Co_3O_4-2 % modified GC electrode shows poor electrocatalytic effect due to the lower amount of graphene nanosheets which eventually allowed the Co_3O_4 to aggregate on the surface of the graphene sheets. The increase in the concentration of GO to 8 and 12 wt. % allows a sufficient number of graphene sheets to decrease the density of the Co_3O_4 nanocubes. Therefore, the rGO-Co_3O_4 modified GC with 8 and 12 wt. % of GO gave poor electrocatalytic activity compared to the rGO-Co_3O_4-4 % modified GC electrode.

The influence of the scan rate on the electrocatalytic oxidation of 5-HT was examined for the rGO-Co_3O_4-4 % modified GC electrode from 10-200 $mV.s^{-1}$ in the presence of 0.5 mM 5-HT in 0.1 M PB (pH 7.2), as shown in Figure 4.6(a). The peak current for oxidation of 5-HT was found to be linear with the square root of the scan rate ($v^{1/2}$) (Figure 4.6(b)) which indicates a typical diffusion controlled process. The positive shift in oxidation peak potential with the increase of the scan rate indicates the slow kinetics of the interfacial electron transfer of 5-HT (Abbaspour *et al.*, 2011). The irreversible electrooxidation of 5-HT is also supported by the linear relation of the peak potential (*Ep*) and the log (ν) (Figure 4.6(c)).

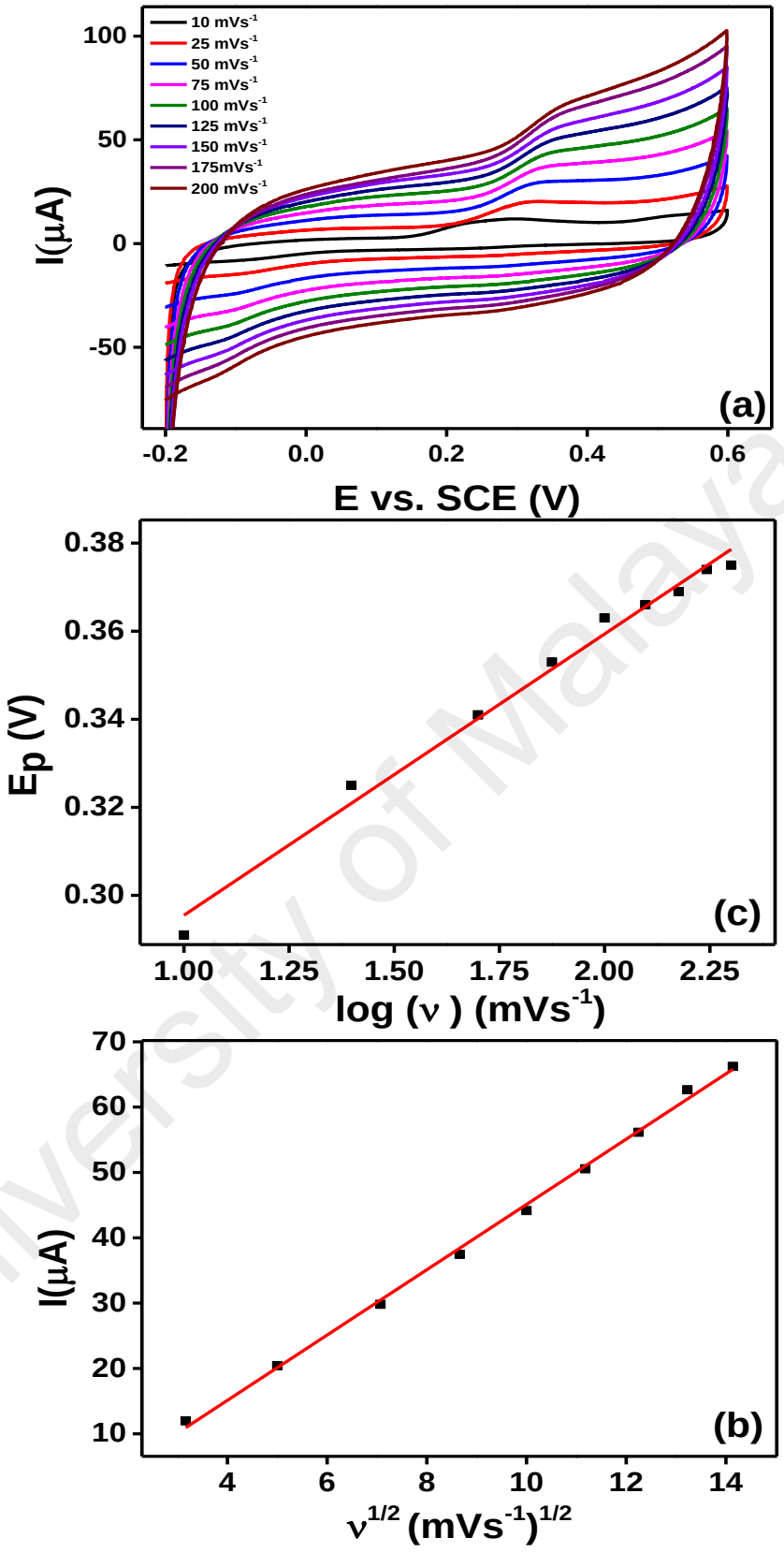

Figure 4.6: (a) Cyclic voltammogram plots obtained for rGO-Co_3O_4-4 % modified electrode in 0.1 M PBS (pH 7.2) in presence of 0.5 mM 5-HT at a scan rate of 10-200 $mV.s^{-1}$. (b) The corresponding calibration plot of anodic peak currents versus square root of scan rate, (c) a relationship between anodic peak potentials versus logarithm of scan rate.

Appendix 5(a) shows the cyclic voltammograms carried out for the rGO-Co_3O_4-4 % modified GC electrode in 0.1 M PB (pH 7.2) at scan rate of 50 $mV.s^{-1}$, with increasing concentration of 5-HT from 0.5 mM to 3 mM. The oxidation peak current is found to increase linearly with a slight shift in the oxidation peak current by increasing the 5-HT concentration. The plot of peak current versus concentration of 5-HT showed a linear response (Appendix 5(b)) which indicates the efficient electrocatalytic ability of the modified electrode.

4.3.4 Amperometric Detection of 5-HT

The rGO-Co_3O_4-4 % modified GC electrode was chosen for further amperometric *i–t* curve due to the outstanding electrochemical behavior and good electrocatalytic oxidation of 5-HT. Figure 4.7(a) shows the typical amperometric curve for the rGO-Co_3O_4-4 % modified GC electrode with successive addition of 1 μM of 5-HT concentration and was increased to 2 μM after 10 injections. The 5-HT solution was spiked after a regular interval of 60 s, once the amperometric curve become stable with an applied potential of + 0.31 V. An obvious enhancement in current response for the successive injection of 5-HT was obtained and the corresponding linear relationship between the current response and 5-HT concentration is shown in Figure 4.7(b). There are two linear ranges plotted ranging from 1 μM to 10 μM and 12 μM to 22 μM based on the results obtained from the amperometric *i–t* curve. The LOD and LOQ were calculated from the first linear range and found to be 1.128 μM and 3.760 μM respectively, with a S/N ratio of 3. The values for LOD and LOQ were calculated by the following equations (4.1) and (4.2):

$$LOD = 3\sigma/m \quad (4.1)$$

$$LOQ = 10\sigma/m \quad (4.2)$$

where σ is the residual standard deviation of the linear regression and m is the slope of the regression line (Reddaiah *et al.*, 2012; Shrivastava *et al.*, 2011). The sensitivity value from the slope of the line was 1.337 $\mu M.\mu M^{-1}$. The comparisons in Table 1 compiles the analytical parameters for the electrochemical detection of 5-HT using different types of modified GC electrodes reported in the literature.

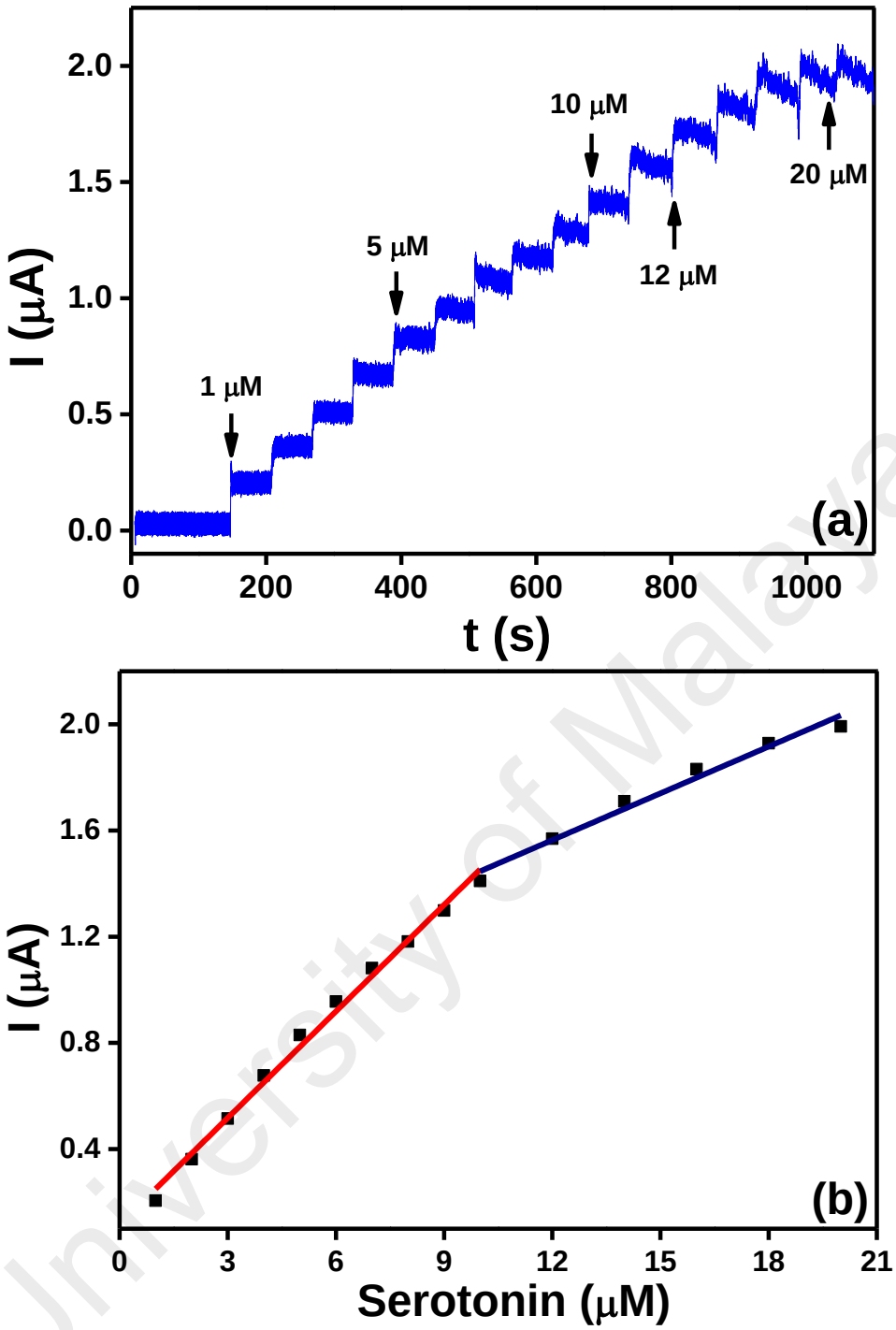

Figure 4.7: (a) Amperometric *i–t* curve obtained at rGO-Co_3O_4-4 % nanocomposite modified GC electrodes for the successive addition of 5-HT with various concentrations in 0.1 M PBS (pH 7.2) at a regular interval of 60 s with two linear ranges. The applied potential was +0.31 V. (b) The calibration plot of peak current versus concentration of 5-HT corresponding to '(a)'.

The selectivity of the prepared sensor was tested in the presence of interfering species such as AA, UA, and DA which is naturally found with 5-HT in the central nervous system, as can be seen in Figure 4.8. These species were added one after the

other, after three successive additions of 5-HT. The results obtained from the selectivity experiments suggests that the rGO-Co_3O_4 modified GC electrode didn't show any response for the AA, DA and UA even with a 50-fold higher concentration. The interference studies show only a small disturbance upon the addition of the spikes of AA. This could arise from the dynamic conditions present due to the almost overlapping potential of the AA and 5-HT. To further confirm the selectivity of the sensor, the 5-HT solution was again spiked and an obvious increase in current values was obtained. However, the present sensor still maintains the high selectivity towards the sensing of 5-HT, even in the presence of 50-fold higher concentration of interference molecules.

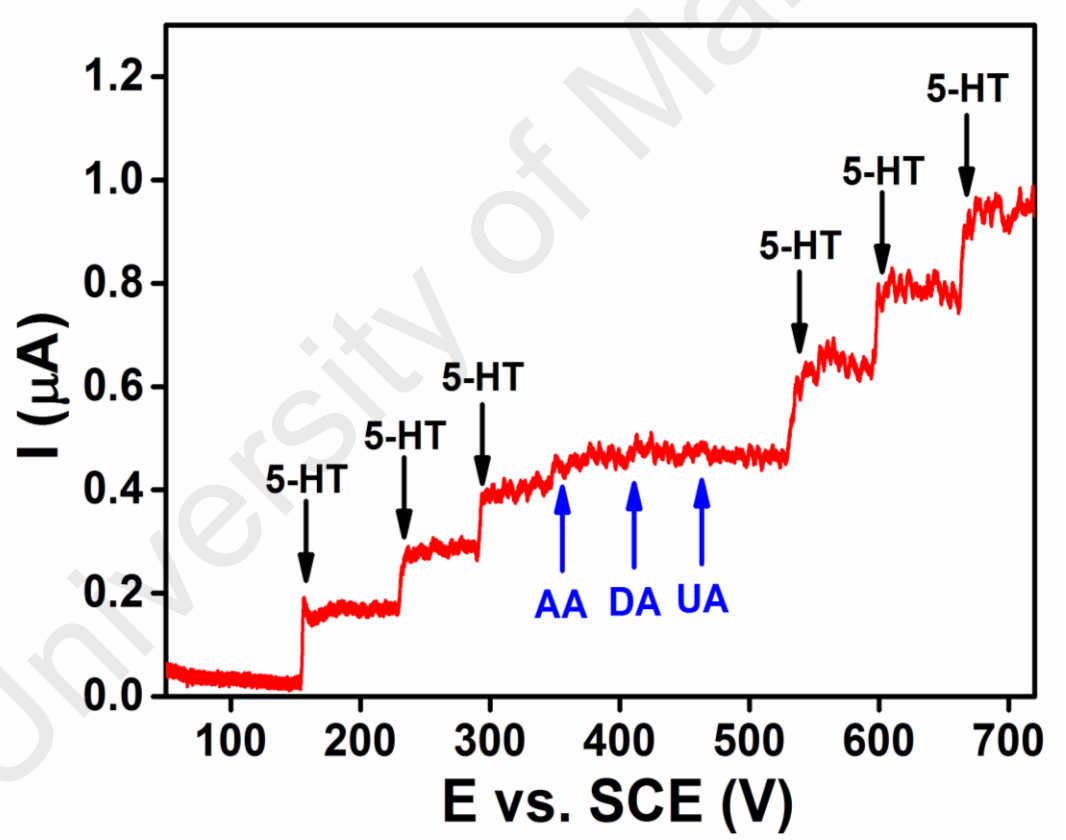

Figure 4.8: Amperometric *i–t* curve obtained at rGO-Co_3O_4-4 % nanocomposite modified GC electrodes for the successive addition of 1 μM 5-HT and each 50 μM of AA, DA, UA in 0.1 M PB (pH 7.2) at a regular interval of 60 s at applied potential of + 0.31 V.

Table 4.1: A comparison of the reported electrochemical sensors for 5-HT detection.

Sensing material[a]	Electrochemical technique[b]	Linear range	LOD (μM)	Interferents Studied	Ref
5-HTP/GCE	DPV	5–35 μM	1.7	-----	(Li *et al.*, 2009)
IL–DC–CNT/GC	DPV	5–900 μM	2.0	AA and UA	(Mazloum-Ardakani *et al.*, 2014)
CNFs	DPV	0.1-10 μM	0.25	AA	(Rand *et al.*, 2013)
rGO-Co_3O_4-4%/GC	Amperometry	1-10 μM 12-20 μM	1.12	AA, DA and UA.	This work

[a] 5-hydroxytryptophan, 7-(1,3-dithiolan-2-yl)-9,10-dihydroxy-6H-benzofuro[3,2-c]chromen-6-one (DC), Carbon nanofibers electrode.
[b] DPV = differential pulse voltammetry

4.4 Conclusions

In this study, the rGO-Co_3O_4-4 % nanocomposite was successfully synthesised by a simple hydrothermal route. The FESEM and EDX elemental mapping analysis confirmed the presence of all the elements in the rGO-Co_3O_4-4 % nanocomposite. The Raman spectra confirms the successful formation of Co_3O_4 and increase in the ratio of *D* and *G* bands (I_D/I_G) of Raman spectra also confirmed the reduction of GO to rGO. An impressive study based on the rGO-Co_3O_4-4 % modified GC electrode was performed and a competitive detection of 5-HT was performed using the amperometric *i*–*t* curve technique. The detection limits for 5-HT was 1.128 μM (LOD) and 3.760 μM (LOQ) while the sensitivity values for rGO-Co_3O_4-4 % nanocomposite was 0.133 $\mu M.\mu M^{-1}$. The rGO-Co_3O_4-4 % nanocomposite based sensor was further investigated for its selectivity and found to be highly selective towards 5-HT detection in the presence of AA, DA and UA.

CHAPTER 5: AN ELECTROCHEMICAL SENSING PLATFORM OF COBALT OXIDE@GOLD NANOCUBES INTERLEAVED REDUCED GRAPHENE OXIDE FOR THE SELECTIVE DETERMINATION OF HYDRAZINE[2]

5.1 Introduction

Hydrazine is a toxic, colorless and flammable molecule (Krittayavathananon *et al.*, 2014). It is classified as a human mutagenic and carcinogen in group B2 by the EPA, United States. It could cause severe injury of lungs, liver, nervous system, spinal cord, temporary blindness and dizziness, pneumonia and kidney damage (Cui *et al.*, 2014; Cui *et al.*, 2014). In addition, acute exposure to hydrazine could result in death (Choudhary *et al.*, 1997). Hydrazine and its offshoots are well-known environmental toxic pollutants, are widely used in rocket fuel (Zhang *et al.*, 2015), fuel cell systems (Madhu *et al.*, 2015), photographic chemicals, insecticides, herbicides, emulsifiers, blowing agents, textile dyes and corrosion inhibitors in various chemical, pharmaceutical and agricultural industries (Ding *et al.*, 2015; Madhu *et al.*, 2015; Wang *et al.*, 2010). Since hydrazine is a suspected carcinogenic and mutagenic agent, the detection of hydrazine in biological systems has attracted considerable attention in recent decades (Karimi-Maleh *et al.*, 2014). There are numerous analytical techniques available for the sensitive determination of hydrazine such as spectrophotometry (Ensafi *et al.*, 1998; Watt *et al.*, 1952), amperometry (Jayasri *et al.*, 2007; Mallela *et al.*, 1977), titrimetry (Budkuley, 1992), chemiluminescence (Safavi *et al.*, 2002), fluorimetry (Safavi *et al.*, 1995), and especially electroanalytical methods (Afzali *et al.*, 2011; Khalilzadeh *et al.*, 2009; Yi *et al.*, 2009). The techniques

[2] This chapter is published as: Shahid, M. M., Rameshkumar, P., Basirunc, W. J., Wijayantha, U., Chiu, W. S., Khiew, P. S., & Huang, N. M. (2018). An electrochemical sensing platform of cobalt oxide@ gold nanocubes interleaved reduced graphene oxide for the selective determination of hydrazine. *Electrochimica Acta, 259*, 606-616.

other than electroanalytical methods are complicated, more laborious and also are unable to determine the real time concentration of hydrazine (Liu *et al.*, 2014). Electrochemical techniques offer the opportunity for a portable, economical, sensitive and rapid method for the determination of hydrazine molecule (Karuppiah *et al.*, 2014). The electrochemical oxidation of hydrazine on carbon electrode produces nitrogen and water that do not cause environmental pollution and have been investigated widely (Antoniadou *et al.*, 1989; Karimi-Maleh *et al.*, 2014). However, the electrochemical oxidation of hydrazine occurs at higher oxidation overpotential due to the sluggish decomposition at the bare electrode surface (Zhang *et al.*, 2010). Therefore, several attempts have been made to circumvent this problem by using CME surface with new class of materials such as metals, metal oxides and their nanocomposites supported by conducting platform (Ding *et al.*, 2015; Rastogi *et al.*, 2014). The CME have the ability to decrease the oxidation overpotential and helps in increasing the oxidation current based on their easy, economical and labor-free operation along with sufficient sensitivity and selectivity (Gholamian *et al.*, 2012; Liu *et al.*, 2014).

Nanotechnology-driven materials have attracted extensive attention in the recent years due to their unique structures and catalytic properties (Gholamian *et al.*, 2012; Khoei *et al.*, 2011). The modification of an electrode by the incorporation of nanomaterials in conjunction with one another to form novel composites such as Pt-Cu@silicon (Ensafi *et al.*, 2016), TiO_2–Pt, Pd-modified TiO_2 (Yi *et al.*, 2011) and Au@Pd (Dutta *et al.*, 2015) is a topic of interest to enhance the sensitivity, selectivity and stability of the electrochemical sensing assay (Ganjali *et al.*, 2010). The synergistic effect of these materials plays a vital role in the determination of the target analyte (Kimmel *et al.*, 2011). Therefore, a considerable attention has also been focused to develop highly conducting materials for supporting nanosized particles such as Ag/PPy/GCE (Ghanbari, 2014), ZnO/MWCNTs/GCE (Fang *et al.*, 2009), AuNPs/GO (Lu *et al.*, 2011) and ZnO–

RGO (Ding *et al.*, 2015). The conducting support materials are widely used in enhancement of catalyst dispersion, heterogeneous catalysis, electrocatalysis and the stability for sensitive determination of hydrazine (Kou *et al.*, 2011; Singh *et al.*, 2012). Because of their extraordinary electronic conductivity and large surface area for the nanosized catalyst, they could enhance the performance in the electrocatalytic activity (Chai *et al.*, 2012; Moghaddam *et al.*, 2012). Graphene has been one of the most interesting material due to its electronic and electrocatalytic properties, and has been widely investigated in electrochemical applications (Choi *et al.*, 2012; Rao *et al.*, 2010). It has attracted much scientific and technological interest due to its physiochemical properties such as high theoretical surface area (2630 m^2) for a single layer graphene sheet (Geim *et al.*, 2007; Park *et al.*, 2009), excellent room temperature thermal conductivity (~5000 W m^{-1} K^{-1}) (Balandin *et al.*, 2008), strong mechanical strength (~40 N/m) , high Young's modulus (~1.0 TPa) (Lee *et al.*, 2008) and excellent electrical conductivity (Service, 2009).

Here, the hydrothermal process was used to synthesize Au nanoparticle deposited rGO-Co_3O_4 nanocubes. The Co_3O_4 nanocubes incorporated into rGO behaved as a template for the growth of Au nanoparticle. The Co_3O_4 nanostructures are considered as promising candidate among other metal oxides, since Co_3O_4 has fascinating optical, magnetic and transport properties. Co_3O_4 has a well-defined electrocatalytic redox activity with high theoretical capacity (890 mAh g^{-1}), low cost and chemically stable state (Shahid *et al.*, 2015; Shahid *et al.*, 2015). The rGO-Co_3O_4@Au nanocomposite modified GC electrode was used as a sensing platform for the detection of hydrazine in phosphate buffer (pH 7.2). The detection limit of hydrazine was found to be 0.443 µM with the sensitivity of 0.58304 ± 0.00466 µA $µM^{-1}$. The lowest possible concentration of Au (0.2133 mM) was used to enhance the sensitivity of rGO-Co_3O_4 nanocubes towards hydrazine detection. The real sample analysis was also carried out in water collected from

different sources and the good recoveries were found. The nanocomposite displayed good sensitivity even in the presence of 50-fold higher concentration of interferent species.

5.2 Experimental Methods

5.2.1 Materials

All chemicals used in this study were of analytical grade and were used as received without further purification. The graphite flakes were purchased from Asbury Inc. (USA). Potassium permanganate ($KMnO_4$, > 99 %), sulphuric acid (H_2SO_4, 98 %), phosphoric acid (H_3PO_4, 98 %), hydrochloric acid (HCl, 35 %), and ammonia solution (NH_3, 25 %) were obtained from R & M Chemicals. Cobalt acetate tetrahydrate ($Co(CH_3COO)_2.4H_2O$) was purchased from Sigma Aldrich. Hydrogen tetrachloroaurate (III) trihydrate ($HAuCl_4 \cdot 3H_2O$) precursor was obtained from abcr GmbH & CO. KG. Hydrogen peroxide (H_2O_2, 35 %) was purchased from Systerm. Hydrazine hydrate ($N_2H_4.H_2O$, 50-60 %) was procured from Sigma Aldrich.

5.2.2 Synthesis of rGO-Co_3O_4@Au Nanocomposite

To prepare the rGO-Co_3O_4@Au nanocomposites, 1 mmol of $Co(CH_3COO)_2.4H_2O$ solution was first prepared in 10 mL of DI water. The solution of $Co(CH_3COO)_2.4H_2O$ was slowly added into the well-sonicated 8 wt. % GO (1 mg/mL) solution under stirring. The solution was allowed to stir for 1 h, so that the cobalt ions could intercalate in between the different layers of graphene sheets. After that, 2 mL of Au (8 mM) solution was drop-wise added to the reaction mixture and stirred for 30 min. A 15 mL ammonia (6 %) solution was added into the above solution and left for another 15 min. Finally, the mixture (75 mL) was transferred into Teflon-lined container with a volume of 100 mL and was subjected to hydrothermal treatment for 12 h at 180 ^oC. The autoclave was cooled down to room temperature and the precipitation was collected and washed with DI water and ethanol several times. The washed product was dried in hot air oven at 60 ^oC for 24

h and the rGO-Co_3O_4@Au nanocomposite powder was collected for further analysis. For the optimization of the Au content, the rGO-Co_3O_4@Au nanocomposites were prepared with 2, 4, 6, 8 and 10 mM of Au by following the same procedure and the nanocomposites were named as rGO-Co_3O_4@Au (2 mM), rGO-Co_3O_4@Au (4 mM), rGO-Co_3O_4@Au (6 mM), rGO-Co_3O_4@Au (8 mM) and rGO-Co_3O_4@Au (10 mM). The controlled materials such as rGO, Co_3O_4 and rGO-Co_3O_4 nanocomposite was prepared in the absence of the other components.

5.2.3 Characterization Techniques

Characterization techniques are as mentioned in Section 4.2.4.

5.2.4 Electrochemical Measurements

A conventional three electrode electrochemical cell was used to carry out all electrochemical studies. The CME was prepared by drop-casting 5 µL of rGO-Co_3O_4@Au nanocomposite (1 mg/mL) on GCE surface (d = 3 mm) and allowing it to dry at room temperature (25 ^oC). The rGO-Co_3O_4@Au coated GCE was used as the WE. Prior to the electrochemical experiments, the GCE was cleaned electrochemically in 0.5 M H_2SO_4 and mechanically polished on 0.05 micron alumina slurry. Nitrogen purged 0.1 M phosphate buffer (pH 7.2) was used as the electrolyte throughout the electrochemical studies. A platinum wire and SCE were the counter and reference electrodes, respectively. Hydrazine hydrate ($N_2H_4.H_2O$) was used as the analyte for detection at the rGO-Co_3O_4@Au modified GCE surface. All the electrochemical studies were carried out by using PAR-VersaSTAT-3 Electrochemical Workstation.

5.3 Results and Discussions

5.3.1 Formation, Morphology and Elemental Mapping Analysis of rGO-Co_3O_4@Au Nanocomposite

In the synthesis of the rGO-Co_3O_4@Au nanocomposite, the Co^{2+} ions were strongly adsorbed on the surface of highly negatively charged GO due to the electrostatic attraction with oxygen functional groups of GO (Jokar *et al.*, 2014). The Co^{2+} ions forms coordination with the ammonia present in the reaction mixture and thus, releases the $[Co(NH_3)_6]^{2+}$ ions. During the hydrothermal treatment, both the oxidation of $[Co(NH_3)_6]^{2+}$ ions as well as the reduction of GO into rGO occurred with the aid of ammonia (Shahid *et al.*, 2015; Yao *et al.*, 2012). The nucleation of Co_3O_4 nanostructure formation was controlled in the presence of ammonia and thereby, it directed the growth of Co_3O_4 nanocubes under the proposed experimental conditions. In addition, these Co_3O_4 nanocubes acted as nanospacers in preventing the restacking of rGO sheets. The Co_3O_4 nanocubes could strongly attach onto the rGO sheets because of the interaction between Co_3O_4 and rGO through the interfacial Co-O-C bonds (Liang *et al.*, 2011). During the hydrothermal process, the reduction of Au^{3+} ions also occurred, and the Au nanoparticles were deposited on the surface of the Co_3O_4 nanocubes. The schematic illustration of the formation of rGO-Co_3O_4@Au nanocomposite is shown in Figure 5.1.

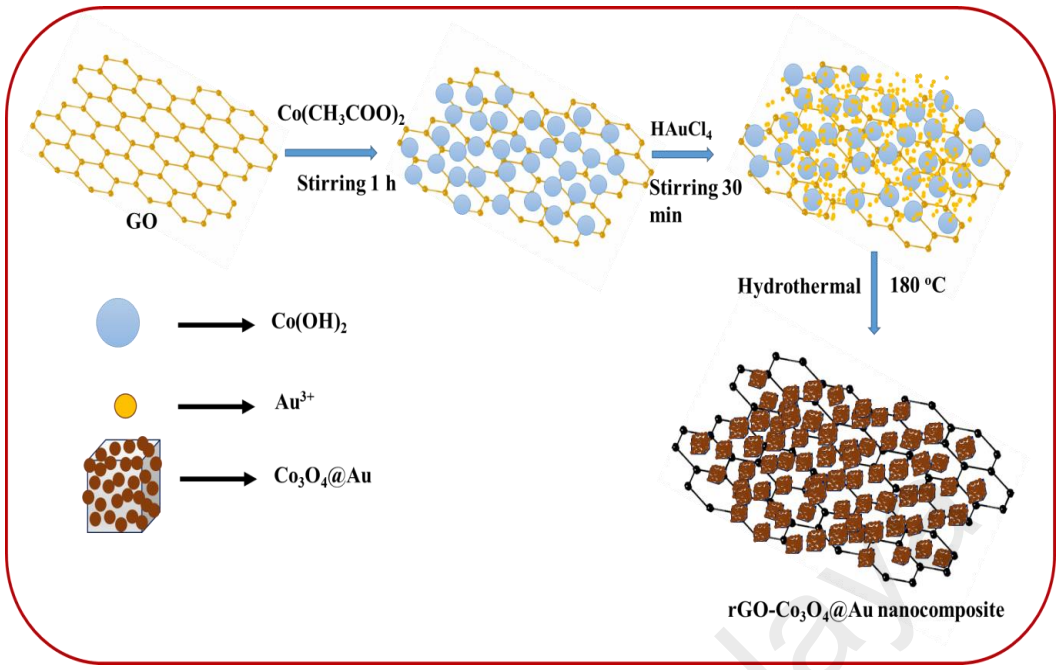

Figure 5.1: Schematic illustration of synthesis of the rGO-Co_3O_4@Au nanocomposite.

The morphology of the rGO-Co_3O_4@Au nanocomposite was studied using the FESEM and HRTEM analyses. Figure 5.2(a & b) displays the FESEM images of the rGO sheets and Co_3O_4 nanocubes. The cubical morphology of the Co_3O_4 nanostructures was retained after the formation of the rGO-Co_3O_4 nanocomposite (Figure 5.2(c)). The rGO sheet prevented the agglomeration of the Co_3O_4 nanocubes and a high population of Co_3O_4 nanocubes was deposited on the rGO sheets. The appearance of the rough surface confirms the formation of the Au nanoparticles on the surface of the Co_3O_4 nanocubes after the formation of the rGO-Co_3O_4@Au nanocomposite (Figure 5.2(d)). From the TEM analysis, a homogeneous dispersion of Co_3O_4@Au nanocubes on the rGO sheets was clearly observed (Figure 5.3). The formation of Au nanoparticles was confirmed from the SPR absorption of Au nanoparticles present in the nanocomposite. Figure 5.3(e) shows the absorption band at 554 nm which corresponds to the SPR feature of the Au nanoparticles. The mean particle size of the Co_3O_4@Au nanocubes was calculated as 35 nm from the FESEM analysis from an observation of 170 particles (Figure 5.3(f)). The *d*-spacing values were calculated from the lattice fringes observed on the surface of the

Co_3O_4@Au nanocubes. On the other hand, the small lattice fringes come under observation belongs to the Au nanoparticles in Figure 5.3(d) with a lattice distance of 0.25 nm corresponding to the Au (1 1 1) plane. This also confirms the formation of Au nanoparticle on the surface of Co_3O_4 nanocubes.

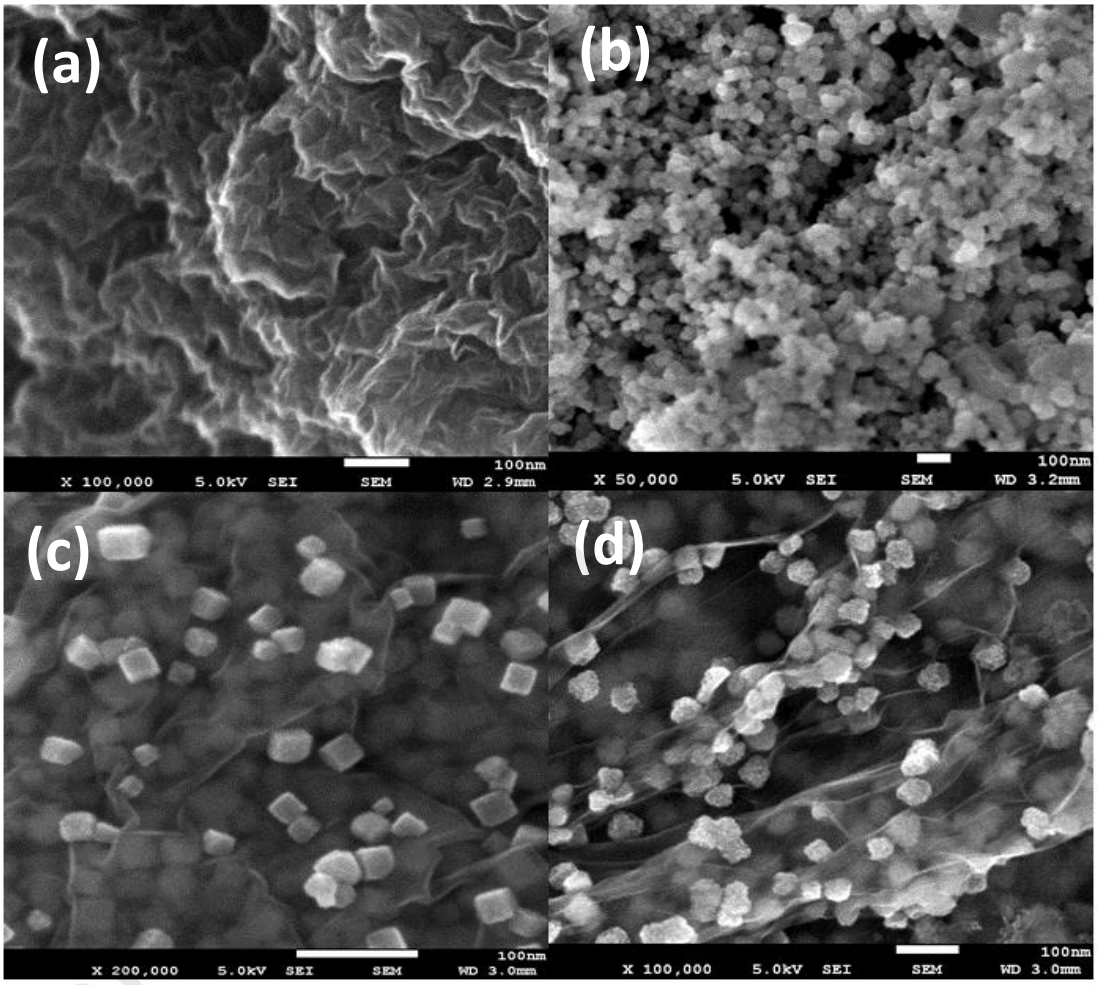

Figure 5.2: FESEM images of (a) rGO sheet, (b) Co_3O_4 nanocubes, (c) rGO-Co_3O_4 nanocomposite and (d) rGO-CO_3O_4@Au (8 mM).

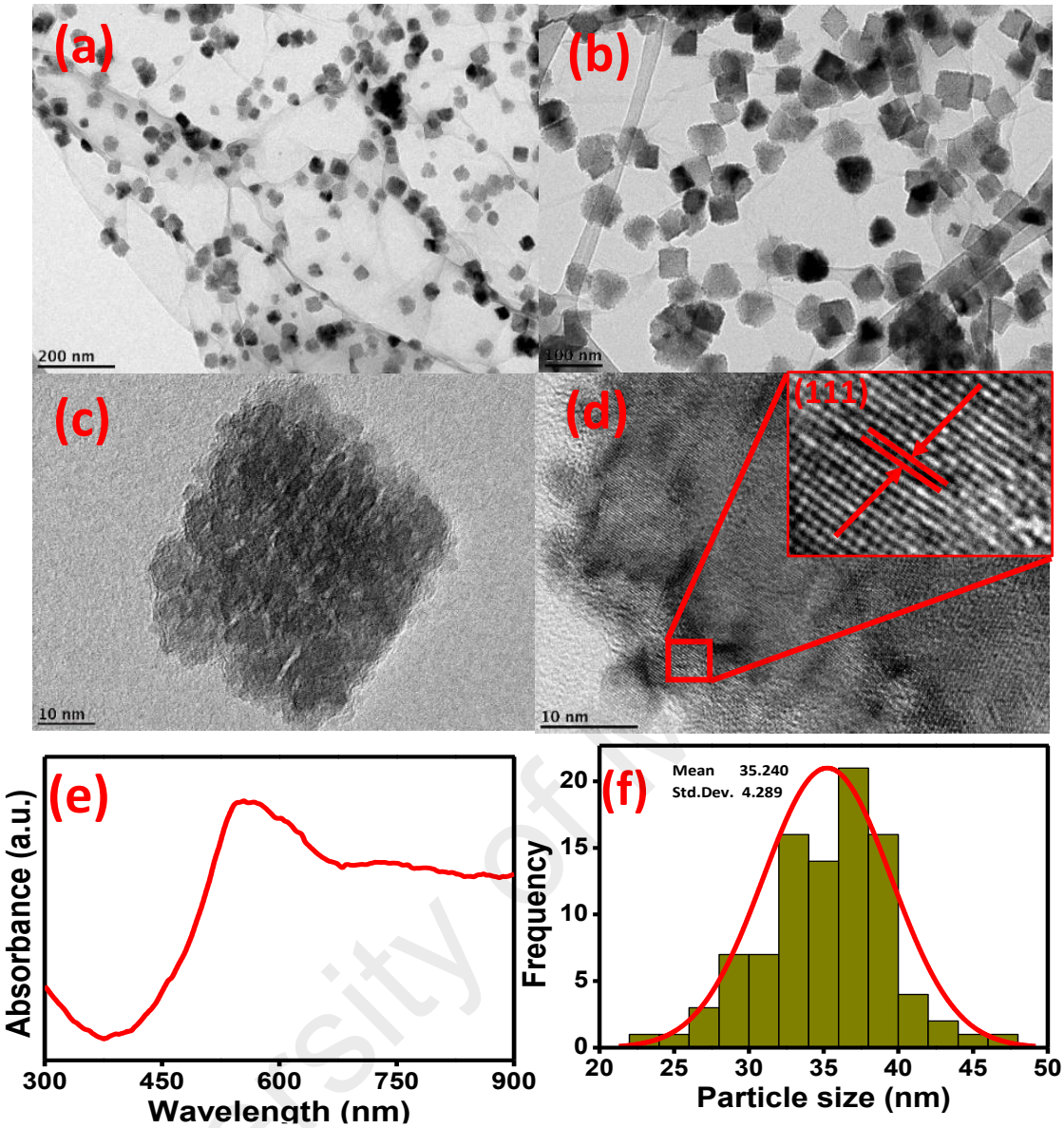

Figure 5.3: (a & b) TEM images of rGO-Co_3O_4@Au (8mM) nanocomposite at different magnifications, (c) single particle of Co_3O_4@Au (8mM), (d) lattice fringes and (e) SPR absorption of Au nanoparticle deposited on Co_3O_4 nanocubes. '(f)' shows the particle size histogram of the Co_3O_4@Au nanocubes.

The distribution of elements present in the rGO-Co_3O_4@Au nanocomposite was studied by EDX elemental mapping analysis (Figure 5.4). The EDX spectrum of the rGO-Co_3O_4@Au nanocomposite showed the signatures of elemental O, Co, C and Au and thereby their confirmed the presence in the nanocomposite (Appendix 6). The elemental peaks of Au have very low intensity due to the very low concentration of Au present in the nanocomposite. Moreover, the wt. % shown in EDX table is in good agreement with the wt. % used for the synthesis of rGO-Co_3O_4@Au. Figure 5.4(a) shows the FESEM image of the nanocomposite and the elements O (black color), Co (green color), C (blue color) and Au (red color) were scanned as shown in the EDX mapping profile of rGO-Co_3O_4@Au nanocomposite (Figure 5.4(b)). The independent elemental O, Co, C and Au distributions are shown in Figure 5.4(c-f) and it displayed a clear distribution of Au nanoparticles on Co_3O_4 nanocubes. The large area coverage of black (Figure 5.4(c)), green (Figure 5.4(d)) and blue (Figure 5.4(f)) colors indicated the dense package of Co_3O_4 nanocubes between the rGO sheets and on the surface of the rGO sheets. Figure 5.4(f) shows the elemental distribution of Au on the surface of Co_3O_4 nanocubes and some area of the image seems to be empty because of the unexposed Co_3O_4@Au nanocubes.

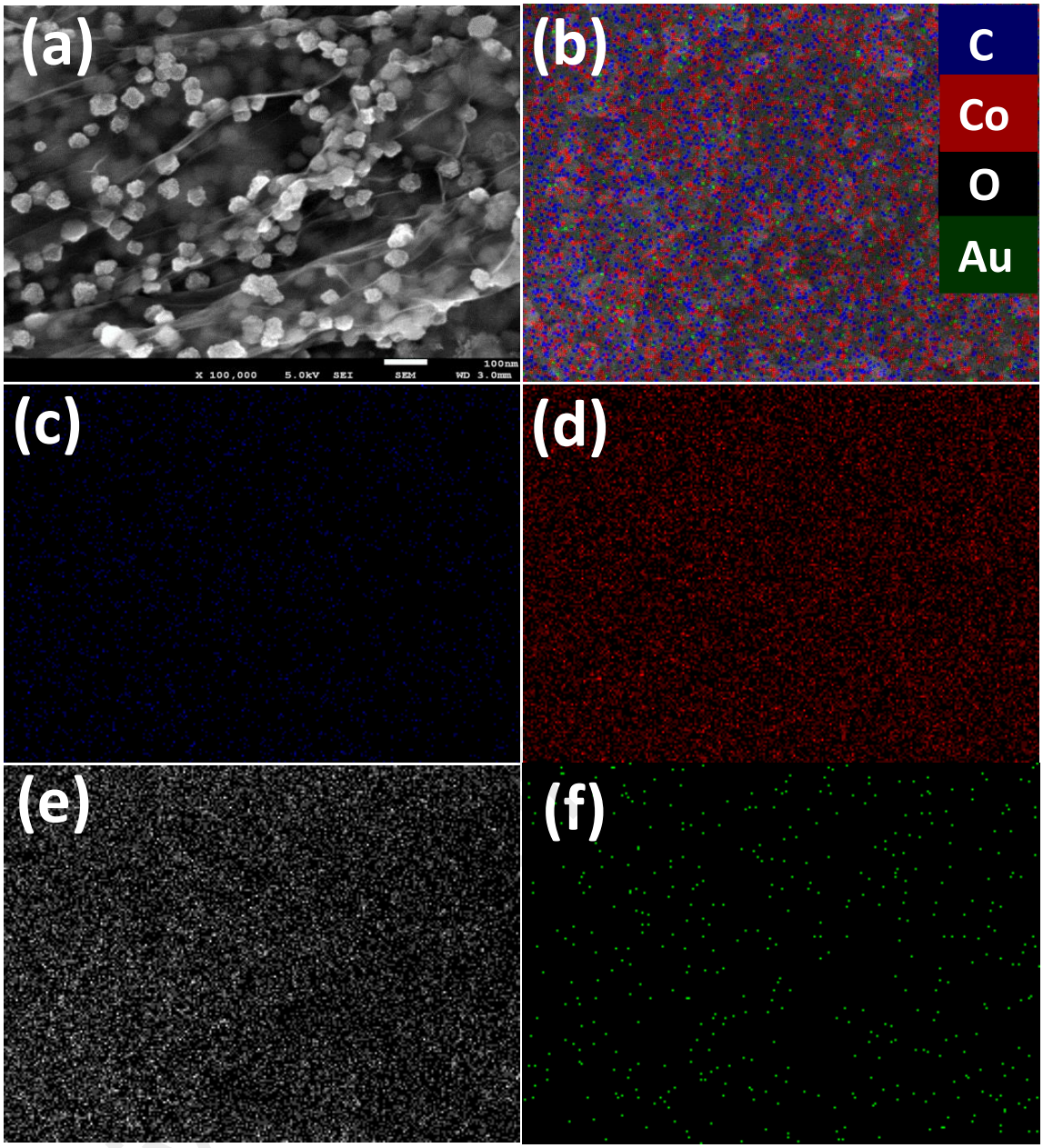

Figure 5.4: (a) FESEM image and (b) EDX elemental mapping of rGO-Co_3O_4@Au (8 mM) nanocomposite: (c) blue, (d) red, (e) black, and (f) green corresponding to the elements C, Co, O, and Au, respectively.

5.3.2 XRD and Raman Analyses

The crystalline nature of the present nanocomposite was studied using XRD analysis. Figure 5.5 depicts the XRD pattern of rGO, Co_3O_4, rGO-Co_3O_4 and rGO-Co_3O_4@Au (8 mM) nanocomposite. The XRD pattern of GO has a sharp and high intensity peak at 2θ value of 10.8 which corresponds to the lattice plane of (0 0 1) before reduction (Appendix 7). The peak was absent after reduction and two more broad peaks

appeared at the 2θ values of 26.0 and 43.1 corresponding to the (0 0 2) and (1 0 0) lattice planes, respectively, thus showed the disorderedly stacking of the rGO in Figure 5.5 (Wang *et al.*, 2008). All the other peaks observed at 31.3°, 36.9°, 44.8°, 55.7°, 59.3°, 65.2°and 77.3° correspond to (2 2 0), (3 1 1), (4 0 0), (4 2 2), (4 4 0), (5 1 1) and (5 3 3) crystal planes of face centered cubic Co_3O_4, respectively (JCPDS Card No. 42-1467) (Wu *et al.*, 2010). There is no peak observed for the rGO due to its very thin and well exfoliated sheets, the Co_3O_4 nanocubes behaves like nanospacers between the different layers of rGO sheets as confirmed by FESEM analysis. This confirms that the Co_3O_4 nanocubes intercalate quiet well and prevents the rGO sheets from restacking after reduction and there is no bulk graphene observed in XRD of rGO-Co_3O_4 (Wu *et al.*, 2010). The XRD pattern recorded for rGO-Co_3O_4@Au (8 mM) nanocomposite in Figure 5.5 showed that the four Au peaks observed at 38.2°, 44.4° ,64.7° and 77.7° which correspond to the Au lattice planes (1 1 1), (2 0 0), (2 2 0) and (3 1 1) have similar 2θ values with Co_3O_4. These Au peaks merged with the Co_3O_4 peaks and it could be seen from the XRD pattern of rGO-Co_3O_4@Au nanocomposites that with the increase in Au contents from 2 mM to 10 mM the Au peaks became more intense in the rGO-Co_3O_4@Au nanocomposites (Appendix 8) (JCPDS 04-0784) (Li *et al.*, 2012). So, the existence of these peaks in the XRD pattern is a further evidence of Au presence/deposition on Co_3O_4 nanocubes, in favor of the FESEM and HRTEM images in Figure 5.2 & 5.3 respectively.

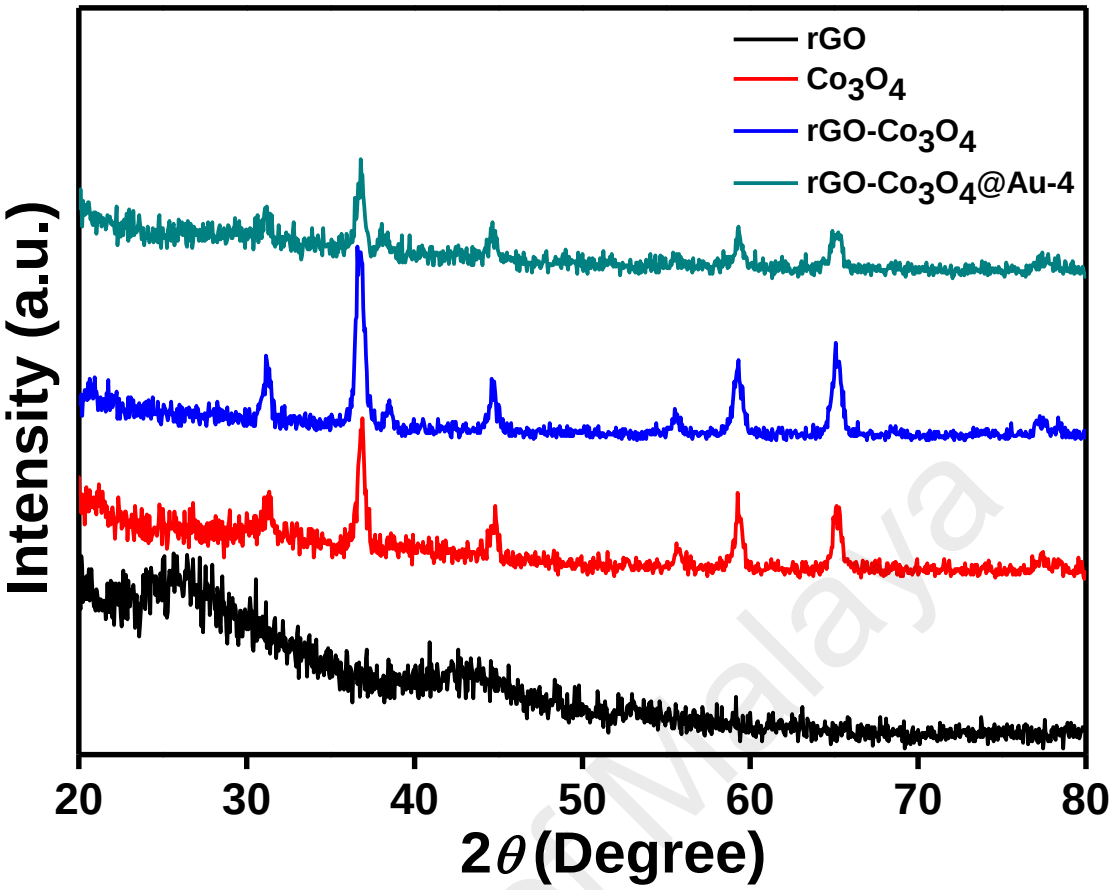

Figure 5.5: XRD patterns of rGO, Co_3O_4, rGO-Co_3O_4 and rGO-Co_3O_4@Au (8 mM) nanocomposites.

Raman spectroscopy is an important conventional tool which is used to characterize the structural changes of carbonaceous materials. Figure 5.6 shows the Raman spectrum of rGO-Co_3O_4@Au (8 mM) nanocomposite. It is can be seen that GO exhibited the *D* (1350 cm^{-1}) mode, related to conversion of sp^2 hybridized carbon to sp^3-hybridized carbon and *G* (1599 cm^{-1}) mode related to vibration of sp^2-hybridized carbon (Figure 5.6 (inset)) (Kang *et al.*, 2009; Li *et al.*, 2010). While the corresponding rGO spectrum with the *D* and *G* bands in Appendix 9 have values of 1352 and 1605 cm^{-1}, respectively. The *D* band to *G* band ratio (I_D/I_G) is 1.07 for rGO which is higher the ratio obtained from GO (I_D/I_G, 0.878). These observations further confirmed the formation of new graphitic domains and successful reduction of GO into rGO after the hydrothermal process (Wang *et al.*, 2010). The Co_3O_4 nanocubes showed characteristic peaks at 192, 476, 518, 614 and 686 cm^{-1} corresponding to F_{2g}, E_g, F_{2g}^2, and A_{1g} modes of the crystalline Co_3O_4 (Kaczmarczyk *et*

al., 2016), respectively, with the D and G bands of rGO confirming the effective formation of the nanocomposite (Figure 5.6). The intensity of the D band is higher than that of the G band of the nanocomposite, which confirmed the reduction of GO during the synthesis of the rGO-Co_3O_4@Au nanocomposite.

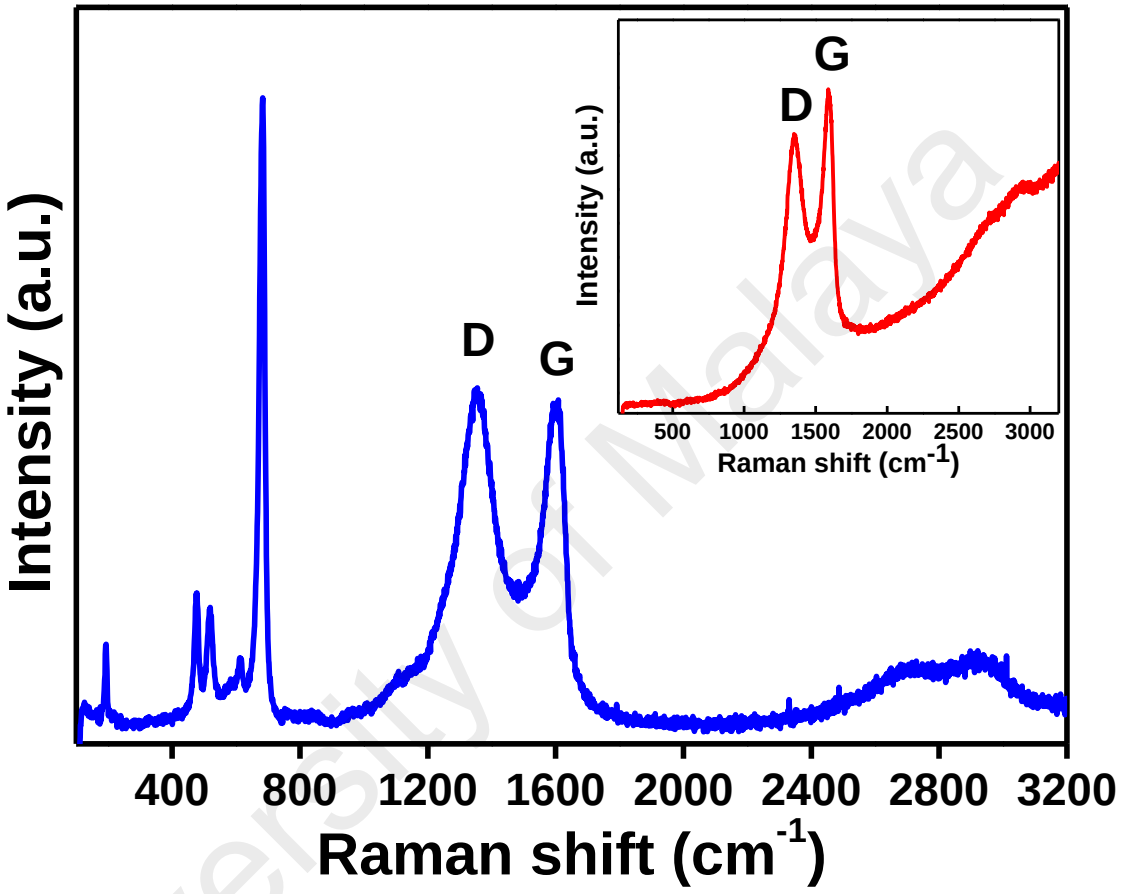

Figure 5.6: Raman spectrum of the rGO-Co_3O_4@Au (8 mM) nanocomposite. Inset shows the Raman spectrum of GO.

5.3.3 Electrocatalytic Oxidation of Hydrazine

The rGO-Co_3O_4@Au nanocomposite was investigated for the electrocatalytic oxidation of hydrazine using CV in 0.1 M phosphate buffer (pH 7.2). Figure 5.7 depicts the cyclic voltammograms corresponding to the oxidation of 0.5 mM of hydrazine at different modified electrodes. The rGO-Co_3O_4@Au nanocomposite shows the oxidation of hydrazine at + 0.079 V with a catalytic current of 29.6 µA (Figure 5.7). No enhanced current response was observed with the rGO-Co_3O_4@Au nanocomposite in the absence

of hydrazine (Figure 5.7). The bare GCE and rGO did not produce faradaic current response from the oxidation of hydrazine (Figure 5.7). However, the cyclic voltammogram of Co_3O_4 nanocubes seems to exhibit the anodic peak of hydrazine oxidation at higher positive potential (Figure 5.7). The hydrazine oxidation was highly facilitated at the rGO-Co_3O_4 nanocubes modified electrode surface and the electrode showed well resolved voltammetric behavior with enormous negative shift in the potential. It showed a catalytic current of 21.57 µA at the peak potential of +0.089 V (Figure 5.7). Graphene is highly conducting platform with higher electron transfer kinetics and it prevents the Co_3O_4 nanocubes from agglomeration (Figure 5.2), so higher electrocatalytic activity is expected due to the synergistic effect of rGO-Co_3O_4 nanocomposite (Shahid *et al.*, 2014). Furthermore, the deposition of very low concentration of Au nanoparticles on the surface of the Co_3O_4 nanocubes improved the electrocatalytic activity of the rGO-Co_3O_4 nanocomposite towards the oxidation of hydrazine. The increase of catalytic current and the decrease of overpotential were attributed to the synergetic effect of the rGO-Co_3O_4 nanocomposite and the highly conductive Au nanoparticles. The surface roughness and increased surface area of the rGO-Co_3O_4@Au nanocomposite also played a crucial role for the enhanced electron transfer process towards the catalytic performance. The cyclic voltammograms were recorded with rGO-Co_3O_4@Au nanocomposite consisting of different concentration of Au (2, 4, 6, 8 and 10 mM) for the electrocatalytic oxidation of hydrazine shown in Appendix 10. It was found that the rGO-Co_3O_4@Au (8 mM) nanocomposite showed the best catalytic response towards the oxidation of hydrazine.

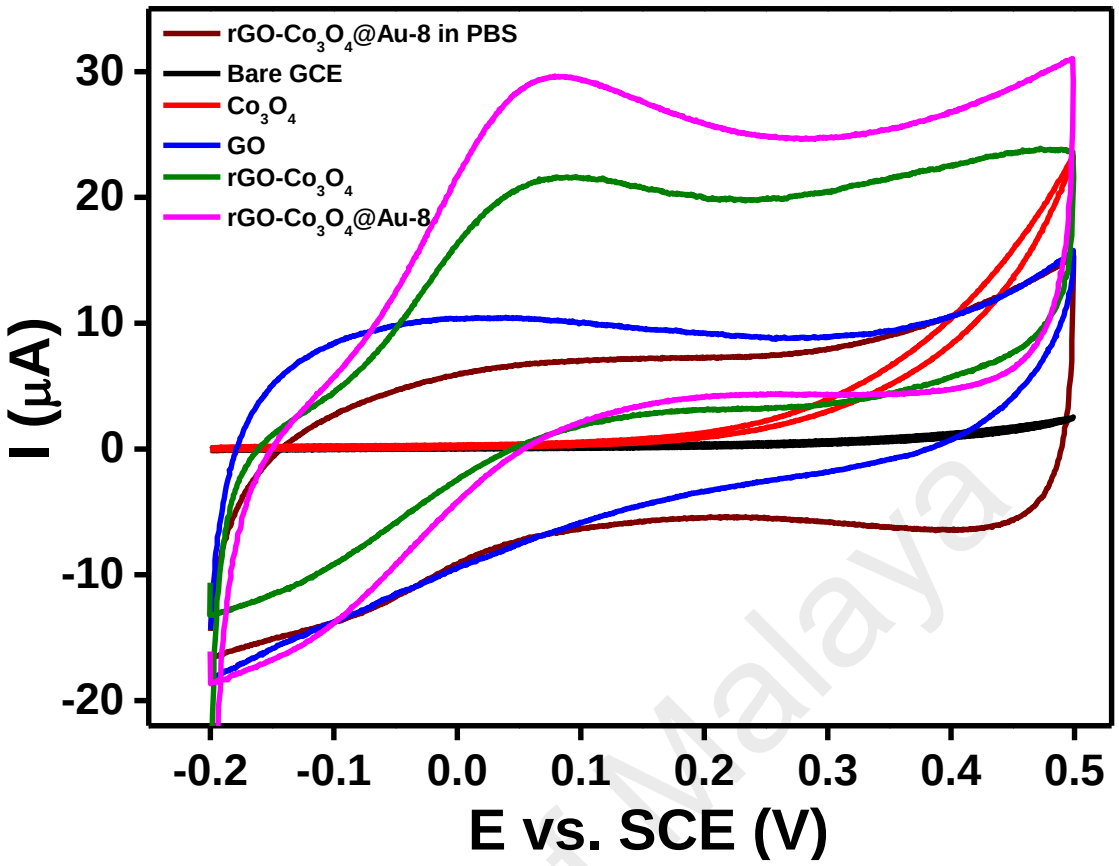

Figure 5.7: Cyclic voltammograms obtained at bare GCE, Co_3O_4 nanocubes, rGO, rGO-Co_3O_4 nanocubes nanocomposite and rGO-Co_3O_4@Au (8 mM) nanocomposite modified electrodes for 0.5 mM of hydrazine in 0.1 M phosphate buffer (pH 7.2) with a scan rate of 50 mV s^{-1}. and cyclic voltammogram of the rGO-Co_3O_4@Au (8 mM) nanocomposite modified electrode without hydrazine.

The influence of concentration was studied at the rGO-Co_3O_4@Au (8mM) modified GCE surface by varying the hydrazine concentration with a scan rate of 50 mV s^{-1} (Figure 5.8(a)). The increase in concentration ranges from 0.5 mM to 5 mM of hydrazine increased the anodic peak current for the oxidation of hydrazine due to the direct electro-oxidation of hydrazine at the rGO-Co_3O_4@Au (8 mM) nanocomposite surface. The plot of peak current versus concentration of hydrazine showed a linear response (Figure 5.8(b)). There was a shift noticed in the peak current toward more positive potential values for hydrazine concentration. The plot in Figure 5.8(b) (inset) showed a linear range with a slope value of 1, the plot of log (I_{pa}) versus log [hydrazine] indicated that the electrooxidation of hydrazine followed the first order kinetics with respect to hydrazine

concentration at the rGO-Co_3O_4@Au (8 mM) nanocomposite modified GC electrode (Figure 5.8(b) (inset)). Cyclic voltammograms were recorded for rGO-Co_3O_4@Au (8 mM) nanocomposite modified GCE for 0.5 mM hydrazine at different scan rates between 10 to 200 mV s^{-1} (Appendix 11(b)). The increase in the current was observed with increasing scan rate and the calibration plot of peak current versus square root of scan rate showed a linear relation in Appendix 11(b). This result indicated that the oxidation of hydrazine was a diffusion controlled process at the rGO-Co_3O_4@Au (8 mM) nanocomposite modified electrode (Tang *et al.*, 2012). Additionally, the CV curves of rGO-Co_3O_4@Au (8 mM) modified GCE showed a peak potential shift towards positive potential with increasing the scan rate. A linear relation between the peak potential (E_{pa}) and log (v) indicated the quasi-reversible oxidation of hydrazine at the nanocomposite modified electrode.

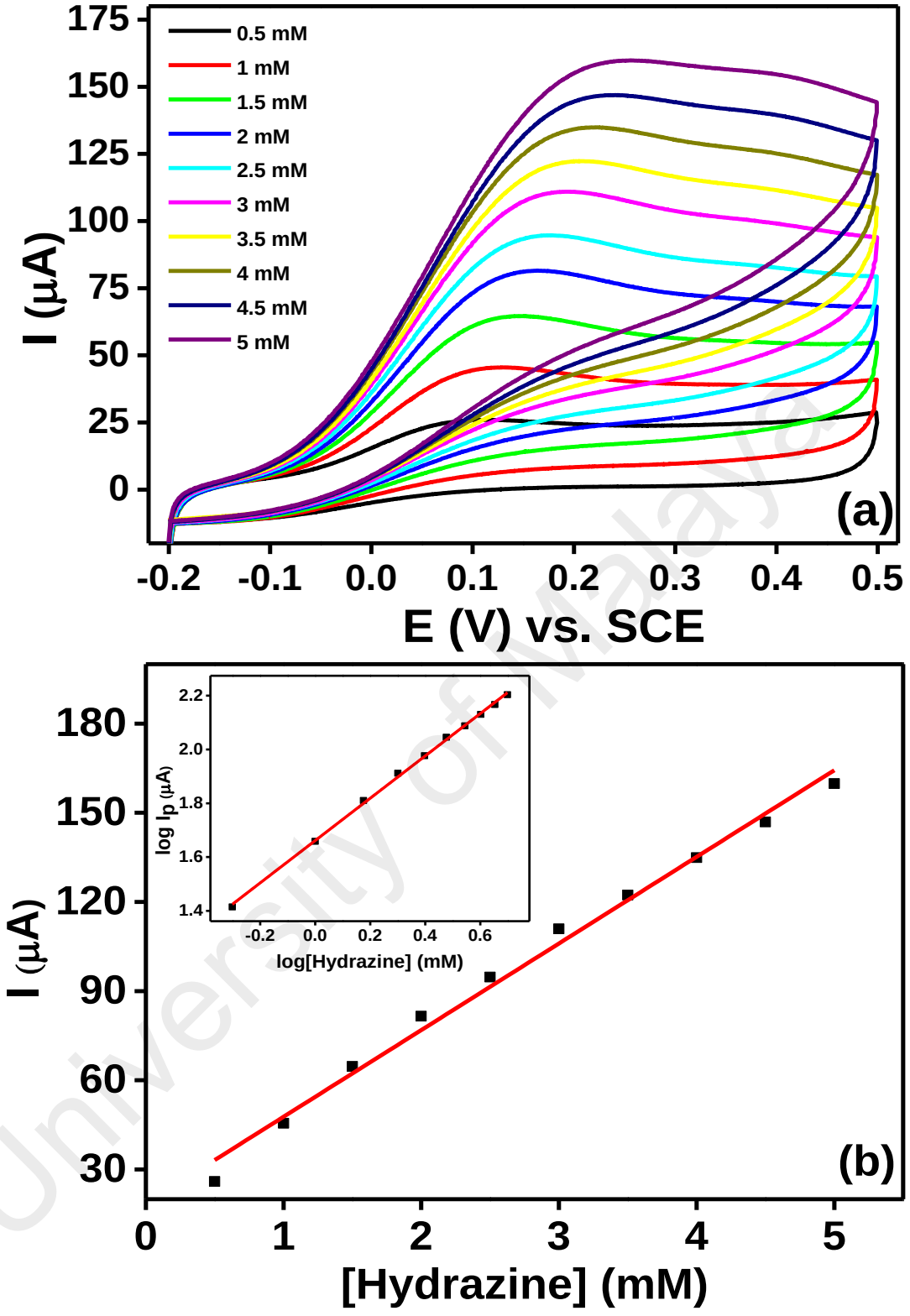

Figure 5.8: (a) Cyclic voltammograms obtained at rGO-Co_3O_4@Au nanocomposite modified electrode during successive addition of different concentrations of hydrazine in 0.1 M phosphate buffer (pH 7.2) with a scan rate of 50 $mV.s^{-1}$. (b) Plot of peak current versus the concentration of hydrazine. Inset shows the plot of log (*Ip*) versus log [hydrazine].

The diffusion coefficient (*D*) of hydrazine during the electrocatalysis was calculated using the Cottrell equation (equation. 5.1).

$$I = nFD^{1/2}\mathrm{A}C_0\pi^{-1/2}t^{-1/2} \quad (5.1)$$

Where *n* is the number of electron involved per hydrazine molecule during oxidation, *F* is the Faraday constant, *A* is the geometric area of the electrode, C_0 is the concentration of hydrazine, and *t* is time. The amperometric *i-t* curves were collected at the nanocomposite modified electrode for the different concentrations of hydrazine (Figure 5.9(a)) and the plot of peak current versus $t^{-1/2}$ showed a linear relation (Figure 5.9(b)). The slopes of the obtained linear lines were plotted against the hydrazine concentrations (Figure 5.9(b) (inset)) and from this plot D was determined to be 0.782×10^{-6} $cm^2.s^{-1}$.

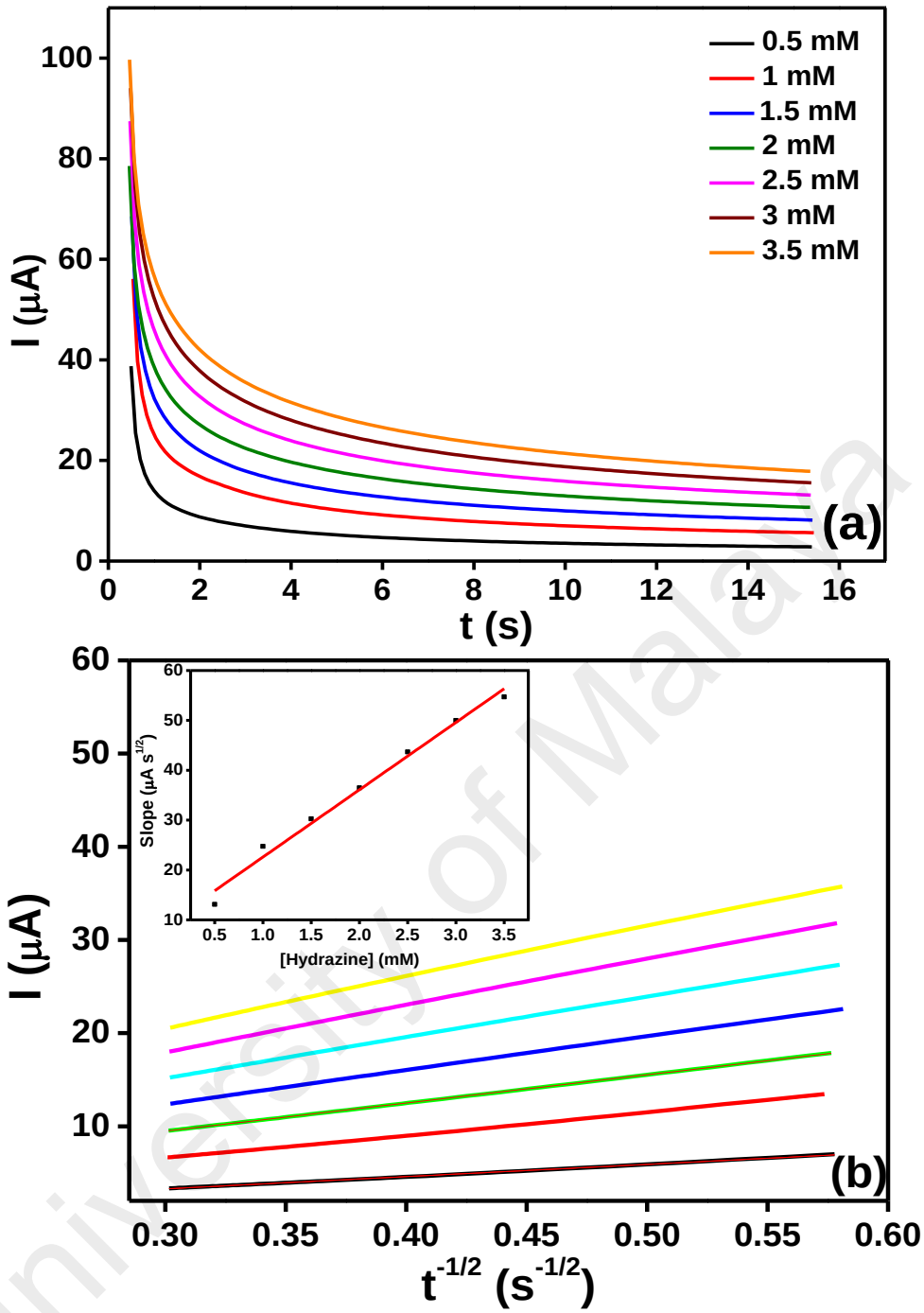

Figure 5.9: (a) Chronoamperograms obtained at rGO-Co_3O_4@Au (8 mM) nanocomposite modified electrode with different concentrations of hydrazine in 0.1 M PBS (pH 7.2). Applied potential was + 0.0179 V. (b) Plot of current versus $t^{-1/2}$ (A). Inset shows the plot of slopes obtained from straight lines versus concentration of hydrazine.

5.3.4 Amperometric Detection of Hydrazine

Chronoamperometry is a convenient technique for the detection of low concentration of analytes and to perform the interference study. Since the rGO-Co_3O_4@Au (8 mM) nanocomposite modified electrode showed higher current response

in the CV, it was used as the amperometric sensor for the detection of hydrazine at low concentration levels. Figure 5.10(a) depicted the amperometric response of the rGO-Co_3O_4@Au (8 mM) nanocomposite for the successive additions of hydrazine at an applied potential of + 0.079 V. The current response was measured from the successive injection of 10 µM and 20 µM concentration of hydrazine at the time interval of 60 s in a continuously stirred 0.1 M phosphate buffer (pH 7.2). The rGO-Co_3O_4@Au (8mM) modified GCE exhibited a significant and quick amperometric response towards each addition of hydrazine. The current reached its steady-state within 3 s indicating the fast electrooxidation of hydrazine at the rGO-Co_3O_4@Au (8 mM) modified GCE surface. The response current increased linearly for each addition of hydrazine over the range between 10 and 740 µM. The corresponding regression plot of current response versus concentration of hydrazine with a linear relation is shown in Figure 5.10(b). The LOD was calculated as 0.443 µM from the expression LOD = 3σ/slope, where, σ is the standard deviation (Devasenathipathy *et al.*, 2014). The sensitivity of the sensor was found to be 0.58304 ± 0.00466 µA μM^{-1} from the slope of the linear regression. Repeated measurements were carried out to check the stability of the sensor and the current responses with negligible decrement were observed at different days. The electrocatalytic activity of the rGO-Co_3O_4 nanocomposite towards the detection of hydrazine was improved by the deposition of minimum amount of Au on the Co_3O_4 nanocubes. The LOD can further be improved by optimizing the rGO content in the nanocomposite because it mainly alters the diffusion layer thickness of the nanocomposite modified electrode.

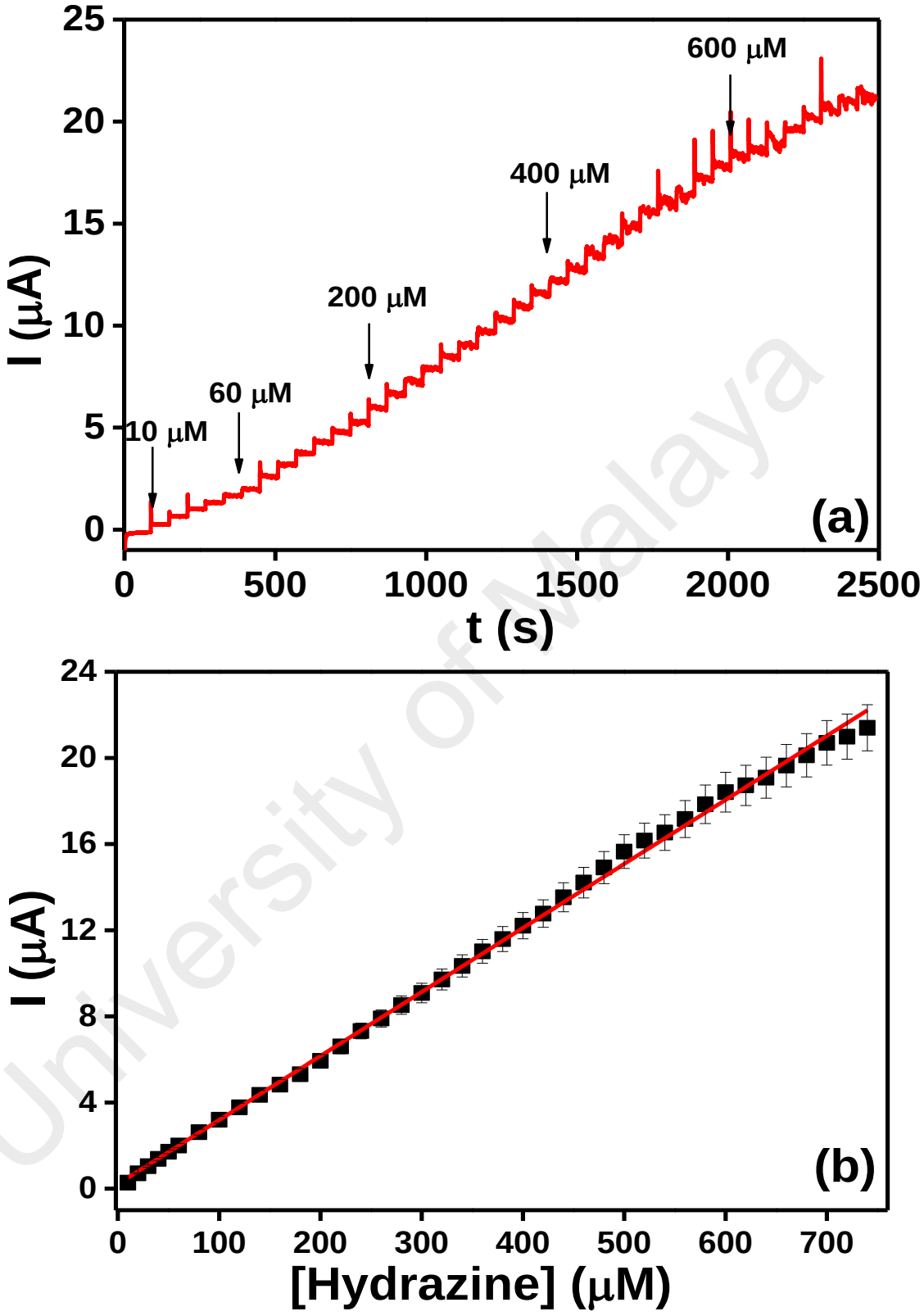

Figure 5.10: (a) Amperometric *i–t* curves obtained at the rGO-Co_3O_4@Au nanocomposite modified GC electrode for the successive addition of hydrazine in phosphate buffer (pH 7.2) at a regular interval of 60 s and (b) corresponding calibration plot of current versus concentration of hydrazine. Applied potential was + 0.079 V.

The selectivity of the rGO-Co_3O_4@Au (8 mM) nanocomposite is an important aspect of the sensor performance. This was assessed by studying the sensor response in the presence of interferents in the same phosphate buffer and the change in current response was monitored. Figure 5.11 shows the amperometric current responses of hydrazine (a) and various interferents such as NO_3^- (b), SO_4^{2-} (c), Cl^- (d), Ag^+ (e), Na^+ (f), K^+ (g), ethanol (h), 4-nitrophenol (i), AA (j) and glucose for studying selectivity of rGO-Co_3O_4@Au (8 mM) nanocomposite. For the first two injections of hydrazine, the nanocomposite behaved efficiently and showed a current response for the hydrazine oxidation. There was no response shown by the rGO-Co_3O_4@Au (8 mM) for the rest of the interferents even at 50-fold higher concentration. Again, for the reconfirmation of selective behavior of rGO-Co_3O_4@Au (8 mM) nanocomposite, hydrazine was injected into homogeneously stirred 0.1 M phosphate buffer and it showed a rapid current response suggesting that the present rGO-Co_3O_4@Au (8 mM) nanocomposite was more selective towards hydrazine oxidation. Moreover, the same magnitude of the current response for the addition of hydrazine was observed and it sustained the steady state current after the 3 s of response time. Two other interferent molecules such as ascorbic acid and glucose were injected after hydrazine and there was no current observed for these molecules. This study revealed the good selectivity of the rGO-Co_3O_4@Au nanocomposite towards hydrazine sensing. Table 1 shows the comparison of analytical performance of the present nanocomposite with other reported nanomaterials. The present work stands for the novel synthesis of the rGO-Co_3O_4@Au nanocomposite using one-pot hydrothermal synthesis and its fast response towards the detection of hydrazine. The proposed modified electrode displayed a satisfactory performance in terms of the detection limit and good selectivity.

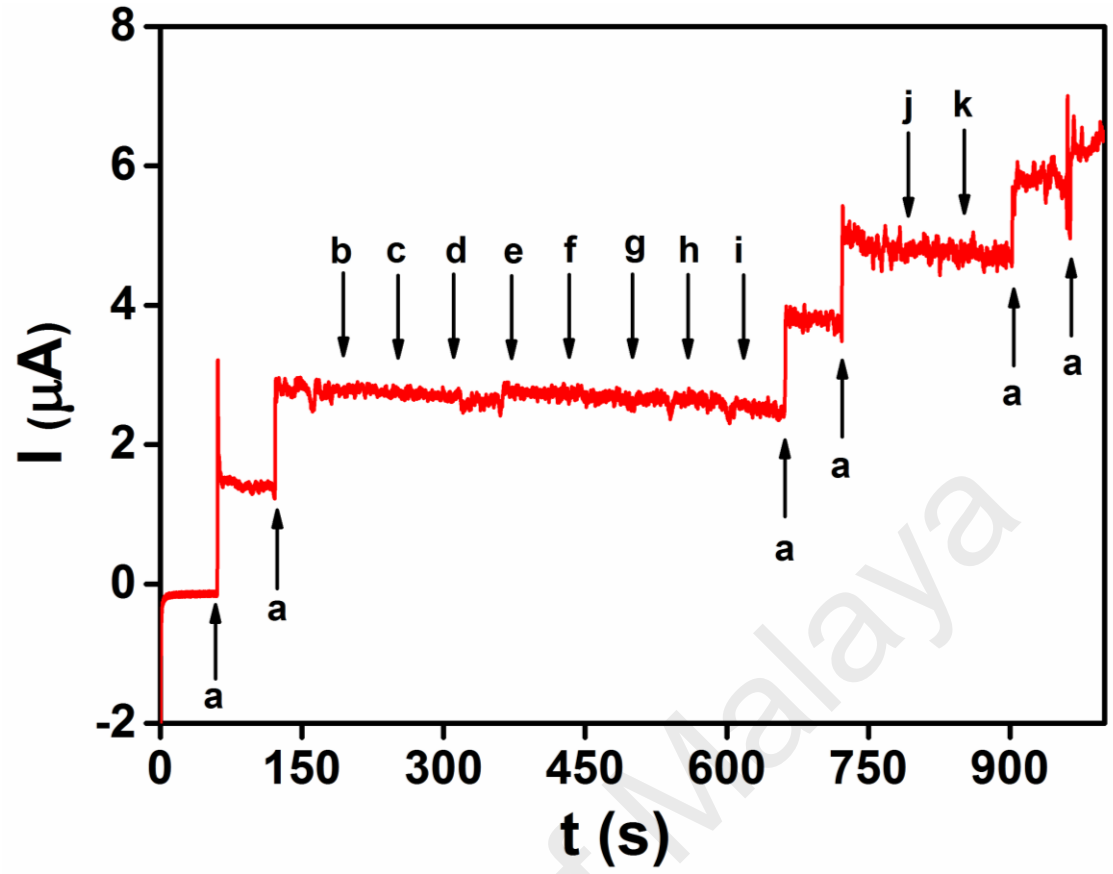

Figure 5.11: Amperometric *i–t* curve obtained at rGO-Co_3O_4@Au nanocomposite modified electrode for the successive addition of 10 µM of hydrazine (a) and each 0.5 mM of NO^{3-} (b), SO42- (c), Cl^- (d) , Ag^+ (e), Na^+ (f), K^+ (g), ethanol (h), 4-nitrophenol (i), ascorbic acid (j) and glucose (k) in phosphate buffer (pH 7.2) at a regular interval of 60 s. Applied potential was + 0.079 V.

Table 5.1: A comparison of some of the reported electrochemical sensors for NO detection.

Sensing material[a]	Electrochemical technique[b]	Linear range (μM)	LOD (μM)	Sensitivity ($\mu A.\mu M^{-1}$)	Reference
Nano-Au/ZnO-MWCNTs/GCE	Amperometry	0.5–1800	0.15	0.0428	(Zhang *et al.*, 2010)
AuPd NCRs	Amperometry	0.10–501	0.02	128.73 & 67.91	(Liu *et al.*, 2016)
Au/SWCNHs/GCE	Amperometry	5–645 & 645–3345	1.1	59.1 & 36.1	(Zhao *et al.*, 2016)
CoHCF-rGO/GCE	Amperometry	0.25–100	0.069	-	(Luo *et al.*, 2015)
AuNP-GPE	SWV Amperometry	25–1000	0.04 3.07	-	(Abdul Aziz *et al.*, 2013)
AuNPs/poly(BCP)/CNT/GCE	LSV	0.5–1000	0.10	-	(Koçak *et al.*, 2014)
Au/PPy/GCE	DPV	1–500 & 500–7500	0.20	126 & 35.6	(Li *et al.*, 2007)
ZrHCF/Au–PtNPs/NFs/GC electrode	Amperometry	0.15–112.5	0.09	-	(Gholivand *et al.*, 2011)
Nano-Au/porous-TiO_2	Amperometry	2.5–500	0.5	0.1722	(Wang *et al.*, 2010)
rGO-Co_3O_4@Au	Amperometry	10-740	0.443	0.5830	This work

[a]AuPd = gold palladium, NRCs = nanorod chains, Au = gold, SWCNHs = single-wall carbon nanohorns, GCE = glassy carbon electrode, CoHCF = cobalt hexacyanoferrate nanocomposite, rGO = reduced graphene oxide, GCE = glassy carbon electrode, AuNP = gold nanoparticle, GPE = graphite pencil electrode, AuNPs = gold nanoparticle, poly(BCP) = Bromocresol purple, CNT = carbon nanotube, GCE = glassy carbon electrode, Au = gold/PPy = polypyrol, GCE = glassy carbon electrode, ZrHCF = zirconium hexacyanoferrate, Au = gold, PtNPs = platinum nanoparticles, NFs = nanofibers, GC = glassy carbon, nano-Au = nano gold, ZnO = zinc oxide, MWCNTs = multi-walled carbon nanotubes, GCE = glassy carbon electrode, Nano-Au = nano gold, Porous-TiO2 = porous titanium dioxide, GCE = glassy carbo electrode, DPV = differential pulse voltammetry; SWV = square wave voltammetry

5.3.5 Application to Real Sample Analysis

To demonstrate the applicability of the present sensor in real sample analysis, the water samples were collected from different places and filtered. The hydrazine stock solution was prepared using real water samples and different concentrations of the sample were spiked into the phosphate buffer. The current response was monitored for the different amounts of hydrazine using amperometry. The measurement results showed the

good recovery of hydrazine for three successive experiments and the experimental results are summarized in Table 5.2.

Table 5.2: Determination of hydrazine in real water samples.

Water sample	Hydrazine added (µM)	Hydrazine found (µM)	RSD (%) (n = 3)	Recovery (%)
Sea water	10	10.30	2.59	103.00
	50	50.06	0.25	100.13
	100	101.33	0.73	101.3
River water	10	10.01	0.22	100.12
	50	50.11	0.92	100.23
	100	102.89	0.38	102.89
Lake water	10	10.01	0.09	100.17
	50	49.65	0.99	99.31
	100	100.26	0.02	100.26

5.3.6 Conclusions

The rGO-Co_3O_4@Au nanocomposite was successfully synthesized and characterized using techniques such as TEM, EDX mapping, XRD and Raman analyses. The temperature and concentration of ammonia were the crucial factors in controlling the morphology of the Co_3O_4 nanocubes. The cubical morphology of Co_3O_4 was confirmed using FESEM and HRTEM analyses and the uniform distribution of Au nanoparticles on the Co_3O_4 surface was demonstrated using EDX elemental mapping analysis. The rGO-Co_3O_4@Au nanocomposite modified GC electrode was demonstrated as an excellent electrochemical sensor for hydrazine detection using amperometry. It showed the linear range of 10-740 µM and the detection limit of 0.443 µM towards hydrazine detection. The nanocomposite showed good selectivity in the detection of hydrazine in the presence of interferents such as NO_3^- , SO_4^{2-} , Cl^-, Ag^+, Na^+, K^+, ethanol, 4-nitrophenol, AA and glucose. The practical use of the sensor was also explored by spiking known concentrations of hydrazine in different water samples and good recoveries were found.

CHAPTER 6: AN ELECTROCHEMICAL SENSING PLATFORM BASED ON REDUCED GRAPHENE OXIDE-COBALT OXIDE NANOCUBES@PLATINUM NANOCOMPOSITE FOR NITRIC OXIDE DETECTION[3]

6.1 Introduction

Nitric oxide (NO) is one of the smallest and simplest biologically important molecules in nature with distinctive and fascinating chemistry.(Taha, 2003) Ignarro, Furchgott and Murad identified NO as endothelium-derived relaxation factor (EDRF) which is responsible for vasodilation and blood pressure regulation in the nervous and cardiovascular systems of mammalian physiology (Furchgott, 1999; Guix *et al.*, 2005; Guo *et al.*, 2012; Ignarro *et al.*, 1987). NO plays extremely important physiological roles as an endogenously-produced antimicrobial agent, (Fang, 1997) as a signaling molecule capable of modulating cytokine production (Schwentker *et al.*, 2002) and also, it plays a key role in wound healing (Luo *et al.*, 2005) and in immune response (Bogdan, 2001). The multi-tasking NO is actually produced endogenously by a class of heme-containing enzymes called nitric oxide synthases (Hetrick *et al.*, 2009; Moncada *et al.*, 1993). Due to the extensive interest in NO from a biochemical and a medical perspective, it is vitally important to monitor the concentration level of NO in physiological system very closely. The concentration of NO varies in the human body from sub-nanomolar to micromolar levels (Privett *et al.*, 2010). Some parameters are very important for the effective detection of NO such as adequate sensitivity, fast response time, wide dynamic range and high selectivity toward NO over the interfering species. Due to the irresistible complexity

[3] This chapter has been published Shahid, M. M., Rameshkumar, P., Pandikumar, A., Lim, H. N., Ng, Y. H., & Huang, N. M. (2015). An electrochemical sensing platform based on a reduced graphene oxide–cobalt oxide nanocube@ platinum nanocomposite for nitric oxide detection. *Journal of Materials Chemistry A*, *3*(27), 14458-14468.

of biological systems, these parameters are often challenging. Besides all the mentioned challenges, the chemical properties of NO make the detection very complex. Fortunately, some analytical techniques including spectroscopic and electrochemical methods are often used for the detection of NO. Among the various methods, electrochemical method is an efficient analytical technique to detect NO because of its long term high calibration stability, fast response, good sensitivity, better selectivity and simplicity(Bedioui *et al.*, 2003).

In recent years, constructing a competent electrochemical sensor is highly pursued among researchers for the sensitive detection of NO. Recently, efforts have been made to increase the sensitivity of the electrochemical detection of NO by engineering the electrode with functional nanomaterials (Privett *et al.*, 2010; Wang *et al.*, 2005). Different type of nanomaterials including single-walled carbon nanotubes (SWCNTs) (Li *et al.*, 2006), multi-walled carbon nanotubes (MWCNTs) (Wu *et al.*, 2002), nano-alumina (He *et al.*, 2009), Nafion-nickel (II) porphyrin film (Malinski *et al.*, 1992) and gold nanoparticles (Thangavel *et al.*, 2008) etc. have been previously used for the detection of NO. Graphene based nanocomposite materials as electrochemical sensors have also been reported for the detection of NO (Jayabal *et al.*, 2014; Li *et al.*, 2011; Wang *et al.*, 2014). Graphene is a two dimensional carbon sheet having single atom thickness, large theoretical surface area (2630 m^2 g^{-1}) with high conductivity at room temperature (10^6 s cm^{-1}) and wide electrochemical window (Chang *et al.*, 2013; Zhu *et al.*, 2010). Graphene nanosheet is an excellent host material for growing nanomaterials for high performance electrochemical applications (Kim *et al.*, 2009; Zhou *et al.*, 2010). To date, a large number of graphene based nanocomposite materials has been synthesized for different applications such as energy storage (Mahmood *et al.*, 2014), biosensor (Karuppiah *et al.*, 2014) and electrocatlaytic (Choi *et al.*, 2012) applications etc. A number of reports on metals, metal oxides and semiconductor nanoparticles grown on graphene nanosheets and

various electrocatalytic applications have been reported (Guo *et al.*, 2009; Kou *et al.*, 2011; Qu *et al.*, 2011; Wu *et al.*, 2010). Among the transition metal oxides, cobalt oxide (Co_3O_4) gathered the attention of many researchers due to its high surface area to volume ratio, high ratio of surface atoms, good chemical stability and it is expected to meet the requirements of future energy applications (Lu *et al.*, 2010). Owing these properties, unaided Co_3O_4 nanoparticles have been used in many reports for variety of applications (Chen *et al.*, 2013; Farhadi *et al.*, 2014; Farhadi *et al.*, 2013; Mu *et al.*, 2013). However, only few attempts have been made to synthesize graphene-cobalt oxide nanocomposite and used for electrocatalytic applications (Karuppiah *et al.*, 2014); (Pan *et al.*, 2013; Xiao *et al.*, 2013). For the synthesis of graphene-metal oxide nanocomposites, hydrothermal synthesis is highly preferred because an appropriate amount of powdered reagents and water are placed in a Teflon-lined autoclave and heated without stirring from moderate to high temperatures and pressures for the desired time, with the possibility of predicting the optimum reaction conditions by electrolyte thermodynamics (Lencka *et al.*, 2000).

In this work, the electrochemical sensing platform based on one-pot hydrothermally synthesized rGO-Co_3O_4@Pt nanocomposite for the detection of in-situ generated NO was investigated. The formation of rGO-Co_3O_4@Pt nanocomposite was confirmed by FESEM, EDX mapping, XRD and Raman analyses. The rGO-Co_3O_4@Pt nanocomposite modified GC electrode displayed better catalytic performance toward the oxidation of NO compared to the other controlled modified electrode investigated in this work. The detection of lower concentration of NO was studied using amperometric *i-t* curve technique and the LOD was 1.73 µM with a signal-to-noise (S/N) ratio ~ 3. The use of lower concentration of Pt improved the sensitivity of the rGO-Co_3O_4@Pt nanocomposite modified electrode. Moreover, the nanocomposite modified electrode was stable, reproducible and showed an excellent selectivity toward the detection of NO in the presence of 100-fold higher concentration of other physiologically important interferents.

6.2 Experimental Methods

6.2.1 Materials

Graphite flakes was purchased from Asbury Inc. (USA). Potassium permanganate ($KMnO_4$, >99 %), sulphuric acid (H_2SO_4, 98 %), hydrochloric acid (HCl, 35 %), and ammonia solution (NH_3, 25 %) were received from R & M Chemicals. Cobalt acetate tetrahydrate ($Co(CH_3COO)_2.4H_2O$) and potassium tetrachloroplatinate (II) (K_2PtCl_4) were obtained from Sigma Aldrich and Acros Organics, respectively. Hydrogen peroxide (H_2O_2) and sodium nitrite ($NaNO_2$) were obtained from Systerm and Merck, respectively. All the chemicals used in this study were of analytical grade. Doubly distilled water was used to prepare the solutions for all the experiments.

6.2.2 Synthesis of rGO-Co_3O_4@Pt Nanocomposite

First, GO was prepared by following the simplified Hummer's method.(Huang *et al.*, 2011) For the preparation of rGO-Co_3O_4@Pt nanocomposite, 12 mL of 1 mmol of $Co(CH_3COO)_2.4H_2O$ solution was mixed with GO solution (8 wt. %) and stirred for 1.5 h to get a homogeneous solution. To this solution, 1 mL of 10 mM K_2PtCl_4 was added slowly with stirring. This was followed by the drop-wise addition of 15 mL of 7.5 % ammonia into the above reaction mixture under vigorous stirring. Then, 75 mL of the reaction mixture was transferred to a 100 mL Teflon-lined stainless steel autoclave for the hydrothermal treatment at 180 °C for 12 h. After the hydrothermal treatment, the precipitate of rGO-Co_3O_4@Pt nanocomposite was washed five times with deionized water and ethanol and dried in a hot air oven at 60 °C. The solid product of the nanocomposite was collected and used for further studies. The synthesis of rGO, Co_3O_4 nanocubes and rGO-Co_3O_4 nanocomposite were followed by using a similar method. For the optimization of GO, rGO-Co_3O_4 nanocomposite was prepared using different amounts of GO (4 and 12 %). The rGO-Co_3O_4 nanocomposite used in this work contains 8 wt. % of GO, unless mentioned otherwise.

6.2.3 Electrochemical Measurements

The rGO-Co_3O_4@Pt nanocomposite modified GC electrode was fabricated by dissolving the nanocomposite in doubly distilled water (1 mg/mL) and 5 μL of the nanocomposite solution was drop-casted on the GC electrode (*d* = 3 mm) surface and allowed to dry at room temperature (25 ^oC) for 2 h. The so fabricated GC was used as a WE. Prior to the modification, the GC electrode was polished with 0.05 micron alumina slurry and cleaned by potential cycling between +1 and -1 V in 0.1 M H_2SO_4 before the experiments. All electrochemical studies were carried out under nitrogen atmosphere using VersaSTAT-3 electrochemical analyser (Princeton Applied Research, USA) with conventional three-electrode system. Platinum (Pt) wire and Ag/AgCl were used as the counter and reference electrodes, respectively. The PBS (pH 2.5) was used as supporting electrolyte and $NaNO_2$ was used as precursor to generate the NO in solution.

6.2.4 Characterization Techniques

Characterization techniques are as mentioned in Section 4.2.4.

6.3 Results and Discussions

6.3.1 Morphological Characterization of rGO-Co_3O_4@Pt Nanocomposite

FESEM analysis was performed to study the morphology of the rGO-Co_3O_4@Pt nanocomposite (Figure 6.1). The FESEM image of rGO (Figure 6.1(a)) shows a sheet like structure and Co_3O_4 appears as cubical nanostructures (Figure 6.1(a)). After the formation of rGO-Co_3O_4 composite, Co_3O_4 nanocubes retained their morphology and are well deposited and distributed on the rGO sheets (Figure 6.1(c)). While some of the Co_3O_4 nanocubes are present in between the rGO sheets and displayed as blurred images, some of the nanocubes are located on the surface of the rGO sheets and exposed as clear images. The morphology of the rGO-Co_3O_4 composite with different concentrations of GO (4 and 12 wt. %) was also evaluated and they also displayed the formation well stabilized cubical

Co_3O_4 nanostructures on the rGO sheets (Appendix 12). The use of ammonia facilitated the precipitation of cobalt ions and the reduction of GO. The Co_3O_4 nanocubes can be strongly anchored onto the rGO matrix due to the interaction between Co_3O_4 and rGO through interfacial Co-O-C bonds formed by the high reactivity of the sp^2 carbon atoms of rGO with electron-rich oxygen species of Co_3O_4 (Nie *et al.*, 2013). During the formation of rGO-Co_3O_4@Pt nanocomposite, Pt nanoparticles are densely decorated on Co_3O_4 without altering the cubical structure of Co_3O_4 and the surface of Co_3O_4 nanocubes became rough after the deposition of Pt (Figure 6.1(d)). Furthermore, it is understood from the FESEM image of the nanocomposite that the rGO sheets prevent the Co_3O_4 nanocubes from agglomeration and Co_3O_4@Pt behaves like a nanospacer between the rGO sheets (Shahid *et al.*, 2014) . The FESEM image of the rGO-Co_3O_4@Pt nanocomposite reveals an efficient decoration of Pt nanoparticles on Co_3O_4 nanocubes in the rGO matrix from the hydrothermal synthesis.

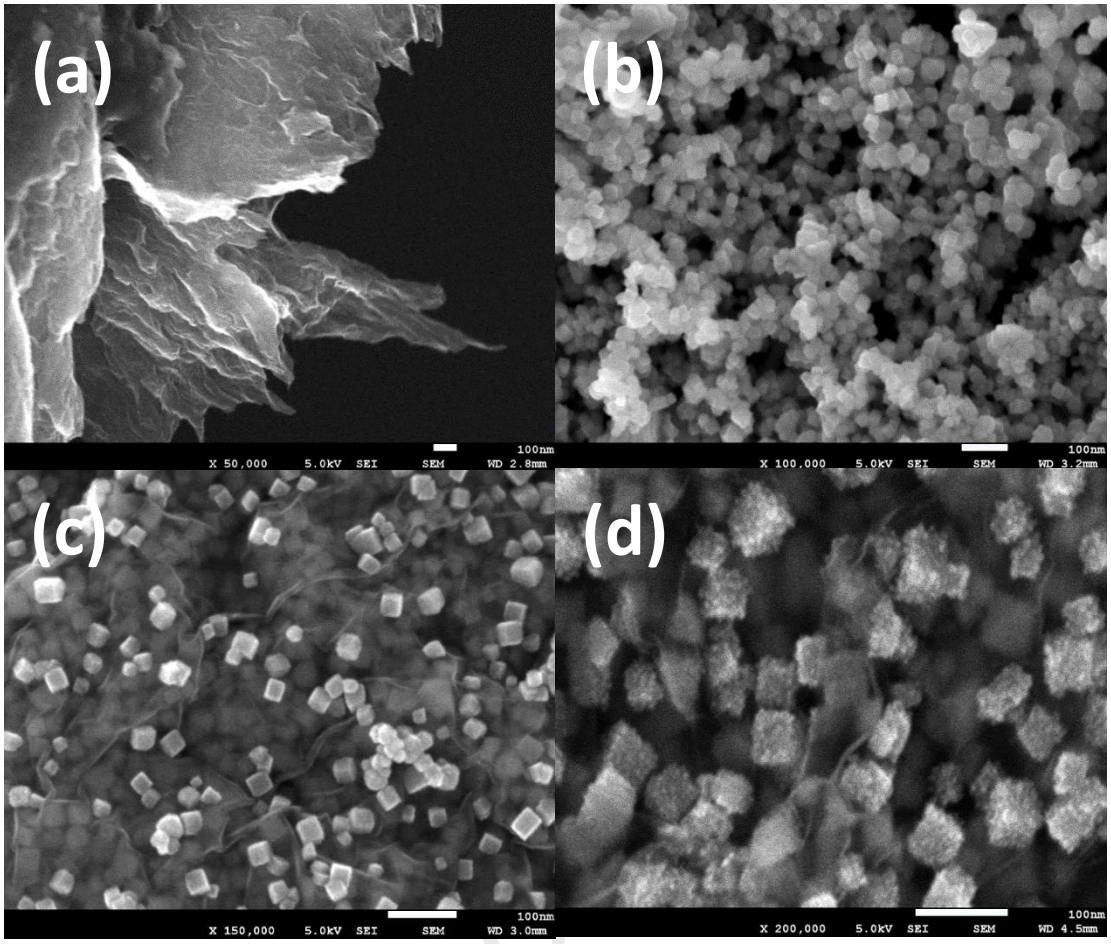

Figure 6.1: FESEM images of (a) rGO sheets, (b) Co_3O_4 nanocubes, (c) rGO-Co_3O_4 nanocomposite and (d) rGO-Co_3O_4@Pt nanocomposite.

The distribution of elements present in the rGO-Co_3O_4@Pt nanocomposite was studied by EDX elemental mapping analysis (Figure 6.2). The EDX spectrum of rGO-Co_3O_4@Pt nanocomposite shows the signatures of elemental O (33.89 wt. %), Co (50.43 wt. %), C (14.74 wt. %) and Pt (0.94 wt. %) and thereby confirms their presence in the nanocomposite (Appendix 13). Figure 6.2(a) shows the FESEM image of the nanocomposite and the elements O (black color), Co (green color), C (blue color) and Pt (red color) were scanned as shown in the EDX mapping profile of rGO-Co_3O_4@Pt nanocomposite (Figure 6.2(b)). The independent elemental O, Co, C and Pt distributions are shown in Figure 6.2(c-f) and it displays a clear distribution of Pt nanoparticles on the Co_3O_4 nanocubes. The large surface coverage of black (Figure 6.2(c)), green (Figure 6.2(d)) and blue (Figure 6.2(e)) colors indicates the dense packing of the Co_3O_4

nanocubes between the rGO sheets and on the surface of the rGO sheets. Figure 6.2(f) shows the elemental distribution of Pt on the surface of Co_3O_4 nanocubes and some area of the image seems to be empty due to the unexposed Co_3O_4@Pt nanocubes.

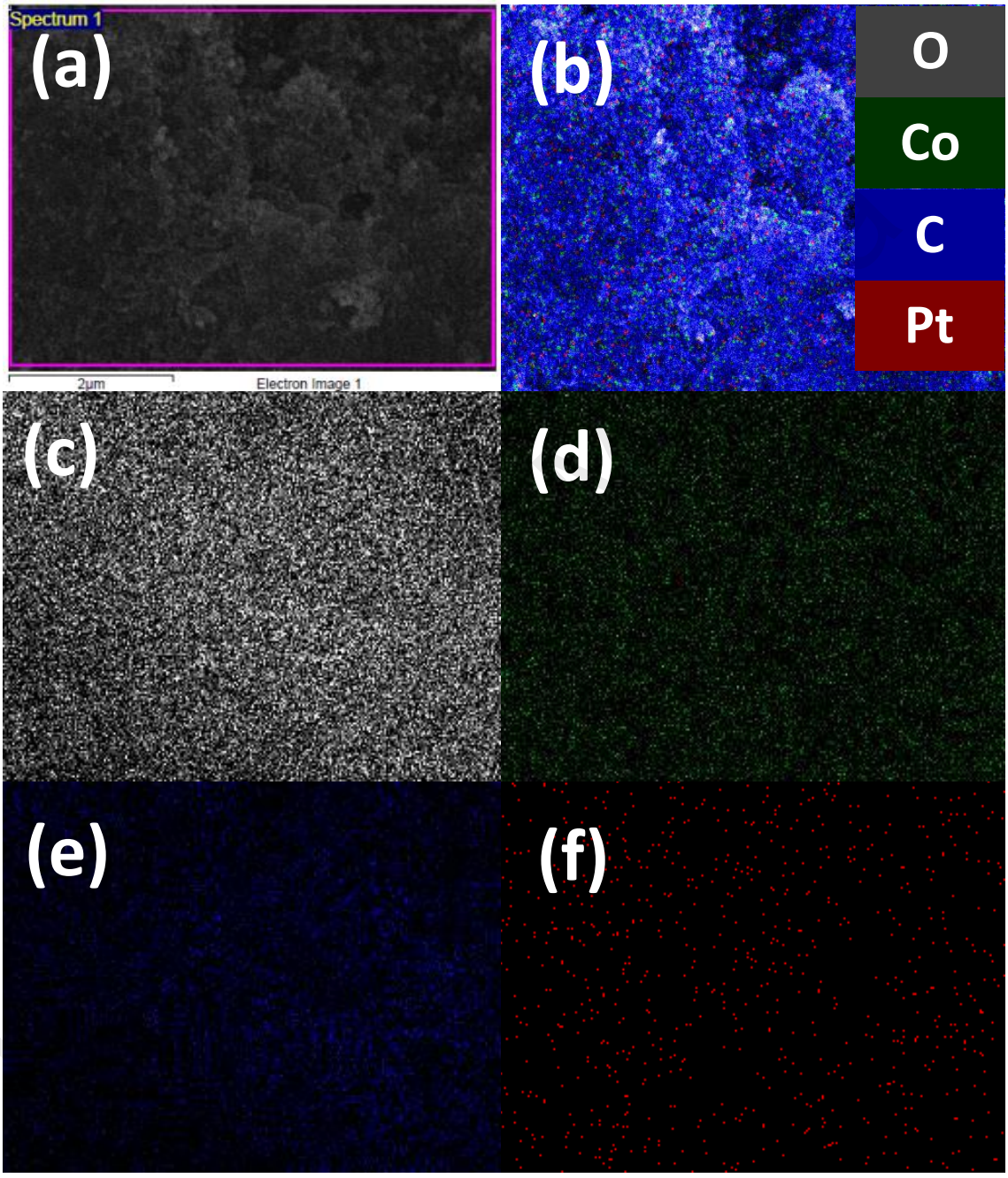

Figure 6.2: FESEM image (a) and EDX elemental mapping (b) of rGO-Co_3O_4@Pt nanocomposite: black (c), green (d), blue (e) and red (f) corresponding to the elements O, Co, C and Pt, respectively.

6.3.2 XRD and Raman analyses

The crystalline nature of the rGO-Co_3O_4@Pt nanocomposite was evaluated by XRD analysis (Figure 6.3). The diffraction peaks observed at 31.2°, 36.8°, 44.7°, 55.5°, 59.2°, 65.1° and 77.2° correspond to the crystal planes of (2 2 0), (3 1 1), (4 0 0), (4 2 2), (4 4 0), (5 1 1) and (5 3 3) of the face centred cubic Co_3O_4 (JCPDS Card No. 42-1467) (Song *et al.*, 2013). The observed 2θ values are in good agreement with the standard database values. The diffraction peaks of Pt nanoparticles might be obscured from the noise and the intense Co_3O_4 diffraction peaks might mask the peaks of Pt since a small amount of Pt was used in the synthesis of rGO-Co_3O_4@Pt nanocomposite. Pt possesses 2θ values of 39.2°, 45.6°, 66.5° and 80.1° corresponding to the (1 1 1), (2 0 0), (2 2 0) and (3 1 1) crystal planes (JCPDS Card No. 88-2343) and these 2θ values are closer to those of Co_3O_4. No distinguishable peak was observed for the carbon diffraction of rGO due to the very thin layer of the rGO sheet.

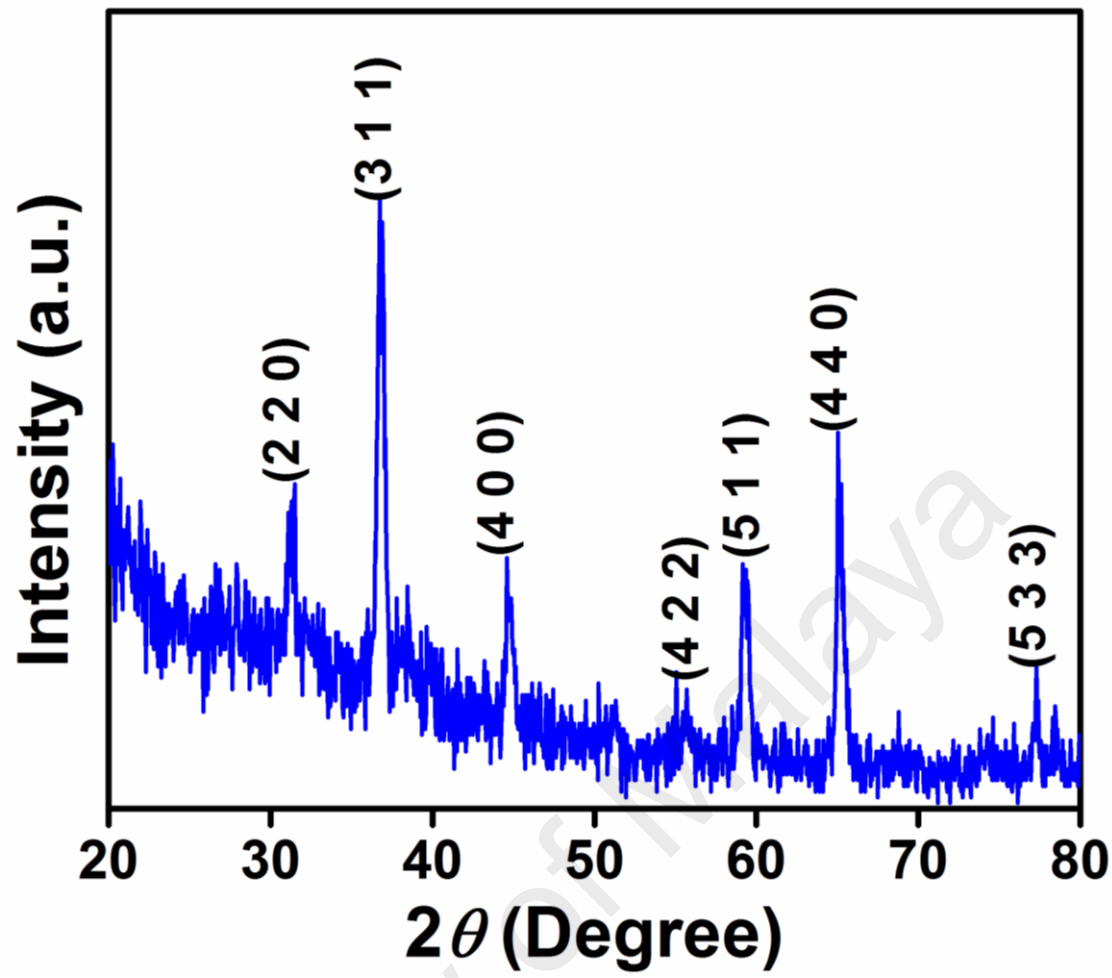

Figure 6.3: XRD pattern of rGO-Co_3O_4@Pt nanocomposite.

Raman spectroscopy is used as a conventional tool to monitor the structural change of graphene-based materials. Figure 6.4 displays the Raman spectra of GO, rGO sheet and rGO-Co_3O_4-Pt nanocomposite. The Raman spectra of both GO (Figure 6.4(a) (inset)) and rGO showed two intense distinguishable peaks at 1356 and 1588 cm^{-1}, corresponding to the *D* and *G* bands, respectively (Figure 6.4(a)). The *D* band is ascribed to the lattice defect induced phonon mode and *G* band refers to the C-C bond expansion or contraction in the hexagonal carbon plane (Li *et al.*, 2014)., (Kim *et al.*, 2014). The degree of disorder and the average size of the in-plane sp^2 domains are specified by the intensity ratio of the *D* to *G* bands (I_D/I_G) (Li *et al.*, 2014). The I_D/I_G of rGO was estimated as 1.02, which is higher than that of GO (0.88), suggesting the formation of partially ordered crystal

structures and the decreased size of in-plane sp^2 domains during the reduction of GO (Li *et al.*, 2014). It is known that *2D* band is valuable to differentiate the monolayer from the multi-layer sheets in graphene based material. It can be seen that there is a slight increase in the *2D* band intensity in the rGO than the GO, which suggests the formation of exfoliated rGO sheets from the densed multilayer GO sheets. The Raman spectrum of rGO-Co_3O_4@Pt nanocomposite retained almost the same value of I_D/I_G for the rGO with the *2D* peak (Figure 6.4(b)). The peaks at 476, 522, 616 and 683 cm^{-1} are attributed to the E_g, F^1_{2g}, F^2_{2g} and A_{1g} modes of Co_3O_4, respectively (Figure 6.4(b) (inset)) (Kim *et al.*, 2011; Liu *et al.*, 2007).

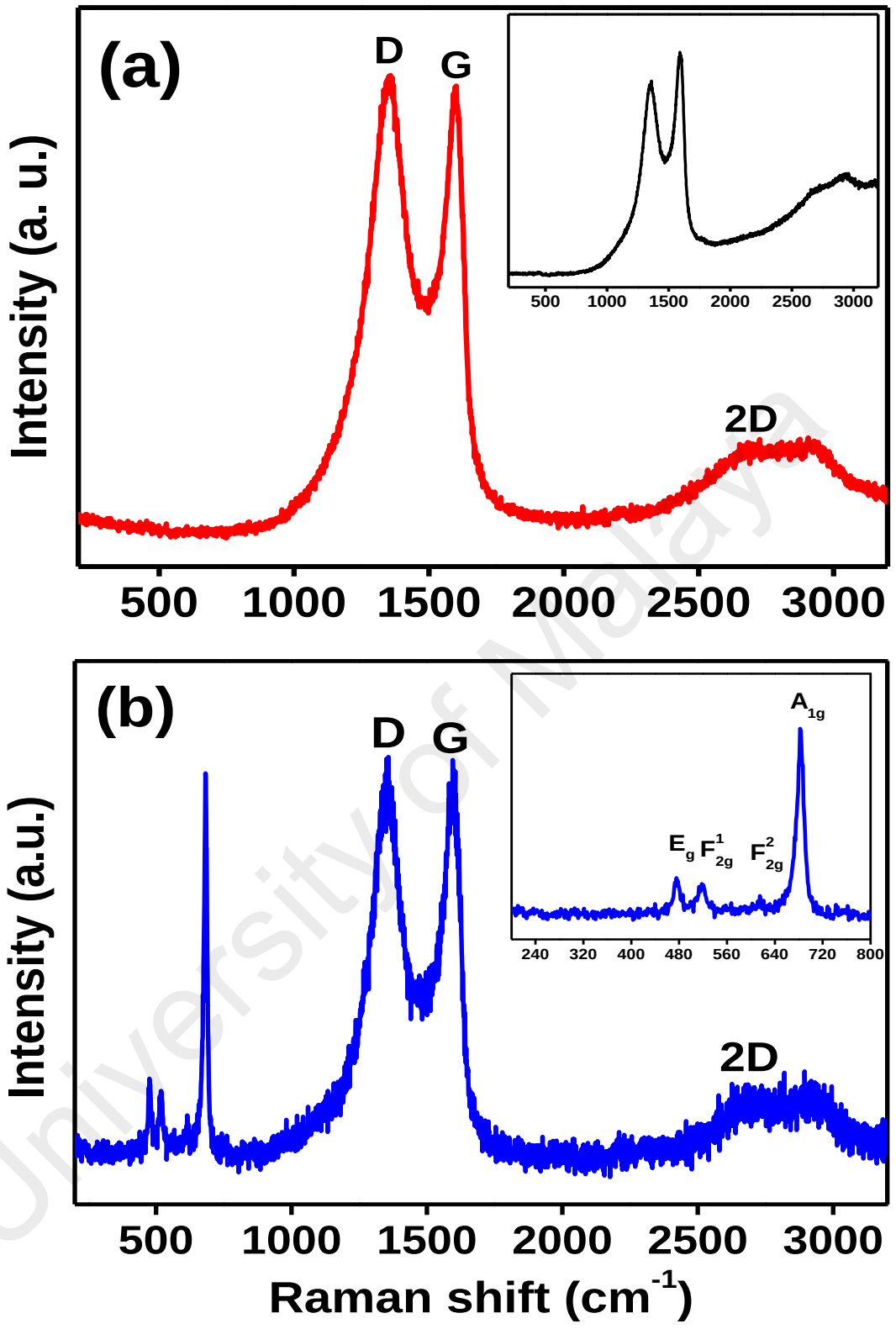

Figure 6.4: (a) Raman spectra of the rGO sheet (Inset: Raman spectrum of GO sheet) and (b) rGO-Co_3O_4@Pt nanocomposite (Inset: expanded view of Raman modes of Co_3O_4.

6.3.3 Electrochemistry of the Redox Marker $[Fe(CN)_6]^{3-/4-}$ and Electrochemical Impedance Spectroscopy Analysis

The redox behavior of $[Fe(CN)_6]^{3-/4-}$ couple is a valuable tool to study the kinetic barrier of the electrode-solution interface since the electron-transfer between the electroactive species in solution and the electrode surface occurs by tunneling of electrons, either through the barrier or through the defects or pinholes present in the barrier (Jia *et al.*, 2002). Figure 6.5 explains the comparison of cyclic voltammetric responses obtained at the bare GC, Co_3O_4 nanocubes, rGO, rGO-Co_3O_4 nanocomposite and rGO-Co_3O_4@Pt nanocomposite modified electrodes for 1 mM $K_3[Fe(CN)_6]$ in 0.1 M KCl at a scan rate of 50 mV s^{-1}. The bare GC electrode shows a reversible votammetric characteristic for the one electron redox process of $[Fe(CN)_6]^{3-/4-}$ couple, with the peak-to-peak separation of 63 mV and an oxidative peak area of 24.016 µC at a scan rate of 50 mV s^{-1}. The Co_3O_4 nanocubes modified electrode shows enhanced redox peak currents with oxidative peak area of 27.176 µC when compared to bare GC. This is due to the higher electrical conductivity of the rGO sheets where the electron transfer kinetics was more facilitated at the rGO modified electrode, thus showed a higher peak current with oxidative peak area of 20.046 µC. The occurrence of a facile electron transfer process at the rGO-Co_3O_4 nanocomposite modified electrode surface is responsible for the enhanced peak current with oxidative peak area of 27.640 µC, compared to the Co_3O_4 nanocubes and rGO modified electrodes. The rGO-Co_3O_4@Pt nanocomposite modified electrode retained the reversible voltammetric response for the $[Fe(CN)_6]^{3-/4-}$ couple and showed higher redox peak currents with an oxidative peak area of 31.884 µC, among the modified electrodes investigated in this work. The redox peak current of rGO-Co_3O_4 nanocomposite was further enhanced by the presence of Pt nanoparticles in the rGO-Co_3O_4@Pt nanocomposite modified electrode. This observation clearly reveals that the rGO-Co_3O_4@Pt nanocomposite acts as a new electrode surface with increased electrode

area and Co_3O_4@Pt has good electrical communication with the underlying electrode surface through the rGO nanosheets.

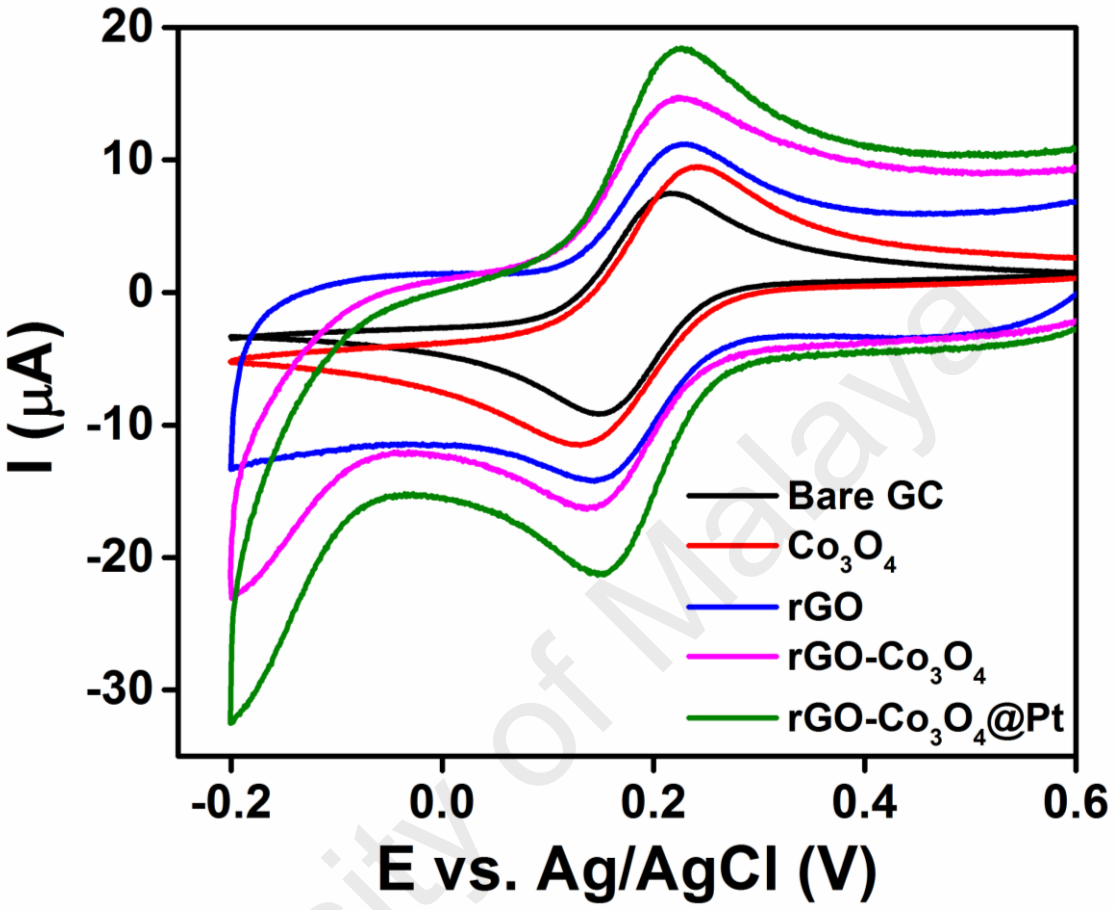

Figure 6.5: Cyclic voltammograms obtained for bare GC, Co_3O_4 nanocubes, rGO, rGO-Co_3O_4 nanocomposite and rGO-Co_3O_4@Pt nanocomposite modified GC electrodes for 1 mM $K_3[Fe(CN)_6]$ in 0.1 M KCl at a scan rate of 50 mV.s^{-1}.

The interfacial properties of surface-modified electrodes were studied by the electrochemical impedance spectroscopy (EIS) (Rubio-Retama *et al.*, 2006). The $[Fe(CN)_6]^{3-/4-}$ couple was used as a redox analyte to study the conducting behavior of the rGO-Co_3O_4@Pt nanocomposite modified electrode. The Nyquist diagram of the complex impedance represents the imaginary versus the real part of the impedance. The semicircle at higher frequencies corresponds to the electron transfer-limited process while the linear portion at lower frequencies corresponds to the diffusion-limited process (Maduraiveeran *et al.*, 2007). The EIS responses were recorded for 1 mM $[Fe(CN)_6]^{3-/4-}$ in 0.1 M KCl for all the modified electrodes (Figure 6.6). The bare GC electrode showed a semicircle-like

shape Nyquist plot with a large diameter, which suggests the hindrance towards the electron-transfer kinetics at the electrode surface (Figure 6.6(black)). When the electrode was modified with Co_3O_4 nanocubes (Figure 6.6(red)) and rGO (Figure 6.6(blue)), the electron transfer resistance (R_{ct}) values decreased from 38400 Ω to 11300 Ω and from 38400 Ω to 830 Ω, respectively. The rGO-Co_3O_4 nanocomposite modified electrode showed only the linear portion at lower frequencies indicating a diffusion-limited process at the electrode-solution interface (Figure 6.6(pink)). The diffusion-limited process is much more facilitated at the rGO-Co_3O_4@Pt nanocomposite modified electrode due to the conducting behavior of Pt in the nanocomposite (Figure 6.6(green)). A perfect linear portion was observed at lower frequencies for the rGO-Co_3O_4@Pt nanocomposite modified electrode compared to the rGO-Co_3O_4 nanocomposite modified electrode. These results indicate that the rGO-Co_3O_4@Pt nanocomposite was successfully formed and it facilitated a diffusion-limited process at the electrode-solution interface. The Bode-phase plots of the modified electrodes were collected in the frequency range of 0.01–10000 Hz (Appendix 14(a)). The phase peaks appeared at a frequency range of 100–1000 Hz which correspond to the charge-transfer resistance of the modified electrodes. The shifting of the peaks toward the low frequency region of 0.1–100 Hz for the rGO-Co_3O_4 and rGO-Co_3O_4@Pt nanocomposite modified electrodes indicates the fast electron-transfer behavior of the nanocomposites. The conducting nature of Pt present in the rGO-Co_3O_4@Pt nanocomposite modified electrode facilitates the peak shift in the Bode plot. The phase angle of the rGO-Co_3O_4@Pt nanocomposite modified electrode is less than 90° at higher frequencies which suggests that the electrode does not behave like an ideal capacitor (Matemadombo *et al.*, 2007). The Bode impedance plot of rGO-Co_3O_4@Pt nanocomposite modified electrode showed a smaller log *Z* value at a low frequency range of 1-100 Hz in logarithm when compared to the other modified electrodes (Appendix 14(b)).

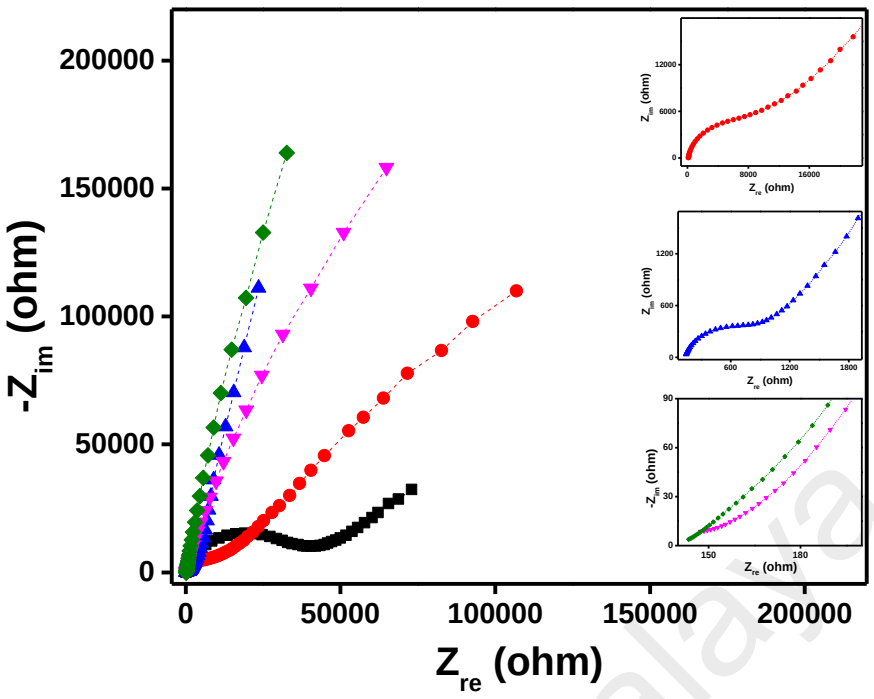

Figure 6.6: Nyquist plots obtained for bare GC (black) Co_3O_4 nanocubes (red), rGO (blue), rGO-Co_3O_4 nanocomposite (pink) and rGO-Co_3O_4@Pt nanocomposite (green) modified GC electrodes for 1 mM $K_3[Fe(CN)_6]$ in 0.1 M KCl. The frequency range was 0.01 Hz to 10 kHz.

6.3.4 Electrocatalysis of Nitric Oxide (NO)

The electrocatlytic oxidation of NO was carried out in 0.1 M PBS (pH 2.5). $NaNO_2$ was used as precursor to produce NO in PBS to study the electrocatalytic activity of the rGO-Co_3O_4@Pt nanocomposite modified electrode. In acidic solution (pH<4), $NaNO_2$ can generate NO by the disproportionation reaction (Equation 6.1) (Thangavel *et al.*, 2008)., (Beltramo *et al.*, 2003). The addition of a known amount of $NaNO_2$ into the bulk electrolyte solution at pH<4 generates a series of concentrations of NO (Thangavel *et al.*, 2008).

$$3HONO \longrightarrow H^+ + 2NO + NO_3^- + H_2O \qquad (6.1)$$

Figure 6.7 displays the cyclic voltammetric responses of the modified electrodes used in this work for the oxidation of NO in 0.1 PBS (pH 2.5) containing 5 mM NO_2^- ions. The rGO-Co_3O_4@Pt nanocomposite modified GC electrode showed catalytic NO oxidation peak at + 0.84 V in 0.1 M PBS containing 5 mM of NO_2^- at a scan rate of 50 mV s^{-1}. However, the nanocomposite modified electrode did not show any voltammetric response

in the absence of NO_2^- (Appendix 15). The Co_3O_4 nanocubes and rGO sheet modified electrodes showed the oxidation peak for NO at almost the same potential (~ + 0.95 V) with smaller difference in the peak current. The rGO-Co_3O_4 nanocomposite modified electrode shifted the oxidation peak potential of NO (+0.87 V) towards less positive potential with a small increment in the peak current. For comparison, the rGO-Pt nanocomposite modified electrode was also fabricated and it showed a peak current of 102 µA at the peak potential of + 0.87 V for NO oxidation. From these results, it can be concluded that the rGO-Co_3O_4@Pt nanocomposite modified electrode displayed a synergistic catalytic effect of the Co_3O_4 nanocubes and Pt nanostructures toward NO oxidation. The Co_3O_4 nanocubes provided a large surface area for Pt deposition and thereby enhanced the electrocatalytic activity of rGO-Co_3O_4@Pt nanocomposite modified electrode. The rGO-Co_3O_4@Pt nanocomposite modified GC electrode efficiently shifted the catalytic peak potential of NO with a peak current of 119 µA, when compared to the other controlled modified electrodes investigated in this work. This reveals that the Pt nanoparticles present in the nanocomposite are in good electrical communication with the rGO-Co_3O_4 which results in an efficient electron-transfer process at the modified electrode toward NO oxidation. The Pt nanoparticles also provide a larger surface area for the effective interaction of NO and thereby improved the electron-transfer kinetics and the electrocatalytic performance. The NO oxidation at the rGO-Co_3O_4@Pt nanocomposite modified electrode possibly proceeds through an electrochemical reaction followed by a chemical reaction (Li *et al.*, 2006). During the electrochemical oxidation of NO, one electron from the NO molecule transfers to the electrode with the formation of the nitrosonium ion (NO^+) (Li *et al.*, 2006). The bare GC electrode also displayed a voltammetric response for the oxidation of NO at +0.94 V with a smaller peak current (79 µA) than the other modified electrodes. The electrocatalytic oxidation of NO was performed using rGO-Co_3O_4 nanocomposite containing different

amounts of GO (4, 8 and 12 wt. % GO) (Appendix 16). The rGO-Co_3O_4 nanocomposite prepared using 8 wt. % GO showed better performance toward the oxidation of NO and the rGO-Co_3O_4@Pt was the preferred nanocomposite. The reproducibility and repeatability of the nanocomposite modified electrode were checked by recording the voltammograms with different electrodes and good reproducible and repeatable results were observed. The stability of the nanocomposite modified electrode was studied for NO oxidation by recording the voltammogram of the same modified electrode after one week and the electrode showed only less than 5 % decrement in the peak current. The modified electrode was stored at room temperature (25 °C) during the period of stability measurements. This infers that the present nanocomposite modified electrode was stable towards the electrocatalytic oxidation of NO.

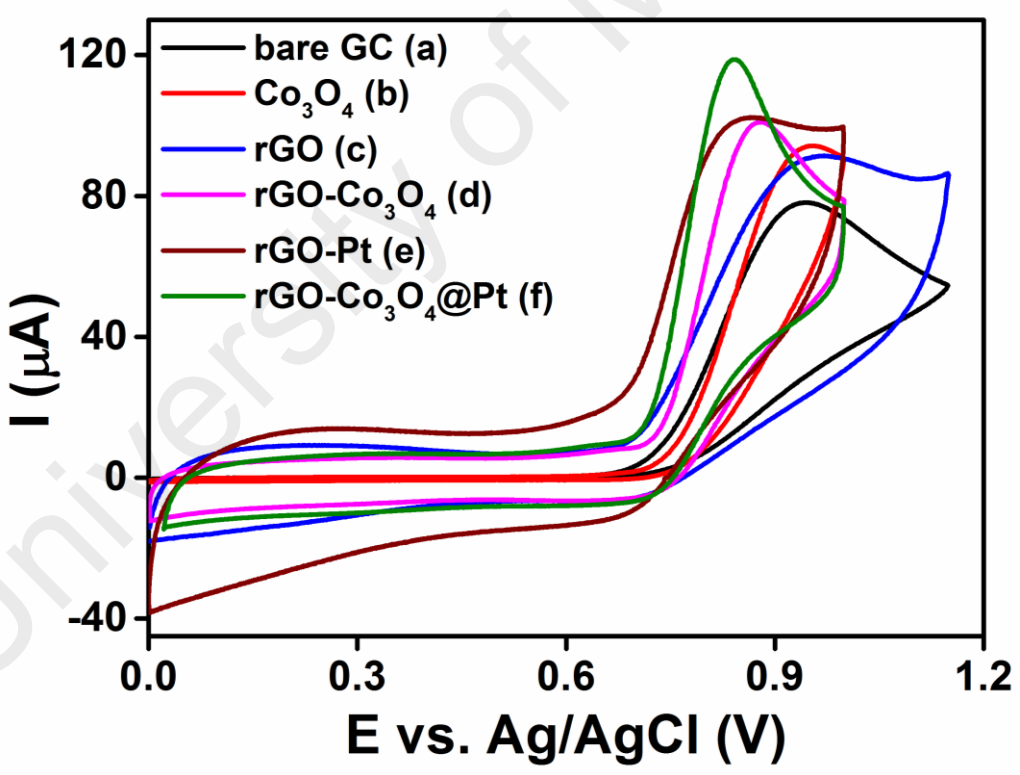

Figure 6.7: Cyclic voltammograms recorded at bare GC, Co_3O_4 nanocubes, rGO, rGO-Co_3O_4 nanocomposite, rGO-Pt nanocomposite and rGO-Co_3O_4@Pt nanocompositen modified electrodes for 5 mM of NO_2^- in 0.1 M PBS (pH 2.5) with a scan rate of 50 mVs^{-1}.

The cyclic voltammograms were recorded at the rGO-Co_3O_4@Pt nanocomposite modified electrode for different concentrations of NO_2^- in 0.1 M PBS (pH 2.5) and the voltammetric curves are displayed in Figure 6.8. The anodic peak current for the oxidation of NO_2^- increased with increasing concentration of NO_2^- and the plot of peak current versus concentration of NO_2^- showed a linear response (Figure 6.8 (inset (a)). The plot of log(I_{pa}) versus log[NO_2^-] showed a linear graph with a slope value approximately equal to 1, which indicates that the electrooxidation of NO follows first order kinetics with respect to NO_2^- concentration at the rGO-Co_3O_4@Pt nanocomposite modified electrode (Figure 6.8(inset b)).

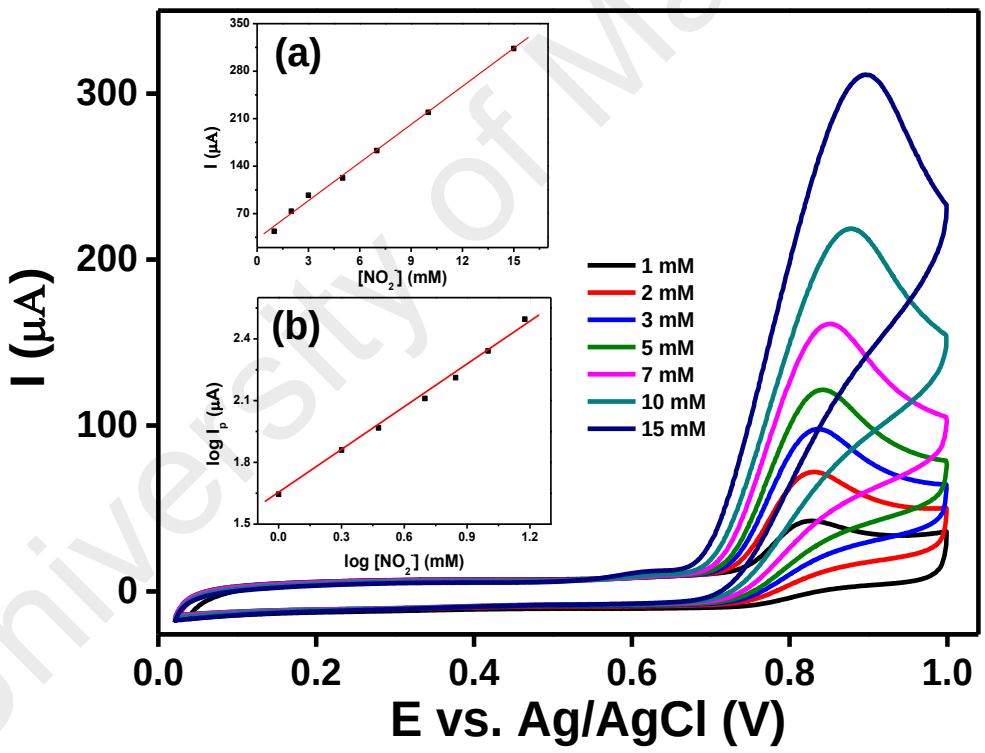

Figure 6.8: Cyclic voltammograms at rGO-Co_3O_4@Pt nanocomposite modified electrode during successive addition of different concentrations of NO_2^- in 0.1 M PBS (pH 2.5) with a scan rate of 50 mV.s^{-1}.

The cyclic voltammograms were recorded for the oxidation of NO at different scan rates and the peak current for NO oxidation was found to be linear with the square root of scan rate ($v^{1/2}$) (Appendix 17(a)). The linear relation indicates that the electrocatalytic

oxidation of NO at the nanocomposite modified electrode is a diffusion controlled process (Rastogi *et al.*, 2014). A gradual increase in the oxidation peak potentials (E_{pa}) with increasing the scan rate (v) indicates the chemical irreversibility of electrocatalytic NO oxidation process at the nanocomposite modified electrode. The quasi-reversible electrooxidation of NO is also supported by the linear relation between peak potential (E_p) and log(v) (Appendix 17(b)) (Zen *et al.*, 2000). The diffusion coefficient (D) of NO was determined for the nanocomposite modified electrode by using Cottrell equation (Equation 6.2).

$$I = nFD^{1/2}\mathrm{A}C_0\pi^{-1/2}t^{-1/2} \qquad (6.2)$$

Where n is the number of electrons transferred per NO molecule during oxidation, F is the Faraday constant, C_0 is the concentration of NO_2^-, A is the geometric area of the electrode and t is time. The chronoamperograms were recorded at the nanocomposite modified electrode for different concentrations of nitrite ions (Appendix 18(a)) and the plot of peak current versus $t^{-1/2}$ showed a linear relationship (Appendix 18(b)). The slopes of the obtained linear lines were plotted against the NO_2^- concentrations (Appendix 18(b)(inset)) and from this plot, D was calculated as 3.8×10^{-5} $cm^2.s^{-1}$.

6.3.5 Amperometric Detection of NO

Amperometric *i-t* curve technique is used as an important analytical tool for the detection of low concentration of analytes and it is a convenient technique to perform the interference study. The sensing ability of the modified electrodes used in this work was investigated one by one, for the successive addition of 1 mM of NO_2^- ions in a homogeneously stirred solution of 0.1 M PBS at a regular time interval of 60 s (Figure 6.9). All the modified electrodes produced current responses for the injection of NO_2^- ions (Figure 6.9(a)) and among them, the rGO-Co_3O_4@Pt modified electrode showed the

highest response for every injection of NO_2^- ions with a good linear range of 1 mM-14 mM (Figure 6.9(b)).

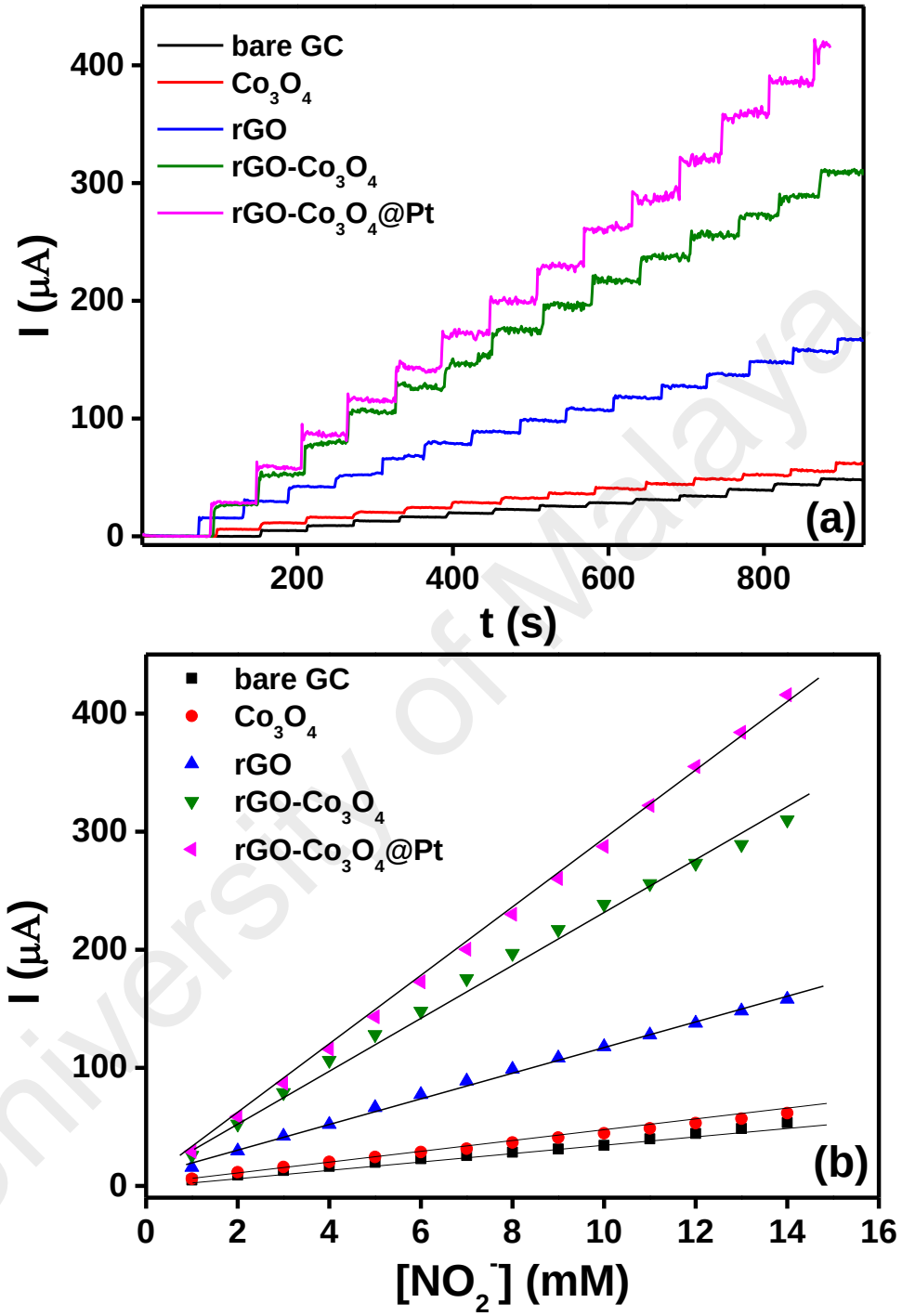

Figure 6.9: (a) Amperometric *i–t* curves obtained at bare GC, Co_3O_4 nanocubes, rGO, rGO-Co_3O_4 nanocomposite and rGO-Co_3O_4@Pt nanocomposite modified GC electrodes for the successive addition of 1 mM NO_2^- in 0.1 M PBS (pH 2.5) at a regular interval of 60 s and (b) corresponding calibration plots of current versus concentration of NO_2^-. Applied potentials were the peak potentials obtained from Figure 6.7.

The presence of Pt nanoparticles on the electrode effectively enhanced the sensing ability of the rGO-Co_3O_4@Pt nanocomposite toward the detection of NO. The rGO-Co_3O_4@Pt nanocomposite was chosen as an electrochemical sensor material for the detection of lower concentration levels of NO in PBS. The amperometric *i-t* curve was obtained at the rGO-Co_3O_4@Pt modified electrode for the successive addition of NO_2^- ions with different concentrations in a homogeneously stirred solution of 0.1 M PBS with an applied potential of +0.84 V (Figure 6.10). For each addition of NO_2^- with a sample interval of 60 s, a significant current response was observed (Figure 6.10(a)) and it suggests that the rGO-Co_3O_4@Pt efficiently promoted the oxidation of NO in 0.1 M PBS (pH 2.5). The plot of current response versus concentration of NO_2^- showed a linear relation for the concentration range of 10 µM to 650 µM (Figure 6.10(b)). Repeated measurements were performed for the detection of NO at lower concentration levels and the current response was reproduced at the nanocomposite modified electrode. The nanocomposite showed the sensitivity of 0.026±0.0002 µA/µM and the LOD was calculated as 1.73 µM for the detection of NO. The comparison of the analytical performance of the present rGO-Co_3O_4@Pt nanocomposite modified GC electrode with some of the reported GC electrode based electrochemical sensors toward the detection of NO is shown in Table 6.1.

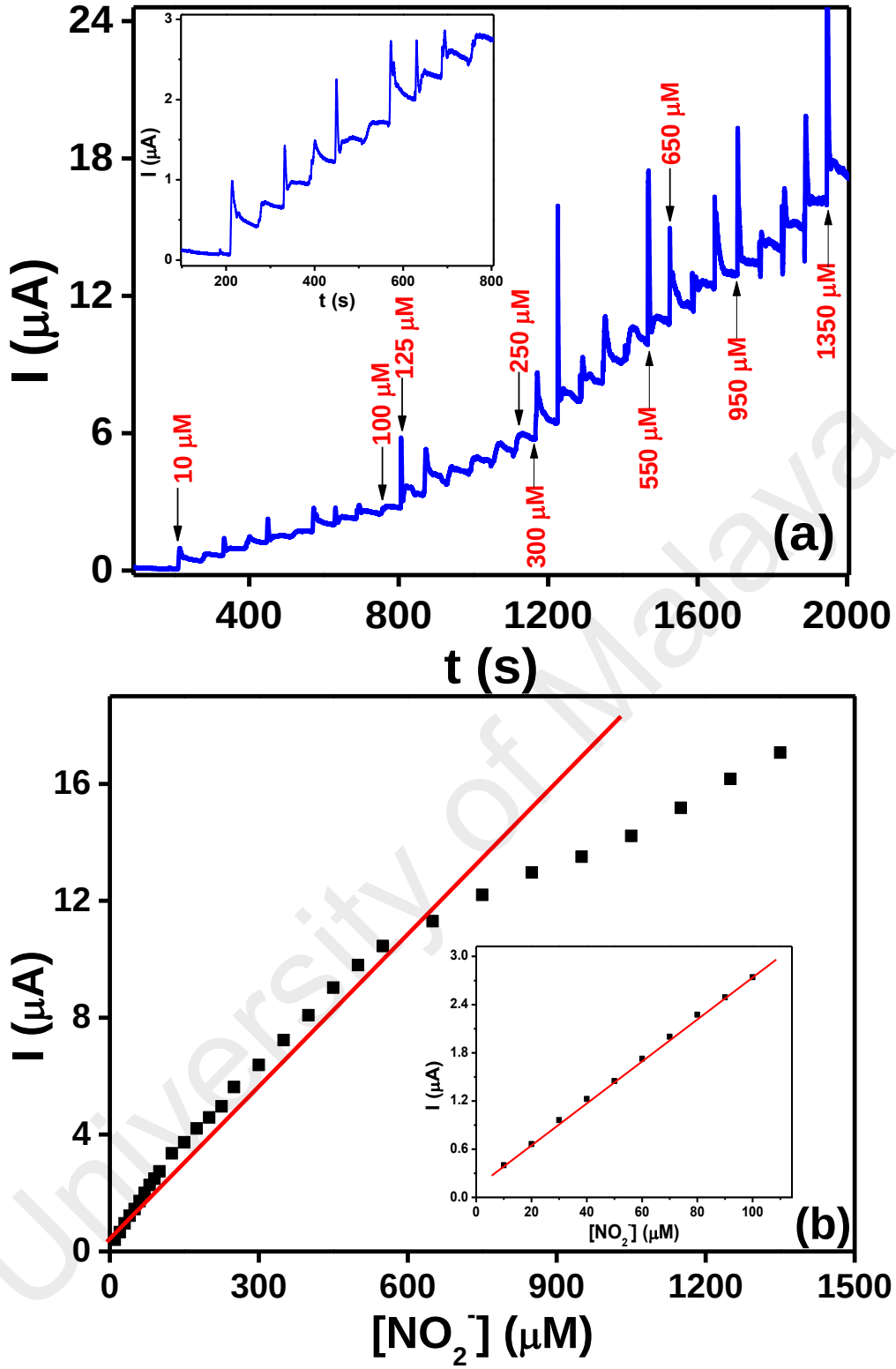

Figure 6.10: (a) Amperometric *i–t* curves obtained at the rGO-Co_3O_4@Pt nanocomposite modified GC electrodes for the successive addition of NO_2^- with various concentrations in 0.1 M PBS (pH 2.5) at a regular interval of 60 s. Inset: expanded view of the i–t curve obtained for the successive addition of 10 µM NO_2^-. The applied potential was +0.84 V. (b) Calibration plot of peak current versus concentration of NO_2^- corresponding to 'A'. Inset: the expanded view of linear calibration plot corresponding to 10 µM NO_2- addition.

Table 6.1: Comparison of some of the reported electrochemical sensors for NO detection.

Modified GC electrode[a]	Technique[b]	Linear range (μM)	LOD (μM)	Reference
GC/PAM/SDS/Cyt c	Amperometry	0.80 μM– 95	0.1	(Chen *et al.*, 2009)
GC/PNMP-b-PGMA/Hb	DPV	0.45 μM–10	0.32	(Jia *et al.*, 2009)
GC/EDAS(TiO_2-Au) nps	SWV	1 μM– 60	1.0	(Pandikumar *et al.*, 2011)
GC/DNA/Cyt c	Amperometry	0.6 μM– 8	0.1	(Liu *et al.*, 2007)
GC/PtNP/AB	Amperometry	0.18 μM– 120	0.05	(Zheng *et al.*, 2012)
GC/AuNP-ERGO	Amperometry	up to 3.38	0.133	(Ting *et al.*, 2013)
GC/SWNT/PVP–Os–EA	Amperometry	0.2 μM– 40	0.05	(Fei *et al.*, 2011)
GC/G-Nf	SWV	50 μM– 450	11.61	(Yusoff *et al.*, 2015)
GC/Hb–CPB/PAM	CV	9.8 μM– 100	9.3	(He *et al.*, 2006)
GC/rGO-Co_3O_4@Pt	Amperometry	10 μM– 650	1.73	Present work

[a] PAM = polyacrylamide; SDS = sodium dodecyl sulfate; Cyt c = cytochrome c; PNMP-b-PGMA = poly [N-(2-methacryloyloxyethyl) pyrrolidone]-blockpoly [glycidyl methacrylate]; Hb = hemoglobin; EDAS = N-[3-(trimethoxysilyl)propyl]ethylene diamine; TiO_2-Au = titanium dioxide-gold nanocomposite; DNA = deoxyribonucleic acid; PtNP = platinum nanoparticle; AB = acetylene black; AuNP = gold nanoparticle; ERGO = electrochemically reduced graphene oxide; SWNT = single-walled carbon nanotube; PVP–Os–EA = Os-bipyridine complex and poly(4-vinylpyridine) (PVP) partially quaternized with 2-bromoethylamine (EA) functionalities; G = graphene; Nf = Nafion; Hb-CPB = hemoglobin-cetylpyridinium bromide. [b] DPV = differential pulse voltammetry; SWV = square wave voltammetry; CV = cyclic voltammetry

The selectivity of the rGO-Co_3O_4@Pt nanocomposite for the detection NO was investigated by injecting various possible physiological interferents in the same homogeneously stirred PBS containing NO and the change in current response was observed. Figure 6.11 explains the continuously recorded amperometric i–t curve response for the successive additions of NO_2^- and interferents in a homogeneously stirred 0.1 M PBS (pH 2.5). The current response of the interferents such as DA, AA and UA was studied by adding them in succession, after the few successive additions of NO_2^- (10

μM) in the same stirred PBS. However, the added interferents did not change the current response even with a 100-fold higher concentration. Again, the injection of NO_2^- in the same solution displayed almost the same magnitude of current response for the oxidation of NO. After few successive additions of NO_2^-, more interferents such as glucose, urea and NaCl were added in succession. The *i-t* curve was recorded with a sampling interval of 60 s and the addition of these interferents did not produce increase in the current response. However, the introduction of 10 μM NO_2^- to the same solution again resulted in a clear and quick response. These results indicated that the present sensor possesses good selectivity and sensitivity towards the determination of NO_2^- even in the presence of 100-fold excess of common physiological interferents.

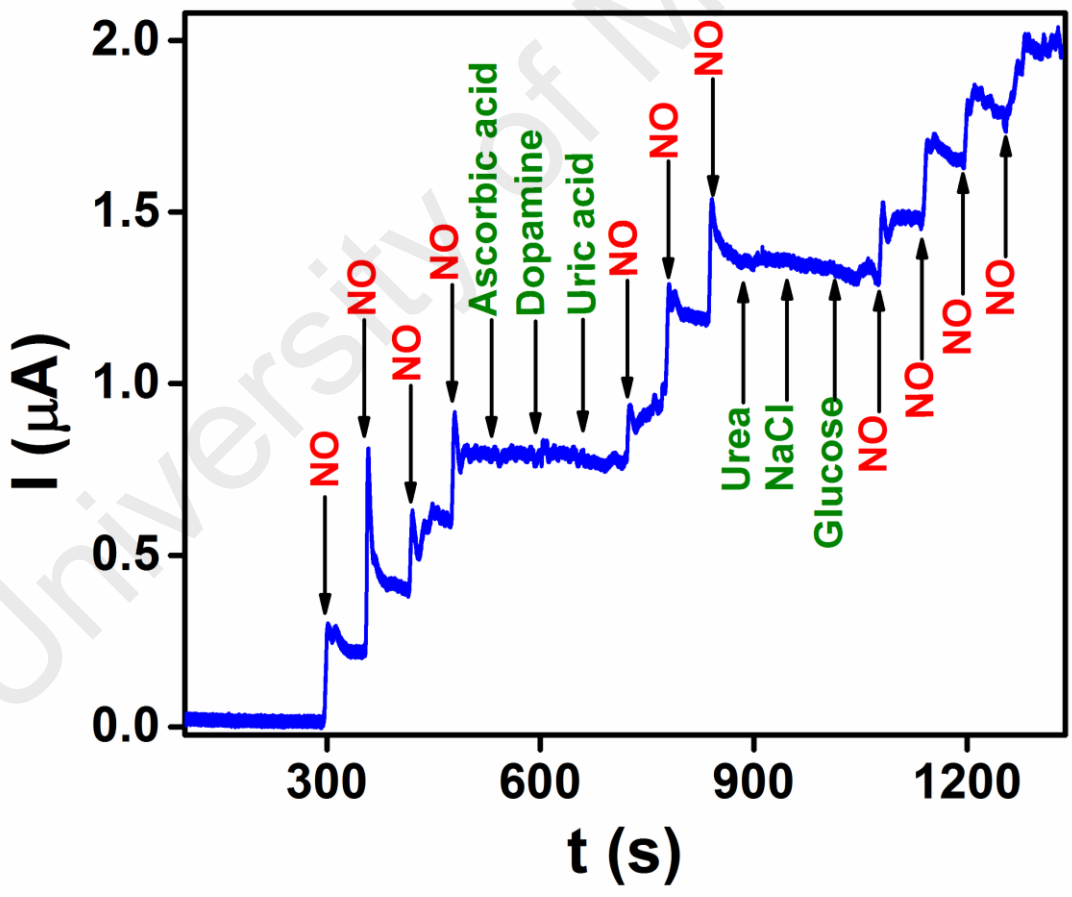

Figure 6.11: Amperometric *i–t* curve obtained at rGO-Co_3O_4@Pt nanocomposite modified GC electrode for the successive addition of 10 μM NO_2^- and each 1 mM of DA, AA, UA, glucose, urea and NaCl in 0.1 M PBS (pH 2.5) at a regular interval of 60 s. Applied potential was + 0.84 V.

6.4 Conclusions

Co_3O_4@Pt nanocubes was successfully synthesized and incorporated to the rGO sheets using the hydrothermal synthesis. The reduction of GO to rGO was confirmed from the increase in the ratio of *D* and *G* bands (I_D/I_G) from the Raman spectra. The morphology of the Co_3O_4 and the deposition of Pt on Co_3O_4 nanocubes were confirmed by the FESEM analysis and the EDX elemental mapping analysis confirmed the presence of all the elements of the rGO-Co_3O_4@Pt nanocomposite. The rGO-Co_3O_4@Pt nanocomposite modified GC electrode shifted the oxidation overpotential of the in-situ generated NO toward smaller positive potential with enhanced catalytic peak current when compared to the other modified electrodes. The higher catalytic effect of the rGO-Co_3O_4@Pt nanocomposite was attributed to the synergistic effect of the Co_3O_4 nanocubes and Pt nanoparticles present in the rGO matrix. The detection of NO was performed using amperometric *i-t* curve technique at the various modified electrodes and among them, the rGO-Co_3O_4@Pt nanocomposite modified electrode showed better performance with the lowest detection limit of 1.73 µM. Also, the nanocomposite modified electrode displayed good selectivity toward NO even in the presence of 100-fold higher concentration of other physiologically analytes. The current sensor was stable and reproducible and adds further credits to the rGO-Co_3O_4 nanocomposite based electrochemical sensors in the contemporary research.

CHAPTER 7: CONCLUSION AND FUTURE WORK

The present study highlights the typical synthesis of Co_3O_4 different nanostructures and Co_3O_4 based nanocomposites for the electrochemical detection of target molecules for the sensor applications. The Co_3O_4 different nanostructures together with Co_3O_4 nanocomposites were designed based upon their inherent properties such as structural affects, catalysis, charge transfer abilities in nanocomposites and sensing capabilities of the materials. The synthesized materials were comprehensively characterized by various techniques such as FESEM fitted with EDX elemental mapping analysis, high resolution transmission electron microscopy (HRTEM), XRD and Raman spectroscopy. The synthesized nanomaterials have demonstrated improved physical and chemical properties for electrochemical sensors applications. Adding into it, the facile method of synthesizing nanomaterials by the hydrothermal technique, their thermal stability, higher electrocatalytic activity and ability to detect the target molecule has made them a very sophisticated material for electrochemical sensors applications.

Co_3O_4 with five different nanostructures were prepared via the hydrothermal route and utilized for the sensing of 4-NP, a water contaminant. The cubical structure of Co_3O_4 presented optimistic results among the other nanostructures (nanocubes, nanowires, nanobundles, nanoplates and nanoflowers) based on their structure, size and crystallinity. All the structures of Co_3O_4 were tested by using cyclic voltammogram techniques for the reduction of 4-NP. A higher current was recorded for 4-NP reduction with a well-defined peak at lower potential as compared to the other nanostructures. So Co_3O_4 with cubical morphology was selected as potential catalyst for the detection of 4-NP. The sensitivity and the lowest LOD for 4-NP were 0.0485±0.00063 µA/µM and 0.93 µM respectively. Based on the results reported in chapter three, Co_3O_4 with cubical structure was selected as potential candidate to fabricate nanocomposites with graphene for another sensor

application. Hence, rGO-Co_3O_4 nanocomposite was prepared by using the same hydrothermal route. In this study, the rGO-Co_3O_4 nanocomposites were prepared with different wt. % of GO (2, 4, 8, 12 and wt. %). The prepared composition with 4 wt. % of GO concentrations was found to be the optimized composition by testing it through cyclic voltammogram technique. All nanocomposites were analyzed to oxidase a depression biomarker called serotonin (5-HT) but promising peak current with lower potential value for the oxidation of biomolecules was displayed by rGO-Co_3O_4-4 %. It was noticed that 2 wt. % of GO results in the agglomeration of Co_3O_4 nanocubes and thus agglomerated particles appears on the surface of graphene sheets. The increase of the GO wt. % provides sufficient numbers of sheets to accommodate the Co_3O_4 nanocubes and hence prevent them from agglomeration for increased electrolyte diffusion into the rGO-Co_3O_4-4 % matrix and boost the catalytic process. Further increase in the GO wt. % results in an increased of stacking graphene sheets lowers the density of Co_3O_4 which produces poor electrocatalytic activity. So rGO-Co_3O_4 was used as an efficient electrode material to detect 5-HT with a LOD of 1.128 μM. Interference studies were also investigated in the presence of co-existing molecules such as AA, DA and UA and sensor was found to be highly selective towards 5-HT. In addition, gold deposited Co_3O_4 nanocubes incorporated into reduced graphene oxide nanocomposites were synthesised by hydrothermal method. In this research, the enhancement in catalytic performance of rGO-Co_3O_4 nanocomposite was tuned by varying the concentration (2, 4, 6, 8 and 10 mM) of Au nanoparticles. It was observed that rGO-Co_3O_4@Au nanocomposite with 8 mM concentration of Au nanoparticle has shown enhanced electrochemical performance. The studies were carried out for the detection of hydrazine, a toxic, colorless and flammable molecule which causes severe injury to the lungs, liver, nervous system and spinal cord etc. The electrochemical detecion of hydrazine was obtained at rGO-Co_3O_4@Au modified GC electrode and the LOD was 0.443 μM and 0.58304 ± 0.00466 μA μM^{-1}. For selectivity

test, the sensor material was tested in the presence of various interfering molecules mentioned in chapter 5. There was no signal detected for the interference species which confirms the selectivity of the rGO-Co_3O_4@Au. Real sample analysis was also studied for the water collected from different areas in Malaysia. Finally, platinum nanoparticle deposited Co_3O_4 nanocubes incorporated into reduced graphene oxide was prepared by hydrothermal method. In this method, rGO-Co_3O_4 nanocomposite with different concentration of GO (2,4,8 and 12 wt. %) were first tested for electrochemical oxidation of NO and it was found that rGO-Co_3O_4 with 8 wt. % of GO showed enhanced electrochemcal signal compared to other compositions. So rGO-Co_3O_4 nanocomposite with 8 wt. % of GO was deposited with platinum nanoparticles and utilized for the detection of NO, a biomolecule responsible for vasodilation and blood pressure regulation in the nervous and cardiovascular systems in mammalian physiology. The detection of NO was carried out on rGO-Co_3O_4@Pt modified GC electrode and LOD was 1.73 μM for the detection of NO. Since NO is a biological molecule which is found togather with other biological molecules, so the detection of NO in the presence of these molecules is very important to check the selectivity of the sensor. It was found that the rGO-Co_3O_4@Pt modified GC electrode is highly selective towards sensing of NO.

Future Work

The current research work focuses on the enhancement of Co_3O_4 nanostruructures as a catalyst for electrochmical sensor applications. In this work, we have used graphene as a superhighway for electrical conduction and Co_3O_4 was used as catalyst material. Graphene facilitated the efficient electron transfer at the interface of the electrode and electrolyte, thus took part in boosting the electrochemical signals. For further enrichment of Co_3O_4 nanocubes, some metal nanoparticles were deposited onto the Co_3O_4 nanocubes. From these results, the proposed future work is listed below:

1. Five different nanostructures of Co_3O_4, have been synthesized but only one type of nanostructured Co_3O_4 was utilized for electrochemical sensors applications based on the performance. The other four nanostructures are still yet to be explored.
2. From the literature, nanowires are considered very promising materials for supercapacitors electrode materials. Nanowires are mostly synthesised by electrodeposition, electrophoretic deposition and chemical vapour deposition methods (e.g. AACVD, MOCVD and HWCVD), but were synthesized by the hydrothermal method in this research.
3. The Co_3O_4 nanowires can be utilized as composite materials with graphene, carbon nanotubes and metal nanoparticles by the same synthetic methods, especially for electrochemcial sensors, supercapacitors and solar cell applications.
4. Similarly, other nanostructures can be utilized for different electrochemical applications or by fabrication into nanocomposites to achieve higher electrocatlaytic performance.

REFERENCES

Abbaspour, A., & Noori, A. (2011). A cyclodextrin host–guest recognition approach to an electrochemical sensor for simultaneous quantification of serotonin and dopamine. *Biosensors and Bioelectronics, 26*(12), 4674-4680.

Abdul Aziz, M., & Kawde, A. N. (2013). Gold nanoparticle-modified graphite pencil electrode for the high-sensitivity detection of hydrazine. *Talanta, 115*, 214-221.

Adler, D. (1968). Insulating and metallic states in transition metal oxides. *Solid State Physics, 21*, 1-113.

Afzali, D., Karimi-Maleh, H., & Khalilzadeh, M. A. (2011). Sensitive and selective determination of phenylhydrazine in the presence of hydrazine at a ferrocene-modified carbon nanotube paste electrode. *Environmental Chemistry Letters, 9*(3), 375-381.

Ahmed, S. R., Ogale, S., Papaefthymiou, G. C., Ramesh, R., & Kofinas, P. (2002). Magnetic properties of $CoFe_2O4$ nanoparticles synthesized through a block copolymer nanoreactor route. *Applied Physics Letters, 80*(9), 1616-1618.

Ajayan, P., & Nalwa, H. (2000). Handbook of Nanostructured Materials and Nanotechnology. *Academic Press, New York*.

Allag, A., Saâd, R., Ouahab, A., Attouche, H., & Kouidri, N. (2016). Optoelectronic properties of SnO_2 thin films sprayed at different deposition times. *Chinese Physics B, 25*(4), 046801.

Alrehaily, L., Joseph, J., Biesinger, M., Guzonas, D., & Wren, J. (2013). Gamma-radiolysis-assisted cobalt oxide nanoparticle formation. *Physical Chemistry Chemical Physics, 15*(3), 1014-1024.

Ando, M., Kadono, K., Kamada, K., & Ohta, K. (2004). Third-order nonlinear optical responses of nanoparticulate Co_3O_4 films. *Thin Solid Films, 446*(2), 271-276.

Anithaa, A. C., Asokan, K., & Sekar, C. (2017). Highly sensitive and selective serotonin sensor based on gamma ray irradiated tungsten trioxide nanoparticles. *Sensors and Actuators B, 238*, 667-675.

Antoniadou, S., Jannakoudakis, A., & Theodoridou, E. (1989). Electrocatalytic reactions on carbon fibre electrodes modified by hemine II. Electro-oxidation of hydrazine. *Synthetic Metals, 30*(3), 295-304.

Arvinte, A., Mahosenaho, M., Pinteala, M., Sesay, A.-M., & Virtanen, V. (2011). Electrochemical oxidation of p-nitrophenol using graphene-modified electrodes, and a comparison to the performance of MWNT-based electrodes. *Microchimica Acta, 174*(3-4), 337-343.

Asif, M. H., Elinder, F., & Willander, M. (2011). Electrochemical biosensors based on ZnO nanostructures to measure intracellular metal ions and glucose. *Journal of Analytical & Bioanalytical Techniques 7*, doi: 10.4172/2155-9872.S7-003.

Augustine, A. K., Nampoori, V., & Kailasnath, M. (2014). Rapid synthesize of gold nanoparticles by microwave irradiation method and its application as an optical limiting material. *Optik-International Journal for Light and Electron Optics, 125*(22), 6696-6699.

Babaei, A., & Taheri, A. R. (2013). Nafion/$Ni(OH)_2$ nanoparticles-carbon nanotube composite modified glassy carbon electrode as a sensor for simultaneous determination of dopamine and serotonin in the presence of ascorbic acid. *Sensors and Actuators B: Chemical, 176*, 543-551.

Baek, H. R., & Eo, I. S. (2017). Electrochemical properties of TiO_2-metal oxide composites for dye-sensitized solar cell. *Current Applied Physics, 17*(6), 854-857.

Bala, H., Fu, W., Yu, Y., Yang, H., & Zhang, Y. (2009). Preparation, optical properties, magnetic properties and thermal stability of core–shell structure cobalt/zinc oxide nanocomposites. *Applied Surface Science, 255*(7), 4050-4055.

Balandin, A. A., Ghosh, S., Bao, W., Calizo, I., Teweldebrhan, D., Miao, F., & Lau, C. N. (2008). Superior thermal conductivity of single-layer graphene. *Nano Letters, 8*(3), 902-907.

Baxter, J. B., & Aydil, E. S. (2005). Nanowire-based dye-sensitized solar cells. *Applied Physics Letters, 86*(5), 053114.

Bedioui, F., & Villeneuve, N. (2003). Electrochemical nitric oxide sensors for biological samples–principle, selected examples and applications. *Electroanalysis, 15*(1), 5-18.

Beltramo, G., & Koper, M. (2003). Nitric oxide reduction and oxidation on stepped Pt [n (111)×(111)] electrodes. *Langmuir, 19*(21), 8907-8915.

Bogdan, C. (2001). Nitric oxide and the immune response. *Nature Immunology*, *2*(10), 907-916.

Borsella, E., Cattaruzza, E., De Marchi, G., Gonella, F., Mattei, G., Mazzoldi, P., Quaranta, A., Battaglin, G., & Polloni, R. (1999). Synthesis of silver clusters in silica-based glasses for optoelectronics applications. *Journal of Non-Crystalline Solids, 245*(1), 122-128.

Brückner, A. (2003). Looking on Heterogeneous Catalytic Systems from Different Perspectives: Multitechnique Approaches as a New Challenge for In Situ Studies. *Catalysis Reviews, 45*(1), 97-150.

Buchsteiner, A., Lerf, A., & Pieper, J. (2006). Water dynamics in graphite oxide investigated with neutron scattering. *The Journal of Physical Chemistry B, 110*(45), 22328-22338.

Budkuley, J. S. (1992). Determination of hydrazine and sulphite in the presence of one another. *Microchimica Acta, 108*(1-2), 103-105.

Byrappa, K., & Yoshimura, M. (2012). *Handbook of hydrothermal technology*: William Andrew.

Cao, L., Zhang, Z., Sun, L., Gao, C., He, M., Wang, Y., Li, Y., Zhang, X., Li, G., & Zhang, J. (2001). Well-Aligned Boron Nanowire Arrays. *Advanced Materials, 13*(22), 1701-1704.

Cao, L. M., Hahn, K., Scheu, C., Rühle, M., Wang, Y. Q., Zhang, Z., Gao, C. X., Li, Y. C., Zhang, X. Y., He, M., Sun, L. L., & Wang, W. K. (2002). Template-catalyst-free growth of highly ordered boron nanowire arrays. *Applied Physics Letters, 80*(22), 4226-4228.

Chai, S.-H., Howe, J. Y., Wang, X., Kidder, M., Schwartz, V., Golden, M. L., Overbury, S. H., Dai, S., & Jiang, D.-e. (2012). Graphitic mesoporous carbon as a support of promoted Rh catalysts for hydrogenation of carbon monoxide to ethanol. *Carbon, 50*(4), 1574-1582.

Chang, H., & Wu, H. (2013). Graphene-based nanocomposites: preparation, functionalization, and energy and environmental applications. *Energy & Environmental Science, 6*(12), 3483.

Chang, W., Skandan, G., Hahn, H., Danforth, S. C., & Kear, B. H. (1994). Chemical vapor condensation of nanostructured ceramic powders. *Nanostructured Materials, 4*(3), 345-351.

Chauveau, J., Fert, V., Morel, A., & Delaage, M. (1991). Rapid and specific enzyme immunoassay of serotonin. *Clinical Chemistry, 37*(7), 1178-1184.

Chen, C.-H., Chen, Y.-C., & Lin, M.-S. (2013). Amperometric determination of NADH with Co_3O_4 nanosheet modifiedelectrode. *Biosensors and Bioelectronics, 42*, 379-384.

Chen, C.-M., Zhang, Q., Yang, M.-G., Huang, C.-H., Yang, Y.-G., & Wang, M.-Z. (2012). Structural evolution during annealing of thermally reduced graphene nanosheets for application in supercapacitors. *Carbon, 50*(10), 3572-3584.

Chen, M., Zhou, W., Qi, M., Zhang, J., Yin, J., & Chen, Q. (2017). Reconstruction of copper shell on metal oxides as enhanced nanoarrays electrodes for lithium ion batteries. *Materials Research Bulletin, 86*, 308-312.

Chen, S., Wu, Q., & Mishra, C. (2012). New graphene-related materials on the horizon. *Nature Materials, 11*, 203-207.

Chen, S., Zhu, J., & Wang, X. (2010). One-Step Synthesis of Graphene-Cobalt Hydroxide Nanocomposites and Their Electrochemical Properties. *Journal of Physical Chemistry C, 114*(27), 11829-11834.

Chen, X., Long, H.-Y., Wu, W.-L., & Yang, Z.-S. (2009). Direct electrochemical behavior of cytochrome c on sodium dodecyl sulfate modified electrode and its application to nitric oxide biosensor. *Thin Solid Films, 517*(8), 2787-2791.

Cheng, C.-S., Serizawa, M., Sakata, H., & Hirayama, T. (1998). Electrical conductivity of Co_3O_4 films prepared by chemical vapour deposition. *Materials Chemistry and Physics, 53*(3), 225-230.

Cho, Y., Parmar, N. S., Nahm, S., & Choi, J.-W. (2017). Full range optical and electrical properties of Zn-doped SnO_2 and oxide/metal/oxide multilayer thin films deposited on flexible PET substrate. *Journal of Alloys and Compounds, 694*, 217-222.

Choi, H.-J., Jung, S.-M., Seo, J.-M., Chang, D. W., Dai, L., & Baek, J.-B. (2012). Graphene for energy conversion and storage in fuel cells and supercapacitors. *Nano Energy, 1*(4), 534-551.

Choi, Y., Gu, M., Park, J., Song, H. K., & Kim, B. S. (2012). Graphene multilayer supported gold nanoparticles for efficient electrocatalysts toward methanol oxidation. *Advanced Energy Materials, 2*(12), 1510-1518.

Chou, S.-L., Wang, J.-Z., Liu, H.-K., & Dou, S.-X. (2008). Electrochemical deposition of porous Co_3O_4 nanostructured thin film for lithium-ion battery. *Journal of Power Sources, 182*(1), 359-364.

Choudhary, G., IIansen, H., Donkin, S., & Kirman, C. (1997). Toxicological profile for hydrazines. *US Department of Health and Human Service*, 5.

Choudhury, C., Bansal, N. K., & Sehgal, H. K. (1983). Heat loss optimisation of a concentric cylindrical solar collector employing a cobalt oxide selective absorber. *Applied Energy, 14*(2), 143-159.

Chu, L., Han, L., & Zhang, X. (2011). Electrochemical simultaneous determination of nitrophenol isomers at nano-gold modified glassy carbon electrode. *Journal of Applied Electrochemistry, 41*(6), 687-694.

Cinthia, A. J., Priyanga, G. S., Rajeswarapalanichamy, R., & Iyakutti, K. (2015). Structural, electronic and mechanical properties of alkaline earth metal oxides MO (M=Be, Mg, Ca, Sr, Ba). *Journal of Physics and Chemistry of Solids, 79*, 23-42.

Conoci, S., Petralia, S., Samorì, P., Raymo, F. M., Di Bella, S., & Sortino, S. (2006). Optically transparent, ultrathin Pt films as versatile metal substrates for molecular optoelectronics. *Advanced Functional Materials, 16*(11), 1425-1432.

Crespi, F., Baumeyer, T., Moebius, C., & Dittrich, J. (1991). Simultaneous in vivo monitoring of dopamine and serotonin by differential pulse conditioning voltammetry with NA-CRO microbiosensors. *Fresenius Journal of Analytical Chemistry, 341*(10), 644.

Cui, L., Ji, C., Peng, Z., Zhong, L., Zhou, C., Yan, L., Qu, S., Zhang, S., Huang, C., & Qian, X. (2014). Unique tri-output optical probe for specific and ultrasensitive detection of hydrazine. *Analytical Chemistry, 86*(9), 4611-4617.

Cui, L., Peng, Z., Ji, C., Huang, J., Huang, D., Ma, J., Zhang, S., Qian, X., & Xu, Y. (2014). Hydrazine detection in the gas state and aqueous solution based on the Gabriel mechanism and its imaging in living cells. *Chemical Communications, 50*(12), 1485-1487.

Dalkıran, B., Esra Erden, P., & Kılıç, E. (2017). Amperometric biosensors based on carboxylated multiwalled carbon nanotubes-metal oxide nanoparticles-7,7,8,8-tetracyanoquinodimethane composite for the determination of xanthine. *Talanta, 167*, 286-295.

de Moraes, A. C. M., Andrade, P. F., de Faria, A. F., Simões, M. B., Salomão, F. C. C. S., Barros, E. B., do Carmo Gonçalves, M., & Alves, O. L. (2015). Fabrication of transparent and ultraviolet shielding composite films based on graphene oxide and cellulose acetate. *Carbohydrate Polymers, 123*, 217-227.

Demuth, J., Hamers, R., Tromp, R., & Welland, M. (1986). A scanning tunneling microscope for surface science studies. *IBM Journal of Research and Development, 30*(4), 396-402.

Devasenathipathy, R., Mani, V., & Chen, S.-M. (2014). Highly selective amperometric sensor for the trace level detection of hydrazine at bismuth nanoparticles decorated graphene nanosheets modified electrode. *Talanta, 124*, 43-51.

Dhas, N. A., Koltypin, Y., & Gedanken, A. (1997). Sonochemical preparation and characterization of ultrafine chromium oxide and manganese oxide powders. *Chemistry of Materials, 9*(12), 3159-3163.

Dinesh, B., Veeramani, V., Chen, S.-M., & Saraswathi, R. (2017). In situ electrochemical synthesis of reduced graphene oxide-cobalt oxide nanocomposite modified electrode for selective sensing of depression biomarker in the presence of ascorbic acid and dopamine. *Journal of Electroanalytical Chemistry, 786*, 169-176.

Ding, J., Zhu, S., Zhu, T., Sun, W., Li, Q., Wei, G., & Su, Z. (2015). Hydrothermal synthesis of zinc oxide-reduced graphene oxide nanocomposites for an electrochemical hydrazine sensor. *RSC Advances, 5*(29), 22935-22942.

Dong, Y., He, K., Yin, L., & Zhang, A. (2007). A facile route to controlled synthesis of Co_3O_4 nanoparticles and their environmental catalytic properties. *Nanotechnology, 18*(43), 435602.

Du, X., He, J., Zhu, J., Sun, L., & An, S. (2012). Ag-deposited silica-coated Fe_3O_4 magnetic nanoparticles catalyzed reduction of p-nitrophenol. *Applied Surface Science, 258*(7), 2717-2723.

Du, X., Skachko, I., Barker, A., & Andrei, E. Y. (2008). Approaching ballistic transport in suspended graphene. *Nature Nanotechnology, 3*(8), 491-495.

Dutta, S., Ray, C., Mallick, S., Sarkar, S., Roy, A., & Pal, T. (2015). Au@ Pd core–shell nanoparticles-decorated reduced graphene oxide: a highly sensitive and selective platform for electrochemical detection of hydrazine. *RSC Advances, 5*(64), 51690-51700.

Ensafi, A. A., Abarghoui, M. M., & Rezaei, B. (2016). Facile synthesis of Pt-Cu@ silicon nanostructure as a new electrocatalyst supported matrix, electrochemical detection of hydrazine and hydrogen peroxide. *Electrochimica Acta, 190*, 199-207.

Ensafi, A. A., & Rezaei, B. (1998). Flow injection determination of hydrazine with fluorimetric detection. *Talanta, 47*(3), 645-649.

Fagan-Murphy, A., Watt, F., Morgan, K. A., & Patel, B. A. (2012). Influence of different biological environments on the stability of serotonin detection on carbon-based electrodes *Journal of Electroanalytical Chemistry, 684*, 1-5.

Fang, B., Zhang, C., Zhang, W., & Wang, G. (2009). A novel hydrazine electrochemical sensor based on a carbon nanotube-wired ZnO nanoflower-modified electrode. *Electrochimica Acta, 55*(1), 178-182.

Fang, F. C. (1997). Perspectives series: host/pathogen interactions. Mechanisms of nitric oxide-related antimicrobial activity. *Journal of Clinical Investigation, 99*(12), 2818.

Farhadi, S., Pourzare, K., & Bazgir, S. (2014). Co_3O_4 nanoplates: Synthesis, characterization and study of optical and magnetic properties. *Journal of Alloys and Compounds, 587*, 632-637.

Farhadi, S., Safabakhsh, J., & Zaringhadam, P. (2013). Synthesis, characterization, and investigation of optical and magnetic properties of cobalt oxide (Co_3O_4) nanoparticles. *Journal of Nanostructure in Chemistry, 3*(1), 1-9.

Fei, J., Hu, S., & Shiu, K.-K. (2011). Amperometric determination of nitric oxide at a carbon nanotube modified electrode with redox polymer coating. *Journal of Solid State Electrochemistry, 15*(3), 519-523.

Fernandez-Garcia, M., Martinez-Arias, A., Hanson, J., & Rodriguez, J. (2004). Nanostructured oxides in chemistry: characterization and properties. *Chemical Reviews, 104*(9), 4063-4104.

Fierro, J. L. G. (2005). *Metal oxides: chemistry and applications*: CRC press, Broken Sound Pkwy NW.

Fiiipponi, L., & Sutherland, D. (2012). *Nanotechnologies: principles, applications, implications and hands-on activities: A compendium for educators*: European Union, Directorate General for Research and Innovation.

Frohlich, K., Luptak, R., Dobrocka, E., Husekova, K., Cico, K., Rosova, A., Lukosius, M., Abrutis, A., Pisecny, P., & Espinos, J. (2006). Characterization of rare earth oxides based MOSFET gate stacks prepared by metal-organic chemical vapour deposition. *Materials Science in Semiconductor Processing, 9*(6), 1065-1072.

Fujishima, A., & Honda, K. (1972). Electrochemical photolysis of water at a semiconductor electrode. *Nature, 238*(5358), 37-38.

Furchgott, R. F. (1999). Endothelium-Derived Relaxing Factor: Discovery, Early Studies, and Identifcation as Nitric Oxide (Nobel Lecture). *Angewandte Chemie International Edition, 38*(13-14), 1870-1880.

Ganjali, M. R., Motakef-Kazami, N., Faridbod, F., Khoee, S., & Norouzi, P. (2010). Determination of Pb 2+ ions by a modified carbon paste electrode based on multi-

walled carbon nanotubes (MWCNTs) and nanosilica. *Journal of Hazardous Materials, 173*(1), 415-419.

Geim, A. K., & Novoselov, K. S. (2007). The rise of graphene. *Nature materials, 6*(3), 183-191.

Ghanbari, K. (2014). Fabrication of silver nanoparticles–polypyrrole composite modified electrode for electrocatalytic oxidation of hydrazine. *Synthetic Metals, 195*, 234-240.

Gholamian, F., Sheikh-Mohseni, M. A., & Naeimi, H. (2012). Simultaneous determination of phenylhydrazine and hydrazine by a nanostructured electrochemical sensor. *Materials Science and Engineering: C, 32*(8), 2344-2348.

Gholivand, M. B., & Azadbakht, A. (2011). A novel hydrazine electrochemical sensor based on a zirconium hexacyanoferrate film-bimetallic Au-Pt inorganic-organic hybrid nanocomposite onto glassy carbon-modified electrode. *Electrochimica Acta, 56*(27), 10044-10054.

Greene, L. E., Law, M., Goldberger, J., Kim, F., Johnson, J. C., Zhang, Y., Saykally, R. J., & Yang, P. (2003). Low-temperature wafer-scale production of ZnO nanowire arrays. *Angewandte Chemie International Edition, 42*(26), 3031-3034.

Greenwood, N., & Earnshaw, A. (1997). *Chemistry of the Elements 2nd Edition*: Butterworth-Heinemann.

Gu, Y.-e., Zhang, Y., Zhang, F., Wei, J., Wang, C., Du, Y., & Ye, W. (2010). Investigation of photoelectrocatalytic activity of Cu_2O nanoparticles for p-nitrophenol using rotating ring-disk electrode and application for electrocatalytic determination. *Electrochimica Acta, 56*(2), 953-958.

Gueell, A. G., Meadows, K. E., Unwin, P. R., & MacPherson, J. V. (2010). Trace voltammetric detection of serotonin at carbon electrodes: comparison of glassy carbon, boron doped diamond and carbon nanotube network electrodes. *Physical Chemistry Chemical Physics, 12*(34), 10108-10114.

Guix, F., Uribesalgo, I., Coma, M., & Munoz, F. (2005). The physiology and pathophysiology of nitric oxide in the brain. *Progress in Neurobiology, 76*(2), 126-152.

Guo, C. X., Ng, S. R., Khoo, S. Y., Zheng, X., Chen, P., & Li, C. M. (2012). RGD-peptide functionalized graphene biomimetic live-cell sensor for real-time detection of nitric oxide molecules. *ACS Nano, 6*(8), 6944-6951.

Guo, S., Dong, S., & Wang, E. (2009). Three-dimensional Pt-on-Pd bimetallic nanodendrites supported on graphene nanosheet: facile synthesis and used as an advanced nanoelectrocatalyst for methanol oxidation. *ACS Nano, 4*(1), 547-555.

Gupta, P., & Goyal, R. N. (2014). Polymelamine modified edge plane pyrolytic graphite sensor for the electrochemical assay of serotonin. *Talanta, 120*, 17-22.

Hai, H. T., Takamura, H., & Koike, J. (2013). Oxidation behavior of Cu–Ag core–shell particles for solar cell applications. *Journal of Alloys and Compounds, 564*, 71-77.

He, Q., Zheng, D., & Hu, S. (2009). Development and application of a nano-alumina based nitric oxide sensor. *Microchimica Acta, 164*(3-4), 459-464.

He, X., & Zhu, L. (2006). Direct electrochemistry of hemoglobin in cetylpyridinium bromide film: Redox thermodynamics and electrocatalysis to nitric oxide. *Electrochemistry Communications, 8*(4), 615-620.

He, Y.-S., Bai, D.-W., Yang, X., Chen, J., Liao, X.-Z., & Ma, Z.-F. (2010). A $Co(OH)_2$-graphene nanosheets composite as a high performance anode material for rechargeable lithium batteries. *Electrochemistry Communications, 12*(4), 570-573.

Henrich, V. E., & Cox, P. A. (1996). *The Surface Science of Metal Oxides*: Cambridge university press, New York.

Henry, P. F., & Weller, M. T. (1998). Ca2AuN: A nitride containing infinite zigzag gold chains. *Angewandte Chemie International Edition, 37*(20), 2855-2857.

7.1.1 Hetrick, E. M., & Schoenfisch, M. H. (2009). Analytical chemistry of nitric oxide. *Annual Review of Analytical Chemistry (Palo Alto Calif), 2*, 409-433.

Hu, H., Wang, X., Wang, J., Wan, L., Liu, F., Zheng, H., Chen, R., & Xu, C. (2010). Preparation and properties of graphene nanosheets–polystyrene nanocomposites via in situ emulsion polymerization. *Chemical Physics Letters, 484*(4), 247-253.

Hu, L., Peng, Q., & Li, Y. (2008). Selective synthesis of Co_3O_4 nanocrystal with different shape and crystal plane effect on catalytic property for methane combustion. *Journal of the American Chemical Society, 130*(48), 16136-16137.

Huang, J., & Wan, Q. (2009). Gas sensors based on semiconducting metal oxide one-dimensional nanostructures. *Sensors, 9*(12), 9903-9924.

Huang, N. M., Lim, H. N., Chia, C. H., Yarmo, M. A., & Muhamad, M. R. (2011). Simple room-temperature preparation of high-yield large-area graphene oxide. *International Journal of Nanomedicine, 6*, 3443-3448.

Huang, W., Yang, C., & Zhang, S. (2003). Simultaneous determination of 2-nitrophenol and 4-nitrophenol based on the multi-wall carbon nanotubes Nafion-modified electrode. *Analytical and Bioanalytical Chemistry, 375*(5), 703-707.

Ignarro, L. J., Buga, G. M., Wood, K. S., Byrns, R. E., & Chaudhuri, G. (1987). Endothelium-derived relaxing factor produced and released from artery and vein is nitric oxide. *Proceedings of the National Academy of Sciences, 84*(24), 9265-9269.

Interrante, L. V., & Hampden-Smith, M. J. (1997). Chemistry of advanced materials: an overview. *Chemistry of Advanced Materials: An Overview, by Leonard V. Interrante (Editor), Mark J. Hampden-Smith (Editor),. Wiley-VCH, 1997.*, 592.

Jain, P. K., Lee, K. S., El-Sayed, I. H., & El-Sayed, M. A. (2006). Calculated absorption and scattering properties of gold nanoparticles of different size, shape, and composition: applications in biological imaging and biomedicine. *Journal of Physical Chemistry B, 110*(14), 7238-7248.

Jang, J. Y., Kim, M. S., Jeong, H. M., & Shin, C. M. (2009). Graphite oxide/poly (methyl methacrylate) nanocomposites prepared by a novel method utilizing macroazoinitiator. *Composites Science and Technology, 69*(2), 186-191.

Jayabal, S., Viswanathan, P., & Ramaraj, R. (2014). Reduced graphene oxide–gold nanorod composite material stabilized in silicate sol–gel matrix for nitric oxide sensor. *RSC Advances, 4*(63), 33541-33548.

Jayasri, D., & Narayanan, S. S. (2007). Amperometric determination of hydrazine at manganese hexacyanoferrate modified graphite–wax composite electrode. *Journal of Hazardous Materials, 144*(1), 348-354.

Jeon, H.-K., Nohta, H., & Ohkura, Y. (1992). High-performance liquid chromatographic determination of catecholamines and their precursor and metabolites in human urine and plasma by postcolumn derivatization involving chemical oxidation followed by fluorescence reaction. *Analytical Biochemistry, 200*(2), 332-338.

Jeong, S. J., Song, J. S., Min, B. K., Lee, W. J., & Park, E. C. (2006). Characteristics of Piezoelectric Multilayer Devices Containing Metal-Oxide Multicomponent Electrode. *Ferroelectrics, 338*(1), 9-16.

Jia, J., Wang, B., Wu, A., Cheng, G., Li, Z., & Dong, S. (2002). A method to construct a third-generation horseradish peroxidase biosensor: self-assembling gold nanoparticles to three-dimensional sol-gel network. *Analytical Chemistry, 74*(9), 2217-2223.

Jia, S., Fei, J., Deng, J., Cai, Y., & Li, J. (2009). Direct electrochemistry and electrocatalysis of hemoglobin immobilized in an amphiphilic diblock copolymer film. *Sensors and Actuators B: Chemical, 138*(1), 244-250.

Jiang, L., Gu, S., Ding, Y., Jiang, F., & Zhang, Z. (2014). Facile and novel electrochemical preparation of a graphene–transition metal oxide nanocomposite for ultrasensitive electrochemical sensing of acetaminophen and phenacetin. *Nanoscale, 6*(1), 207-214.

Jiang, Y., Zheng, B., Du, J., Liu, G., Guo, Y., & Xiao, D. (2013). Electrophoresis deposition of Ag nanoparticles on TiO_2 nanotube arrays electrode for hydrogen peroxide sensing. *Talanta, 112*, 129-135.

Jiang, Z., Jiang, Z.-J., Maiyalagan, T., & Manthiram, A. (2016). Cobalt oxide-coated N- and B-doped graphene hollow spheres as bifunctional electrocatalysts for oxygen reduction and oxygen evolution reactions. *Journal of Materials Chemistry A, 4*(16), 5877-5889.

Jiao, F., & Frei, H. (2009). Nanostructured Cobalt Oxide Clusters in Mesoporous Silica as Efficient Oxygen-Evolving Catalysts. *Angewandte Chemie International Edition, 48*(10), 1841-1844.

Jiao, F., & Frei, H. (2010). Nanostructured cobalt and manganese oxide clusters as efficient water oxidation catalysts. *Energy & Environmental Science, 3*(8), 1018-1027.

Jokar, E., & Shahrokhian, S. (2014). Growth control of cobalt oxide nanoparticles on reduced graphene oxide for enhancement of electrochemical capacitance. *International Journal of Hydrogen Energy, 39*(36), 21068-21075.

Jonker, G., & Van Santen, J. (1950). Physica (Utrecht) 16, 337 (1950). *CrossRef Google Scholar*.

Kaczmarczyk, J., Zasada, F., Janas, J., Indyka, P., Piskorz, W., Kotarba, A., & Sojka, Z. (2016). Thermodynamic Stability, Redox Properties and Reactivity of Mn_3O_4, Fe_3O_4, and Co_3O_4 Model Catalysts for N_2O Decomposition–Resolving the Origins of Steady Turnover. *ACS Catalysis*.

Kang, H., Kulkarni, A., Stankovich, S., Ruoff, R. S., & Baik, S. (2009). Restoring electrical conductivity of dielectrophoretically assembled graphite oxide sheets by thermal and chemical reduction techniques. *Carbon, 47*(6), 1520-1525.

Kang, M.-G., Park, H. J., Ahn, S. H., & Guo, L. J. (2010). Transparent Cu nanowire mesh electrode on flexible substrates fabricated by transfer printing and its application in organic solar cells. *Solar Energy Materials and Solar Cells, 94*(6), 1179-1184.

Kang, T.-T., Liu, X., Zhang, R. Q., Hu, W. G., Cong, G., Zhao, F.-A., & Zhu, Q. (2006). InN nanoflowers grown by metal organic chemical vapor deposition. *Applied Physics Letters, 89*(7), 071113.

Karabacak, T., Mallikarjunan, A., Singh, J. P., Ye, D., Wang, G.-C., & Lu, T.-M. (2003). β-phase tungsten nanorod formation by oblique-angle sputter deposition. *Applied Physics Letters, 83*(15), 3096-3098.

Karimi-Maleh, H., Moazampour, M., Ensafi, A. A., Mallakpour, S., & Hatami, M. (2014). An electrochemical nanocomposite modified carbon paste electrode as a sensor for simultaneous determination of hydrazine and phenol in water and wastewater samples. *Environmental Science and Pollution Research, 21*(9), 5879-5888.

Karuppiah, C., Palanisamy, S., Chen, S.-M., Ramaraj, S. K., & Periakaruppan, P. (2014). A novel and sensitive amperometric hydrazine sensor based on gold nanoparticles decorated graphite nanosheets modified screen printed carbon electrode. *Electrochimica Acta, 139*, 157-164.

Karuppiah, C., Palanisamy, S., Chen, S.-M., Veeramani, V., & Periakaruppan, P. (2014). A novel enzymatic glucose biosensor and sensitive non-enzymatic hydrogen peroxide sensor based on graphene and cobalt oxide nanoparticles composite modified glassy carbon electrode. *Sensors and Actuators B: Chemical, 196*, 450-456.

Kelly, R., Miotello, A., Chrisey, D., & Hubler, G. (1994). Pulsed Laser Deposition of Thin Films. *by DB Chrisey and GK Hubler (Wiley, New York, 1994) p, 55*.

Khalilzadeh, M. A., & Karimi-Maleh, H. (2009). Sensitive and selective determination of phenylhydrazine in the presence of hydrazine at a ferrocene monocarboxylic acid modified carbon nanotube paste electrode. *Analytical Letters, 43*(1), 186-196.

Khlebtsov, N., & Dykman, L. (2011). Biodistribution and toxicity of engineered gold nanoparticles: a review of in vitro and in vivo studies. *Chemical Society Reviews, 40*(3), 1647-1671.

Khoei, A., Ban, E., Banihashemi, P., & Qomi, M. A. (2011). Effects of temperature and torsion speed on torsional properties of single-walled carbon nanotubes. *Materials Science and Engineering: C, 31*(2), 452-457.

Kim, H., Seo, D.-H., Kim, S.-W., Kim, J., & Kang, K. (2011). Highly reversible Co_3O_4/graphene hybrid anode for lithium rechargeable batteries. *Carbon, 49*(1), 326-332.

Kim, K., Zhao, Y., Jang, H., Lee, S., Kim, J., Kim, K., & Ahn, J. (2009). P. kim, J.-Y. Choi and BH Hong. *Nature, 457*, 706.

Kim, K. S., Zhao, Y., Jang, H., Lee, S. Y., Kim, J. M., Kim, K. S., Ahn, J.-H., Kim, P., Choi, J.-Y., & Hong, B. H. (2009). Large-scale pattern growth of graphene films for stretchable transparent electrodes. *Nature, 457*(7230), 706-710.

Kim, Y., Noh, Y., Lim, E. J., Lee, S., Choi, S. M., & Kim, W. B. (2014). Star-shaped Pd@ Pt core–shell catalysts supported on reduced graphene oxide with superior electrocatalytic performance. *Journal of Materials Chemistry A, 2*(19), 6976-6986.

Kimmel, D. W., LeBlanc, G., Meschievitz, M. E., & Cliffel, D. E. (2011). Electrochemical sensors and biosensors. *Analytical Chemistry, 84*(2), 685-707.

Koçak, S., & Aslışen, B. (2014). Hydrazine oxidation at gold nanoparticles and poly(bromocresol purple) carbon nanotube modified glassy carbon electrode. *Sensors and Actuators B: Chemical, 196*, 610-618.

Kou, R., Shao, Y., Mei, D., Nie, Z., Wang, D., Wang, C., Viswanathan, V. V., Park, S., Aksay, I. A., & Lin, Y. (2011). Stabilization of electrocatalytic metal nanoparticles at metal− metal oxide− graphene triple junction points. *Journal of the American Chemical Society, 133*(8), 2541-2547.

Krittayavathananon, A., Srimuk, P., Luanwuthi, S., & Sawangphruk, M. (2014). Palladium nanoparticles decorated on reduced graphene oxide rotating disk electrodes toward ultrasensitive hydrazine detection: effects of particle size and hydrodynamic diffusion. *Analytical Chemistry, 86*(24), 12272-12278.

Kumar, R. V., Diamant, Y., & Gedanken, A. (2000). Sonochemical synthesis and characterization of nanometer-size transition metal oxides from metal acetates. *Chemistry of Materials, 12*(8), 2301-2305.

Kung, H. H. (1989). *Transition Metal Oxides: Surface Chemistry and Catalysis* (Vol. 45): Elsevier, Amsterdam.

Lee, C., Wei, X., Kysar, J. W., & Hone, J. (2008). Measurement of the elastic properties and intrinsic strength of monolayer graphene. *Science, 321*(5887), 385-388.

Lencka, M. M., Oledzka, M., & Riman, R. E. (2000). Hydrothermal synthesis of sodium and potassium bismuth titanates. *Chemistry of Materials, 12*(5), 1323-1330.

Lesiak, M., Binczarski, M., Karski, S., Maniukiewicz, W., Rogowski, J., Szubiakiewicz, E., Berlowska, J., Dziugan, P., & Witońska, I. (2014). Hydrogenation of furfural over Pd–Cu/Al_2O_3 catalysts. The role of interaction between palladium and copper on determining catalytic properties. *Journal of Molecular Catalysis A: Chemical, 395*, 337-348.

Li, C. C., Chen, L. B., Li, Q. H., & Wang, T. H. (2012). Seed-free, aqueous synthesis of gold nanowires. *CrystEngComm, 14*(22), 7549-7551.

Li, C. M., Zang, J., Zhan, D., Chen, W., Sun, C. Q., Teo, A. L., Chua, Y., Lee, V., & Moochhala, S. (2006). Electrochemical detection of nitric oxide on a SWCNT/RTIL composite gel microelectrode. *Electroanalysis, 18*(7), 713-718.

Li, D., Müller, M. B., Gilje, S., Kaner, R. B., & Wallace, G. G. (2008). Processable aqueous dispersions of graphene nanosheets. *Nature Nanotechnology, 3*(2), 101-105.

Li, J., Kuang, D., Feng, Y., Zhang, F., Xu, Z., & Liu, M. (2012). A graphene oxide-based electrochemical sensor for sensitive determination of 4-nitrophenol. *Journal of Hazardous Materials, 201*, 250-259.

Li, J., & Lin, X. (2007). Electrocatalytic oxidation of hydrazine and hydroxylamine at gold nanoparticle—polypyrrole nanowire modified glassy carbon electrode. *Sensors and Actuators B: Chemical, 126*(2), 527-535.

Li, S.-J., Du, J.-M., Zhang, J.-P., Zhang, M.-J., & Chen, J. (2014). A glassy carbon electrode modified with a film composed of cobalt oxide nanoparticles and graphene for electrochemical sensing of H_2O_2. *Microchimica Acta, 181*(5-6), 631-638.

Li, S.-S., Zheng, J.-N., Ma, X., Hu, Y.-Y., Wang, A.-J., Chen, J.-R., & Feng, J.-J. (2014). Facile synthesis of hierarchical dendritic PtPd nanogarlands supported on reduced graphene oxide with enhanced electrocatalytic properties. *Nanoscale, 6*(11), 5708-5713.

Li, W.-Y., Xu, L.-N., & Chen, J. (2005). Co_3O_4 nanomaterials in lithium-ion batteries and gas sensors. *Advanced Functional Materials, 15*(5), 851-857.

Li, W., Geng, X., Guo, Y., Rong, J., Gong, Y., Wu, L., Zhang, X., Li, P., Xu, J., & Cheng, G. (2011). Reduced graphene oxide electrically contacted graphene sensor for highly sensitive nitric oxide detection. *ACS Nano, 5*(9), 6955-6961.

Li, W., Gong, B., Wu, P., Yang, S., Yang, Q., Dang, Z., & Zhu, N. (2017). Evaluation of the physiochemical properties and catalytic performance of mixed metal oxides-carbon nanotubes nanohybrids containing carbon nanotubes with different diameters. *Applied Clay Science, 135*, 95-102.

Li, W., Jung, H., Hoa, N. D., Kim, D., Hong, S.-K., & Kim, H. (2010). Nanocomposite of cobalt oxide nanocrystals and single-walled carbon nanotubes for a gas sensor application. *Sensors and Actuators B: Chemical, 150*(1), 160-166.

Li, X., Wang, L., Wu, Q., Chen, Z., & Lin, X. (2014). A nonenzymatic hydrogen peroxide sensor based on Au–Ag nanotubes and chitosan film. *Journal of Electroanalytical Chemistry, 735*, 19-23.

Li, Y.-P., Cao, H.-B., Liu, C.-M., & Zhang, Y. (2007). Electrochemical reduction of nitrobenzene at carbon nanotube electrode. *Journal of Hazardous Materials, 148*(1), 158-163.

Li, Y., Huang, X., Chen, Y., Wang, L., & Lin, X. (2009). Simultaneous determination of dopamine and serotonin by use of covalent modification of 5-hydroxytryptophan on glassy carbon electrode. *Microchimica Acta, 164*(1-2), 107-112.

Li, Z., Yao, Y., Lin, Z., Moon, K.-S., Lin, W., & Wong, C. (2010). Ultrafast, dry microwave synthesis of graphene sheets. *Journal of Materials Chemistry, 20*(23), 4781-4783.

7.1.2 Liang, Y., Li, Y., Wang, H., Zhou, J., Wang, J., Regier, T., & Dai, H. (2011). Co_3O_4 nanocrystals on graphene as a synergistic catalyst for oxygen reduction reaction. *Nature Materials, 10*(10), 780-786.

Lin, X., Chen, Y., & Li, S. (2013). Spectrophotometric determination of trace p-nitrophenol enriched by 1-hydroxy-2-naphthoic acid-modified nanometer TiO_2 in water. *Analytical Methods, 5*(22), 6480-6485.

Liu, A. (2008). Towards development of chemosensors and biosensors with metal-oxide-based nanowires or nanotubes. *Biosensors and Bioelectronics, 24*(2), 167-177.

Liu, B., Wang, T., Yin, C., & Wei, Z. (2014). Electrochemical analysis of p-nitrophenol in acidic or alkaline medium using silver nanoparticle decorated multi-walled carbon nanotubes. *Journal of Materials Science, 49*(15), 5398-5405.

Liu, H.-C., & Yen, S.-K. (2007). Characterization of electrolytic Co_3O_4 thin films as anodes for lithium-ion batteries. *Journal of Power Sources, 166*(2), 478-484.

Liu, M., Hu, J., Ma, T., Wang, S., & Ding, H. (2011). Application of a disposable screen-printed electrode to depression diagnosis for laboratory rats based on blood serotonin detection. *Analytical Sciences, 27*(8), 839-843.

Liu, M., Xiang, J., Zhou, J., & Ding, H. (2010). A disposable amperometric sensor for rapid detection of serotonin in the blood and brain of the depressed mice based on Nafion membrane-coated colloidal gold screen-printed electrode. *Journal of Electroanalytical Chemistry, 640*(1), 1-7.

Liu, X., Zhu, H., & Yang, X. (2014). An electrochemical sensor for dopamine based on poly(o-phenylenediamine) functionalized with electrochemically reduced graphene oxide. *RSC Advances, 4*(8), 3706-3712.

Liu, Y.-C., Zhao, J., Wu, W.-L., & Yang, Z.-S. (2007). Direct electrochemical behavior of cytochrome c on DNA modified glassy carbon electrode and its application to nitric oxide biosensor. *Electrochimica Acta, 52*(14), 4848-4852.

Liu, Y., Chen, S.-S., Wang, A.-J., Feng, J.-J., Wu, X., & Weng, X. (2016). An ultra-sensitive electrochemical sensor for hydrazine based on AuPd nanorod alloy nanochains. *Electrochimica Acta, 195*, 68-76.

Liu, Z., Du, J., Qiu, C., Huang, L., Ma, H., Shen, D., & Ding, Y. (2009). Electrochemical sensor for detection of p-nitrophenol based on nanoporous gold. *Electrochemistry Communications, 11*(7), 1365-1368.

Lou, X. W., Deng, D., Lee, J. Y., Feng, J., & Archer, L. A. (2008). Self-supported formation of needlelike Co_3O_4 nanotubes and their application as lithium-ion battery electrodes. *Advanced Materials, 20*(2), 258-262.

Lu, W., Ning, R., Qin, X., Zhang, Y., Chang, G., Liu, S., Luo, Y., & Sun, X. (2011). Synthesis of Au nanoparticles decorated graphene oxide nanosheets: Noncovalent functionalization by TWEEN 20 in situ reduction of aqueous chloroaurate ions for hydrazine detection and catalytic reduction of 4-nitrophenol. *Journal of Hazardous Materials, 197*, 320-326.

Lu, Y., Wang, Y., Zou, Y., Jiao, Z., Zhao, B., He, Y., & Wu, M. (2010). Macroporous Co_3O_4 platelets with excellent rate capability as anodes for lithium ion batteries. *Electrochemistry Communications, 12*(1), 101-105.

Luo, J.-d., & Chen, A. F. (2005). Nitric oxide: a newly discovered function on wound healing. *Acta Pharmacologica Sinica, 26*(3), 259-264.

Luo, X., Pan, J., Pan, K., Yu, Y., Zhong, A., Wei, S., Li, J., Shi, J., & Li, X. (2015). An electrochemical sensor for hydrazine and nitrite based on graphene–cobalt hexacyanoferrate nanocomposite: Toward environment and food detection. *Journal of Electroanalytical Chemistry, 745*, 80-87.

Madhu, R., Dinesh, B., Chen, S.-M., Saraswathi, R., & Mani, V. (2015). An electrochemical synthesis strategy for composite based ZnO microspheres–Au nanoparticles on reduced graphene oxide for the sensitive detection of hydrazine in water samples. *RSC Advances, 5*(67), 54379-54386.

Madhu, R., Karuppiah, C., Chen, S.-M., Veerakumar, P., & Liu, S.-B. (2014). Electrochemical detection of 4-nitrophenol based on biomass derived activated carbons. *Analytical Methods, 6*(14), 5274-5280.

Maduraiveeran, G., & Ramaraj, R. (2007). Gold nanoparticles embedded in silica sol–gel matrix as an amperometric sensor for hydrogen peroxide. *Journal of Electroanalytical Chemistry, 608*(1), 52-58.

Maduraiveeran, G., & Ramaraj, R. (2009). Potential sensing platform of silver nanoparticles embedded in functionalized silicate shell for nitroaromatic compounds. *Analytical Chemistry, 81*(18), 7552-7560.

Mahmood, N., Zhang, C., Yin, H., & Hou, Y. (2014). Graphene-based nanocomposites for energy storage and conversion in lithium batteries, supercapacitors and fuel cells. *Journal of Materials Chemistry A, 2*(1), 15-32.

Makhlouf, S. A. (2002). Magnetic properties of Co_3O_4 nanoparticles. *Journal of Magnetism and Magnetic Materials, 246*(1), 184-190.

Malinski, T., & Taha, Z. (1992). Nitric oxide release from a single cell measured in situ by a porphyrinic-based microsensor. *Nature, 358*(6388), 676-678.

Mallela, S., & Khandelwal, B. (1977). Use of the rotating platinum electrode for microdetermination of hydrazine, hydroxylamine, nitrite, ascorbic acid, oxalic acid and thiourea with manganese (III) pyrophosphate. *Microchimica Acta, 68*(3-4), 245-248.

Matemadombo, F., & Nyokong, T. (2007). Characterization of self-assembled monolayers of iron and cobalt octaalkylthiosubstituted phthalocyanines and their use in nitrite electrocatalytic oxidation. *Electrochimica Acta, 52*(24), 6856-6864.

Mazloum-Ardakani, M., & Khoshroo, A. (2014). High sensitive sensor based on functionalized carbon nanotube/ionic liquid nanocomposite for simultaneous determination of norepinephrine and serotonin. *Journal of Electroanalytical Chemistry, 717-718*, 17-23.

Middelkoop, C. M., Dekker, G. A., Kraayenbrink, A. A., & Popp-Snijders, C. (1993). Platelet-poor plasma serotonin in normal and preeclamptic pregnancy. *Clinical Chemistry, 39*(8), 1675-1678.

Ming-Jay, D., Fu-Lu, H., Sun, I. W., Wen-Ta, T., & Jeng-Kuei, C. (2009). An entirely electrochemical preparation of a nano-structured cobalt oxide electrode with superior redox activity. *Nanotechnology, 20*(17), 175602.

Mini, V., Archana, K., Raghu, S., Sharanappa, C., & Devendrappa, H. (2016). Nanostructured multifunctional core/shell ternary composite of polyaniline-chitosan-cobalt oxide: Preparation, electrical and optical properties. *Materials Chemistry and Physics, 170*, 90-98.

Miotello, A., & Kelly, R. (1999). Laser-induced phase explosion: new physical problems when a condensed phase approaches the thermodynamic critical temperature. *Applied Physics A, 69*(1), S67-S73.

Moghaddam, R. B., & Pickup, P. G. (2012). Support effects on the oxidation of ethanol at Pt nanoparticles. *Electrochimica Acta, 65*, 210-215.

Mogudi, B. M., Ncube, P., & Meijboom, R. (2016). Catalytic activity of mesoporous cobalt oxides with controlled porosity and crystallite sizes: Evaluation using the reduction of 4-nitrophenol. *Applied Catalysis B: Environmental, 198*, 74-82.

Moncada, S., & Higgs, A. (1993). The L-arginine-nitric oxide pathway. *The New England Journal of Medicine, 329*(27), 2002-2012.

Morris, R., Fagan-Murphy, A., MacEachern, S. J., Covill, D., & Patel, B. A. (2016). Electrochemical fecal pellet sensor for simultaneous real-time ex vivo detection of colonic serotonin signalling and motility. *Scientific reports*, *6*, 23442.

Mu, J., Zhang, L., Zhao, M., & Wang, Y. (2013). Co_3O_4 nanoparticles as an efficient catalase mimic: Properties, mechanism and its electrocatalytic sensing application for hydrogen peroxide. *Journal of Molecular Catalysis A: Chemical, 378*, 30-37.

Ndlovu, T., Arotiba, O. A., Krause, R. W., & Mamba, B. B. (2010). Electrochemical detection of o-nitrophenol on a poly (propyleneimine)-gold nanocomposite modified glassy carbon electrode. *International Journal of Electrochemical Science, 5*, 117-1186.

Ng, H. T., Li, J., Smith, M. K., Nguyen, P., Cassell, A., Han, J., & Meyyappan, M. (2003). Growth of Epitaxial Nanowires at the Junctions of Nanowalls. *Science, 300*(5623), 1249-1249.

Nguyen, T. T., Nguyen, V. H., Deivasigamani, R. K., Kharismadewi, D., Iwai, Y., & Shim, J.-J. (2016). Facile synthesis of cobalt oxide/reduced graphene oxide composites for electrochemical capacitor and sensor applications. *Solid State Sciences, 53*, 71-77.

Ni, M., Leung, M. K., Leung, D. Y., & Sumathy, K. (2007). A review and recent developments in photocatalytic water-splitting using TiO2 for hydrogen production. *Renewable and Sustainable Energy Reviews, 11*(3), 401-425.

Nie, R., Shi, J., Du, W., Ning, W., Hou, Z., & Xiao, F.-S. (2013). A sandwich N-doped graphene/Co 3 O 4 hybrid: an efficient catalyst for selective oxidation of olefins and alcohols. *Journal of Materials Chemistry A, 1*(32), 9037-9045.

Niu, L. M., Lian, K. Q., Shi, H. M., Wu, Y. B., Kang, W. J., & Bi, S. Y. (2013). Characterization of an ultrasensitive biosensor based on a nano-Au/DNA/nano-Au/poly (SFR) composite and its application in the simultaneous determination of dopamine, uric acid, guanine, and adenine. *Sensors and Actuators B: Chemical, 178*, 10-18.

Noguera, C. (1996). *Physics and chemistry at oxide surfaces*: Cambridge University Press, Orsay.

Novoselov, K. S., Geim, A. K., Morozov, S. V., Jiang, D., Zhang, Y., Dubonos, S. V., Grigorieva, I. V., & Firsov, A. A. (2004). Electric field effect in atomically thin carbon films. *Science, 306*(5696), 666-669.

Numan, A., Duraisamy, N., Saiha Omar, F., Mahipal, Y. K., Ramesh, K., & Ramesh, S. (2016). Enhanced electrochemical performance of cobalt oxide nanocube intercalated reduced graphene oxide for supercapacitor application. *RSC Advances, 6*(41), 34894-34902.

Numan, A., Shahid, M. M., Omar, F. S., Ramesh, K., & Ramesh, S. (2017). Facile fabrication of cobalt oxide nanograin-decorated reduced graphene oxide composite as ultrasensitive platform for dopamine detection. *Sensors and Actuators B: Chemical, 238*, 1043-1051.

O'Donoghue, M. (1983). *A guide to Man-made Gemstones*: Van Nostrand Reinhold Company.

Ohkubo, I., Matsumoto, Y., Hasegawa, T., Ueno, K., Itaka, K., Ahmet, P., Chikyow, T., Kawasaki, M., & Koinuma, H. (2001). Pulsed laser epitaxy and magnetic properties of single phase Y-type magnetoplumbite thin films. *Japanese Journal of Applied Physics, 40*(12B), L1343.

Pan, L., Li, L., & Chen, Y. (2012). Synthesis of NiO nanomaterials with various morphologies and their electrocatalytic performances for p-nitrophenol reduction. *Journal of sol-gel science and technology, 62*(3), 364-369.

Pan, L., Tang, J., & Wang, F. (2013). Synthesis and electrocatalytic performance for p-nitrophenol reduction of rod-like Co_3O_4 and Ag/Co_3O_4 composites. *Materials Research Bulletin, 48*(7), 2648-2653.

Pan, L., Zhao, H., Shen, W., Dong, X., & Xu, J. (2013). Surfactant-assisted synthesis of a Co_3O_4/reduced graphene oxide composite as a superior anode material for Li-ion batteries. *Journal of Materials Chemistry A, 1*(24), 7159-7166.

Pandikumar, A., & Ramaraj, R. (2011). Aminosilicate sol-gel embedded core-shell (TiO_2-Au) nps nanomaterials modified electrode for the electrochemical detection of nitric oxide. *Indian Journal of Chemistry, 50A*, 1388-1393.

Panholzer, T. J., Beyer, J., & Lichtwald, K. (1999). Coupled-column liquid chromatographic analysis of catecholamines, serotonin, and metabolites in human urine. *Clinical Chemistry, 45*(2), 262-268.

Paredes, J., Villar-Rodil, S., Martínez-Alonso, A., & Tascon, J. (2008). Graphene oxide dispersions in organic solvents. *Langmuir, 24*(19), 10560-10564.

Park, D.-H., Lim, S.-T., & Hwang, S.-J. (2006). A soft chemical route to multicomponent lithium transition metal oxide nanowires as promising cathode materials for lithium secondary batteries. *Electrochimica Acta, 52*(4), 1462-1466.

Park, S., & Ruoff, R. S. (2009). Chemical methods for the production of graphenes. *Nature Nanotechnology, 4*(4), 217-224.

Poizot, P., Laruelle, S., Grugeon, S., Dupont, L., & Tarascon, J. (2000). Nano-sized transition-metal oxides as negative-electrode materials for lithium-ion batteries. *Nature, 407*(6803), 496-499.

Pravinraj, S., Vijayakumar, M., & Marimuthu, K. (2017). Enhanced luminescence behaviour of Eu^{3+} doped heavy metal oxide telluroborate glasses for Laser and LED applications. *Physica B: Condensed Matter, 509*, 84-93.

Privett, B. J., Shin, J. H., & Schoenfisch, M. H. (2010). Electrochemical nitric oxide sensors for physiological measurements. *Chemical Society Reviews, 39*(6), 1925-1935.

Qu, Q., Yang, S., & Feng, X. (2011). 2D Sandwich-like Sheets of Iron Oxide Grown on Graphene as High Energy Anode Material for Supercapacitors. *Advanced Materials, 23*(46), 5574-5580.

Rafique, S., Abdullah, S. M., Shahid, M. M., Ansari, M. O., & Sulaiman, K. (2017). Significantly improved photovoltaic performance in polymer bulk heterojunction solar cells with graphene oxide/PEDOT: PSS double decked hole transport layer. *Scientific Reports, 7*, doi**:** 10.1038/srep39555.

Rahman, M. M., Khan, S. B., Faisal, M., Rub, M. A., Al-Youbi, A. O., & Asiri, A. M. (2012). Electrochemical determination of olmesartan medoxomil using hydrothermally prepared nanoparticles composed SnO_2– Co_3O_4 nanocubes in tablet dosage forms. *Talanta, 99*, 924-931.

Rahman, M. M., Wang, J.-Z., Deng, X.-L., Li, Y., & Liu, H.-K. (2009). Hydrothermal synthesis of nanostructured Co_3O_4 materials under pulsed magnetic field and with an aging technique, and their electrochemical performance as anode for lithium-ion battery. *Electrochimica Acta, 55*(2), 504-510.

Rahman, M. M., Wang, J.-Z., Deng, X.-L., Li, Y., & Liu, H.-K. (2009). Hydrothermal synthesis of nanostructured Co_3O_4 materials under pulsed magnetic field and with an aging technique, and their electrochemical performance as anode for lithium-ion battery. *Electrochimica Acta, 55*(2), 504-510.

Rajput, N. (2015). Methods of preparation of nanoparticles-A review. *International Journal Of Advances in Engineering & Technology, 7*(6), 1806-1811.

Rameshkumar, P., & Ramaraj, R. (2014). Electroanalysis of nitrobenzene derivatives and nitrite ions using silver nanoparticles deposited silica spheres modified electrode. *Journal of Electroanalytical Chemistry, 731*, 72-77.

Ran, G., Chen, C., & Gu, C. (2015). Serotonin sensor based on a glassy carbon electrode modified with multiwalled carbon nanotubes, chitosan and poly(p-aminobenzenesulfonate). *Microchimica Acta, 182*(7), 1323-1328.

Rand, E., Periyakaruppan, A., Tanaka, Z., Zhang, D. A., Marsh, M. P., Andrews, R. J., Lee, K. H., Chen, B., Meyyappan, M., & Koehne, J. E. (2013). A carbon nanofiber based biosensor for simultaneous detection of dopamine and serotonin in the presence of ascorbicacid. *Biosensors and Bioelectronics, 42*, 434-438.

Rao, C., Sood, A., Voggu, R., & Subrahmanyam, K. (2010). Some novel attributes of graphene. *The Journal of Physical Chemistry Letters, 1*(2), 572-580.

Rastogi, P. K., Ganesan, V., & Krishnamoorthi, S. (2014a). Palladium nanoparticles decorated gaur gum based hybrid material for electrocatalytic hydrazine determination. *Electrochimica Acta, 125*, 593-600.

Rastogi, P. K., Ganesan, V., & Krishnamoorthi, S. (2014b). A promising electrochemical sensing platform based on a silver nanoparticles decorated copolymer for sensitive nitrite determination. *Journal of Materials Chemistry A, 2*(4), 933-943.

Razmi, H., & Habibi, E. (2010). Amperometric detection of acetaminophen by an electrochemical sensor based on cobalt oxide nanoparticles in a flow injection system. *Electrochimica Acta, 55*(28), 8731-8737.

Reddaiah, K., Reddy, T. M., & Raghu, P. (2012). Electrochemical investigation of L-dopa and simultaneous resolution in the presence of uric acid and ascorbic acid at a poly (methyl orange) film coated electrode: A voltammetric study. *Journal of Electroanalytical Chemistry, 682*, 164-171.

Rout, C. S., Krishna, S. H., Vivekchand, S., Govindaraj, A., & Rao, C. (2006). Hydrogen and ethanol sensors based on ZnO nanorods, nanowires and nanotubes. *Chemical Physics Letters, 418*(4), 586-590.

Rubio-Retama, J., Hernando, J., Lopez-Ruiz, B., Härtl, A., Steinmüller, D., Stutzmann, M., Lopez-Cabarcos, E., & Antonio Garrido, J. (2006). Synthetic nanocrystalline diamond as a third-generation biosensor support. *Langmuir, 22*(13), 5837-5842.

Safavi, A., & Ensafi, A. A. (1995). Kinetic spectrophotometric determination of hydrazine. *Analytica Chimica Acta, 300*(1), 307-311.

Safavi, A., & Karimi, M. A. (2002). Flow injection chemiluminescence determination of hydrazine by oxidation with chlorinated isocyanurates. *Talanta, 58*(4), 785-792.

Sankur, H., Gunning, W., DeNatale, J., & Flintoff, J. (1989). High-quality optical and epitaxial Ge films formed by laser evaporation. *Journal of Applied Physics, 65*(6), 2475-2478.

Santhiago, M., Henry, C. S., & Kubota, L. T. (2014). Low cost, simple three dimensional electrochemical paper-based analytical device for determination of p-nitrophenol. *Electrochimica Acta, 130*, 771-777.

Schwentker, A., Vodovotz, Y., Weller, R., & Billiar, T. R. (2002). Nitric oxide and wound repair: role of cytokines? *Nitric oxide, 7*(1), 1-10.

Service, R. F. (2009). Materials science. Carbon sheets an atom thick give rise to graphene dreams. *Science (New York, NY), 324*(5929), 875-877.

Shahabuddin, S., Sarih, N. M., Ismail, F. H., Shahid, M. M., & Huang, N. M. (2015). Synthesis of chitosan grafted-polyaniline/ Co_3O_4 nanocube nanocomposites and their photocatalytic activity toward methylene blue dye degradation. *RSC Advances, 5*(102), 83857-83867.

Shahid, M. M., Pandikumar, A., Golsheikh, A. M., Huang, N. M., & Lim, H. N. (2014). Enhanced electrocatalytic performance of cobalt oxide nanocubes incorporating reduced graphene oxide as a modified platinum electrode for methanol oxidation. *RSC Advances, 4*(107), 62793-62801.

Shahid, M. M., Rameshkumar, P., Basirun, W. J., Juan, J. C., & Huang, N. M. (2017). Cobalt oxide nanocubes interleaved reduced graphene oxide as an efficient electrocatalyst for oxygen reduction reaction in alkaline medium. *Electrochimica Acta, 237*, 61-68.

Shahid, M. M., Rameshkumar, P., & Huang, N. M. (2015). Morphology dependent electrocatalytic properties of hydrothermally synthesized cobalt oxide nanostructures. *Ceramics International, 41*(10), 13210-13217.

Shahid, M. M., Rameshkumar, P., Pandikumar, A., Lim, H. N., Ng, Y. H., & Huang, N. M. (2015). An electrochemical sensing platform based on a reduced graphene oxide-cobalt oxide nanocube@platinum nanocomposite for nitric oxide detection. *Journal of Materials Chemistry A, 3*(27), 14458-14468.

Shalini, K., Mane, A. U., Shivashankar, S., Rajeswari, M., & Choopun, S. (2001). Epitaxial growth of Co_3O_4 films by low temperature, low pressure chemical vapour deposition. *Journal of Crystal Growth, 231*(1), 242-247.

Shaoqing, Y., Jun, H., & Jianlong, W. (2010). Radiation-induced catalytic degradation of p-nitrophenol (PNP) in the presence of TiO2 nanoparticles. *Radiation Physics and Chemistry*, *79*(10), 1039-1046.

Sharifi, S., Shakur, H., Mirzaei, A., & Hosseini, M. (2013). Characterization of cobalt oxide Co_3O_4 nanoparticles prepared by various methods: Effect of calcination temperatures on size, dimension and catalytic decomposition of hydrogen peroxide. *International Journal of Nanoscience and Nanotechnology*, *9*(1), 51-58.

Shi, R., Chen, G., Ma, W., Zhang, D., Qiu, G., & Liu, X. (2012). Shape-controlled synthesis and characterization of cobalt oxides hollow spheres and octahedra. *Dalton Transactions, 41*(19), 5981-5987.

Shimizu, M., Suzuki, M., Iguchi, F., & Yugami, H. (2014). High-temperature Solar Selective Absorbers Using Transparent Conductive Oxide Coated Metal. *Energy Procedia*, *57*, 418-426.

Shrivastava, A., & Gupta, V. (2011). Methods for the determination of limit of detection and limit of quantitation of the analytical methods. *Chronicles of Young Scientists, 2*(1), 21-21.

Singh, B., Dempsey, E., Dickinson, C., & Laffir, F. (2012). Inside/outside Pt nanoparticles decoration of functionalised carbon nanofibers (Pt 19.2/f-CNF 80.8) for sensitive non-enzymatic electrochemical glucose detection. *Analyst, 137*(7), 1639-1648.

Song, Z., Zhang, Y., Liu, W., Zhang, S., Liu, G., Chen, H., & Qiu, J. (2013). Hydrothermal synthesis and electrochemical performance of Co_3O_4/reduced graphene oxide nanosheet composites for supercapacitors. *Electrochimica Acta, 112*, 120-126.

Stankovich, S., Dikin, D. A., Piner, R. D., Kohlhaas, K. A., Kleinhammes, A., Jia, Y., Wu, Y., Nguyen, S. T., & Ruoff, R. S. (2007). Synthesis of graphene-based nanosheets via chemical reduction of exfoliated graphite oxide. *Carbon, 45*(7), 1558-1565.

Stroyuk, A. L., Shvalagin, V. V., & Kuchmii, S. Y. (2005). Photochemical synthesis and optical properties of binary and ternary metal–semiconductor composites based

on zinc oxide nanoparticles. *Journal of Photochemistry and Photobiology A: Chemistry, 173*(2), 185-194.

Su, J., Gherasimova, M., Cui, G., Tsukamoto, H., Han, J., Onuma, T., Kurimoto, M., Chichibu, S., Broadbridge, C., & He, Y. (2005). Growth of AlGaN nanowires by metalorganic chemical vapor deposition. *Applied Physics Letters, 87*(18), 183108.

Sun, M., Liu, H., Liu, Y., Qu, J., & Li, J. (2015). Graphene-based transition metal oxide nanocomposites for the oxygen reduction reaction. *Nanoscale, 7*(4), 1250-1269.

Taha, Z. H. (2003). Nitric oxide measurements in biological samples. *Talanta, 61*(1), 3-10.

Takada, S., Fujii, M., Kohiki, S., Babasaki, T., Deguchi, H., Mitome, M., & Oku, M. (2001). Intraparticle magnetic properties of Co_3O_4 nanocrystals. *Nano Letters, 1*(7), 379-382.

Tang, Y.-Y., Kao, C.-L., & Chen, P.-Y. (2012). Electrochemical detection of hydrazine using a highly sensitive nanoporous gold electrode. *Analytica Chimica Acta, 711*, 32-39.

Tang, Y., Huang, R., Liu, C., Yang, S., Lu, Z., & Luo, S. (2013). Electrochemical detection of 4-nitrophenol based on a glassy carbon electrode modified with a reduced graphene oxide/Au nanoparticle composite. *Analytical Methods, 5*(20), 5508-5514.

Thangavel, S., & Ramaraj, R. (2008). Polymer membrane stabilized gold nanostructures modified electrode and its application in nitric oxide detection. *The Journal of Physical Chemistry C, 112*(50), 19825-19830.

Thanh, T. D., Balamurugan, J., Kim, N. H., Lee, S. H., & Lee, J. H. (2016). Effective seed-assisted synthesis of gold nanoparticles anchored nitrogen-doped graphene for electrochemical detection of glucose and dopamine. *Biosensors and Bioelectronics, 81*, 259-267.

Thompson, L., & Doraiswamy, L. (1999). Sonochemistry: science and engineering. *Industrial & Engineering Chemistry Research, 38*(4), 1215-1249.

Ting, S. L., Guo, C. X., Leong, K. C., Kim, D.-H., Li, C. M., & Chen, P. (2013). Gold nanoparticles decorated reduced graphene oxide for detecting the presence and cellular release of nitric oxide. *Electrochimica Acta, 111*, 441-446.

Tsuda, N., Nasu, K., Fujimori, A., & Siratori, K. (2013). *Electronic Conduction in Oxides* (Vol. 94): Springer Science & Business Media, Hiedelberg.

Tsunoda, M., Takezawa, K., Santa, T., & Imai, K. (1999). Simultaneous automatic determination of catecholamines and their 3-O-methyl metabolites in rat plasma by high-performance liquid chromatography using peroxyoxalate chemiluminescence reaction. *Analytical Biochemistry, 269*(2), 386-392.

Van Lier, G., Van Alsenoy, C., Van Doren, V., & Geerlings, P. (2000). Ab initio study of the elastic properties of single-walled carbon nanotubes and graphene. *Chemical Physics Letters, 326*(1), 181-185.

Védrine, J. C. (2002). The Role of Redox, Acid-Base and Collective Properties and of Cristalline State of Heterogeneous Catalysts in the Selective Oxidation of Hydrocarbons. *Topics in Catalysis, 21*(1), 97-106.

Viinikanoja, A., Wang, Z., Kauppila, J., & Kvarnström, C. (2012). Electrochemical reduction of graphene oxide and its in situ spectroelectrochemical characterization. *Physical Chemistry Chemical Physics, 14*(40), 14003-14009.

Wang, F., Wu, Y., Lu, K., & Ye, B. (2013). A simple but highly sensitive and selective calixarene-based voltammetric sensor for serotonin. *Electrochimica Acta, 87*, 756-762.

Wang, G., Yang, J., Park, J., Gou, X., Wang, B., Liu, H., & Yao, J. (2008). Facile synthesis and characterization of graphene nanosheets. *The Journal of Physical Chemistry C, 112*(22), 8192-8195.

Wang, G., Zhang, C., He, X., Li, Z., Zhang, X., Wang, L., & Fang, B. (2010). Detection of hydrazine based on Nano-Au deposited on Porous-TiO2 film. *Electrochimica Acta, 55*(24), 7204-7210.

Wang, J., Xie, Y., Zhang, Z., Li, J., Li, C., Zhang, L., Xing, Z., Xu, R., & Zhang, X. (2010). Photocatalytic degradation of organic dyes by Er3+:$YAlO_3$/TiO_2 composite under solar light. *Environmental Chemistry Letters, 8*(1), 87-93.

Wang, S., & Lin, X. (2005). Electrodeposition of Pt–Fe (III) nanoparticle on glassy carbon electrode for electrochemical nitric oxide sensor. *Electrochimica Acta, 50*(14), 2887-2891.

Wang, X., Tian, W., Zhai, T., Zhi, C., Bando, Y., & Golberg, D. (2012). Cobalt(ii,iii) oxide hollow structures: fabrication, properties and applications. *Journal of Materials Chemistry, 22*(44), 23310-23326.

Wang, Y., Jin, A., & Zhang, Z. (2002). Cu/SiO 2− x nanowires with compositional modulation structure grown via thermal evaporation. *Applied Physics Letters, 81*(23), 4425-4427.

Wang, Y., Song, B., Xu, J., & Hu, S. (2014). An amperometric sensor for nitric oxide based on a glassy carbon electrode modified with graphene, Nafion, and electrodeposited gold nanoparticles. *Microchimica Acta, 182*(3-4), 711-718.

Wang, Y., Wan, Y., & Zhang, D. (2010). Reduced graphene sheets modified glassy carbon electrode for electrocatalytic oxidation of hydrazine in alkaline media. *Electrochemistry Communications, 12*(2), 187-190.

Watt, G. W., & Chrisp, J. D. (1952). Spectrophotometric method for determination of hydrazine. *Analytical Chemistry, 24*(12), 2006-2008.

Willmott, P., Manoravi, P., & Holliday, K. (2000). Production and characterization of Nd, Cr: GSGG thin films on Si (001) grown by pulsed laser ablation. *Applied Physics A: Materials Science & Processing, 70*(4), 425-429.

Wu, F.-H., Zhao, G.-C., & Wei, X.-W. (2002). Electrocatalytic oxidation of nitric oxide at multi-walled carbon nanotubes modified electrode. *Electrochemistry Communications, 4*(9), 690-694.

Wu, J., Wang, Q., Umar, A., Sun, S., Huang, L., Wang, J., & Gao, Y. (2014). Highly sensitive p-nitrophenol chemical sensor based on crystalline α-MnO_2 nanotubes. *New Journal of Chemistry, 38*(9), 4420-4426.

Wu, R.-J., Hu, C.-H., Yeh, C.-T., & Su, P.-G. (2003). Nanogold on powdered cobalt oxide for carbon monoxide sensor. *Sensors and Actuators B: Chemical, 96*(3), 596-601.

Wu, Z.-S., Ren, W., Wen, L., Gao, L., Zhao, J., Chen, Z., Zhou, G., Li, F., & Cheng, H.-M. (2010). Graphene anchored with Co_3O_4 nanoparticles as anode of lithium ion batteries with enhanced reversible capacity and cyclic performance. *ACS nano, 4*(6), 3187-3194.

Wu, Z. S., Wang, D. W., Ren, W., Zhao, J., Zhou, G., Li, F., & Cheng, H. M. (2010). Anchoring Hydrous RuO2 on Graphene Sheets for High-Performance Electrochemical Capacitors. *Advanced Functional Materials, 20*(20), 3595-3602.

Xia, X., Tu, J., Zhang, J., Xiang, J., Wang, X., & Zhao, X. (2010). Fast electrochromic properties of self-supported Co 3 O 4 nanowire array film. *Solar Energy Materials and Solar Cells, 94*(2), 386-389.

Xiao, J., Kuang, Q., Yang, S., Xiao, F., Wang, S., & Guo, L. (2013). Surface Structure Dependent Electrocatalytic Activity of Co_3O_4 Anchored on Graphene Sheets toward Oxygen Reduction Reaction. *Scientific reports, 3*.

Xiao, S. Q., Wang, H., Zhao, Z. C., Xia, Y. X., & Wang, Z. H. (2008). Magnetic and transport properties in metal-oxide-semiconductor structures of Co_3Mn_2O/SiO_2 /Si. *Journal of Physics D: Applied Physics, 41*(4), 045005.

Xu, C.-X., Huang, K.-J., Fan, Y., Wu, Z.-W., Li, J., & Gan, T. (2012). Simultaneous electrochemical determination of dopamine and tryptophan using a TiO_2-graphene/poly (4-aminobenzenesulfonic acid) composite film based platform. *Materials Science and Engineering: C, 32*(4), 969-974.

Xu, G., Li, B., Wang, X., & Luo, X. (2014). Electrochemical sensor for nitrobenzene based on carbon paste electrode modified with a poly (3, 4-ethylenedioxythiophene) and carbon nanotube nanocomposite. *Microchimica Acta, 181*(3-4), 463-469.

Xu, M., Ye, L., Wang, J., Wei, Z., & Cheng, S. (2017). Quality tracing of peanuts using an array of metal-oxide based gas sensors combined with chemometrics methods. *Postharvest Biology and Technology, 128*, 98-104.

Xu, X., Liu, Z., Zhang, X., Duan, S., Xu, S., & Zhou, C. (2011). β-Cyclodextrin functionalized mesoporous silica for electrochemical selective sensor:

Simultaneous determination of nitrophenol isomers. *Electrochimica Acta, 58*, 142-149.

Xue, P., Zhang, L., Zhang, L., Feng, X., Zhang, Y., Hao, W., Wang, H., & Zheng, H. (2014). In-plane Vacancy-Induced Growth of Ultra-High Loading Cobalt Oxide-Graphene Composite for High-Performance Lithium-Ion Batteries. *Electrochimica Acta, 136*, 330-339.

Yang, J., Liu, G., Lu, J., Qiu, Y., & Yang, S. (2007). Electrochemical route to the synthesis of ultrathin ZnO nanorod/nanobelt arrays on zinc substrate. *Applied Physics Letters, 90*(10), 103109.

Yang, W., Gao, Z., Wang, J., Wang, B., Liu, Q., Li, Z., Mann, T., Yang, P., Zhang, M., & Liu, L. (2012). Synthesis of reduced graphene nanosheet/urchin-like manganese dioxide composite and high performance as supercapacitor electrode. *Electrochimica Acta, 69*, 112-119.

Yao, Y., Yang, Z., Sun, H., & Wang, S. (2012). Hydrothermal synthesis of Co_3O_4–graphene for heterogeneous activation of peroxymonosulfate for decomposition of phenol. *Industrial & Engineering Chemistry Research, 51*(46), 14958-14965.

Yao, Z., Yue, R., Zhai, C., Jiang, F., Wang, H., Du, Y., Wang, C., & Yang, P. (2013). Electrochemical layer-by-layer fabrication of a novel three-dimensional Pt/graphene/carbon fiber electrode and its improved catalytic performance for methanol electrooxidation in alkaline medium. *International Journal of Hydrogen Energy, 38*(15), 6368-6376.

Yeh, M.-H., Sun, C.-L., Su, J.-S., Lin, L.-Y., Lee, C.-P., Chen, C.-Y., Wu, C.-G., Vittal, R., & Ho, K.-C. (2012). A low-cost counter electrode of ITO glass coated with a graphene/Nafion® composite film for use in dye-sensitized solar cells. *Carbon, 50*(11), 4192-4202.

Yi, Q., Niu, F., & Yu, W. (2011). Pd-modified TiO_2 electrode for electrochemical oxidation of hydrazine, formaldehyde and glucose. *Thin Solid Films, 519*(10), 3155-3161.

Yi, Q., & Yu, W. (2009). Nanoporous gold particles modified titanium electrode for hydrazine oxidation. *Journal of Electroanalytical Chemistry, 633*(1), 159-164.

Yin, H., Zhou, Y., Ai, S., Ma, Q., Zhu, L., & Lu, L. (2012). Electrochemical oxidation determination and voltammetric behaviour of 4-nitrophenol based on Cu2O nanoparticles modified glassy carbon electrode. *International Journal of Environmental Analytical Chemistry, 92*(6), 742-754.

Yuan, C.-X., Fan, Y.-R., Guo, H.-X., Zhang, J.-X., Wang, Y.-L., Shan, D.-L., & Lu, X.-Q. (2014). A new electrochemical sensor of nitro aromatic compound based on three-dimensional porous Pt–Pd nanoparticles supported by graphene–multiwalled carbon nanotube composite. *Biosensors and Bioelectronics, 58*, 85-91.

Yusoff, N., Pandikumar, A., Huang, N. M., & Lim, H. N. (2015). Facile synthesis of nanosized graphene/Nafion hybrid materials and their application in electrochemical sensing of nitric oxide. *Analytical Methods, 7*(8), 3537-3544.

Yusoff, N., Rameshkumar, P., Mehmood, M. S., Pandikumar, A., Lee, H. W., & Huang, N. M. (2017). Ternary nanohybrid of reduced graphene oxide-nafion@ silver nanoparticles for boosting the sensor performance in non-enzymatic amperometric detection of hydrogen peroxide. *Biosensors and Bioelectronics, 87*, 1020-1028.

Yusoff, N., Rameshkumar, P., Shahid, M. M., Huang, S.-T., & Huang, N. M. (2017). Amperometric detection of nitric oxide using a glassy carbon electrode modified with gold nanoparticles incorporated into a nanohybrid composed of reduced graphene oxide and nafion. *Microchimica Acta, 184*(9), 3291–3299.

Zecchina, A., Scarano, D., Bordiga, S., Spoto, G., & Lamberti, C. (2001). Surface structures of oxides and halides and their relationships to catalytic properties. *Advances in Catalysis, 46*, 265-397.

Zen, J.-M., Kumar, A. S., & Wang, H.-F. (2000). A dual electrochemical sensor for nitrite and nitric oxide. *Analyst, 125*(12), 2169-2172.

Zeng, Y., Zhou, Y., Zhou, T., & Shi, G. (2014). A novel composite of reduced graphene oxide and molecularly imprinted polymer for electrochemical sensing 4-nitrophenol. *Electrochimica Acta, 130*, 504-511.

Zhai, T., Fang, X., Liao, M., Xu, X., Zeng, H., Yoshio, B., & Golberg, D. (2009). A comprehensive review of one-dimensional metal-oxide nanostructure photodetectors. *Sensors, 9*(8), 6504-6529.

Zhang, C., Wang, G., Ji, Y., Liu, M., Feng, Y., Zhang, Z., & Fang, B. (2010). Enhancement in analytical hydrazine based on gold nanoparticles deposited on ZnO-MWCNTs films. *Sensors and Actuators B: Chemical, 150*(1), 247-253.

Zhang, C., Yang, J., & Wu, Z. (2000). Electroreduction of nitrobenzene on titanium electrode implanted with platinum. *Materials Science and Engineering: B, 68*(3), 138-142.

Zhang, H.-X., Cao, A.-M., Hu, J.-S., Wan, L.-J., & Lee, S.-T. (2006). Electrochemical sensor for detecting ultratrace nitroaromatic compounds using mesoporous SiO_2-modified electrode. *Analytical Chemistry, 78*(6), 1967-1971.

Zhang, J., Gao, W., Dou, M., Wang, F., Liu, J., Li, Z., & Ji, J. (2015). Nanorod-constructed porous Co_3O_4 nanowires: highly sensitive sensors for the detection of hydrazine. *Analyst, 140*(5), 1686-1692.

Zhang, Y., Chen, Y., Wang, T., Zhou, J., & Zhao, Y. (2008). Synthesis and magnetic properties of nanoporous Co_3O_4 snanoflowers. *Microporous and Mesoporous Materials, 114*(1), 257-261.

Zhao, S., Wang, L., Wang, T., Han, Q., & Xu, S. (2016). A high-performance hydrazine electrochemical sensor based on gold nanoparticles/single-walled carbon nanohorns composite film. *Applied Surface Science, 369*, 36-42.

Zheng, D., Liu, X., Zhou, D., & Hu, S. (2012). Sensing of nitric oxide using a glassy carbon electrode modified with an electrocatalytic film composed of dihexadecyl hydrogen phosphate, platinum nanoparticles, and acetylene black. *Microchimica Acta, 176*(1-2), 49-55.

Zhou, Y.-G., Chen, J.-J., Wang, F.-b., Sheng, Z.-H., & Xia, X.-H. (2010). A facile approach to the synthesis of highly electroactive Pt nanoparticles on graphene as an anode catalyst for direct methanol fuel cells. *Chemical Communications, 46*(32), 5951-5953.

7.1.3 Zhu, Y., Murali, S., Cai, W., Li, X., Suk, J. W., Potts, J. R., & Ruoff, R. S. (2010). Graphene and graphene oxide: synthesis, properties, and applications. *Advanced Materials, 22*(35), 3906-3924.

LIST OF PUBLICATIONS AND PAPERS PRESENTED

Publications

1. **Shahid, M. M.**, Rameshkumar, P., & Huang, N. M. (2015). Morphology dependent electrocatalytic properties of hydrothermally synthesized cobalt oxide nanostructures. *Ceramics International*, *41*(10), 13210-13217.

2. **Shahid, M. M**., Rameshkumar, P., Basirunc, W. J., Wijayantha, U., Chiu, W. S., Khiew, P. S., & Huang, N. M. (2018). An electrochemical sensing platform of cobalt oxide@ gold nanocubes interleaved reduced graphene oxide for the selective determination of hydrazine. *Electrochimica Acta*, *259*, 606-616.

3. **Shahid, M. M**., Rameshkumar, P., Pandikumar, A., Lim, H. N., Ng, Y. H., & Huang, N. M. (2015). An electrochemical sensing platform based on a reduced graphene oxide–cobalt oxide nanocube@ platinum nanocomposite for nitric oxide detection. *Journal of Materials Chemistry A*, *3*(27), 14458-14468.

Paper Presented in Internstional Conferences

1. **Shahid, M. M**., Nay Ming Huang, Cobalt oxide nanostructures based electrochemical sensing platform for the detection of water contaminant 4-nitrophenol. *International Conference on Waste Management and Environment (ICWME-2015)*. 9-11 September 2015, University of Malaya, Kuala Lumpur, Malaysia.

2. **Shahid, M. M**., Nay Ming Huang, A highly active and durable electrocatalyst; based on cobalt oxide nanocubes incorporated reduced graphene oxide a modified platinum electrode for methanol oxidation. *International Conference on Emerging research in sciences & humanities (ERSH-2016).* 16-17 May 2016. Pearl International Hotel, Kuala Lumpur, Malaysia.

APPENDIX

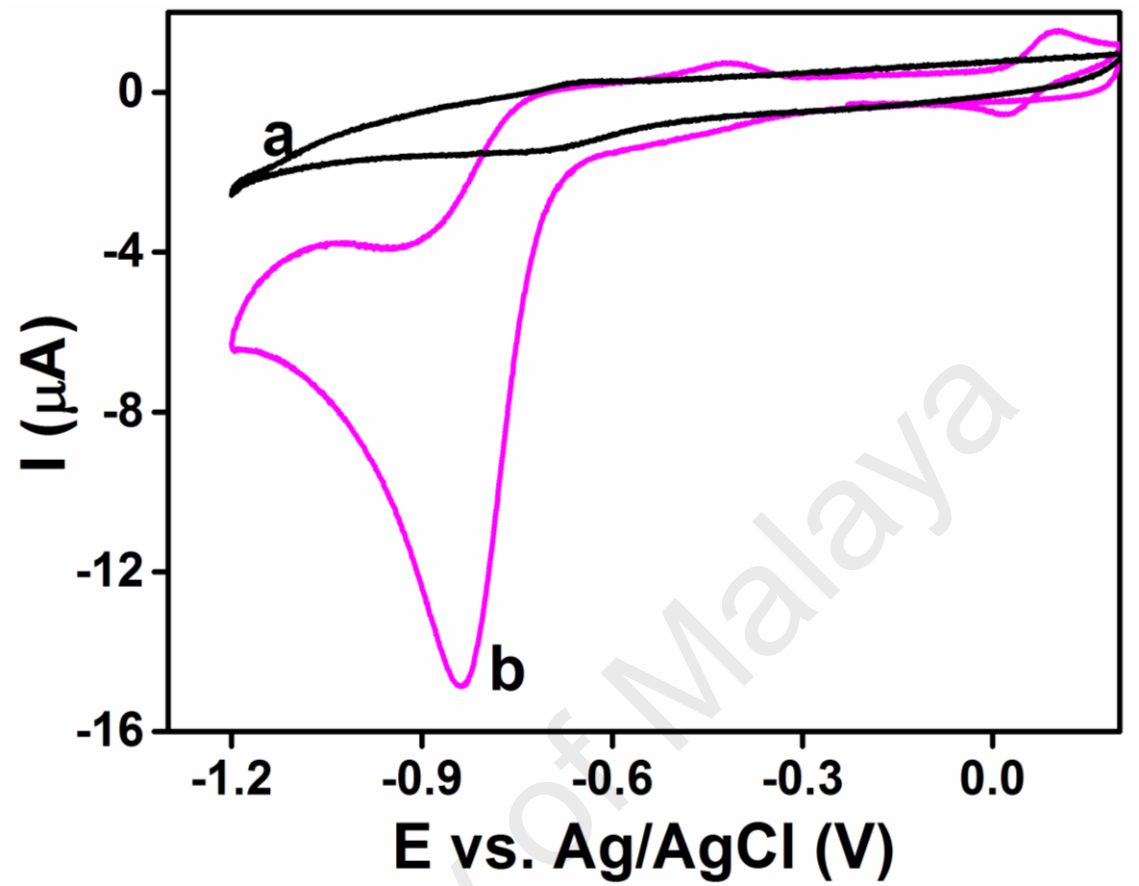

Appendix 1: CV recorded at GC/Co_3O_4 nanocubes.

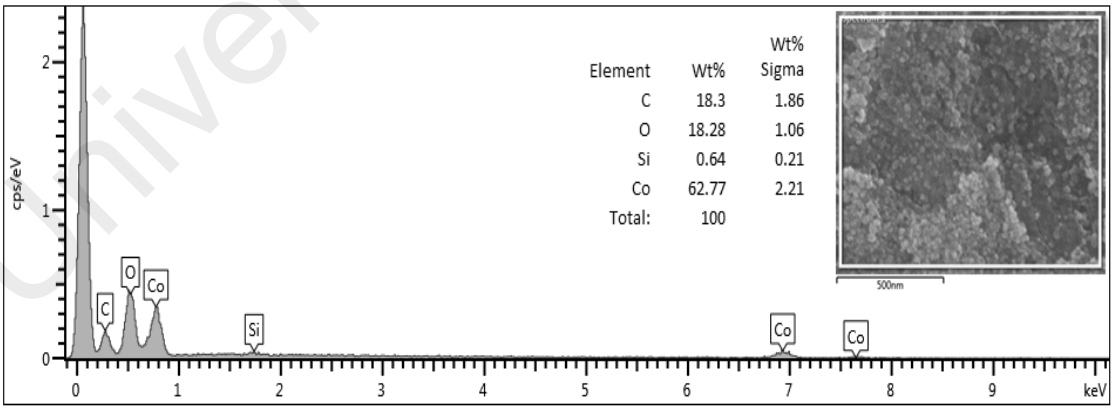

Appendix 2: EDX spectrum of rGO-Co_3O_4-4 % nanocomposite.

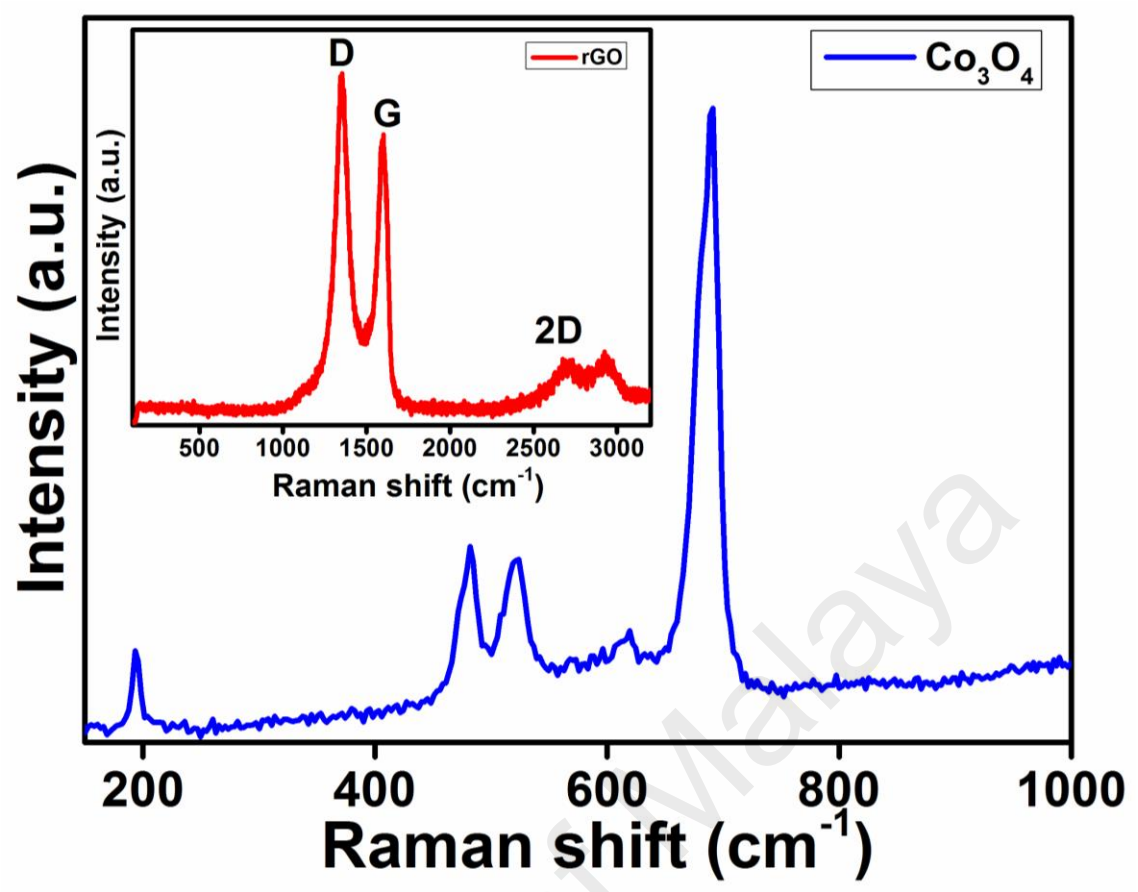

Appendix 3: Raman spectra of pure Co_3O_4 and rGO (inset).

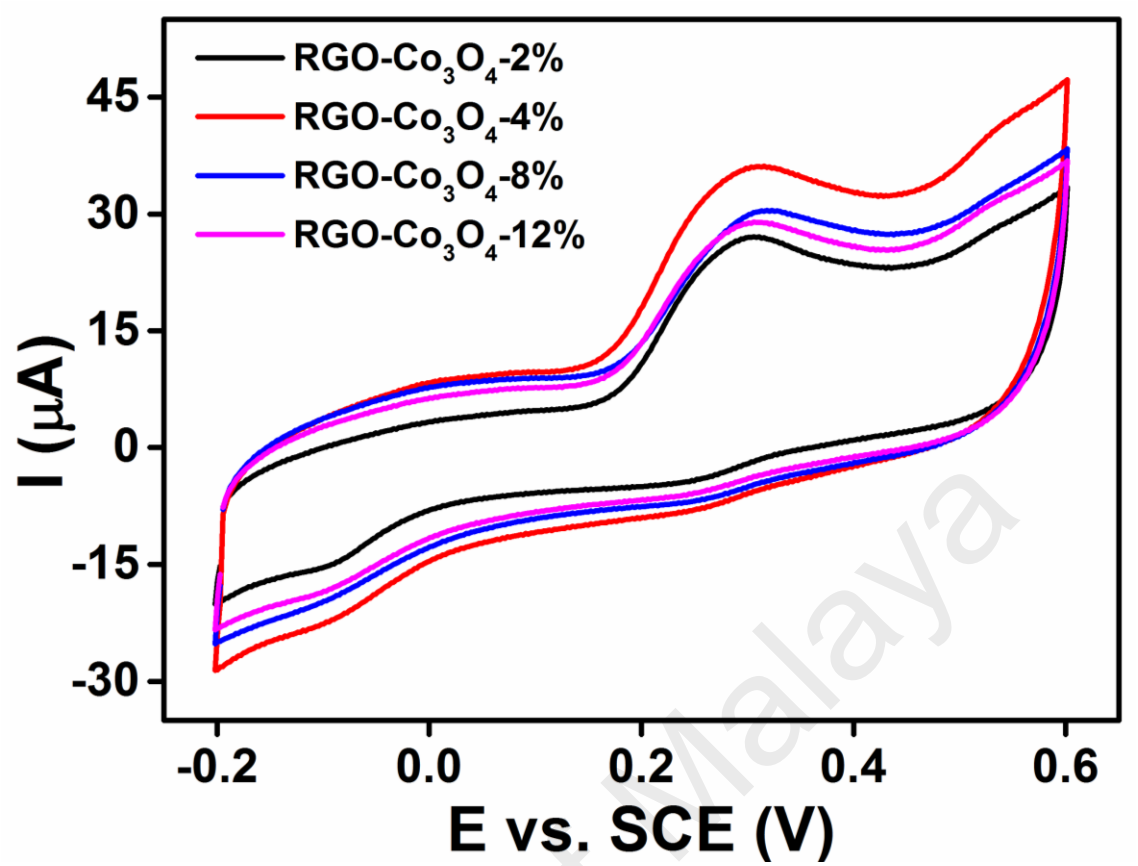

Appendix 4: CV recorded for rGO-Co_3O_4 nanocomposites.

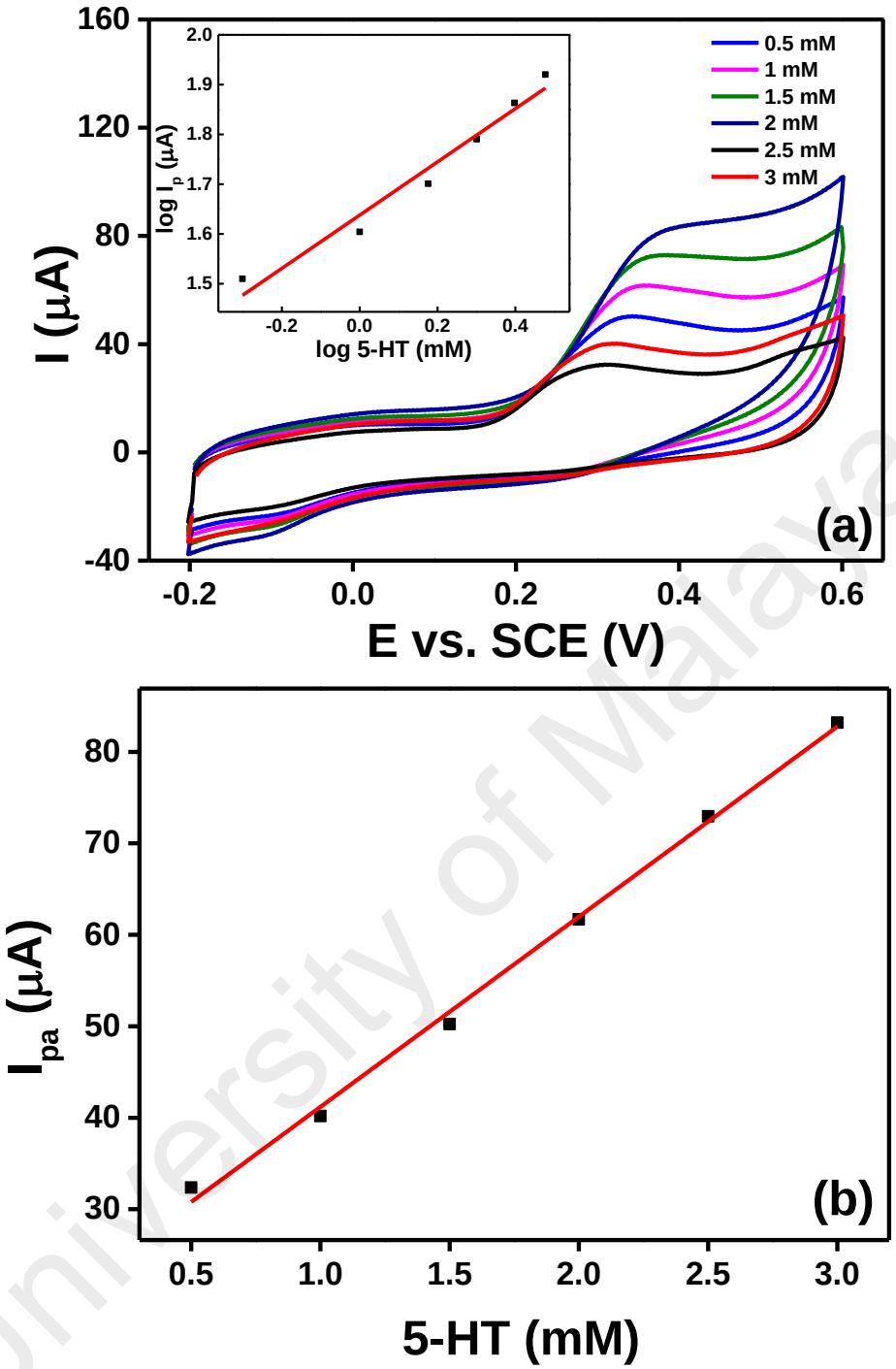

Appendix 5: (a) CV obtained at rGO-Co_3O_4-4 % nanocomposite for various concentration, (b) shows the corresponding calibration plot of serotonine concentrations versus current.

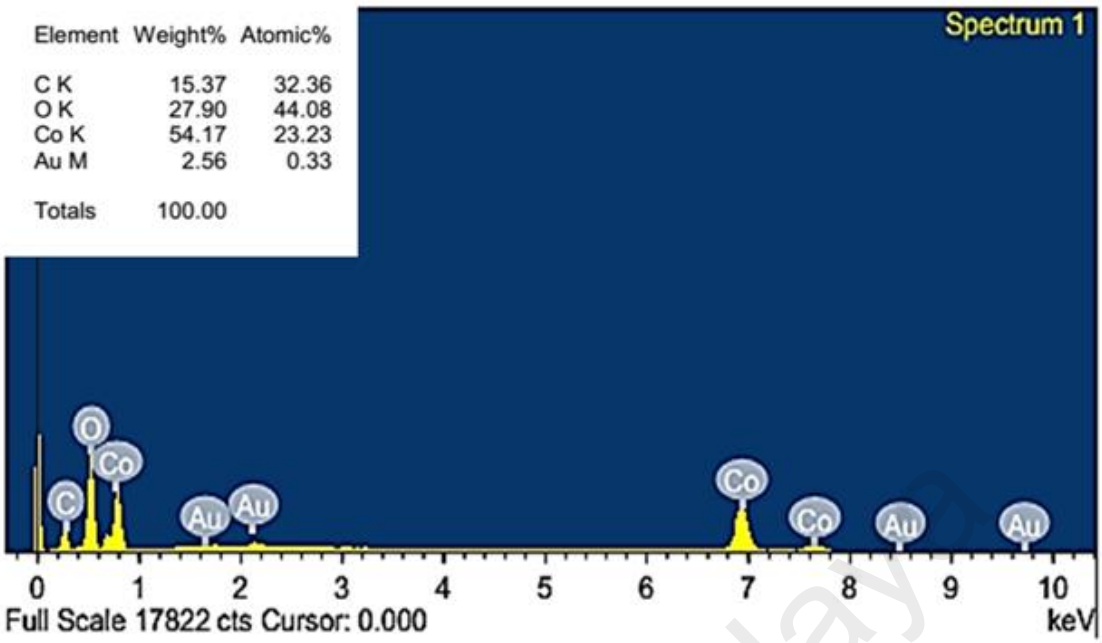

Appendix 6: EDX spectrum of the rGO-Co_3O_4@Au nanocomposite.

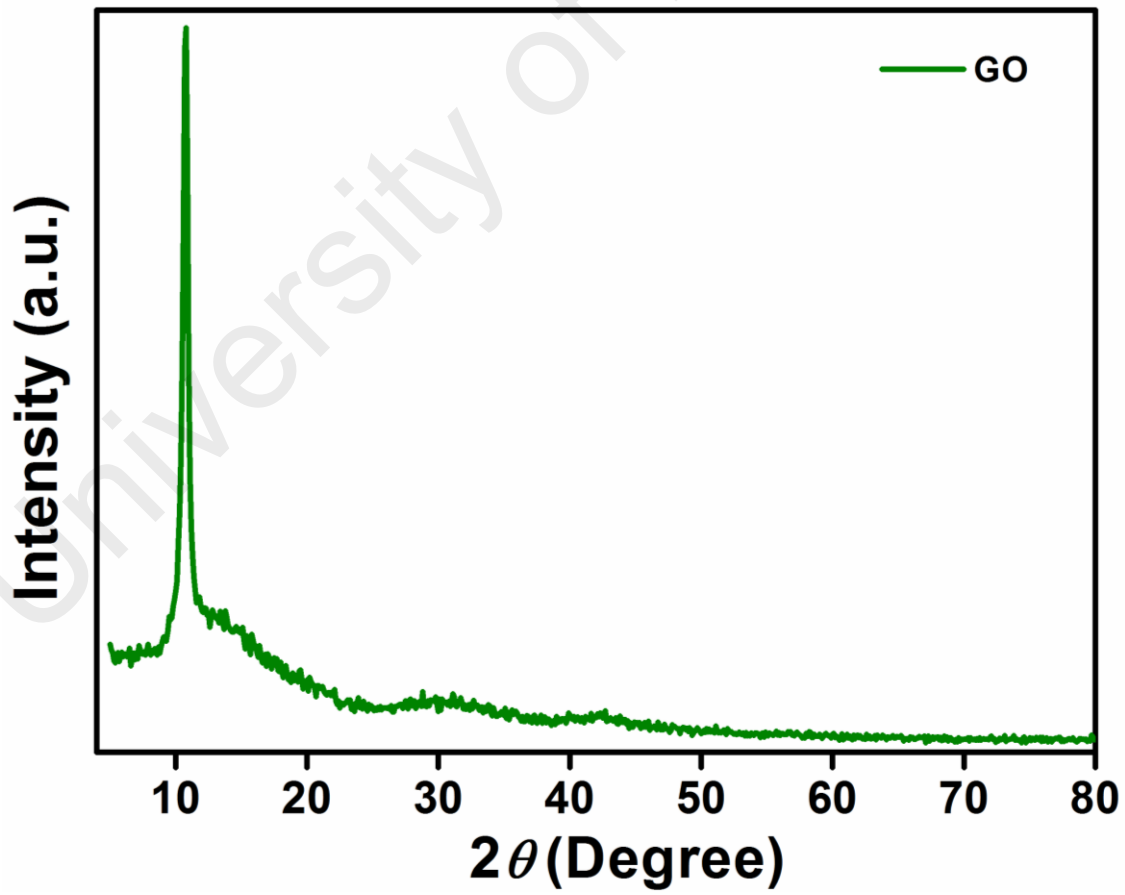

Appendix 7: XRD pattern of GO.

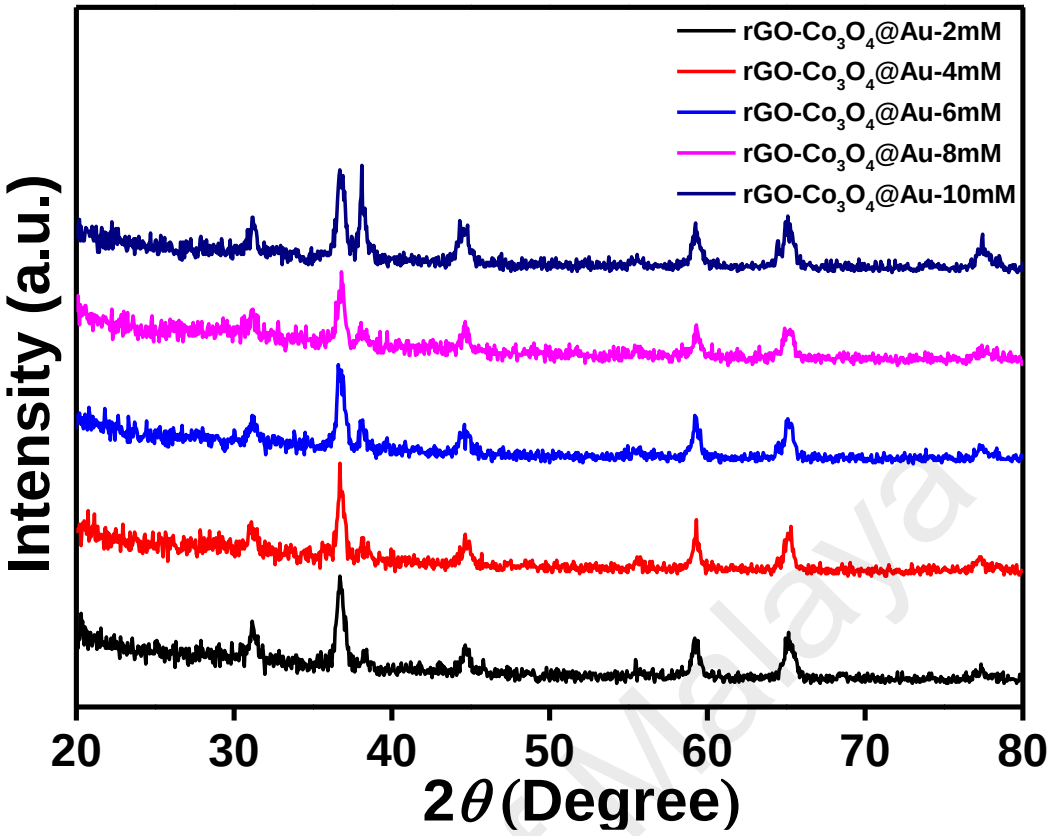

Appendix 8: XRD pattern of a) rGO-Co_3O_4@Au (2 mM), b) rGO-Co_3O_4@Au (4 mM), c) rGO-Co_3O_4@Au (6 mM), d) rGO-Co_3O_4@Au (8mM), e) rGO-Co_3O_4@Au (10 mM).

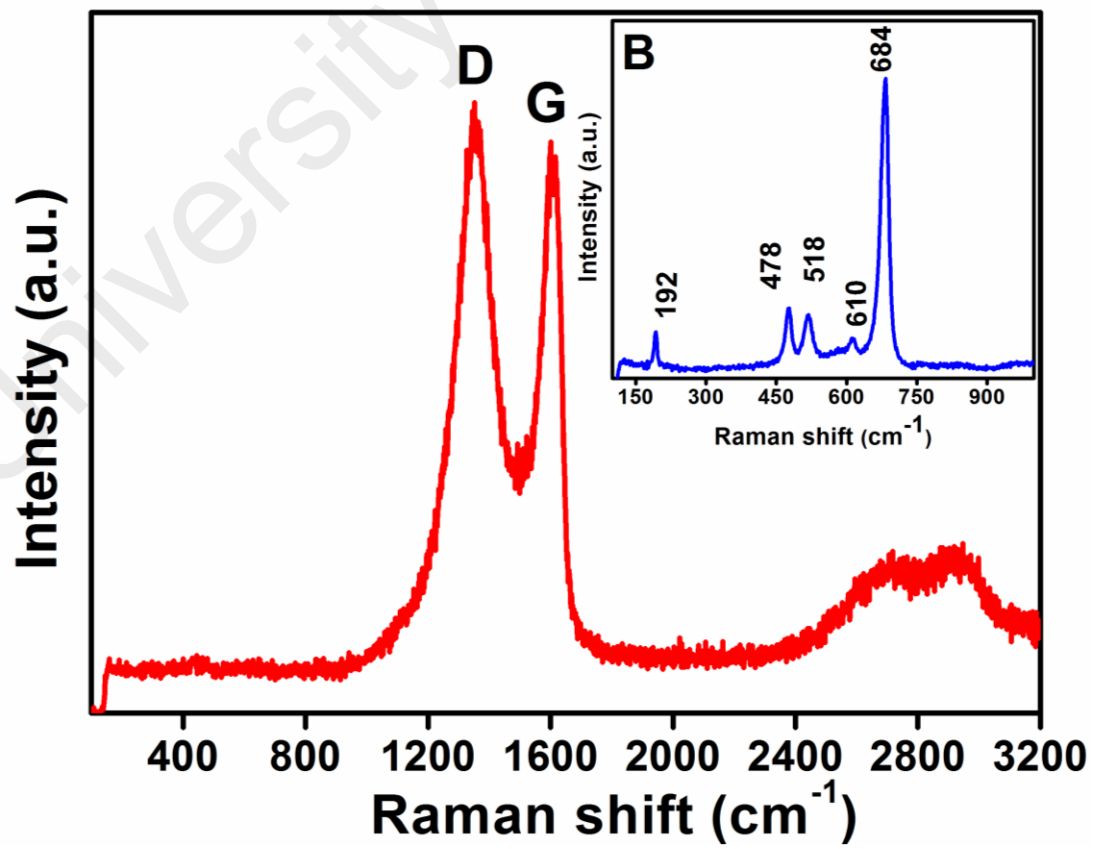

Appendix 9: Raman spectra of rGO, and Co_3O_4 nanocube (inset).

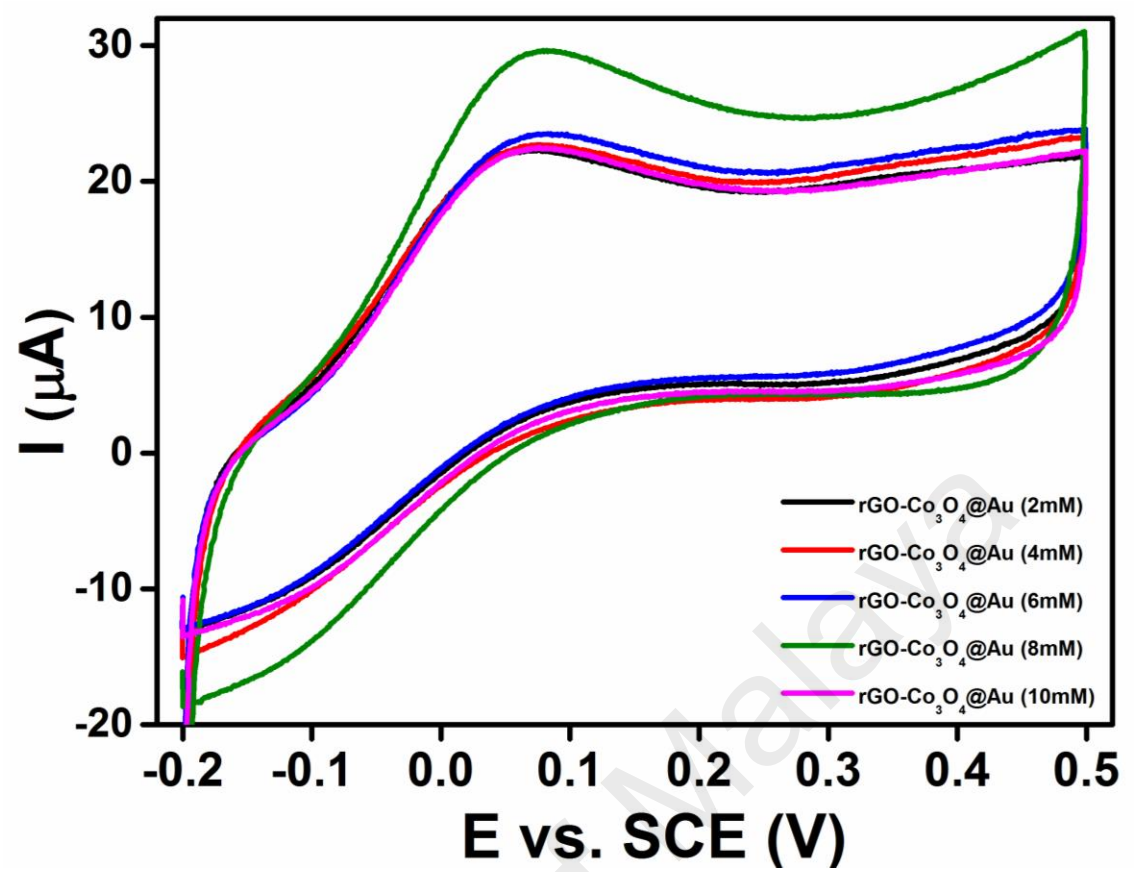

Appendix 10: Cyclic voltammograms recorded at rGO-Co_3O_4@Au nanocomposite with different amounts of Au modified electrodes for 0.5 mM of hydrazine in 0.1 M PBS at a scan rate of 50 mV s^{-1}.

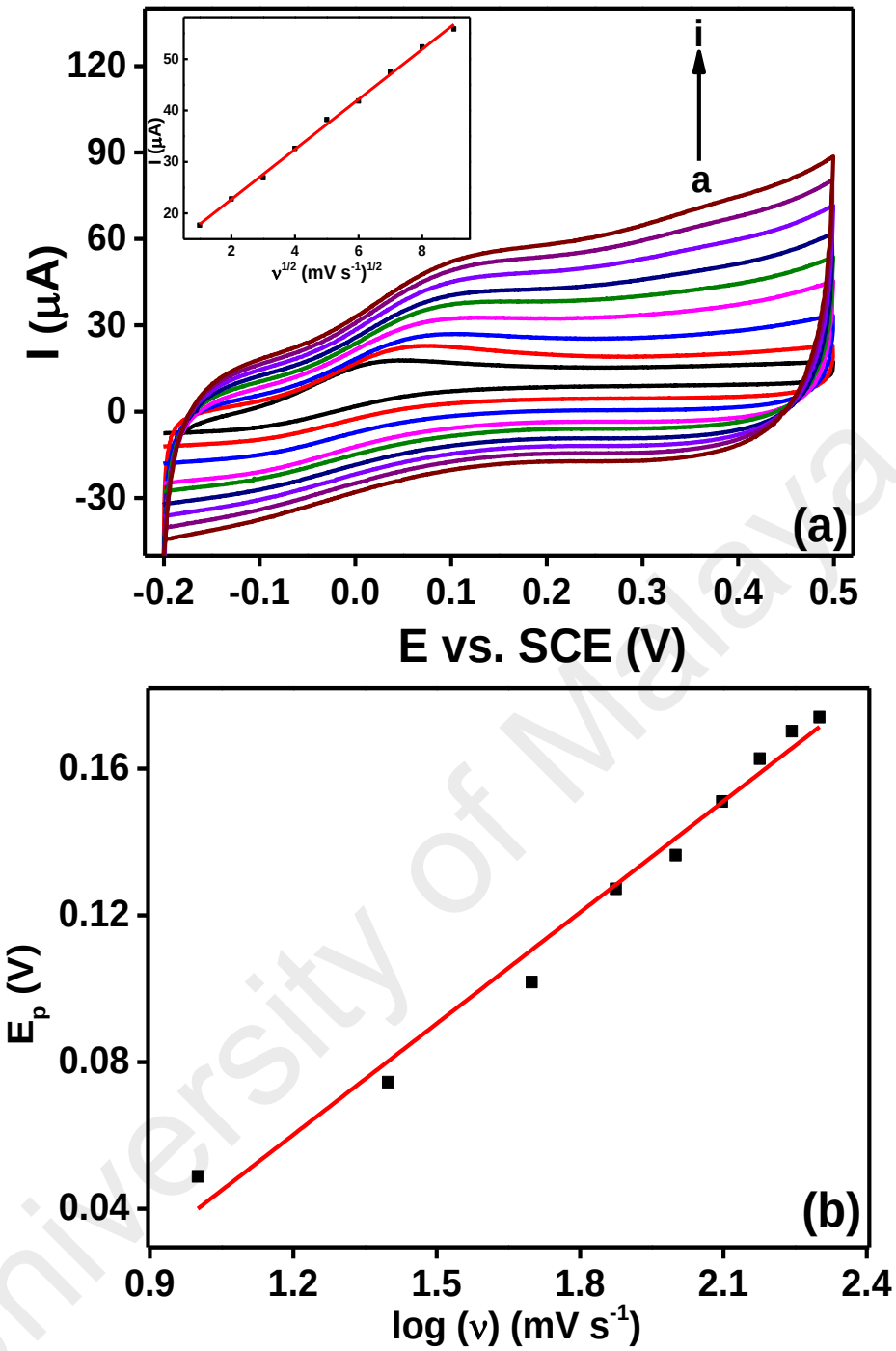

Appendix 11: (a) Cyclic voltammograms obtained at rGO-Co_3O_4@Au 8mM nanocomposite modified electrode for 0.5 mM hydrazine in 0.1 M phosphate buffer with different scan rates a: 10 mVs^{-1}, b: 25 mVs^{-1}, c: 50 mVs^{-1}, d: 75 mVs^{-1}, e: 100 mVs^{-1}, f: 125 mVs^{-1}, g: 150 mVs^{-1}, h: 175 mVs^{-1}, i: 200 mVs^{-1} Inset: Plot of peak current versus square root of scan rate and (b) the corresponding calibration plot of log for different scan rate versus peak current.

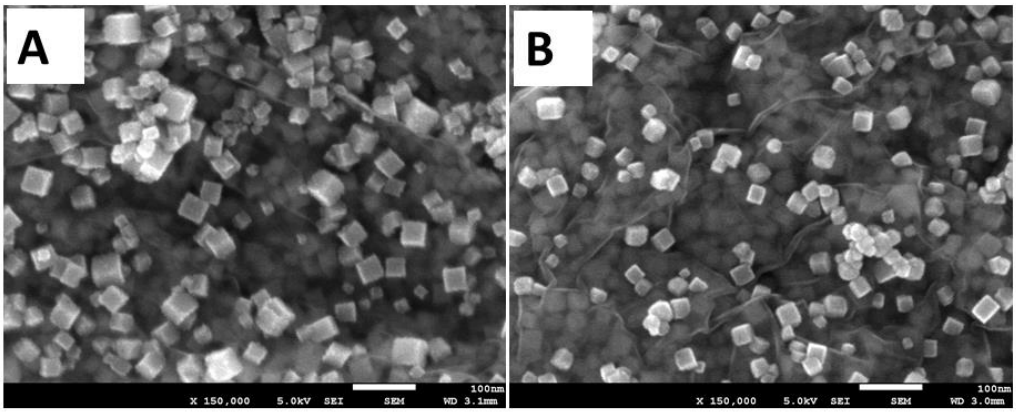

Appendix 12: FESEM images of rGO-Co_3O_4 nanocomposite.

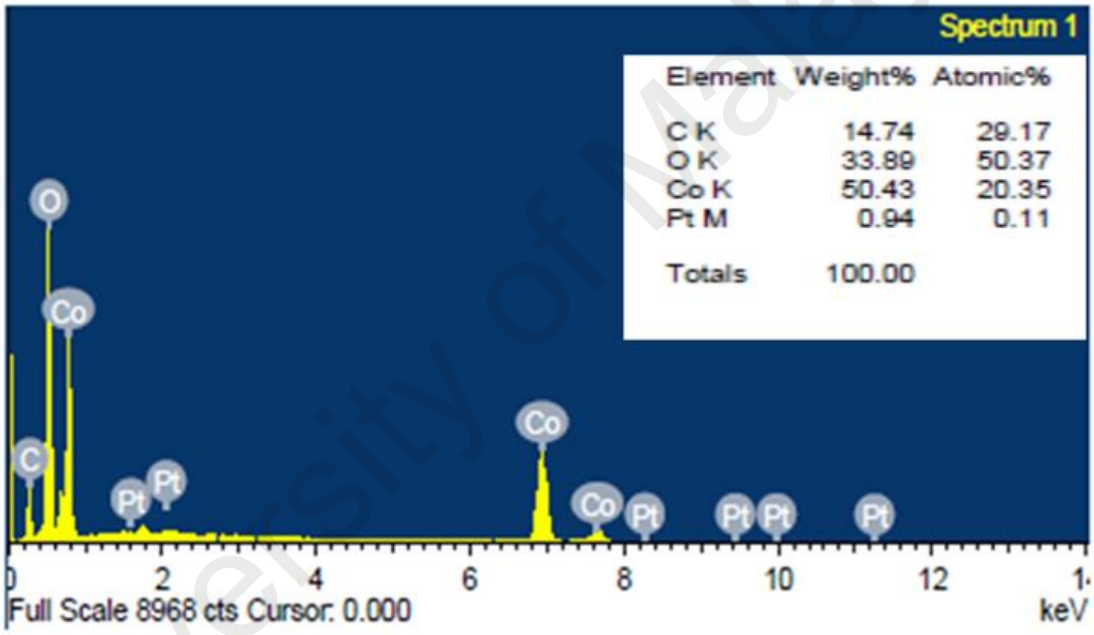

Appendix 13: EDX spectrum of rGO-Co_3O_4@Pt nanocomposite.

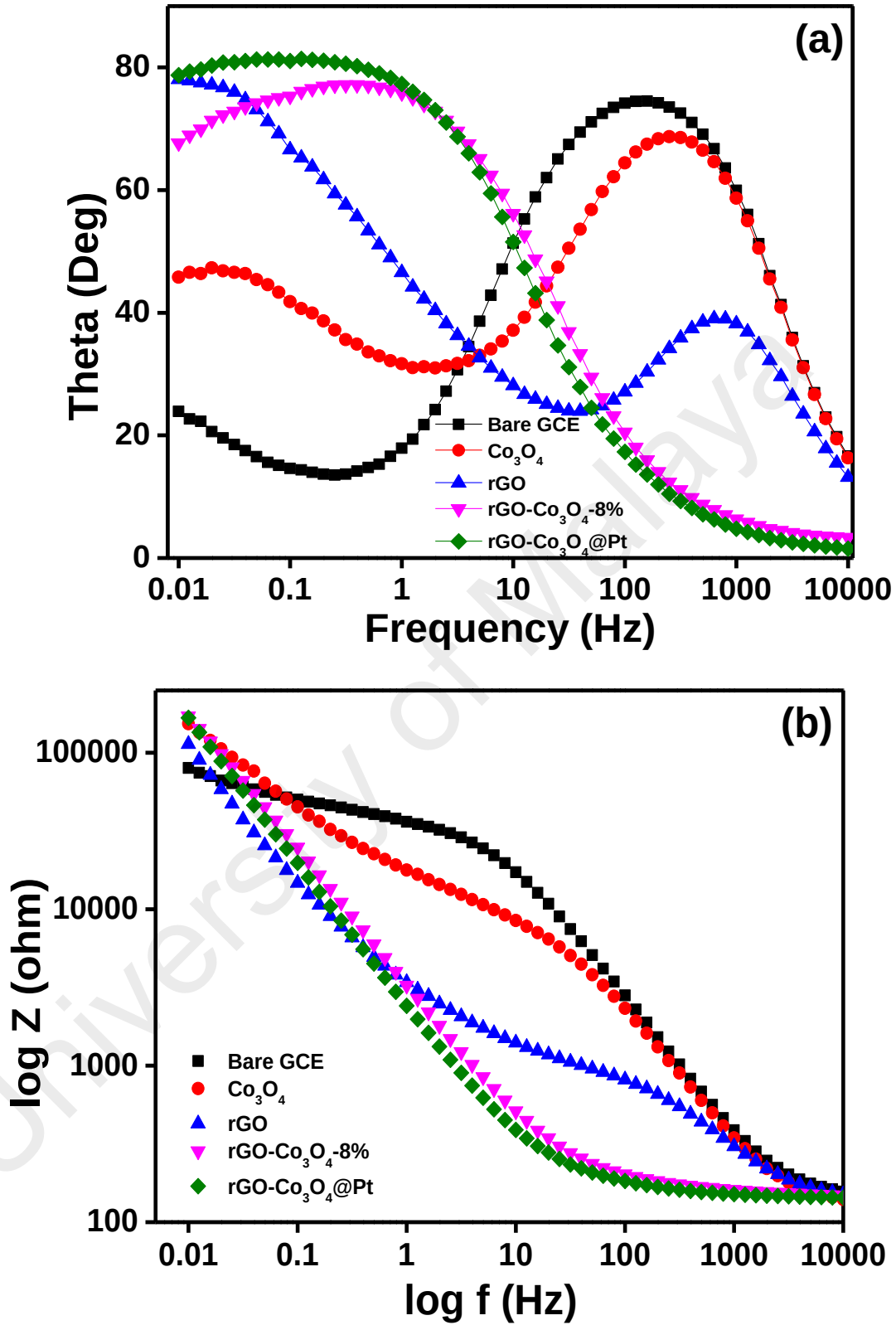

Appendix 14: (a) Bode phase plots (A) and Bode impedance plots (log Z *vs.* log f) (b) obtained for bare GC, Co_3O_4 nanocubes, rGO, rGO-Co_3O_4 nanocomposite and rGO-Co_3O_4@Pt nanocomposite modified GC electrodes for 1 mM $K_3[Fe(CN)_6]$ in 0.1 M KCl.

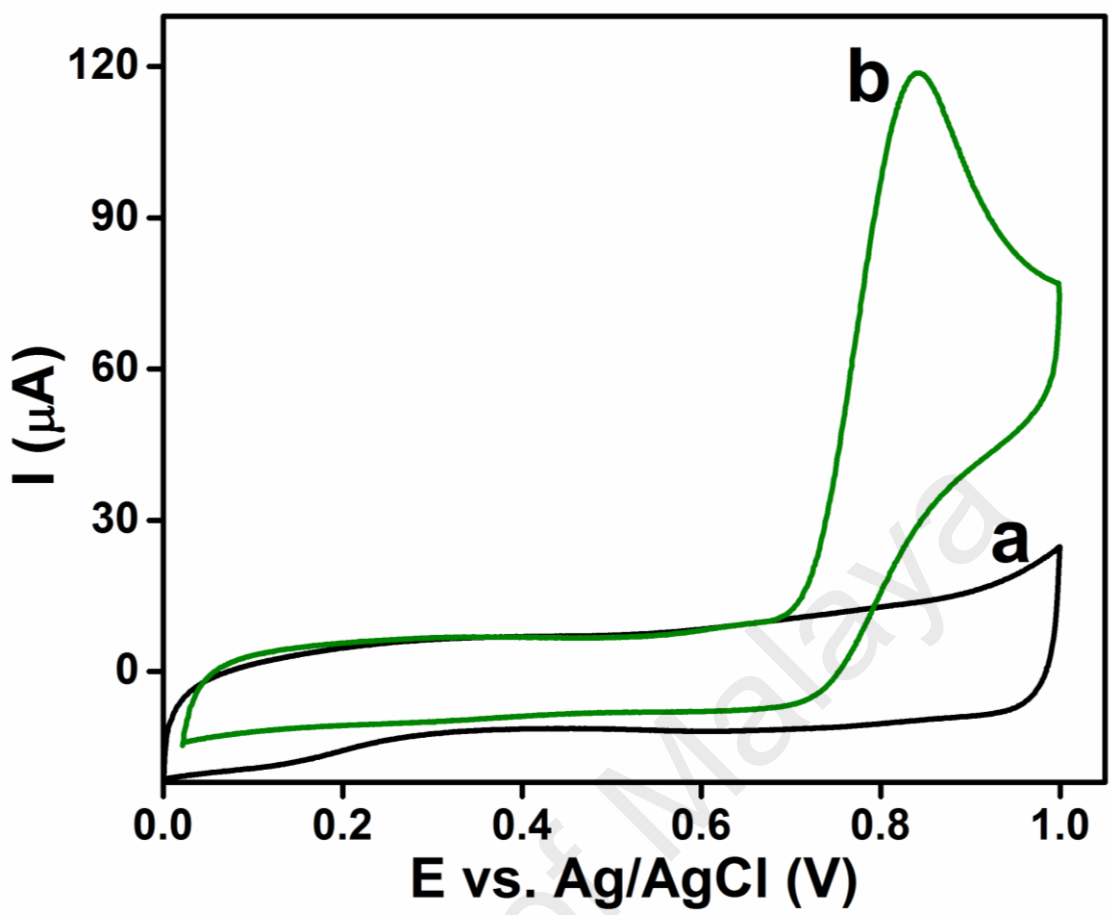

Appendix 15: Cyclic voltammograms recorded at rGO-Co_3O_4@Pt nanocomposite modified electrode in the absence (a) and presence (b) of 5 mM NO_2- in 0.1 M PBS (pH 2.5) at a scan rate of 50 mV s^{-1}.

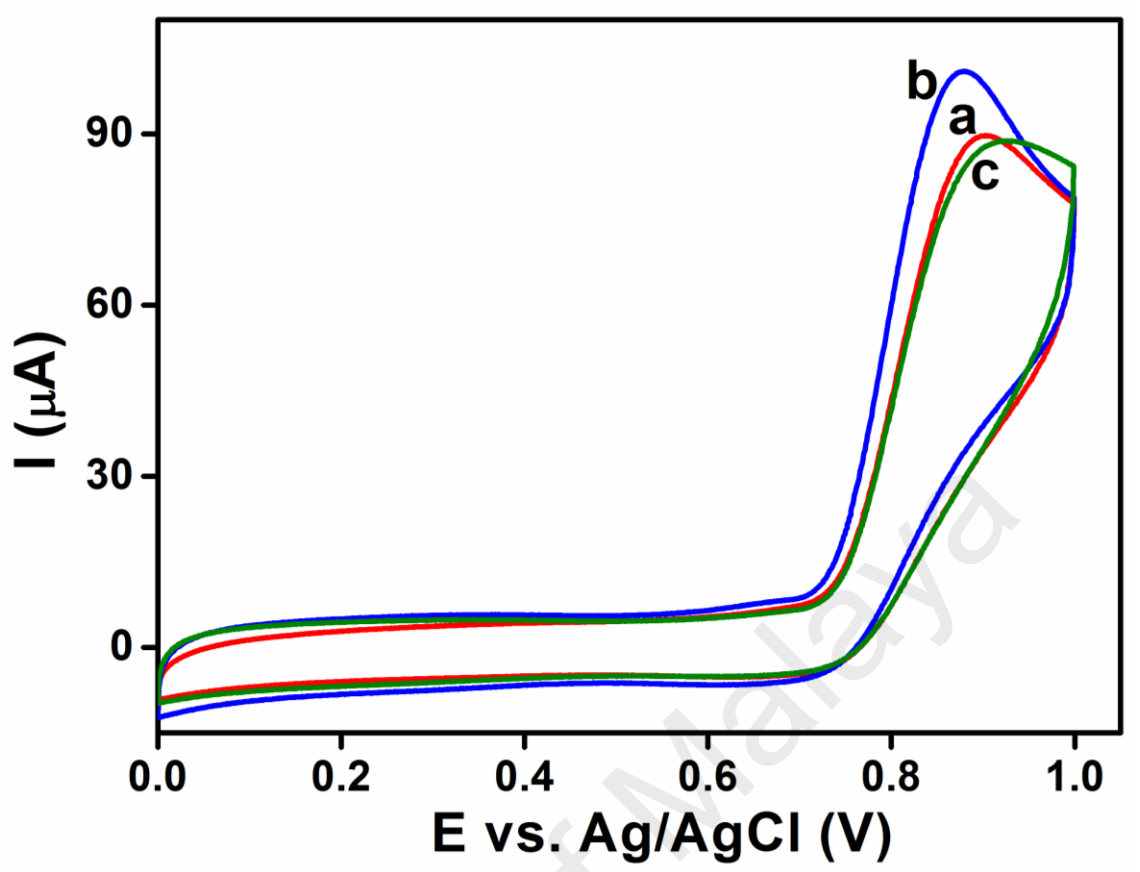

Appendix 16: Cyclic voltammograms recorded at rGO-Co_3O_4 nanocomposite modified electrode with different amounts of GO (a: 4, b: 8 and c: 12 wt %) for 5 mM of NO_2- in 0.1 M PBS (pH 2.5) at a scan rate of 50 mV s^{-1}.

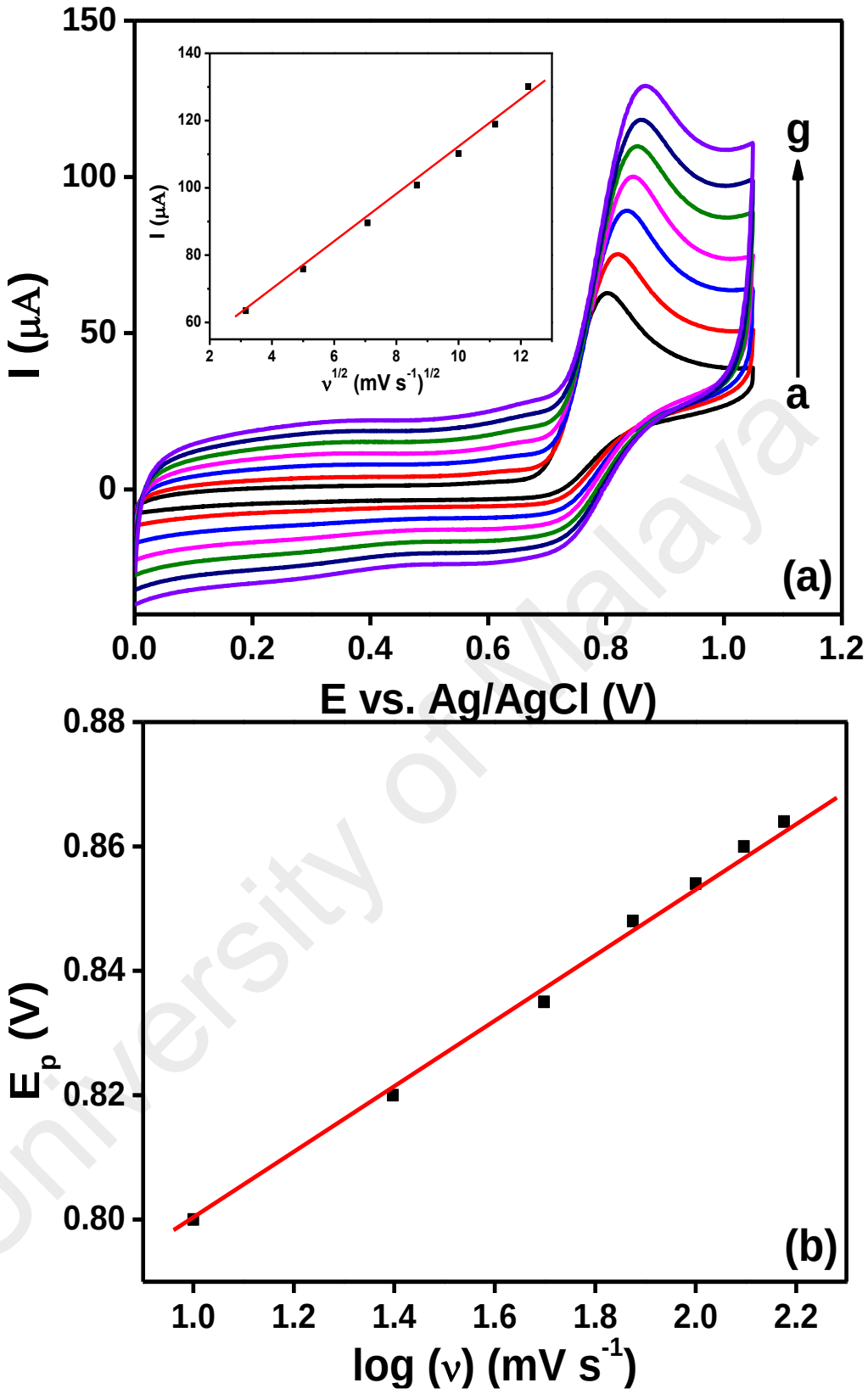

Appendix 17: (a) Cyclic voltammograms recorded at rGO-Co_3O_4@Pt nanocomposite modified electrode for 5 mM of NO_2- in 0.1 M PBS with various scan rates (a: 10, b: 25, c: 50, d: 75, e: 100, f: 125 and g: 150 mV s^{-1}). Inset: Plot of peak current versus square root of scan rate. (b) Plot of peak potential from (a) versus log (scan rate).

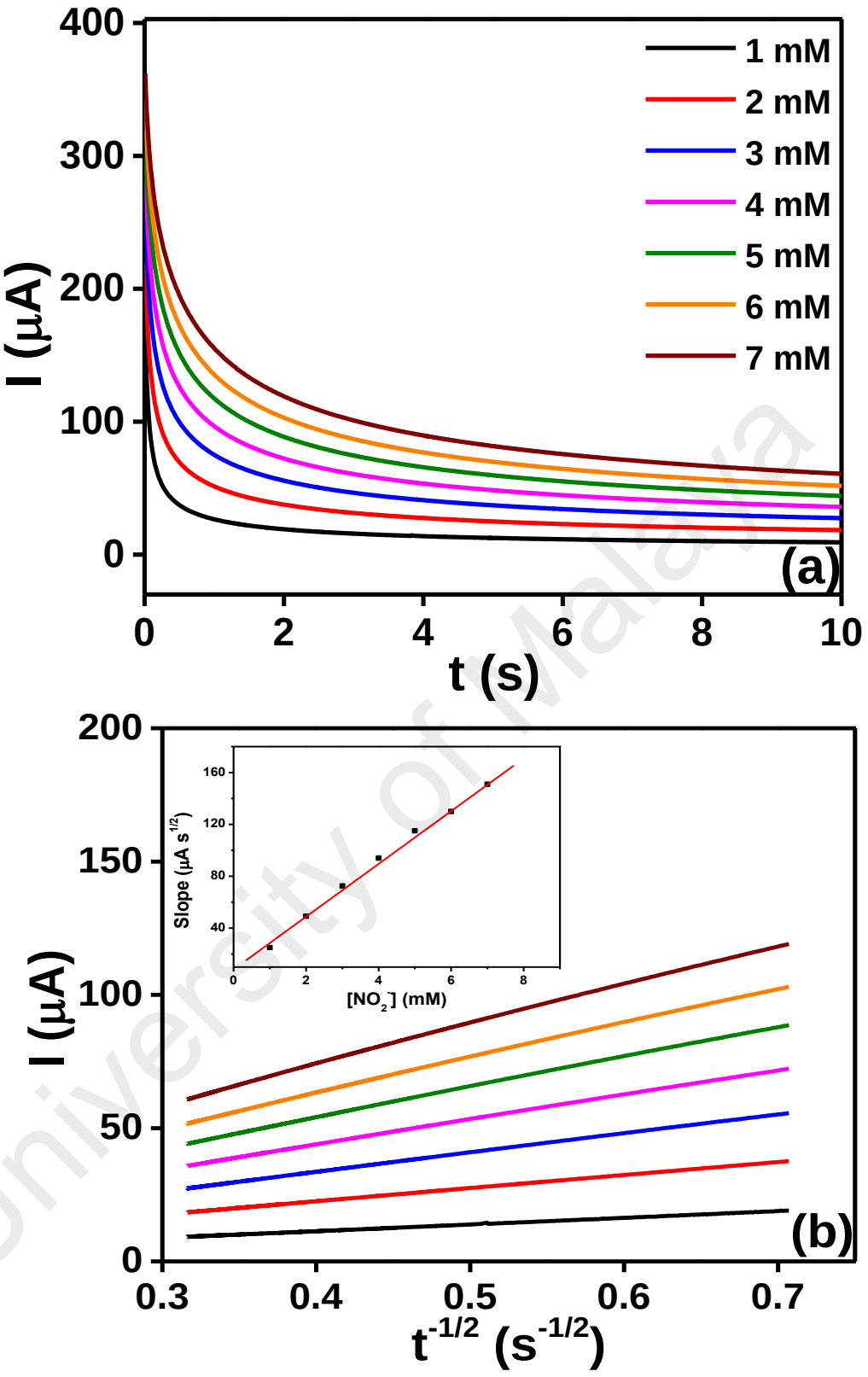

Appendix 18: (a) Chronoamperograms obtained at rGO-Co_3O_4@Pt nanocomposite modified electrode with different concentrations of NO_2^- in 0.1 M PBS (pH 2.5). (b) Plot of current versus $t^{-1/2}$. Inset: Plot of slopes obtained from straight lines of 'b' versus concentration of NO_2^-.

Abbaspour, A., & Noori, A. (2011). A cyclodextrin host–guest recognition approach to an electrochemical sensor for simultaneous quantification of serotonin and dopamine. *Biosensors and Bioelectronics, 26*(12), 4674-4680.

Abdul Aziz, M., & Kawde, A. N. (2013). Gold nanoparticle-modified graphite pencil electrode for the high-sensitivity detection of hydrazine. *Talanta, 115*, 214-221.

Adler, D. (1968). Insulating and metallic states in transition metal oxides. *Solid State Physics, 21*, 1-113.

Afzali, D., Karimi-Maleh, H., & Khalilzadeh, M. A. (2011). Sensitive and selective determination of phenylhydrazine in the presence of hydrazine at a ferrocene-modified carbon nanotube paste electrode. *Environmental chemistry letters, 9*(3), 375-381.

Ahmed, S. R., Ogale, S., Papaefthymiou, G. C., Ramesh, R., & Kofinas, P. (2002). Magnetic properties of cofe2o4 nanoparticles synthesized through a block copolymer nanoreactor route. *Applied physics letters, 80*(9), 1616-1618.

Ajayan, P., & Nalwa, H. (2000). Handbook of nanostructured materials and nanotechnology. *Academic Press, New York*.

Allag, A., Saâd, R., Ouahab, A., Attouche, H., & Kouidri, N. (2016). Optoelectronic properties of sno 2 thin films sprayed at different deposition times. *Chinese Physics B, 25*(4), 046801.

Alrehaily, L., Joseph, J., Biesinger, M., Guzonas, D., & Wren, J. (2013). Gamma-radiolysis-assisted cobalt oxide nanoparticle formation. *Physical Chemistry Chemical Physics, 15*(3), 1014-1024.

Ando, M., Kadono, K., Kamada, K., & Ohta, K. (2004). Third-order nonlinear optical responses of nanoparticulate co 3 o 4 films. *Thin Solid Films, 446*(2), 271-276.

Anithaa, A. C., Asokan, K., & Sekar, C. (2017). Highly sensitive and selective serotonin sensor based on gamma ray irradiated tungsten trioxide nanoparticles. *Sensors and Actuators B, 238*, 667-675.

Antoniadou, S., Jannakoudakis, A., & Theodoridou, E. (1989). Electrocatalytic reactions on carbon fibre electrodes modified by hemine ii. Electro-oxidation of hydrazine. *Synthetic metals, 30*(3), 295-304.

Arvinte, A., Mahosenaho, M., Pinteala, M., Sesay, A.-M., & Virtanen, V. (2011). Electrochemical oxidation of p-nitrophenol using graphene-modified electrodes, and a comparison to the performance of mwnt-based electrodes. *Microchimica Acta, 174*(3-4), 337-343.

Asif, M. H., Elinder, F., & Willander, M. (2011). Electrochemical biosensors based on zno nanostructures to measure intracellular metal ions and glucose. *Journal of Analytical & Bioanalytical Techniques 7*.

Augustine, A. K., Nampoori, V., & Kailasnath, M. (2014). Rapid synthesize of gold nanoparticles by microwave irradiation method and its application as an optical

limiting material. *Optik-International Journal for Light and Electron Optics, 125*(22), 6696-6699.

Babaei, A., & Taheri, A. R. (2013). Nafion/ni(oh)2 nanoparticles-carbon nanotube composite modified glassy carbon electrode as a sensor for simultaneous determination of dopamine and serotonin in the presence of ascorbic acid. *Sensors and Actuators B: Chemical, 176*, 543-551.

Baek, H. R., & Eo, I. S. (2017). Electrochemical properties of tio2-metal oxide composites for dye-sensitized solar cell. *Current Applied Physics, 17*(6), 854-857.

Bala, H., Fu, W., Yu, Y., Yang, H., & Zhang, Y. (2009). Preparation, optical properties, magnetic properties and thermal stability of core–shell structure cobalt/zinc oxide nanocomposites. *Applied Surface Science, 255*(7), 4050-4055.

Balandin, A. A., Ghosh, S., Bao, W., Calizo, I., Teweldebrhan, D., Miao, F., & Lau, C. N. (2008). Superior thermal conductivity of single-layer graphene. *Nano Letters, 8*(3), 902-907.

Baxter, J. B., & Aydil, E. S. (2005). Nanowire-based dye-sensitized solar cells. *Applied physics letters, 86*(5), 053114.

Bedioui, F., & Villeneuve, N. (2003). Electrochemical nitric oxide sensors for biological samples–principle, selected examples and applications. *Electroanalysis, 15*(1), 5-18.

Beltramo, G., & Koper, M. (2003). Nitric oxide reduction and oxidation on stepped pt [n (111)×(111)] electrodes. *Langmuir, 19*(21), 8907-8915.

Bogdan, C. (2001). Nitric oxide and the immune response. *Nature immunology, 2*(10), 907-916.

Borsella, E., Cattaruzza, E., De Marchi, G., Gonella, F., Mattei, G., Mazzoldi, P., Quaranta, A., Battaglin, G., & Polloni, R. (1999). Synthesis of silver clusters in silica-based glasses for optoelectronics applications. *Journal of non-crystalline solids, 245*(1), 122-128.

Brückner, A. (2003). Looking on heterogeneous catalytic systems from different perspectives: Multitechnique approaches as a new challenge for in situ studies. *Catalysis Reviews, 45*(1), 97-150.

Buchsteiner, A., Lerf, A., & Pieper, J. (2006). Water dynamics in graphite oxide investigated with neutron scattering. *The Journal of Physical Chemistry B, 110*(45), 22328-22338.

Budkuley, J. S. (1992). Determination of hydrazine and sulphite in the presence of one another. *Microchimica Acta, 108*(1-2), 103-105.

Byrappa, K., & Yoshimura, M. (2012). *Handbook of hydrothermal technology*: William Andrew.

Cao, L., Zhang, Z., Sun, L., Gao, C., He, M., Wang, Y., Li, Y., Zhang, X., Li, G., & Zhang, J. (2001). Well-aligned boron nanowire arrays. *Advanced Materials, 13*(22), 1701-1704.

Cao, L. M., Hahn, K., Scheu, C., Rühle, M., Wang, Y. Q., Zhang, Z., Gao, C. X., Li, Y. C., Zhang, X. Y., He, M., Sun, L. L., & Wang, W. K. (2002). Template-catalyst-free growth of highly ordered boron nanowire arrays. *Applied physics letters, 80*(22), 4226-4228.

Chai, S.-H., Howe, J. Y., Wang, X., Kidder, M., Schwartz, V., Golden, M. L., Overbury, S. H., Dai, S., & Jiang, D.-e. (2012). Graphitic mesoporous carbon as a support of promoted rh catalysts for hydrogenation of carbon monoxide to ethanol. *carbon, 50*(4), 1574-1582.

Chang, H., & Wu, H. (2013). Graphene-based nanocomposites: Preparation, functionalization, and energy and environmental applications. *Energy & Environmental Science, 6*(12), 3483.

Chang, W., Skandan, G., Hahn, H., Danforth, S. C., & Kear, B. H. (1994). Chemical vapor condensation of nanostructured ceramic powders. *Nanostructured Materials, 4*(3), 345-351.

Chauveau, J., Fert, V., Morel, A., & Delaage, M. (1991). Rapid and specific enzyme immunoassay of serotonin. *Clinical chemistry, 37*(7), 1178-1184.

Chen, C.-H., Chen, Y.-C., & Lin, M.-S. (2013). Amperometric determination of nadh with co 3 o 4 nanosheet modifiedelectrode. *Biosensors and Bioelectronics, 42*, 379-384.

Chen, C.-M., Zhang, Q., Yang, M.-G., Huang, C.-H., Yang, Y.-G., & Wang, M.-Z. (2012). Structural evolution during annealing of thermally reduced graphene nanosheets for application in supercapacitors. *carbon, 50*(10), 3572-3584.

Chen, M., Zhou, W., Qi, M., Zhang, J., Yin, J., & Chen, Q. (2017). Reconstruction of copper shell on metal oxides as enhanced nanoarrays electrodes for lithium ion batteries. *Materials Research Bulletin, 86*, 308-312.

Chen, S., Wu, Q., & Mishra, C. (2012). New graphene-related materials on the horizon. *Nat. Mater, 11*, 203-207.

Chen, S., Zhu, J., & Wang, X. (2010). One-step synthesis of graphene-cobalt hydroxide nanocomposites and their electrochemical properties. *Journal of Physical Chemistry C, 114*(27), 11829-11834.

Chen, X., Long, H.-Y., Wu, W.-L., & Yang, Z.-S. (2009). Direct electrochemical behavior of cytochrome c on sodium dodecyl sulfate modified electrode and its application to nitric oxide biosensor. *Thin Solid Films, 517*(8), 2787-2791.

Cheng, C.-S., Serizawa, M., Sakata, H., & Hirayama, T. (1998). Electrical conductivity of co 3 o 4 films prepared by chemical vapour deposition. *Materials Chemistry and Physics, 53*(3), 225-230.

Cho, Y., Parmar, N. S., Nahm, S., & Choi, J.-W. (2017). Full range optical and electrical properties of zn-doped sno2 and oxide/metal/oxide multilayer thin films deposited on flexible pet substrate. *Journal of Alloys and Compounds, 694*, 217-222.

Choi, H.-J., Jung, S.-M., Seo, J.-M., Chang, D. W., Dai, L., & Baek, J.-B. (2012). Graphene for energy conversion and storage in fuel cells and supercapacitors. *Nano Energy, 1*(4), 534-551.

Choi, Y., Gu, M., Park, J., Song, H. K., & Kim, B. S. (2012). Graphene multilayer supported gold nanoparticles for efficient electrocatalysts toward methanol oxidation. *Advanced Energy Materials, 2*(12), 1510-1518.

Chou, S.-L., Wang, J.-Z., Liu, H.-K., & Dou, S.-X. (2008). Electrochemical deposition of porous co 3 o 4 nanostructured thin film for lithium-ion battery. *Journal of Power Sources, 182*(1), 359-364.

Choudhary, G., IIansen, H., Donkin, S., & Kirman, C. (1997). Toxicological profile for hydrazines. *US Department of Health and Human Service*, 5.

Choudhury, C., Bansal, N. K., & Sehgal, H. K. (1983). Heat loss optimisation of a concentric cylindrical solar collector employing a cobalt oxide selective absorber. *Applied Energy, 14*(2), 143-159.

Chu, L., Han, L., & Zhang, X. (2011). Electrochemical simultaneous determination of nitrophenol isomers at nano-gold modified glassy carbon electrode. *Journal of Applied Electrochemistry, 41*(6), 687-694.

Cinthia, A. J., Priyanga, G. S., Rajeswarapalanichamy, R., & Iyakutti, K. (2015). Structural, electronic and mechanical properties of alkaline earth metal oxides mo (m=be, mg, ca, sr, ba). *Journal of Physics and Chemistry of Solids, 79*, 23-42.

Conoci, S., Petralia, S., Samorì, P., Raymo, F. M., Di Bella, S., & Sortino, S. (2006). Optically transparent, ultrathin pt films as versatile metal substrates for molecular optoelectronics. *Advanced Functional Materials, 16*(11), 1425-1432.

Crespi, F., Baumeyer, T., Moebius, C., & Dittrich, J. (1991). Simultaneous in vivo monitoring of dopamine and serotonin by differential pulse conditioning voltammetry with na-cro microbiosensors. *Fresenius. J. Anal. Chem., 341*(10), 644.

Cui, L., Ji, C., Peng, Z., Zhong, L., Zhou, C., Yan, L., Qu, S., Zhang, S., Huang, C., & Qian, X. (2014). Unique tri-output optical probe for specific and ultrasensitive detection of hydrazine. *Analytical chemistry, 86*(9), 4611-4617.

Cui, L., Peng, Z., Ji, C., Huang, J., Huang, D., Ma, J., Zhang, S., Qian, X., & Xu, Y. (2014). Hydrazine detection in the gas state and aqueous solution based on the gabriel mechanism and its imaging in living cells. *Chemical Communications, 50*(12), 1485-1487.

Dalkıran, B., Esra Erden, P., & Kılıç, E. (2017). Amperometric biosensors based on carboxylated multiwalled carbon nanotubes-metal oxide nanoparticles-7,7,8,8-

tetracyanoquinodimethane composite for the determination of xanthine. *Talanta, 167*, 286-295.

de Moraes, A. C. M., Andrade, P. F., de Faria, A. F., Simões, M. B., Salomão, F. C. C. S., Barros, E. B., do Carmo Gonçalves, M., & Alves, O. L. (2015). Fabrication of transparent and ultraviolet shielding composite films based on graphene oxide and cellulose acetate. *Carbohydrate polymers, 123*, 217-227.

Demuth, J., Hamers, R., Tromp, R., & Welland, M. (1986). A scanning tunneling microscope for surface science studies. *IBM journal of research and development, 30*(4), 396-402.

Devasenathipathy, R., Mani, V., & Chen, S.-M. (2014). Highly selective amperometric sensor for the trace level detection of hydrazine at bismuth nanoparticles decorated graphene nanosheets modified electrode. *Talanta, 124*, 43-51.

Dhas, N. A., Koltypin, Y., & Gedanken, A. (1997). Sonochemical preparation and characterization of ultrafine chromium oxide and manganese oxide powders. *Chemistry of materials, 9*(12), 3159-3163.

Dinesh, B., Veeramani, V., Chen, S.-M., & Saraswathi, R. (2017). In situ electrochemical synthesis of reduced graphene oxide-cobalt oxide nanocomposite modified electrode for selective sensing of depression biomarker in the presence of ascorbic acid and dopamine. *J. Electroanal. Chem., 786*, 169-176.

Ding, J., Zhu, S., Zhu, T., Sun, W., Li, Q., Wei, G., & Su, Z. (2015). Hydrothermal synthesis of zinc oxide-reduced graphene oxide nanocomposites for an electrochemical hydrazine sensor. *RSC Advances, 5*(29), 22935-22942.

Dong, Y., He, K., Yin, L., & Zhang, A. (2007). A facile route to controlled synthesis of co3o4 nanoparticles and their environmental catalytic properties. *Nanotechnology, 18*(43), 435602.

Du, X., He, J., Zhu, J., Sun, L., & An, S. (2012). Ag-deposited silica-coated fe3o4 magnetic nanoparticles catalyzed reduction of p-nitrophenol. *Applied Surface Science, 258*(7), 2717-2723.

Du, X., Skachko, I., Barker, A., & Andrei, E. Y. (2008). Approaching ballistic transport in suspended graphene. *Nature nanotechnology, 3*(8), 491-495.

Dutta, S., Ray, C., Mallick, S., Sarkar, S., Roy, A., & Pal, T. (2015). Au@ pd core–shell nanoparticles-decorated reduced graphene oxide: A highly sensitive and selective platform for electrochemical detection of hydrazine. *RSC Advances, 5*(64), 51690-51700.

Ensafi, A. A., Abarghoui, M. M., & Rezaei, B. (2016). Facile synthesis of pt-cu@ silicon nanostructure as a new electrocatalyst supported matrix, electrochemical detection of hydrazine and hydrogen peroxide. *Electrochimica Acta, 190*, 199-207.

Ensafi, A. A., & Rezaei, B. (1998). Flow injection determination of hydrazine with fluorimetric detection. *Talanta, 47*(3), 645-649.

Fagan-Murphy, A., Watt, F., Morgan, K. A., & Patel, B. A. (2012). Influence of different biological environments on the stability of serotonin detection on carbon-based electrodes. *J. Electroanal. Chem., 684*, 1-5.

Fang, B., Zhang, C., Zhang, W., & Wang, G. (2009). A novel hydrazine electrochemical sensor based on a carbon nanotube-wired zno nanoflower-modified electrode. *Electrochimica Acta, 55*(1), 178-182.

Fang, F. C. (1997). Perspectives series: Host/pathogen interactions. Mechanisms of nitric oxide-related antimicrobial activity. *Journal of Clinical Investigation, 99*(12), 2818.

Farhadi, S., Pourzare, K., & Bazgir, S. (2014). Co 3 o 4 nanoplates: Synthesis, characterization and study of optical and magnetic properties. *Journal of Alloys and Compounds, 587*, 632-637.

Farhadi, S., Safabakhsh, J., & Zaringhadam, P. (2013). Synthesis, characterization, and investigation of optical and magnetic properties of cobalt oxide (co3o4) nanoparticles. *Journal of Nanostructure in Chemistry, 3*(1), 1-9.

Fei, J., Hu, S., & Shiu, K.-K. (2011). Amperometric determination of nitric oxide at a carbon nanotube modified electrode with redox polymer coating. *Journal of Solid State Electrochemistry, 15*(3), 519-523.

Fernandez-Garcia, M., Martinez-Arias, A., Hanson, J., & Rodriguez, J. (2004). Nanostructured oxides in chemistry: Characterization and properties. *Chemical Reviews, 104*(9), 4063-4104.

Fierro, J. L. G. (2005). *Metal oxides: Chemistry and applications*: CRC press.

Fiiipponi, L., & Sutherland, D. (2012). *Nanotechnologies: Principles, applications, implications and hands-on activities: A compendium for educators*: European Union, Directorate General for Research and Innovation.

Frohlich, K., Luptak, R., Dobrocka, E., Husekova, K., Cico, K., Rosova, A., Lukosius, M., Abrutis, A., Pisecny, P., & Espinos, J. (2006). Characterization of rare earth oxides based mosfet gate stacks prepared by metal-organic chemical vapour deposition. *Materials science in semiconductor processing, 9*(6), 1065-1072.

Fujishima, A., & Honda, K. (1972). Electrochemical photolysis of water at a semiconductor electrode. *nature, 238*(5358), 37-38.

Furchgott, R. F. (1999). Endothelium-derived relaxing factor: Discovery, early studies, and identifcation as nitric oxide (nobel lecture). *Angewandte Chemie International Edition, 38*(13-14), 1870-1880.

Ganjali, M. R., Motakef-Kazami, N., Faridbod, F., Khoee, S., & Norouzi, P. (2010). Determination of pb 2+ ions by a modified carbon paste electrode based on multi-walled carbon nanotubes (mwcnts) and nanosilica. *Journal of hazardous materials, 173*(1), 415-419.

Geim, A. K., & Novoselov, K. S. (2007). The rise of graphene. *Nature materials, 6*(3), 183-191.

Ghanbari, K. (2014). Fabrication of silver nanoparticles–polypyrrole composite modified electrode for electrocatalytic oxidation of hydrazine. *Synthetic metals, 195,* 234-240.

Gholamian, F., Sheikh-Mohseni, M. A., & Naeimi, H. (2012). Simultaneous determination of phenylhydrazine and hydrazine by a nanostructured electrochemical sensor. *Materials Science and Engineering: C, 32*(8), 2344-2348.

Gholivand, M. B., & Azadbakht, A. (2011). A novel hydrazine electrochemical sensor based on a zirconium hexacyanoferrate film-bimetallic au-pt inorganic-organic hybrid nanocomposite onto glassy carbon-modified electrode. *Electrochim. Acta, 56*(27), 10044-10054.

Greene, L. E., Law, M., Goldberger, J., Kim, F., Johnson, J. C., Zhang, Y., Saykally, R. J., & Yang, P. (2003). Low-temperature wafer-scale production of zno nanowire arrays. *Angewandte Chemie International Edition, 42*(26), 3031-3034.

Greenwood, N., & Earnshaw, A. (1997). *Chemistry of the elements 2nd edition*: Butterworth-Heinemann.

Gu, Y.-e., Zhang, Y., Zhang, F., Wei, J., Wang, C., Du, Y., & Ye, W. (2010). Investigation of photoelectrocatalytic activity of cu 2 o nanoparticles for p-nitrophenol using rotating ring-disk electrode and application for electrocatalytic determination. *Electrochimica Acta, 56*(2), 953-958.

Gueell, A. G., Meadows, K. E., Unwin, P. R., & MacPherson, J. V. (2010). Trace voltammetric detection of serotonin at carbon electrodes: Comparison of glassy carbon, boron doped diamond and carbon nanotube network electrodes. *Phys. Chem. Chem. Phys., 12*(34), 10108-10114.

Guix, F., Uribesalgo, I., Coma, M., & Munoz, F. (2005). The physiology and pathophysiology of nitric oxide in the brain. *Progress in neurobiology, 76*(2), 126-152.

Guo, C. X., Ng, S. R., Khoo, S. Y., Zheng, X., Chen, P., & Li, C. M. (2012). Rgd-peptide functionalized graphene biomimetic live-cell sensor for real-time detection of nitric oxide molecules. *ACS nano, 6*(8), 6944-6951.

Guo, S., Dong, S., & Wang, E. (2009). Three-dimensional pt-on-pd bimetallic nanodendrites supported on graphene nanosheet: Facile synthesis and used as an advanced nanoelectrocatalyst for methanol oxidation. *ACS nano, 4*(1), 547-555.

Gupta, P., & Goyal, R. N. (2014). Polymelamine modified edge plane pyrolytic graphite sensor for the electrochemical assay of serotonin. *Talanta, 120*, 17-22.

Hai, H. T., Takamura, H., & Koike, J. (2013). Oxidation behavior of cu–ag core–shell particles for solar cell applications. *Journal of Alloys and Compounds, 564*, 71-77.

He, Q., Zheng, D., & Hu, S. (2009). Development and application of a nano-alumina based nitric oxide sensor. *Microchimica Acta, 164*(3-4), 459-464.

He, X., & Zhu, L. (2006). Direct electrochemistry of hemoglobin in cetylpyridinium bromide film: Redox thermodynamics and electrocatalysis to nitric oxide. *Electrochemistry Communications, 8*(4), 615-620.

He, Y.-S., Bai, D.-W., Yang, X., Chen, J., Liao, X.-Z., & Ma, Z.-F. (2010). A co(oh)2-graphene nanosheets composite as a high performance anode material for rechargeable lithium batteries. *Electrochem. Commun., 12*(4), 570-573.

Henrich, V. E., & Cox, P. A. (1996). *The surface science of metal oxides*: Cambridge university press.

Henry, P. F., & Weller, M. T. (1998). Ca2aun: A nitride containing infinite zigzag gold chains. *Angewandte Chemie International Edition, 37*(20), 2855-2857.

Hetrick, E. M., & Schoenfisch, M. H. (2009). Analytical chemistry of nitric oxide. *Annual review of analytical chemistry (Palo Alto, Calif.), 2*, 409.

Hu, H., Wang, X., Wang, J., Wan, L., Liu, F., Zheng, H., Chen, R., & Xu, C. (2010). Preparation and properties of graphene nanosheets–polystyrene nanocomposites via in situ emulsion polymerization. *Chemical Physics Letters, 484*(4), 247-253.

Hu, L., Peng, Q., & Li, Y. (2008). Selective synthesis of co3o4 nanocrystal with different shape and crystal plane effect on catalytic property for methane combustion. *Journal of the American Chemical Society, 130*(48), 16136-16137.

Huang, J., & Wan, Q. (2009). Gas sensors based on semiconducting metal oxide one-dimensional nanostructures. *Sensors, 9*(12), 9903-9924.

Huang, N., Lim, H., Chia, C., Yarmo, M., & Muhamad, M. (2011). Simple room-temperature preparation of high-yield large-area graphene oxide. *International Journal of Nanomedicine, 6*, 3443.

Huang, N. M., Lim, H. N., Chia, C. H., Yarmo, M. A., & Muhamad, M. R. (2011). Simple room-temperature preparation of high-yield large-area graphene oxide. *International Journal of Nanomedicine, 6*, 3443-3448.

Huang, W., Yang, C., & Zhang, S. (2003). Simultaneous determination of 2-nitrophenol and 4-nitrophenol based on the multi-wall carbon nanotubes nafion-modified electrode. *Analytical and bioanalytical chemistry, 375*(5), 703-707.

Ignarro, L. J., Buga, G. M., Wood, K. S., Byrns, R. E., & Chaudhuri, G. (1987). Endothelium-derived relaxing factor produced and released from artery and vein is nitric oxide. *Proceedings of the National Academy of Sciences, 84*(24), 9265-9269.

Interrante, L. V., & Hampden-Smith, M. J. (1997). Chemistry of advanced materials: An overview. *Chemistry of Advanced Materials: An Overview, by Leonard V. Interrante (Editor), Mark J. Hampden-Smith (Editor), pp. 592. ISBN 0-471-18590-6. Wiley-VCH, December 1997.*, 592.

Jain, P. K., Lee, K. S., El-Sayed, I. H., & El-Sayed, M. A. (2006). Calculated absorption and scattering properties of gold nanoparticles of different size, shape, and composition: Applications in biological imaging and biomedicine. *J. Phys. Chem. B, 110*(14), 7238-7248.

Jang, J. Y., Kim, M. S., Jeong, H. M., & Shin, C. M. (2009). Graphite oxide/poly (methyl methacrylate) nanocomposites prepared by a novel method utilizing macroazoinitiator. *Composites Science and Technology, 69*(2), 186-191.

Jayabal, S., Viswanathan, P., & Ramaraj, R. (2014). Reduced graphene oxide–gold nanorod composite material stabilized in silicate sol–gel matrix for nitric oxide sensor. *RSC Advances, 4*(63), 33541-33548.

Jayasri, D., & Narayanan, S. S. (2007). Amperometric determination of hydrazine at manganese hexacyanoferrate modified graphite–wax composite electrode. *Journal of hazardous materials, 144*(1), 348-354.

Jeon, H.-K., Nohta, H., & Ohkura, Y. (1992). High-performance liquid chromatographic determination of catecholamines and their precursor and metabolites in human urine and plasma by postcolumn derivatization involving chemical oxidation followed by fluorescence reaction. *Analytical biochemistry, 200*(2), 332-338.

Jeong, S. J., Song, J. S., Min, B. K., Lee, W. J., & Park, E. C. (2006). Characteristics of piezoelectric multilayer devices containing metal-oxide multicomponent electrode. *Ferroelectrics, 338*(1), 9-16.

Jia, J., Wang, B., Wu, A., Cheng, G., Li, Z., & Dong, S. (2002). A method to construct a third-generation horseradish peroxidase biosensor: Self-assembling gold nanoparticles to three-dimensional sol-gel network. *Analytical chemistry, 74*(9), 2217-2223.

Jia, S., Fei, J., Deng, J., Cai, Y., & Li, J. (2009). Direct electrochemistry and electrocatalysis of hemoglobin immobilized in an amphiphilic diblock copolymer film. *Sensors and Actuators B: Chemical, 138*(1), 244-250.

Jiang, L., Gu, S., Ding, Y., Jiang, F., & Zhang, Z. (2014). Facile and novel electrochemical preparation of a graphene–transition metal oxide nanocomposite for ultrasensitive electrochemical sensing of acetaminophen and phenacetin. *Nanoscale, 6*(1), 207-214.

Jiang, Y., Zheng, B., Du, J., Liu, G., Guo, Y., & Xiao, D. (2013). Electrophoresis deposition of ag nanoparticles on tio 2 nanotube arrays electrode for hydrogen peroxide sensing. *Talanta, 112*, 129-135.

Jiang, Z., Jiang, Z.-J., Maiyalagan, T., & Manthiram, A. (2016). Cobalt oxide-coated n- and b-doped graphene hollow spheres as bifunctional electrocatalysts for oxygen reduction and oxygen evolution reactions. *Journal of Materials Chemistry A, 4*(16), 5877-5889.

Jiao, F., & Frei, H. (2009). Nanostructured cobalt oxide clusters in mesoporous silica as efficient oxygen-evolving catalysts. *Angewandte Chemie International Edition, 48*(10), 1841-1844.

Jiao, F., & Frei, H. (2010). Nanostructured cobalt and manganese oxide clusters as efficient water oxidation catalysts. *Energy & Environmental Science, 3*(8), 1018-1027.

Jokar, E., & Shahrokhian, S. (2014). Growth control of cobalt oxide nanoparticles on reduced graphene oxide for enhancement of electrochemical capacitance. *International Journal of Hydrogen Energy, 39*(36), 21068-21075.

Jonker, G., & Van Santen, J. (1950). Physica (utrecht) 16, 337 (1950). *CrossRef Google Scholar*.

Kaczmarczyk, J., Zasada, F., Janas, J., Indyka, P., Piskorz, W., Kotarba, A., & Sojka, Z. (2016). Thermodynamic stability, redox properties and reactivity of mn3o4, fe3o4, and co3o4 model catalysts for n2o decomposition–resolving the origins of steady turnover. *ACS Catalysis*.

Kang, H., Kulkarni, A., Stankovich, S., Ruoff, R. S., & Baik, S. (2009). Restoring electrical conductivity of dielectrophoretically assembled graphite oxide sheets by thermal and chemical reduction techniques. *carbon, 47*(6), 1520-1525.

Kang, M.-G., Park, H. J., Ahn, S. H., & Guo, L. J. (2010). Transparent cu nanowire mesh electrode on flexible substrates fabricated by transfer printing and its application in organic solar cells. *Solar Energy Materials and Solar Cells, 94*(6), 1179-1184.

Kang, T.-T., Liu, X., Zhang, R. Q., Hu, W. G., Cong, G., Zhao, F.-A., & Zhu, Q. (2006). Inn nanoflowers grown by metal organic chemical vapor deposition. *Applied physics letters, 89*(7), 071113.

Karabacak, T., Mallikarjunan, A., Singh, J. P., Ye, D., Wang, G.-C., & Lu, T.-M. (2003). B-phase tungsten nanorod formation by oblique-angle sputter deposition. *Applied physics letters, 83*(15), 3096-3098.

Karimi-Maleh, H., Moazampour, M., Ensafi, A. A., Mallakpour, S., & Hatami, M. (2014). An electrochemical nanocomposite modified carbon paste electrode as a sensor for simultaneous determination of hydrazine and phenol in water and wastewater samples. *Environmental Science and Pollution Research, 21*(9), 5879-5888.

Karuppiah, C., Palanisamy, S., Chen, S.-M., Ramaraj, S. K., & Periakaruppan, P. (2014). A novel and sensitive amperometric hydrazine sensor based on gold nanoparticles decorated graphite nanosheets modified screen printed carbon electrode. *Electrochimica Acta, 139*, 157-164.

Karuppiah, C., Palanisamy, S., Chen, S. M., Veeramani, V., & Periakaruppan, P. (2014). A novel enzymatic glucose biosensor and sensitive non-enzymatic hydrogen peroxide sensor based on graphene and cobalt oxide nanoparticles composite modified glassy carbon electrode. *Sensors and Actuators B-Chemical, 196*, 450-456.

Kelly, R., Miotello, A., Chrisey, D., & Hubler, G. (1994). Pulsed laser deposition of thin films. *by DB Chrisey and GK Hubler (Wiley, New York, 1994) p, 55*.

Khalilzadeh, M. A., & Karimi-Maleh, H. (2009). Sensitive and selective determination of phenylhydrazine in the presence of hydrazine at a ferrocene monocarboxylic acid modified carbon nanotube paste electrode. *Analytical Letters, 43*(1), 186-196.

Khlebtsov, N., & Dykman, L. (2011). Biodistribution and toxicity of engineered gold nanoparticles: A review of in vitro and in vivo studies. *Chemical Society Reviews, 40*(3), 1647-1671.

Khoei, A., Ban, E., Banihashemi, P., & Qomi, M. A. (2011). Effects of temperature and torsion speed on torsional properties of single-walled carbon nanotubes. *Materials Science and Engineering: C, 31*(2), 452-457.

Kim, H., Seo, D.-H., Kim, S.-W., Kim, J., & Kang, K. (2011). Highly reversible co 3 o 4/graphene hybrid anode for lithium rechargeable batteries. *carbon, 49*(1), 326-332.

Kim, K., Zhao, Y., Jang, H., Lee, S., Kim, J., Kim, K., & Ahn, J. (2009). P. Kim, j.-y. Choi and bh hong. *nature, 457*, 706.

Kim, K. S., Zhao, Y., Jang, H., Lee, S. Y., Kim, J. M., Kim, K. S., Ahn, J.-H., Kim, P., Choi, J.-Y., & Hong, B. H. (2009). Large-scale pattern growth of graphene films for stretchable transparent electrodes. *nature, 457*(7230), 706-710.

Kim, Y., Noh, Y., Lim, E. J., Lee, S., Choi, S. M., & Kim, W. B. (2014). Star-shaped pd@ pt core–shell catalysts supported on reduced graphene oxide with superior electrocatalytic performance. *Journal of Materials Chemistry A, 2*(19), 6976-6986.

Kimmel, D. W., LeBlanc, G., Meschievitz, M. E., & Cliffel, D. E. (2011). Electrochemical sensors and biosensors. *Analytical chemistry, 84*(2), 685-707.

Koçak, S., & Aslışen, B. (2014). Hydrazine oxidation at gold nanoparticles and poly(bromocresol purple) carbon nanotube modified glassy carbon electrode. *Sensors and Actuators B: Chemical, 196*, 610-618.

Kou, R., Shao, Y., Mei, D., Nie, Z., Wang, D., Wang, C., Viswanathan, V. V., Park, S., Aksay, I. A., & Lin, Y. (2011). Stabilization of electrocatalytic metal nanoparticles at metal− metal oxide− graphene triple junction points. *Journal of the American Chemical Society, 133*(8), 2541-2547.

Krittayavathananon, A., Srimuk, P., Luanwuthi, S., & Sawangphruk, M. (2014). Palladium nanoparticles decorated on reduced graphene oxide rotating disk electrodes toward ultrasensitive hydrazine detection: Effects of particle size and hydrodynamic diffusion. *Analytical chemistry, 86*(24), 12272-12278.

Kumar, R. V., Diamant, Y., & Gedanken, A. (2000). Sonochemical synthesis and characterization of nanometer-size transition metal oxides from metal acetates. *Chemistry of materials, 12*(8), 2301-2305.

Kung, H. H. (1989). *Transition metal oxides: Surface chemistry and catalysis* (Vol. 45): Elsevier.

Lee, C., Wei, X., Kysar, J. W., & Hone, J. (2008). Measurement of the elastic properties and intrinsic strength of monolayer graphene. *Science, 321*(5887), 385-388.

Lencka, M. M., Oledzka, M., & Riman, R. E. (2000). Hydrothermal synthesis of sodium and potassium bismuth titanates. *Chemistry of materials, 12*(5), 1323-1330.

Lesiak, M., Binczarski, M., Karski, S., Maniukiewicz, W., Rogowski, J., Szubiakiewicz, E., Berlowska, J., Dziugan, P., & Witońska, I. (2014). Hydrogenation of furfural over pd–cu/al 2 o 3 catalysts. The role of interaction between palladium and copper on determining catalytic properties. *Journal of Molecular Catalysis A: Chemical, 395*, 337-348.

Li, C. C., Chen, L. B., Li, Q. H., & Wang, T. H. (2012). Seed-free, aqueous synthesis of gold nanowires. *CrystEngComm, 14*(22), 7549-7551.

Li, C. M., Zang, J., Zhan, D., Chen, W., Sun, C. Q., Teo, A. L., Chua, Y., Lee, V., & Moochhala, S. (2006). Electrochemical detection of nitric oxide on a swcnt/rtil composite gel microelectrode. *Electroanalysis*, *18*(7), 713-718.

Li, D., Müller, M. B., Gilje, S., Kaner, R. B., & Wallace, G. G. (2008). Processable aqueous dispersions of graphene nanosheets. *Nature nanotechnology, 3*(2), 101-105.

Li, J., Kuang, D., Feng, Y., Zhang, F., Xu, Z., & Liu, M. (2012). A graphene oxide-based electrochemical sensor for sensitive determination of 4-nitrophenol. *Journal of hazardous materials, 201*, 250-259.

Li, J., & Lin, X. (2007). Electrocatalytic oxidation of hydrazine and hydroxylamine at gold nanoparticle—polypyrrole nanowire modified glassy carbon electrode. *Sensors and Actuators B: Chemical, 126*(2), 527-535.

Li, S.-J., Du, J.-M., Zhang, J.-P., Zhang, M.-J., & Chen, J. (2014). A glassy carbon electrode modified with a film composed of cobalt oxide nanoparticles and graphene for electrochemical sensing of h2o2. *Microchimica Acta, 181*(5-6), 631-638.

Li, S.-S., Zheng, J.-N., Ma, X., Hu, Y.-Y., Wang, A.-J., Chen, J.-R., & Feng, J.-J. (2014). Facile synthesis of hierarchical dendritic ptpd nanogarlands supported on reduced graphene oxide with enhanced electrocatalytic properties. *Nanoscale, 6*(11), 5708-5713.

Li, W.-Y., Xu, L.-N., & Chen, J. (2005). Co3o4 nanomaterials in lithium-ion batteries and gas sensors. *Advanced Functional Materials, 15*(5), 851-857.

Li, W., Geng, X., Guo, Y., Rong, J., Gong, Y., Wu, L., Zhang, X., Li, P., Xu, J., & Cheng, G. (2011). Reduced graphene oxide electrically contacted graphene sensor for highly sensitive nitric oxide detection. *ACS nano, 5*(9), 6955-6961.

Li, W., Gong, B., Wu, P., Yang, S., Yang, Q., Dang, Z., & Zhu, N. (2017). Evaluation of the physiochemical properties and catalytic performance of mixed metal oxides-carbon nanotubes nanohybrids containing carbon nanotubes with different diameters. *Applied Clay Science, 135*, 95-102.

Li, W., Jung, H., Hoa, N. D., Kim, D., Hong, S.-K., & Kim, H. (2010). Nanocomposite of cobalt oxide nanocrystals and single-walled carbon nanotubes for a gas sensor application. *Sensors and Actuators B: Chemical, 150*(1), 160-166.

Li, X., Wang, L., Wu, Q., Chen, Z., & Lin, X. (2014). A nonenzymatic hydrogen peroxide sensor based on au–ag nanotubes and chitosan film. *Journal of Electroanalytical Chemistry, 735*, 19-23.

Li, Y.-P., Cao, H.-B., Liu, C.-M., & Zhang, Y. (2007). Electrochemical reduction of nitrobenzene at carbon nanotube electrode. *Journal of hazardous materials, 148*(1), 158-163.

Li, Y., Huang, X., Chen, Y., Wang, L., & Lin, X. (2009). Simultaneous determination of dopamine and serotonin by use of covalent modification of 5-hydroxytryptophan on glassy carbon electrode. *Microchimica Acta, 164*(1-2), 107-112.

Li, Z., Yao, Y., Lin, Z., Moon, K.-S., Lin, W., & Wong, C. (2010). Ultrafast, dry microwave synthesis of graphene sheets. *Journal of Materials Chemistry, 20*(23), 4781-4783.

Liang, Y., Li, Y., Wang, H., Zhou, J., Wang, J., Regier, T., & Dai, H. (2011). Co3o4 nanocrystals on graphene as a synergistic catalyst for oxygen reduction reaction. *Nat Mater, 10*(10), 780-786.

Lin, X., Chen, Y., & Li, S. (2013). Spectrophotometric determination of trace p-nitrophenol enriched by 1-hydroxy-2-naphthoic acid-modified nanometer tio2 in water. *Analytical Methods, 5*(22), 6480.

Liu, A. (2008). Towards development of chemosensors and biosensors with metal-oxide-based nanowires or nanotubes. *Biosensors and Bioelectronics, 24*(2), 167-177.

Liu, B., Wang, T., Yin, C., & Wei, Z. (2014). Electrochemical analysis of p-nitrophenol in acidic or alkaline medium using silver nanoparticle decorated multi-walled carbon nanotubes. *Journal of Materials Science, 49*(15), 5398-5405.

Liu, H.-C., & Yen, S.-K. (2007). Characterization of electrolytic co 3 o 4 thin films as anodes for lithium-ion batteries. *Journal of Power Sources, 166*(2), 478-484.

Liu, M., Hu, J., Ma, T., Wang, S., & Ding, H. (2011). Application of a disposable screen-printed electrode to depression diagnosis for laboratory rats based on blood serotonin detection. *Anal. Sci., 27*(8), 839-843.

Liu, M., Xiang, J., Zhou, J., & Ding, H. (2010). A disposable amperometric sensor for rapid detection of serotonin in the blood and brain of the depressed mice based on nafion membrane-coated colloidal gold screen-printed electrode. *Journal of Electroanalytical Chemistry, 640*(1), 1-7.

Liu, X., Zhu, H., & Yang, X. (2014). An electrochemical sensor for dopamine based on poly(o-phenylenediamine) functionalized with electrochemically reduced graphene oxide. *RSC Adv., 4*(8), 3706-3712.

Liu, Y.-C., Zhao, J., Wu, W.-L., & Yang, Z.-S. (2007). Direct electrochemical behavior of cytochrome c on DNA modified glassy carbon electrode and its application to nitric oxide biosensor. *Electrochimica Acta, 52*(14), 4848-4852.

Liu, Y., Chen, S.-S., Wang, A.-J., Feng, J.-J., Wu, X., & Weng, X. (2016). An ultra-sensitive electrochemical sensor for hydrazine based on aupd nanorod alloy nanochains. *Electrochimica Acta, 195*, 68-76.

Liu, Z., Du, J., Qiu, C., Huang, L., Ma, H., Shen, D., & Ding, Y. (2009). Electrochemical sensor for detection of p-nitrophenol based on nanoporous gold. *Electrochemistry Communications, 11*(7), 1365-1368.

Lou, X. W., Deng, D., Lee, J. Y., Feng, J., & Archer, L. A. (2008). Self-supported formation of needlelike co3o4 nanotubes and their application as lithium-ion battery electrodes. *Advanced Materials, 20*(2), 258-262.

Lu, W., Ning, R., Qin, X., Zhang, Y., Chang, G., Liu, S., Luo, Y., & Sun, X. (2011). Synthesis of au nanoparticles decorated graphene oxide nanosheets: Noncovalent functionalization by tween 20 in situ reduction of aqueous chloroaurate ions for hydrazine detection and catalytic reduction of 4-nitrophenol. *Journal of hazardous materials, 197*, 320-326.

Lu, Y., Wang, Y., Zou, Y., Jiao, Z., Zhao, B., He, Y., & Wu, M. (2010). Macroporous co 3 o 4 platelets with excellent rate capability as anodes for lithium ion batteries. *Electrochemistry Communications, 12*(1), 101-105.

Luo, J.-d., & Chen, A. F. (2005). Nitric oxide: A newly discovered function on wound healing. *Acta Pharmacologica Sinica, 26*(3), 259-264.

Luo, X., Pan, J., Pan, K., Yu, Y., Zhong, A., Wei, S., Li, J., Shi, J., & Li, X. (2015). An electrochemical sensor for hydrazine and nitrite based on graphene–cobalt hexacyanoferrate nanocomposite: Toward environment and food detection. *Journal of Electroanalytical Chemistry, 745*, 80-87.

Madhu, R., Dinesh, B., Chen, S.-M., Saraswathi, R., & Mani, V. (2015). An electrochemical synthesis strategy for composite based zno microspheres–au nanoparticles on reduced graphene oxide for the sensitive detection of hydrazine in water samples. *RSC Advances, 5*(67), 54379-54386.

Madhu, R., Karuppiah, C., Chen, S.-M., Veerakumar, P., & Liu, S.-B. (2014). Electrochemical detection of 4-nitrophenol based on biomass derived activated carbons. *Analytical Methods, 6*(14), 5274-5280.

Maduraiveeran, G., & Ramaraj, R. (2007). Gold nanoparticles embedded in silica sol–gel matrix as an amperometric sensor for hydrogen peroxide. *Journal of Electroanalytical Chemistry, 608*(1), 52-58.

Maduraiveeran, G., & Ramaraj, R. (2009). Potential sensing platform of silver nanoparticles embedded in functionalized silicate shell for nitroaromatic compounds. *Analytical chemistry, 81*(18), 7552-7560.

Mahmood, N., Zhang, C., Yin, H., & Hou, Y. (2014). Graphene-based nanocomposites for energy storage and conversion in lithium batteries, supercapacitors and fuel cells. *Journal of Materials Chemistry A, 2*(1), 15-32.

Makhlouf, S. A. (2002). Magnetic properties of co 3 o 4 nanoparticles. *Journal of magnetism and magnetic materials, 246*(1), 184-190.

Malinski, T., & Taha, Z. (1992). Nitric oxide release from a single cell measured in situ by a porphyrinic-based microsensor.

Mallela, S., & Khandelwal, B. (1977). Use of the rotating platinum electrode for microdetermination of hydrazine, hydroxylamine, nitrite, ascorbic acid, oxalic acid and thiourea with manganese (iii) pyrophosphate. *Microchimica Acta, 68*(3-4), 245-248.

Matemadombo, F., & Nyokong, T. (2007). Characterization of self-assembled monolayers of iron and cobalt octaalkylthiosubstituted phthalocyanines and their use in nitrite electrocatalytic oxidation. *Electrochimica Acta, 52*(24), 6856-6864.

Mazloum-Ardakani, M., & Khoshroo, A. (2014). High sensitive sensor based on functionalized carbon nanotube/ionic liquid nanocomposite for simultaneous determination of norepinephrine and serotonin. *Journal of Electroanalytical Chemistry, 717-718*, 17-23.

Middelkoop, C. M., Dekker, G. A., Kraayenbrink, A. A., & Popp-Snijders, C. (1993). Platelet-poor plasma serotonin in normal and preeclamptic pregnancy. *Clinical chemistry, 39*(8), 1675-1678.

Ming-Jay, D., Fu-Lu, H., Sun, I. W., Wen-Ta, T., & Jeng-Kuei, C. (2009). An entirely electrochemical preparation of a nano-structured cobalt oxide electrode with superior redox activity. *Nanotechnology, 20*(17), 175602.

Ming, H. N. (2010). Simple room-temperature preparation of high-yield large-area graphene oxide. *International Journal of Nanomedicine, 6*.

Mini, V., Archana, K., Raghu, S., Sharanappa, C., & Devendrappa, H. (2016). Nanostructured multifunctional core/shell ternary composite of polyaniline-chitosan-cobalt oxide: Preparation, electrical and optical properties. *Materials Chemistry and Physics, 170*, 90-98.

Miotello, A., & Kelly, R. (1999). Laser-induced phase explosion: New physical problems when a condensed phase approaches the thermodynamic critical temperature. *Applied Physics A, 69*(1), S67-S73.

Moghaddam, R. B., & Pickup, P. G. (2012). Support effects on the oxidation of ethanol at pt nanoparticles. *Electrochimica Acta, 65*, 210-215.

Mogudi, B. M., Ncube, P., & Meijboom, R. (2016). Catalytic activity of mesoporous cobalt oxides with controlled porosity and crystallite sizes: Evaluation using the reduction of 4-nitrophenol. *Applied Catalysis B: Environmental, 198*, 74-82.

Moncada, S., & Higgs, A. (1993). The l-arginine-nitric oxide pathway. *The New England journal of medicine, 329*(27), 2002-2012.

Morris, R., Fagan-Murphy, A., MacEachern, S. J., Covill, D., & Patel, B. A. (2016). Electrochemical fecal pellet sensor for simultaneous real-time ex vivo detection of colonic serotonin signalling and motility. *6*, 23442.

Mu, J., Zhang, L., Zhao, M., & Wang, Y. (2013). Co 3 o 4 nanoparticles as an efficient catalase mimic: Properties, mechanism and its electrocatalytic sensing application for hydrogen peroxide. *Journal of Molecular Catalysis A: Chemical, 378*, 30-37.

Ndlovu, T., Arotiba, O. A., Krause, R. W., & Mamba, B. B. (2010). Electrochemical detection of o-nitrophenol on a poly (propyleneimine)-gold nanocomposite modified glassy carbon electrode. *International Journal of Electrochemical Science, 5*, 117-1186.

Ng, H. T., Li, J., Smith, M. K., Nguyen, P., Cassell, A., Han, J., & Meyyappan, M. (2003). Growth of epitaxial nanowires at the junctions of nanowalls. *Science, 300*(5623), 1249-1249.

Nguyen, T. T., Nguyen, V. H., Deivasigamani, R. K., Kharismadewi, D., Iwai, Y., & Shim, J.-J. (2016). Facile synthesis of cobalt oxide/reduced graphene oxide composites for electrochemical capacitor and sensor applications. *Solid State Sciences, 53*, 71-77.

Ni, M., Leung, M. K., Leung, D. Y., & Sumathy, K. (2007). A review and recent developments in photocatalytic water-splitting using tio2 for hydrogen production. *Renewable and Sustainable Energy Reviews, 11*(3), 401-425.

Nie, R., Shi, J., Du, W., Ning, W., Hou, Z., & Xiao, F.-S. (2013). A sandwich n-doped graphene/co 3 o 4 hybrid: An efficient catalyst for selective oxidation of olefins and alcohols. *Journal of Materials Chemistry A, 1*(32), 9037-9045.

Niu, L. M., Lian, K. Q., Shi, H. M., Wu, Y. B., Kang, W. J., & Bi, S. Y. (2013). Characterization of an ultrasensitive biosensor based on a nano-au/DNA/nano-au/poly (sfr) composite and its application in the simultaneous determination of dopamine, uric acid, guanine, and adenine. *Sensors and Actuators B: Chemical, 178*, 10-18.

Noguera, C. (1996). *Physics and chemistry at oxide surfaces*: Cambridge University Press.

Novoselov, K. S., Geim, A. K., Morozov, S. V., Jiang, D., Zhang, Y., Dubonos, S. V., Grigorieva, I. V., & Firsov, A. A. (2004). Electric field effect in atomically thin carbon films. *Science, 306*(5696), 666-669.

Numan, A., Duraisamy, N., Saiha Omar, F., Mahipal, Y. K., Ramesh, K., & Ramesh, S. (2016). Enhanced electrochemical performance of cobalt oxide nanocube intercalated reduced graphene oxide for supercapacitor application. *RSC Advances, 6*(41), 34894-34902.

Numan, A., Shahid, M. M., Omar, F. S., Ramesh, K., & Ramesh, S. (2017). Facile fabrication of cobalt oxide nanograin-decorated reduced graphene oxide composite as ultrasensitive platform for dopamine detection. *Sensors and Actuators B: Chemical, 238*, 1043-1051.

O'Donoghue, M. (1983). *A guide to man-made gemstones*: Van Nostrand Reinhold Company.

Ohkubo, I., Matsumoto, Y., Hasegawa, T., Ueno, K., Itaka, K., Ahmet, P., Chikyow, T., Kawasaki, M., & Koinuma, H. (2001). Pulsed laser epitaxy and magnetic properties of single phase y-type magnetoplumbite thin films. *Japanese journal of applied physics, 40*(12B), L1343.

Pan, L., Li, L., & Chen, Y. (2012). Synthesis of nio nanomaterials with various morphologies and their electrocatalytic performances for p-nitrophenol reduction. *Journal of sol-gel science and technology, 62*(3), 364-369.

Pan, L., Tang, J., & Wang, F. (2013). Synthesis and electrocatalytic performance for p-nitrophenol reduction of rod-like co3o4 and ag/co3o4 composites. *Materials Research Bulletin, 48*(7), 2648-2653.

Pan, L., Zhao, H., Shen, W., Dong, X., & Xu, J. (2013). Surfactant-assisted synthesis of a co 3 o 4/reduced graphene oxide composite as a superior anode material for li-ion batteries. *Journal of Materials Chemistry A, 1*(24), 7159-7166.

Pandikumar, A., & Ramaraj, R. (2011). Aminosilicate sol-gel embedded core-shell (tio 2-au) nps nanomaterials modified electrode for the electrochemical detection of nitric oxide.

Panholzer, T. J., Beyer, J., & Lichtwald, K. (1999). Coupled-column liquid chromatographic analysis of catecholamines, serotonin, and metabolites in human urine. *Clinical chemistry, 45*(2), 262-268.

Paredes, J., Villar-Rodil, S., Martínez-Alonso, A., & Tascon, J. (2008). Graphene oxide dispersions in organic solvents. *Langmuir, 24*(19), 10560-10564.

Park, D.-H., Lim, S.-T., & Hwang, S.-J. (2006). A soft chemical route to multicomponent lithium transition metal oxide nanowires as promising cathode materials for lithium secondary batteries. *Electrochimica Acta, 52*(4), 1462-1466.

Park, S., & Ruoff, R. S. (2009). Chemical methods for the production of graphenes. *Nature nanotechnology, 4*(4), 217-224.

Poizot, P., Laruelle, S., Grugeon, S., Dupont, L., & Tarascon, J. (2000). Nano-sized transition-metal oxides as negative-electrode materials for lithium-ion batteries. *nature, 407*(6803), 496-499.

Pravinraj, S., Vijayakumar, M., & Marimuthu, K. (2017). Enhanced luminescence behaviour of eu3+ doped heavy metal oxide telluroborate glasses for laser and led applications. *Physica B: Condensed Matter, 509*, 84-93.

Privett, B. J., Shin, J. H., & Schoenfisch, M. H. (2010). Electrochemical nitric oxide sensors for physiological measurements. *Chemical Society Reviews, 39*(6), 1925-1935.

Qu, Q., Yang, S., & Feng, X. (2011). 2d sandwich-like sheets of iron oxide grown on graphene as high energy anode material for supercapacitors. *Advanced Materials, 23*(46), 5574-5580.

Rafique, S., Abdullah, S. M., Shahid, M. M., Ansari, M. O., & Sulaiman, K. (2017). Significantly improved photovoltaic performance in polymer bulk heterojunction solar cells with graphene oxide/pedot: Pss double decked hole transport layer. *Scientific reports, 7*.

Rahman, M. M., Khan, S. B., Faisal, M., Rub, M. A., Al-Youbi, A. O., & Asiri, A. M. (2012). Electrochemical determination of olmesartan medoxomil using hydrothermally prepared nanoparticles composed sno 2–co 3 o 4 nanocubes in tablet dosage forms. *Talanta, 99*, 924-931.

Rahman, M. M., Wang, J.-Z., Deng, X.-L., Li, Y., & Liu, H.-K. (2009). Hydrothermal synthesis of nanostructured co3o4 materials under pulsed magnetic field and with an aging technique, and their electrochemical performance as anode for lithium-ion battery. *Electrochimica Acta, 55*(2), 504-510.

Rahman, M. M., Wang, J.-Z., Deng, X.-L., Li, Y., & Liu, H.-K. (2009). Hydrothermal synthesis of nanostructured co 3 o 4 materials under pulsed magnetic field and with an aging technique, and their electrochemical performance as anode for lithium-ion battery. *Electrochimica Acta, 55*(2), 504-510.

Rajput, N. (2015). Methods of preparation of nanoparticles-a review. *International Journal Of Advances In Engineering & Technology, 7*(6), 1806.

Rameshkumar, P., & Ramaraj, R. (2014). Electroanalysis of nitrobenzene derivatives and nitrite ions using silver nanoparticles deposited silica spheres modified electrode. *Journal of Electroanalytical Chemistry, 731*, 72-77.

Ran, G., Chen, C., & Gu, C. (2015). Serotonin sensor based on a glassy carbon electrode modified with multiwalled carbon nanotubes, chitosan and poly(p-aminobenzenesulfonate). *Microchimica Acta, 182*(7), 1323-1328.

Rand, E., Periyakaruppan, A., Tanaka, Z., Zhang, D. A., Marsh, M. P., Andrews, R. J., Lee, K. H., Chen, B., Meyyappan, M., & Koehne, J. E. (2013). A carbon nanofiber based biosensor for simultaneous detection of dopamine and serotonin in the presence of ascorbicacid. *Biosensors and Bioelectronics, 42*, 434-438.

Rao, C., Sood, A., Voggu, R., & Subrahmanyam, K. (2010). Some novel attributes of graphene. *The Journal of Physical Chemistry Letters, 1*(2), 572-580.

Rastogi, P. K., Ganesan, V., & Krishnamoorthi, S. (2014). Palladium nanoparticles decorated gaur gum based hybrid material for electrocatalytic hydrazine determination. *Electrochimica Acta, 125*, 593-600.

Rastogi, P. K., Ganesan, V., & Krishnamoorthi, S. (2014). A promising electrochemical sensing platform based on a silver nanoparticles decorated copolymer for sensitive nitrite determination. *Journal of Materials Chemistry A, 2*(4), 933-943.

Razmi, H., & Habibi, E. (2010). Amperometric detection of acetaminophen by an electrochemical sensor based on cobalt oxide nanoparticles in a flow injection system. *Electrochimica Acta, 55*(28), 8731-8737.

Reddaiah, K., Reddy, T. M., & Raghu, P. (2012). Electrochemical investigation of l-dopa and simultaneous resolution in the presence of uric acid and ascorbic acid at a poly (methyl orange) film coated electrode: A voltammetric study. *Journal of Electroanalytical Chemistry, 682*, 164-171.

Rout, C. S., Krishna, S. H., Vivekchand, S., Govindaraj, A., & Rao, C. (2006). Hydrogen and ethanol sensors based on zno nanorods, nanowires and nanotubes. *Chemical Physics Letters, 418*(4), 586-590.

Rubio-Retama, J., Hernando, J., Lopez-Ruiz, B., Härtl, A., Steinmüller, D., Stutzmann, M., Lopez-Cabarcos, E., & Antonio Garrido, J. (2006). Synthetic nanocrystalline diamond as a third-generation biosensor support. *Langmuir, 22*(13), 5837-5842.

Safavi, A., & Ensafi, A. A. (1995). Kinetic spectrophotometric determination of hydrazine. *Analytica chimica acta, 300*(1), 307-311.

Safavi, A., & Karimi, M. A. (2002). Flow injection chemiluminescence determination of hydrazine by oxidation with chlorinated isocyanurates. *Talanta, 58*(4), 785-792.

Sankur, H., Gunning, W., DeNatale, J., & Flintoff, J. (1989). High-quality optical and epitaxial ge films formed by laser evaporation. *Journal of Applied Physics, 65*(6), 2475-2478.

Santhiago, M., Henry, C. S., & Kubota, L. T. (2014). Low cost, simple three dimensional electrochemical paper-based analytical device for determination of p-nitrophenol. *Electrochimica Acta, 130*, 771-777.

Schwentker, A., Vodovotz, Y., Weller, R., & Billiar, T. R. (2002). Nitric oxide and wound repair: Role of cytokines? *Nitric oxide, 7*(1), 1-10.

Service, R. F. (2009). Materials science. Carbon sheets an atom thick give rise to graphene dreams. *Science (New York, NY), 324*(5929), 875.

Shahabuddin, S., Sarih, N. M., Ismail, F. H., Shahid, M. M., & Huang, N. M. (2015). Synthesis of chitosan grafted-polyaniline/co 3 o 4 nanocube nanocomposites and their photocatalytic activity toward methylene blue dye degradation. *RSC Advances, 5*(102), 83857-83867.

Shahid, M. M., Pandikumar, A., Golsheikh, A. M., Huang, N. M., & Lim, H. N. (2014). Enhanced electrocatalytic performance of cobalt oxide nanocubes incorporating reduced graphene oxide as a modified platinum electrode for methanol oxidation. *RSC Adv., 4*(107), 62793-62801.

Shahid, M. M., Rameshkumar, P., Basirun, W. J., Juan, J. C., & Huang, N. M. (2017). Cobalt oxide nanocubes interleaved reduced graphene oxide as an efficient electrocatalyst for oxygen reduction reaction in alkaline medium. *Electrochimica Acta, 237*, 61-68.

Shahid, M. M., Rameshkumar, P., & Huang, N. M. (2015). Morphology dependent electrocatalytic properties of hydrothermally synthesized cobalt oxide nanostructures. *Ceramics International, 41*(10), 13210-13217.

Shahid, M. M., Rameshkumar, P., Pandikumar, A., Lim, H. N., Ng, Y. H., & Huang, N. M. (2015). An electrochemical sensing platform based on a reduced graphene oxide-cobalt oxide nanocube@platinum nanocomposite for nitric oxide detection. *Journal of Materials Chemistry A, 3*(27), 14458-14468.

Shalini, K., Mane, A. U., Shivashankar, S., Rajeswari, M., & Choopun, S. (2001). Epitaxial growth of co 3 o 4 films by low temperature, low pressure chemical vapour deposition. *Journal of crystal growth, 231*(1), 242-247.

Shaoqing, Y., Jun, H., & Jianlong, W. (2010). Radiation-induced catalytic degradation of p-nitrophenol (pnp) in the presence of tio2 nanoparticles. *Radiation Physics and Chemistry*, *79*(10), 1039-1046.

Sharifi, S., Shakur, H., Mirzaei, A., & Hosseini, M. (2013). Characterization of cobalt oxide co3o4 nanoparticles prepared by various methods: Effect of calcination temperatures on size, dimension and catalytic decomposition of hydrogen peroxide. *International Journal of Nanoscience and Nanotechnology*, *9*(1), 51-58.

Shi, R., Chen, G., Ma, W., Zhang, D., Qiu, G., & Liu, X. (2012). Shape-controlled synthesis and characterization of cobalt oxides hollow spheres and octahedra. *Dalton Transactions, 41*(19), 5981-5987.

Shimizu, M., Suzuki, M., Iguchi, F., & Yugami, H. (2014). High-temperature solar selective absorbers using transparent conductive oxide coated metal. *Energy Procedia*, *57*, 418-426.

Shrivastava, A., & Gupta, V. (2011). Methods for the determination of limit of detection and limit of quantitation of the analytical methods. *Chronicles of Young Scientists, 2*(1), 21-21.

Singh, B., Dempsey, E., Dickinson, C., & Laffir, F. (2012). Inside/outside pt nanoparticles decoration of functionalised carbon nanofibers (pt 19.2/f-cnf 80.8) for sensitive non-enzymatic electrochemical glucose detection. *Analyst, 137*(7), 1639-1648.

Song, Z., Zhang, Y., Liu, W., Zhang, S., Liu, G., Chen, H., & Qiu, J. (2013). Hydrothermal synthesis and electrochemical performance of co 3 o 4/reduced graphene oxide nanosheet composites for supercapacitors. *Electrochimica Acta, 112*, 120-126.

Stankovich, S., Dikin, D. A., Piner, R. D., Kohlhaas, K. A., Kleinhammes, A., Jia, Y., Wu, Y., Nguyen, S. T., & Ruoff, R. S. (2007). Synthesis of graphene-based

nanosheets via chemical reduction of exfoliated graphite oxide. *carbon, 45*(7), 1558-1565.

Stroyuk, A. L., Shvalagin, V. V., & Kuchmii, S. Y. (2005). Photochemical synthesis and optical properties of binary and ternary metal–semiconductor composites based on zinc oxide nanoparticles. *Journal of Photochemistry and Photobiology A: Chemistry, 173*(2), 185-194.

Su, J., Gherasimova, M., Cui, G., Tsukamoto, H., Han, J., Onuma, T., Kurimoto, M., Chichibu, S., Broadbridge, C., & He, Y. (2005). Growth of algan nanowires by metalorganic chemical vapor deposition. *Applied physics letters, 87*(18), 183108.

Sun, M., Liu, H., Liu, Y., Qu, J., & Li, J. (2015). Graphene-based transition metal oxide nanocomposites for the oxygen reduction reaction. *Nanoscale, 7*(4), 1250-1269.

Taha, Z. H. (2003). Nitric oxide measurements in biological samples. *Talanta, 61*(1), 3-10.

Takada, S., Fujii, M., Kohiki, S., Babasaki, T., Deguchi, H., Mitome, M., & Oku, M. (2001). Intraparticle magnetic properties of co3o4 nanocrystals. *Nano Letters, 1*(7), 379-382.

Tang, Y.-Y., Kao, C.-L., & Chen, P.-Y. (2012). Electrochemical detection of hydrazine using a highly sensitive nanoporous gold electrode. *Analytica chimica acta, 711*, 32-39.

Tang, Y., Huang, R., Liu, C., Yang, S., Lu, Z., & Luo, S. (2013). Electrochemical detection of 4-nitrophenol based on a glassy carbon electrode modified with a reduced graphene oxide/au nanoparticle composite. *Analytical Methods, 5*(20), 5508-5514.

Thangavel, S., & Ramaraj, R. (2008). Polymer membrane stabilized gold nanostructures modified electrode and its application in nitric oxide detection. *The Journal of Physical Chemistry C, 112*(50), 19825-19830.

Thanh, T. D., Balamurugan, J., Kim, N. H., Lee, S. H., & Lee, J. H. (2016). Effective seed-assisted synthesis of gold nanoparticles anchored nitrogen-doped graphene for electrochemical detection of glucose and dopamine. *Biosens Bioelectron, 81*, 259-267.

Thompson, L., & Doraiswamy, L. (1999). Sonochemistry: Science and engineering. *Industrial & Engineering Chemistry Research, 38*(4), 1215-1249.

Ting, S. L., Guo, C. X., Leong, K. C., Kim, D.-H., Li, C. M., & Chen, P. (2013). Gold nanoparticles decorated reduced graphene oxide for detecting the presence and cellular release of nitric oxide. *Electrochimica Acta, 111*, 441-446.

Tsuda, N., Nasu, K., Fujimori, A., & Siratori, K. (2013). *Electronic conduction in oxides* (Vol. 94): Springer Science & Business Media.

Tsunoda, M., Takezawa, K., Santa, T., & Imai, K. (1999). Simultaneous automatic determination of catecholamines and their 3-o-methyl metabolites in rat plasma

by high-performance liquid chromatography using peroxyoxalate chemiluminescence reaction. *Analytical biochemistry, 269*(2), 386-392.

Van Lier, G., Van Alsenoy, C., Van Doren, V., & Geerlings, P. (2000). Ab initio study of the elastic properties of single-walled carbon nanotubes and graphene. *Chemical Physics Letters, 326*(1), 181-185.

Védrine, J. C. (2002). The role of redox, acid-base and collective properties and of cristalline state of heterogeneous catalysts in the selective oxidation of hydrocarbons. *Topics in Catalysis, 21*(1), 97-106.

Viinikanoja, A., Wang, Z., Kauppila, J., & Kvarnström, C. (2012). Electrochemical reduction of graphene oxide and its in situ spectroelectrochemical characterization. *Physical Chemistry Chemical Physics, 14*(40), 14003-14009.

Wang, F., Wu, Y., Lu, K., & Ye, B. (2013). A simple but highly sensitive and selective calixarene-based voltammetric sensor for serotonin. *Electrochimica Acta, 87*, 756-762.

Wang, G., Yang, J., Park, J., Gou, X., Wang, B., Liu, H., & Yao, J. (2008). Facile synthesis and characterization of graphene nanosheets. *The Journal of Physical Chemistry C, 112*(22), 8192-8195.

Wang, G., Zhang, C., He, X., Li, Z., Zhang, X., Wang, L., & Fang, B. (2010). Detection of hydrazine based on nano-au deposited on porous-tio2 film. *Electrochimica Acta, 55*(24), 7204-7210.

Wang, J., Xie, Y., Zhang, Z., Li, J., Li, C., Zhang, L., Xing, Z., Xu, R., & Zhang, X. (2010). Photocatalytic degradation of organic dyes by er3+:Yalo3/tio2 composite under solar light. *Environmental chemistry letters, 8*(1), 87-93.

Wang, S., & Lin, X. (2005). Electrodeposition of pt–fe (iii) nanoparticle on glassy carbon electrode for electrochemical nitric oxide sensor. *Electrochimica Acta, 50*(14), 2887-2891.

Wang, X., Tian, W., Zhai, T., Zhi, C., Bando, Y., & Golberg, D. (2012). Cobalt(ii,iii) oxide hollow structures: Fabrication, properties and applications. *Journal of Materials Chemistry, 22*(44), 23310-23326.

Wang, Y., Jin, A., & Zhang, Z. (2002). Cu/sio 2− x nanowires with compositional modulation structure grown via thermal evaporation. *Applied physics letters, 81*(23), 4425-4427.

Wang, Y., Song, B., Xu, J., & Hu, S. (2014). An amperometric sensor for nitric oxide based on a glassy carbon electrode modified with graphene, nafion, and electrodeposited gold nanoparticles. *Microchimica Acta, 182*(3-4), 711-718.

Wang, Y., Wan, Y., & Zhang, D. (2010). Reduced graphene sheets modified glassy carbon electrode for electrocatalytic oxidation of hydrazine in alkaline media. *Electrochemistry Communications, 12*(2), 187-190.

Watt, G. W., & Chrisp, J. D. (1952). Spectrophotometric method for determination of hydrazine. *Analytical chemistry, 24*(12), 2006-2008.

Willmott, P., Manoravi, P., & Holliday, K. (2000). Production and characterization of nd, cr: Gsgg thin films on si (001) grown by pulsed laser ablation. *Applied Physics A: Materials Science & Processing, 70*(4), 425-429.

Wu, F.-H., Zhao, G.-C., & Wei, X.-W. (2002). Electrocatalytic oxidation of nitric oxide at multi-walled carbon nanotubes modified electrode. *Electrochemistry Communications, 4*(9), 690-694.

Wu, J., Wang, Q., Umar, A., Sun, S., Huang, L., Wang, J., & Gao, Y. (2014). Highly sensitive p-nitrophenol chemical sensor based on crystalline α-mno2nanotubes. *New Journal of Chemistry, 38*(9), 4420.

Wu, R.-J., Hu, C.-H., Yeh, C.-T., & Su, P.-G. (2003). Nanogold on powdered cobalt oxide for carbon monoxide sensor. *Sensors and Actuators B: Chemical, 96*(3), 596-601.

Wu, Z.-S., Ren, W., Wen, L., Gao, L., Zhao, J., Chen, Z., Zhou, G., Li, F., & Cheng, H.-M. (2010). Graphene anchored with co3o4 nanoparticles as anode of lithium ion batteries with enhanced reversible capacity and cyclic performance. *ACS nano, 4*(6), 3187-3194.

Wu, Z. S., Wang, D. W., Ren, W., Zhao, J., Zhou, G., Li, F., & Cheng, H. M. (2010). Anchoring hydrous ruo2 on graphene sheets for high-performance electrochemical capacitors. *Advanced Functional Materials, 20*(20), 3595-3602.

Xia, X., Tu, J., Zhang, J., Xiang, J., Wang, X., & Zhao, X. (2010). Fast electrochromic properties of self-supported co 3 o 4 nanowire array film. *Solar Energy Materials and Solar Cells, 94*(2), 386-389.

Xiao, J., Kuang, Q., Yang, S., Xiao, F., Wang, S., & Guo, L. (2013). Surface structure dependent electrocatalytic activity of co3o4 anchored on graphene sheets toward oxygen reduction reaction. *Scientific reports, 3*.

Xiao, S. Q., Wang, H., Zhao, Z. C., Xia, Y. X., & Wang, Z. H. (2008). Magnetic and transport properties in metal-oxide-semiconductor structures of co 3 mn 2 o/sio 2 /si. *Journal of Physics D: Applied Physics, 41*(4), 045005.

Xu, C.-X., Huang, K.-J., Fan, Y., Wu, Z.-W., Li, J., & Gan, T. (2012). Simultaneous electrochemical determination of dopamine and tryptophan using a tio 2-graphene/poly (4-aminobenzenesulfonic acid) composite film based platform. *Materials Science and Engineering: C, 32*(4), 969-974.

Xu, G., Li, B., Wang, X., & Luo, X. (2014). Electrochemical sensor for nitrobenzene based on carbon paste electrode modified with a poly (3, 4-ethylenedioxythiophene) and carbon nanotube nanocomposite. *Microchimica Acta, 181*(3-4), 463-469.

Xu, M., Ye, L., Wang, J., Wei, Z., & Cheng, S. (2017). Quality tracing of peanuts using an array of metal-oxide based gas sensors combined with chemometrics methods. *Postharvest Biology and Technology, 128*, 98-104.

Xu, X., Liu, Z., Zhang, X., Duan, S., Xu, S., & Zhou, C. (2011). B-cyclodextrin functionalized mesoporous silica for electrochemical selective sensor: Simultaneous determination of nitrophenol isomers. *Electrochimica Acta, 58*, 142-149.

Xue, P., Zhang, L., Zhang, L., Feng, X., Zhang, Y., Hao, W., Wang, H., & Zheng, H. (2014). In-plane vacancy-induced growth of ultra-high loading cobalt oxide-graphene composite for high-performance lithium-ion batteries. *Electrochimica Acta, 136*, 330-339.

Yang, J., Liu, G., Lu, J., Qiu, Y., & Yang, S. (2007). Electrochemical route to the synthesis of ultrathin zno nanorod/nanobelt arrays on zinc substrate. *Applied physics letters, 90*(10), 103109.

Yang, W., Gao, Z., Wang, J., Wang, B., Liu, Q., Li, Z., Mann, T., Yang, P., Zhang, M., & Liu, L. (2012). Synthesis of reduced graphene nanosheet/urchin-like manganese dioxide composite and high performance as supercapacitor electrode. *Electrochimica Acta, 69*, 112-119.

Yao, Y., Yang, Z., Sun, H., & Wang, S. (2012). Hydrothermal synthesis of co3o4–graphene for heterogeneous activation of peroxymonosulfate for decomposition of phenol. *Industrial & Engineering Chemistry Research, 51*(46), 14958-14965.

Yao, Z., Yue, R., Zhai, C., Jiang, F., Wang, H., Du, Y., Wang, C., & Yang, P. (2013). Electrochemical layer-by-layer fabrication of a novel three-dimensional pt/graphene/carbon fiber electrode and its improved catalytic performance for methanol electrooxidation in alkaline medium. *International Journal of Hydrogen Energy, 38*(15), 6368-6376.

Yeh, M.-H., Sun, C.-L., Su, J.-S., Lin, L.-Y., Lee, C.-P., Chen, C.-Y., Wu, C.-G., Vittal, R., & Ho, K.-C. (2012). A low-cost counter electrode of ito glass coated with a graphene/nafion® composite film for use in dye-sensitized solar cells. *carbon, 50*(11), 4192-4202.

Yi, Q., Niu, F., & Yu, W. (2011). Pd-modified tio 2 electrode for electrochemical oxidation of hydrazine, formaldehyde and glucose. *Thin Solid Films, 519*(10), 3155-3161.

Yi, Q., & Yu, W. (2009). Nanoporous gold particles modified titanium electrode for hydrazine oxidation. *Journal of Electroanalytical Chemistry, 633*(1), 159-164.

Yin, H., Zhou, Y., Ai, S., Ma, Q., Zhu, L., & Lu, L. (2012). Electrochemical oxidation determination and voltammetric behaviour of 4-nitrophenol based on cu2o nanoparticles modified glassy carbon electrode. *International Journal of Environmental Analytical Chemistry, 92*(6), 742-754.

Yuan, C.-X., Fan, Y.-R., Guo, H.-X., Zhang, J.-X., Wang, Y.-L., Shan, D.-L., & Lu, X.-Q. (2014). A new electrochemical sensor of nitro aromatic compound based on three-dimensional porous pt–pd nanoparticles supported by graphene–multiwalled carbon nanotube composite. *Biosensors and Bioelectronics, 58*, 85-91.

Yusoff, N., Pandikumar, A., Huang, N. M., & Lim, H. N. (2015). Facile synthesis of nanosized graphene/nafion hybrid materials and their application in electrochemical sensing of nitric oxide. *Analytical Methods, 7*(8), 3537-3544.

Yusoff, N., Rameshkumar, P., Mehmood, M. S., Pandikumar, A., Lee, H. W., & Huang, N. M. (2017). Ternary nanohybrid of reduced graphene oxide-nafion@ silver nanoparticles for boosting the sensor performance in non-enzymatic amperometric detection of hydrogen peroxide. *Biosensors and Bioelectronics, 87*, 1020-1028.

Yusoff, N., Rameshkumar, P., Shahid, M. M., Huang, S.-T., & Huang, N. M. (2017). Amperometric detection of nitric oxide using a glassy carbon electrode modified with gold nanoparticles incorporated into a nanohybrid composed of reduced graphene oxide and nafion. *Microchimica Acta*.

Zecchina, A., Scarano, D., Bordiga, S., Spoto, G., & Lamberti, C. (2001). Surface structures of oxides and halides and their relationships to catalytic properties. *Advances in catalysis, 46*, 265-397.

Zen, J.-M., Kumar, A. S., & Wang, H.-F. (2000). A dual electrochemical sensor for nitrite and nitric oxide. *Analyst, 125*(12), 2169-2172.

Zeng, Y., Zhou, Y., Zhou, T., & Shi, G. (2014). A novel composite of reduced graphene oxide and molecularly imprinted polymer for electrochemical sensing 4-nitrophenol. *Electrochimica Acta, 130*, 504-511.

Zhai, T., Fang, X., Liao, M., Xu, X., Zeng, H., Yoshio, B., & Golberg, D. (2009). A comprehensive review of one-dimensional metal-oxide nanostructure photodetectors. *Sensors, 9*(8), 6504-6529.

Zhang, C., Wang, G., Ji, Y., Liu, M., Feng, Y., Zhang, Z., & Fang, B. (2010). Enhancement in analytical hydrazine based on gold nanoparticles deposited on zno-mwcnts films. *Sensors and Actuators B: Chemical, 150*(1), 247-253.

Zhang, C., Yang, J., & Wu, Z. (2000). Electroreduction of nitrobenzene on titanium electrode implanted with platinum. *Materials Science and Engineering: B, 68*(3), 138-142.

Zhang, H.-X., Cao, A.-M., Hu, J.-S., Wan, L.-J., & Lee, S.-T. (2006). Electrochemical sensor for detecting ultratrace nitroaromatic compounds using mesoporous sio2-modified electrode. *Analytical chemistry, 78*(6), 1967-1971.

Zhang, J., Gao, W., Dou, M., Wang, F., Liu, J., Li, Z., & Ji, J. (2015). Nanorod-constructed porous co 3 o 4 nanowires: Highly sensitive sensors for the detection of hydrazine. *Analyst, 140*(5), 1686-1692.

Zhang, Y., Chen, Y., Wang, T., Zhou, J., & Zhao, Y. (2008). Synthesis and magnetic properties of nanoporous co3o4 nanoflowers. *Microporous and Mesoporous Materials, 114*(1), 257-261.

Zhao, S., Wang, L., Wang, T., Han, Q., & Xu, S. (2016). A high-performance hydrazine electrochemical sensor based on gold nanoparticles/single-walled carbon nanohorns composite film. *Applied Surface Science, 369*, 36-42.

Zheng, D., Liu, X., Zhou, D., & Hu, S. (2012). Sensing of nitric oxide using a glassy carbon electrode modified with an electrocatalytic film composed of dihexadecyl hydrogen phosphate, platinum nanoparticles, and acetylene black. *Microchimica Acta, 176*(1-2), 49-55.

Zhou, Y.-G., Chen, J.-J., Wang, F.-b., Sheng, Z.-H., & Xia, X.-H. (2010). A facile approach to the synthesis of highly electroactive pt nanoparticles on graphene as an anode catalyst for direct methanol fuel cells. *Chemical Communications, 46*(32), 5951-5953.

Zhu, Y., Murali, S., Cai, W., Li, X., Suk, J. W., Potts, J. R., & Ruoff, R. S. (2010). Graphene and graphene oxide: Synthesis, properties, and applications. *Adv Mater, 22*(35), 3906-3924.